NMR INVESTIGATIONS OF DYNAMIC PHENOMENA IN CRYSTALLINE ORGANIC SOLIDS

Kenneth Stuart Cameron

A Thesis Submitted for the Degree of PhD
at the
University of St Andrews

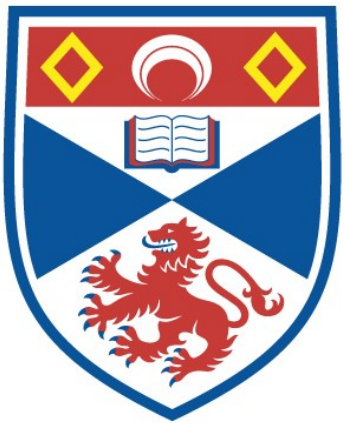

1977

NMR INVESTIGATIONS OF DYNAMIC PHENOMENA IN CRYSTALLINE ORGANIC SOLIDS.

a thesis presented by

Kenneth Stuart Cameron

to the

University of St. Andrews

in application for

THE DEGREE OF DOCTOR OF PHILOSOPHY

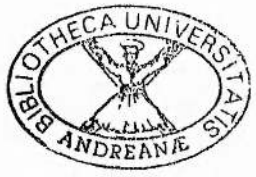

St. Andrews

September 1996

ProQuest LLC.
789 East Eisenhower Parkway
P.O. Box 1346
Ann Arbor, MI 48106 – 1346

Copyright

Declaration

I, Kenneth Stuart Cameron, hereby certify that this thesis, which is approximately 37,000 words in length, has been written by me, that it is a record of work carried out by me and that it has not been submitted in any previous application for a higher degree.

signature: , date: 27-9-96

I was admitted as a research student October 1992 and as a candidate for the degree of Ph.D. in October 1993; the higher study for which this is a record was carried out in the University of St. Andrews between 1992 and 1996.

signature: date: 27-9-96

I hereby certify that the candidate has fulfilled the conditions of the Resolution and Regulations appropriate for the degree of Ph.D. in the University of St. Andrews and that the candidate is qualified to submit this thesis in application for that degree.

signature of supervisor: date: 27-09-96

Dedicated To

My Family

Acknowledgements

I extend many thanks to my supervisor, Dr F.G. Riddell for his support, encouragement and boundless enthusiasm throughout this project. I also thank the EPSRC for funding for this project.

The people that have shared a lab with me over the years deserve a great big thank you for contributing to an excellent lab atmosphere. In particular I would like to thank the gang from 229 of John 'Big Jock' Smith, Doctor Shirley, Janice 'Bloodsucker' Bramham and Martin 'Dr Who' Rogerson. Thanks especially to Martin who moved with me to the new lab and with whom I had many a discussion on everything, but mainly on Dr Who! I also extend thanks to Marc a fellow chemist and flatmate. I can only say that I am sorry about all those dirty dishes, okay! I would also like to mention Josep who was a great friend during his year in St. Andrews. He adapted well to the dreach Scottish weather from the sunshine of Barcelona and showed even showed potential for golf. Speaking of golf brings me to my other great friend, Roger, who not only shared a lab but also dared to share a country cottage. Those great moments of footballing skill on the famous sloping Kingask pitch will live long. To my other chemists, friends and regular golf partners Malcolm and Doug, many thanks for all those early morning tee offs. Additional thanks goes to Doug for his contribution to the work in the thesis.

Thanks to the technical staff in particular John for his help. Melanja 'Mrs MHz' deserves special mention for being so cheery in dealing with that brute Boris.

An extra special thanks goes to Panthea.

Abstract

The study of the following compounds is based on the premiss that high symmetry in molecules should lead to low barriers to molecular motion even in the solid state i.e. the principle of least distress. The study of 3,3-diethylpentane is a very nice example of a phase change which results in no chemical shift changes but, produces a sharp discontinuity in the rate of ethyl group rotation. A large discontinuity in rate of molecular motion is also observed in 4,4-dipropylheptane which is also due to a phase change. The following study of tetraalkyl ammonium halides revealed both alkyl group rotation and cation tumbling to be occurring. This is most significant in the tetramethyl ammonium halides where the effects of methyl rotation and cation tumbling are shown to overlap considerably. The activation energies for the cation tumbling in the tetramethyl ammonium halides are E_a = 30 - 36 kJ mol^{-1} and for ethyl group rotation in tetraethyl ammonium chloride are, $\Delta H^{\ddagger}$ = 57.8 kJ mol^{-1} and $\Delta S^{\ddagger}$ = 45.9 J K^{-1} mol^{-1}. The chemical shift differences in each chain due to different chain lengths is seen in tetrabutyl ammonium iodate which also shows a sudden coalescence and introduction of rapid molecular motion after two small phase changes. This compound has a large phase change which also affects the rate of molecular motion. The tetraalkyl phosphonium halides have a greater degree of molecular motion than the ammoniums in the temperature range studied and also offer the chance to use ^{31}P $T_{1\rho}$ measurements. The tetramethyl phosphonium halides show a distinct cation tumbling as opposed to the ammoniums. The process in the chloride and bromide which have hexagonal structures gives $\Delta H^{\ddagger} \approx$ 30 kJ mol^{-1} and negative $\Delta S^{\ddagger}$ values and the lower symmetry iodide has $\Delta H^{\ddagger}$ = 45.2 kJ mol^{-1} and a positive value of $\Delta S^{\ddagger}$. The tetraethyl phosphonium halides show ethyl group rotations measurable to varying degrees by ^{13}C $T_{1\rho}$. The tetrabutyl phosphonium halides also have the different chain lengths as seen for the ammonium compounds. They also show bond rotations which are quite difficult to measure by ^{13}C $T_{1\rho}$ values. The study of bis-(hydroxymethyl)cyclopentane (BHMCP) in an attempt to study ring puckering/pseudorotation in cyclopentane derivatives in the solid state reveals a hydrogen bond exchange process ($\Delta G_c^{\ddagger} \approx$ 60 kJ mol^{-1}). The bicyclic derivatives of BHMCP showed no such molecular motions but did reveal some interesting solid-solid phase transitions and chemical shift changes. The study of *trans*-cyclopentanediol yields $\Delta H^{\ddagger}$ = 77.0 and $\Delta S^{\ddagger}$ = 184 J K^{-1} mol^{-1} for the processes involved. The study of 4,4-dimethyl-*trans*-1,2-cyclopentanediol reveals two processes. One results in the coalescence of resonances and appears to be a hydrogen bonding exchange process. The other is a much lower energy process ($E_a \approx$ 26 kJ mol^{-1}) which could be a ring puckering process. The study of sulpholane also shows significant molecular motion with $\Delta H^{\ddagger}$ = 50.6 kJ mol^{-1} and $\Delta S^{\ddagger}$ = 77.9 J K^{-1} mol^{-1}.

Contents

CHAPTER 1

1. Introduction[1]

The origins of Nuclear Magnetic Resonance (NMR) were in the USA where two separate groups of Physicists led by Felix Bloch and Edward Purcell carried out the first experiments in 1946. These first NMR experiments were carried out on solids and NMR was rapidly seen as "a powerful tool for studying the internal static and dynamic properties of matter, in particular the finest details of structures and motions."[1(a)] There are however, two severe restrictions when studying solids. The first is dipolar coupling and the second is chemical shielding anisotropy (CSA) and both are dependent on orientation in the magnetic field and both give rise to large linewidths. In liquids and gases this is cancelled by rapid molecular reorientation. In solids there is in some respects an over-abundance of information and so modern techniques have in the main simplified spectra (i.e. removed information). In solid state NMR it is possible to study a number of features not possible in high resolution (e.g. solution) NMR:

1. Solid state phenomena such as superconductivity and rates of diffusion.

2. The dependence of NMR phenomena to the external magnetic field with respect to the crystal axes e.g. chemical shielding anisotropy and dipolar couplings.

3. Dipolar spin-spin coupling is often much stronger than the spin-lattice interaction, and so allows double resonance spectroscopy which can achieve very high sensitivity (e.g. cross polarisation).

This over-abundance of information meant that until about twenty years ago chemists did not use NMR for solids, the main problem being line broadening, which when using a simple one pulse sequence on an organic solid for proton and carbon analysis typically gives linewidths of many kilohertz. In order to achieve the high resolution spectra that have been used for a large proportion of this work it is crucial to restrict the effects of chemical shielding anisotropy (CSA) and dipolar coupling.

Another problem is the long spin-lattice relaxation times in solids, which in solution NMR are relatively short due to rapid molecular tumbling. Spin-lattice relaxation becomes much less efficient in solids due to the rigid structure. This can, under certain circumstances, lead to long acquisition times and therefore, instead of experiments taking minutes, as in solution, it can more commonly take hours to achieve good signal to noise in a spectrum.

1.1 Theory of Line Broadening in Solids

1.1.1 Chemical Shielding Anisotropy (CSA)

The theory of CSA can be explained by looking at a simple molecule like carbon dioxide (Fig. 1.1). Chemical shift is produced by the shielding of nuclei by local electrons from the applied magnetic field, B_0. The field experienced by the central carbon nucleus depends on the orientation of the molecule with respect to the magnetic field B_0, because of the directionality of the electron distribution. The effect of this directionality is shown by aliphatic and aromatic or carbonyl carbons which have CSA of 10 ppm and >100ppm respectively.

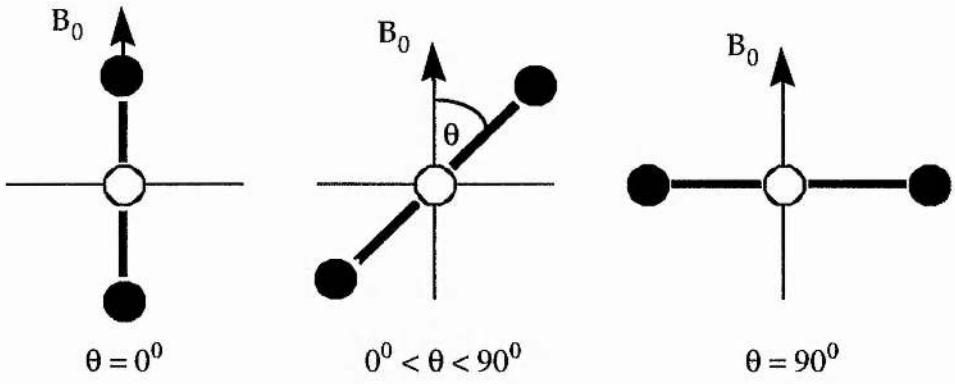

Fig. 1.1: Different orientations of a CO_2 molecule with respect to the magnetic field B_0.

It is clear from Fig. 1.1 that when $\theta = 0^{\circ}$ the central carbon experiences a different magnetic field from the case when $0^{\circ} < \theta < 90^{\circ}$ and also when $\theta = 90^{\circ}$ and so for a powdered crystalline material this gives rise to a range of chemical shifts. There are more ways that the molecules can be arranged when $\theta = 90^{\circ}$, therefore, there is greater intensity of the spectrum when $\theta = 90^{\circ}$ (perpendicular) than for $\theta = 0^{\circ}$ (parallel) (Fig. 1.2).

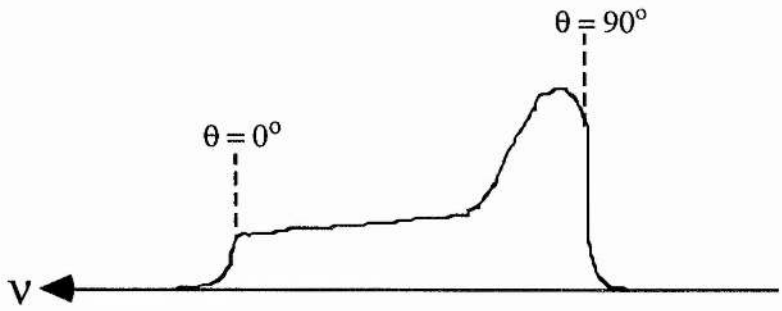

Fig. 1.2 Powder pattern for an axially symmetrical molecule such as CO_2.

From geometric considerations CSA depends on $3\cos^2\theta-1$ and this is crucial in the way that CSA can at least be partially removed from solid state NMR spectra.

1.1.2 Dipolar Interactions

Dipole-dipole interactions are generated when nuclei have I = 1/2. This is the dominant source of broadening for dipolar nuclei in solids containing ^1H (and ^{19}F). These can occur between isolated pairs of nuclei and for I = 1/2 nuclei e.g. ^1H, ^{13}C the through space coupling $J \alpha [k(3\cos^2\theta-1)]/r^3$ where k is a constant reflecting the magnetic properties of the two coupled nuclei and r is their distance apart.

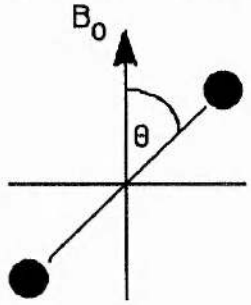

Fig. 1.3: Definition of θ for dipolar interactions.

^1H is an abundant spin (100%) nucleus and ^{13}C is a rare spin (1%) nucleus, therefore, ^1H-^1H interactions dominate the ^1H spectrum and $^1H/^{13}C$ interactions are important in the ^{13}C spectrum but $^{13}C/^{13}C$ interactions can be neglected. Dipolar interactions of abundant spins give rise to the so called "Pake pattern" (Fig. 1.4)[2] where each spin affects the other and in the case of an axially symmetrical molecule gives a spectrum similar to that in Figure 1.4. For a many spin system i.e. a real compound the linewidths are many kHz (Fig. 1.4), this is because the spins are interconnected. For dilute spins e.g. ^{13}C in an organic solid, they are coupled to the entire proton spin system and this produces broad lines even in single crystals.

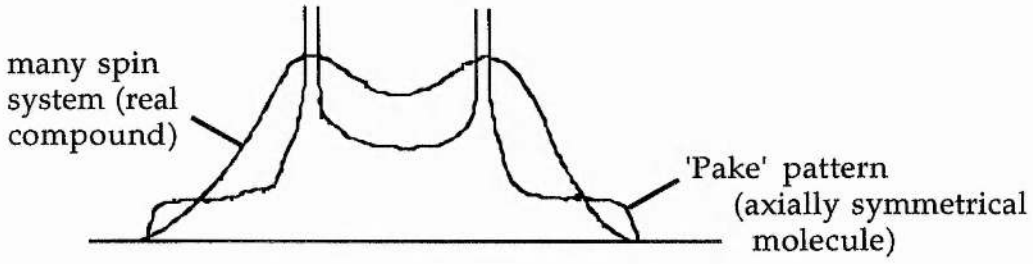

Fig. 1.4: Pake pattern for an axially symmetrical molecule and the pattern for a many spin sytem.

1.1.3 Spin Relaxation Times

The spin-spin relaxation time (T_2) is inversely proportional to NMR linewidths. The T_2 relaxation time is the decay of magnetisation in the x,y plane ($M_{x,y}$) and is shortened by field inhomogeneity. In solids it is affected by interactions of the static dipolar fields, set up due to the lack of motion in the solid. The Larmor frequency of $M_{x,y}$ changes and thus the magnetisation spreads out. T_2 is very small when the Larmor frequency changes periodically e.g. dynamic processes, proton transfer, conformational equilibria and valence tautomerism. Therefore, linewidths can be temperature dependent.

Quadrupolar nuclei have a quadrupole moment, Q, which can interact with the electric field gradient at the nucleus and cause very short T_1 values, and thus line broadening occurs because of the uncertainty in determining the energy difference between the excited and ground states. For covalently bound Cl, Br and I the lines are effectively too broad to measure. In ^{14}N and ^{2}H the quadrupolar relaxation is less effective but the lines can be up to 300 kHz and 100-200 kHz broad respectively.

1.2 Spectral Improvement

1.2.1 Magic angle spinning

To simplify the spectra and sharpen lines methods for removing some of the solid state nuclear interactions were sought. One such method is magic angle spinning (MAS).

Dipolar broadening and CSA both have an angular dependence $3\cos^2\theta-1$, where θ is the angle as shown in Fig. 1.3. The interaction between two nuclei (A and B) containing the term $3\cos^2\theta-1$ can be removed by so called magic angle spinning (Fig. 1.5).

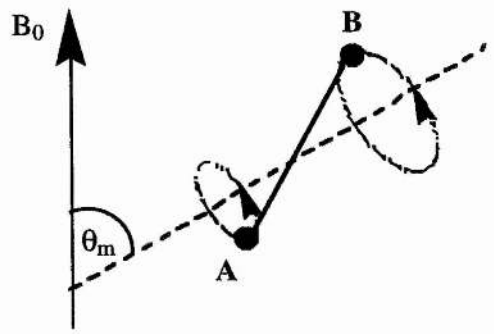

Fig. 1.5: Relation of the angle θ to B_0 and the AB vector.

The angle θ_m which is known as the magic angle, is the angle at which $3\cos^2\theta - 1 = 0$. The magic angle (θ_m) is the angle between opposing vertices of a cube (Fig. 1.6).

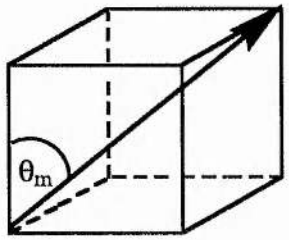

Fig. 1.6: Origin of the magic angle.

When the sample is spun, the average orientation of any internuclear vector AB (Fig. 1.5) will be equal to the magic angle. The rate of spinning has to be greater than the CSA linewidth or a set of lines is produced centred on the isotropic chemical shift. MAS will also help to sharpen dipolar broadened lines, because the dipolar coupling term contains $(3\cos^2\theta - 1)$, but the dipolar interactions in most organic compounds are so large that the sample cannot be spun fast enough to average them out.

Relatively narrow lines are generated but, they have side bands associated with them them occurring at integral multiples of the spinning speed which reflect the CSA pattern. For this reason the compounds are generally run at different spinning speeds since the spinning side bands move out the faster the sample is spun and so are easily identifiable. The spinning speed has to be in the kHz range, because to average out the CSA it must be rapid compared to the static linewidths. In fact, the complete removal of spinning side bands requires the spinning speed to be greater than the CSA (in Hz).

In plastic crystals, where the molecules occupy well defined lattice positions, but are free to rotate sharp lines can be generated by MAS alone. The motion needs to be fast enough to generate dipolar decoupling then the MAS can further reduce the linewidths to less than the chemical shift differences (e.g. adamantane).

1.2.2 Dipolar Decoupling

In general the coupling of ^{13}C to ^{1}H can be removed by high power heteronuclear decoupling. The interactions may be of the order of tens of kilohertz and, therefore, the power required is high e.g. 10^2-10^3 W compared to *ca* 5-50W for solution NMR.

The combination of MAS and high power heteronuclear decoupling produces linewidths for ^{13}C typically of the order of 50 Hz and even less in favourable cases. In some cases, however, it is impossible to remove all the effects of CSA and this gives rise to spinning side bands (ssb). These occur at multiples of the spinning speed and although they can yield additional information they often obscure resonances. However, CSA is generally only significant in organic molecules with planar or linear functionalities such as aromatic, olefinic, acetylenic and carbonyl carbons.

1.2.3 Cross Polarisation

The low abundance of ^{13}C and its long relaxation times in the solid state give rise to further problems. The problem is overcome by a technique known as cross polarisation (CP), by exciting the abundant protons and transferring their magnetisation to the carbon nuclei. The pulse sequence involved (Fig. 1.7) shows the contact pulse which is typically 1 ms compared with the microsecond 90° pulses that are typically used for most purposes.

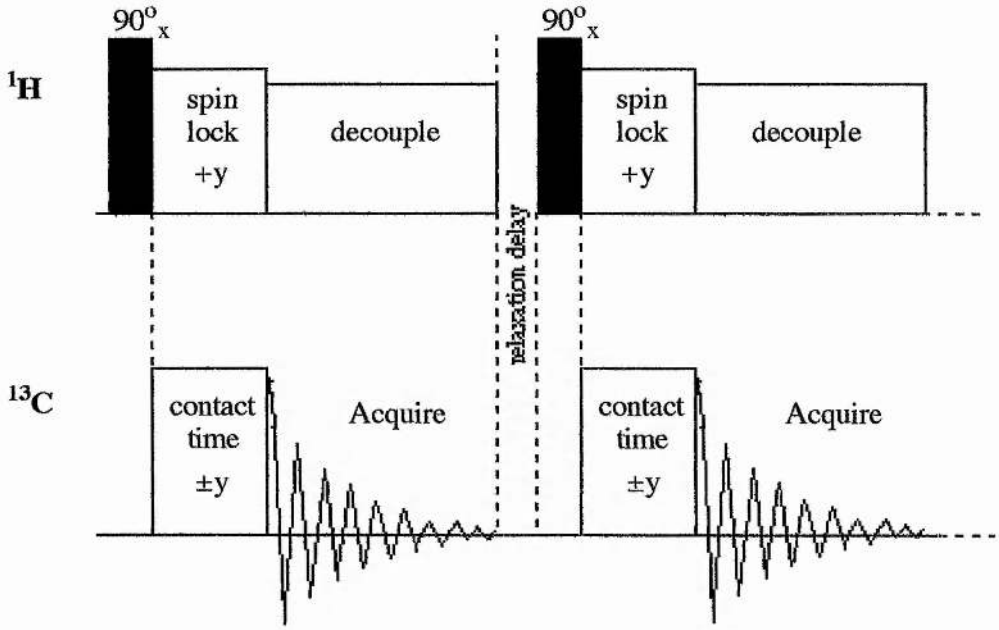

Fig. 1.7: The cross polarisation pulse sequence.

This can be shown in the rotating frame of reference (Fig. 1.8).

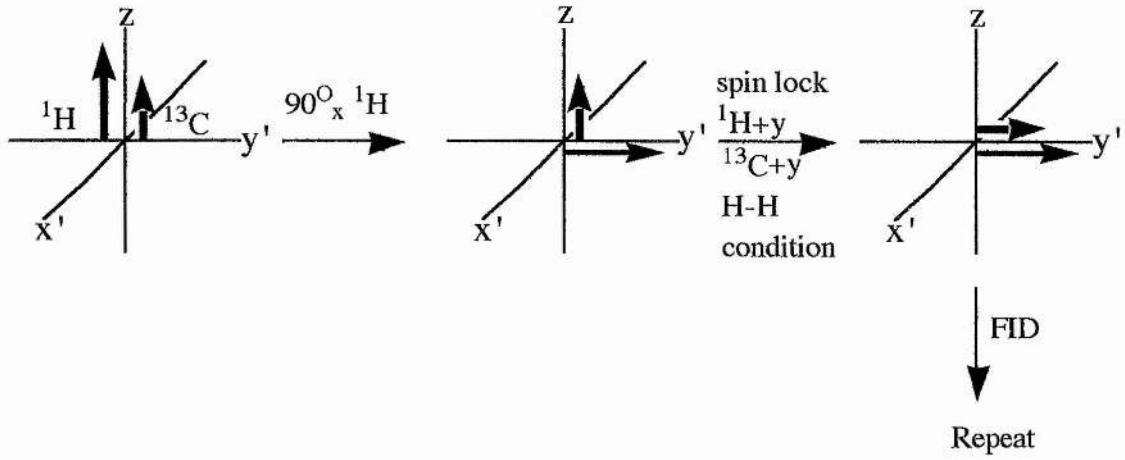

Fig. 1.8: The cross polarisation pulse sequence in the rotating frame of reference.

During the contact pulse the magnetisation is transferred from the ^{1}H reservoir, spin-locked along the y'-axis to the ^{13}C nuclei. The carbon magnetisation is also forced to precess along the y'-axis and if the two rf power levels are adjusted so that the two nuclei are made to precess at the same frequency then they can undergo mutual spin flips or mutual relaxation. This is known as the Hartmann-Hahn condition and is given in (eqn.1). The result is a transfer of magnetisation from the abundant ^{1}H pool to the ^{13}C pool.

$$\gamma_H H_H = \gamma_C H_C \qquad \textbf{eqn.1}$$

H_H is the field for irradiating ^1H

H_C is the field for irradiating ^{13}C

γ are the gyromagnetic ratios of the given nucleus which relates the moment μ with the angular moment I.

This arises from the relationship;

$$\nu = \gamma H_o/2\pi$$

At the Hartmann-Hahn condition $\nu_1 = \nu_2$, and therefore,

$$\gamma_1 H_1/2\pi = \gamma_2 H_2/2\pi$$

The precessional frequency is, therefore, the same for both ^1H and ^{13}C and this allows a 'thermal' contact and thus cross polarisation.

Each nucleus has a different gyromagnetic ratio and so the precessional frequency of a nucleus is proportional to the applied magnetic field. The cross polarisation enhances the ^{13}C magnetisation because the signal intensity is directly proportional to γ_H/γ_C which is *ca* 4. The recycle times are also reduced because the experiment is dependent on proton spin-lattice relaxation rather than the carbon relaxation which is an order of magnitude slower.

Thus the combined so called CP/MAS experiment using high powered decoupling gives good high resolution spectra for solids, in a shorter time.

1.3 Solid state NMR and rate determination

1.3.1 Relaxation times

Longitudinal magnetisation in the z-axis and transverse magnetisation in the x,y plane are time dependent and are, therefore, subject to relaxation phenomena. This manifests in the spin-lattice (longitudinal) relaxation time (T_1) and the spin-spin (transverse) relaxation time (T_2):

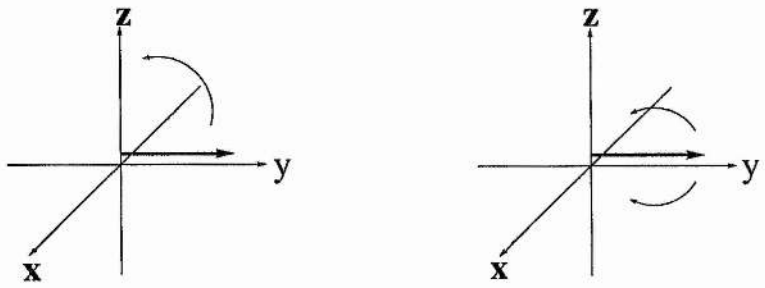

Fig. 1.9: (a) Longitudinal relaxation. (b) Transverse relaxation

These are the two basic relaxation times, but there are others e.g. $T_{1\rho}$, T_{1D} and T_2^* and some of these will be dealt with at a later stage. It can be seen from the nomenclature that these relaxation times are in some ways similar to T_1 and T_2.

1.3.1.1 Spin-lattice relaxation time

The relaxation time (T_1) is the time constant associated with the rate at which equilibrium magnetisation (M_0) is reached after exposure to an external magnetic field B_0. The build up of the magnetisation in the z-axis is given by a first order rate equation:

$$\frac{dM_Z}{dt} = \frac{M_0 - M_Z}{T_1} \qquad \textbf{eqn.2}$$

During this process energy is transferred from the relaxing spins to other spins in the lattice and hence T_1 is called the spin-lattice relaxation time. T_1 occurs because molecular tumbling creates fluctuating magnetic fields which have components $B_{x'}$ and $B_{y'}$ with a wide range of frequencies which act as built in r.f. transmitters and stimulate transitions. Relaxation occurs when the tumbling has a component at close

to ω_0, enabling magnetisation to be transferred. The magnetic energy lost is then received by the lattice and finishes up in the form of thermal energy.

T_1 has many contributing factors i.e. T_{1DD}, dipolar; T_{1CSA}, chemical shielding anisotropy; T_{1Q}, quadrupolar and T_{1SC}, scalar. This leads to the overall rate for the observed longitudinal relaxation:

$$\frac{1}{T_{1obs}} = \frac{1}{T_{1DD}} + \frac{1}{T_{1CSA}} + \frac{1}{T_{1Q}} + \frac{1}{T_{1SC}} \qquad \textbf{eqn.3}$$

In solids the motions are obviously much more restricted and so T_1 relaxation becomes less efficient and this leads to long recycle delays (5-60s commonly) even for protons, while the signal decays in milliseconds. There is, however, a difference between abundant nuclei and dilute spin systems. In the abundant nuclei case (e.g. protons) the strengths of the dipolar interactions are such that all of the nuclei have a single common set of relaxation times. In the dilute spin case (e.g. ^{13}C) the nuclei do not share a common relaxation time and so the relaxation times and hence dynamics of each atom in a molecule can in principle be determined. T_1 will only give information about the dynamics in the frequency range of ω_0 i.e. in the MHz region.

In general proton relaxation is facilitated by intermolecular interactions because they are on the outside of molecules. ^{13}C nuclei are shielded and so the relaxation is dominated by relaxation is dominated by intramolecular interactions. The rate of relaxation for carbons in a ^{13}C, ^{1}H spin system is given by:**1(b)**

$$R_1^{DD} = \frac{1}{T_1} = \frac{m_o}{2\pi} (h^2 \gamma_{^{13}C}^2 \gamma_{^{1}H}^2 r_{CH}^{-6} \tau_C)$$

m_o: constant
r: distance between the C and H considered
τ_c: correlation time of motion.

eqn.4

Both in solution and in the solid state T_1 values for protons are shorter than for carbons because the dipole-dipole interaction is dependent on the square of the magnetogyric ratios.

One commonly used method of measuring T_1 (Fig. 1.10) is the inversion recovery method, 180-τ-90, where τ is varied and the peak intensity is measured. A plot of ln (intensity) vs. τ then gives a straight line with slope T_1.

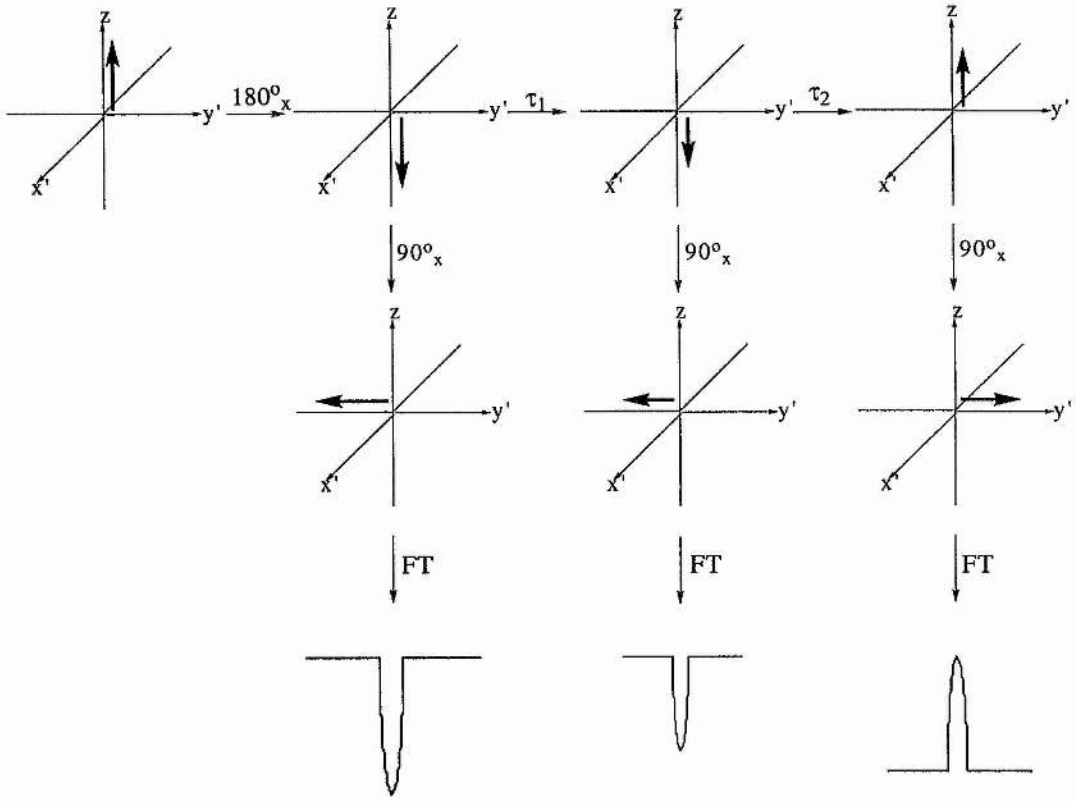

Fig. 1.10: Measurement of T_1 by inversion recovery method.

The variation of T_1 with temperature can be calculated from eqn.5, where K includes the factors in eqn. 4 that are independent of temperature and frequency.[3]

$$1/T_1 = K\left[\frac{\tau_c}{1+\omega_o^2\tau_c^2} + \frac{2\tau_c}{1+4\omega_o^2\tau_c^2}\right]$$

K: constant
ω_o: Larmor frequency

eqn.5

Where τ_c causes random modulation of the dipole Hamiltonian. Assuming that the process has an activation energy (E_a) then the variation of τ_c with temperature will follow the Arrhenius equation:[4]

$\tau_c = \tau_o \exp(E_a/RT)$ R - gas constant.

Therefore, a plot of ln τ_c against 1/T gives E_a, or alternatively if ln T_1 vs. 1/T is plotted the asymptotic regions become linear (Fig. 1.11) and the upper and lower limits give $-E_a/R$ and $+E_a/R$ respectively.

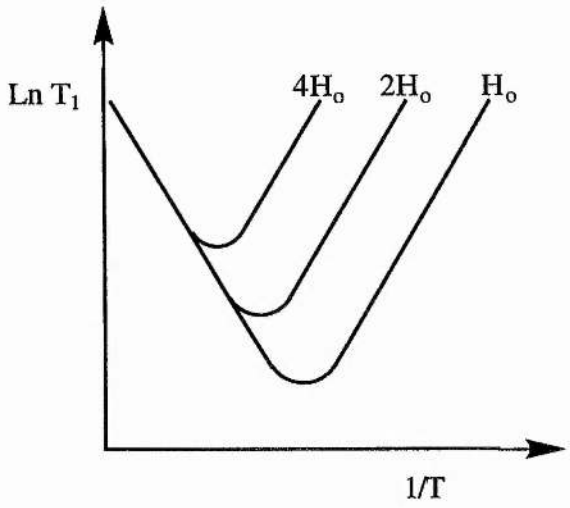

Fig. 1.11: Dependence of the T_1 minimum on H_o.

T_1 is sensitive to motion occurring at the Larmor frequency in the applied field (e.g. 500.13 MHz and 125.758 MHz for ^1H and ^{13}C respectively on the spectrometer used at St. Andrews) and considering eqn.4 the T_1 minimum will occur at lower temperatures (τ_c longer) and will be deeper for smaller ω (H_o) (Fig. 1.11). Therefore, T_1 is generally only used for dynamic proton NMR although modulation of ^{13}C T_1 values by methyl group rotations are possible below ambient temperature. Above ambient temperature it is necessary to move to lower frequencies to measure molecular motions by ^{13}C T_1 values.

1.3.1.2 Spin-lattice relaxation time in the rotating frame ($T_{1\rho}$)

This relaxation time occurs when an external field H_1 is applied and forces the nuclei to precess at a tip angle of ϑ to the static magnetic field. The rate of relaxation for $\vartheta = 90^0$ (i.e. 90^0 pulse) and $\omega_1 \ll \omega_o$, is given by:[5]

$$\frac{1}{T_{1\rho}} = K\left[\frac{3}{2}\left(\frac{\tau_c}{1+4\omega_1^2\tau_c^2}\right) + \frac{5}{2}\left(\frac{\tau_c}{1+\omega_o^2\tau_c^2}\right) + \frac{\tau_c}{1+4\omega_o^2\tau_c^2}\right]$$

K: constant
ω_1: precessional frequency of the spin lock field.

eqn.6

Assuming that $\omega_o\tau_c \gg 1$ (i.e. the contributions at ω_o are negligible) then eqn.5

reduces to:[6]

$$1/T_{1\rho} = \frac{3}{2}K\left[\frac{\tau_c}{1+4\omega_1^2\tau_c^2}\right] \qquad \textbf{eqn.7}$$

In the heteronuclear case eqn.7 becomes:[7]

$$1/T_{1\rho} = \frac{B^2\tau_c}{1+\omega_1^2\tau_c^2} \qquad \textbf{eqn.8}$$

B^2 : C-H interaction strength

The pulse sequence for measuring homonuclear $T_{1\rho}$ (e.g. ^1H) (Fig. 1.12) shows that there is a initial pulse of 90^0 on x' and that the second pulse on y' is the spin-locking field of variable length (τ).

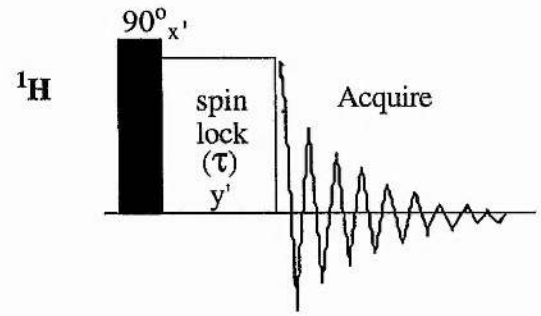

Fig. 1.12: Pulse sequence for measuring ^1H $T_{1\rho}$.

To measure heteronuclear ^{13}C $T_{1\rho}$ values the cross polarisation pulse sequence (Fig. 1.7) is used, by varying the length of the spin lock, as shown for the homonuclear case (Fig. 1.12).

The magnetisation along the y' axis decays with a time constant $T_{1\rho}$ and so by varying the length of the spin-lock (τ), $T_{1\rho}$ values are obtained from the gradient of a plot of ln (intensity) vs. τ. Therefore, a plot of ln τ_c vs. 1/T yields E_a in the same way as for T_1. It can be shown that the asymptotic plot of ln $T_{1\rho}$ vs. 1/T yields $-E_a/R$ and $+E_a/R$ for the upper and lower limits respectively in the same way as T_1:

If $\omega_1^2\tau_c^2 \ll 0$ then eqn.8 reduces to:

$$1/T_{1\rho} = \frac{B^2\tau_c}{1}$$

therefore,

$$k = 1/\tau_c = B^2T_{1\rho}$$

and so a plot of ln $T_{1\rho}$ vs. 1/T gives a gradient of $-E_a/R$ and an intercept of ln B^2 + preexponential factor.

and if $\omega_1^2\tau_c^2 \gg 0$ then eqn.8 reduces to:

$$1/T_{1\rho} = \frac{B^2\tau_c}{\omega_1^2\tau_c^2}$$

and so,

$$k = 1/\tau_c = (\omega_1^2/B^2)\ T_{1\rho}$$

and a plot of ln $T_{1\rho}$ vs. 1/T now has a gradient of E_a/R with an intercept of ln (ω_1^2/B^2) + the preexponential factor.

It is however, possible to extend this theory to get values of free energy of activation and the entropy of activation:

If eqn.8 is considered then, at the minimum of the function;

$$\omega_1^2\tau^2 = 1 \qquad \textbf{eqn.9}$$

and,

$$T_{1\rho}(\min) = \frac{2}{B^2\tau} \qquad \textbf{eqn. 10}$$

and from eqn.9:

$$\tau^2 = \frac{1}{\omega_1^2}$$

This, therefore allows the calculation of B^2 values and from this the rate of the process follows:

$$k = \frac{1}{\tau}$$

Eqn.8 can be written as a quadratic equation:

$$\omega_1^2\tau^2 - T_{1\rho}B^2\tau + 1 = 0 \qquad \textbf{eqn.8'}$$

Therefore, by finding B^2 from the $T_{1\rho}$ minimum the quadratic can be solved for τ. The correct value for τ is easily determined from the two values obtained for τ by taking the low value at low temperatures and after the minimum taking the high value.

The calculation of rate parameters then proceeds as for transition state theory, which gives the following equation:

$$k = \frac{kT}{h} e^{\frac{-\Delta H^{\ddagger}}{RT}} e^{\frac{-\Delta S^{\ddagger}}{R}}$$

k: Boltzman constant

h: Planck's constant

eqn. 11

Thus a plot of ln (k/T) against 1/T will be a straight line with gradient $-\Delta H^{\ddagger}/RT$ and a y intercept of ln (k/h) + $\Delta S^{\ddagger}/R$.

As with T_1 relaxation the relaxation of nuclei in the applied field (H_1) is facilitated by molecular motions of the same order of magnitude as ω_1. Such molecular motions modulate the local field to which the nuclei are subject and, therefore, the relaxation is more efficient.

A spin-lock field is routinely used in the CP/MAS pulse sequence for the enhancement of ^{13}C NMR signals (section 1.23). Therefore, the ^{13}C nuclei are forced to precess at a frequency ω_1 ($= \gamma H_1$). The spin-lock field used for CP is 50-100 kHz and so $T_{1\rho}$ is sensitive to motions in this frequency range (say 10^4 to 10^7 sec^{-1}). The spin-lock field (ω_1) is much lower in frequency than ω_o and so $T_{1\rho}$ can be

a valuable technique for the study of mechanical relaxations (e.g. alkyl group rotations and molecular motion in polymers).[8]

1.3.1.3 Relaxation in a dipolar field

In order for a sample to display relaxation in a dipolar field (T_{1D}) it must have good dipolar coupling (i.e. short T_2) and a long T_1. The sample, when introduced to a strong magnetic field, has an initial magnetisation, M. If it is slowly removed adiabatically from the magnetic field residual pockets of magnetisation are set up randomly throughout the sample along local fields. These local fields are very small, but if the sample is reintroduced into the strong magnetic field at the same rate it was removed then all the magnetisation (M) will reappear in a time short compared with T_1. The total time for the experiment , however, must be short compared to T_1. The time decay along each local field vector is governed by T_{1D}, the dipolar relaxation time. The relaxation is therefore, sensitive to motions at the frequency of the local field, which is of the order of a few kilohertz (i.e. low frequency and high energy motions). Experimentally the conversion of the magnetisation to the dipolar state can be done using a pulse sequence (Fig. 1.13) and, therefore, the measurement of T_{1D}:[9]

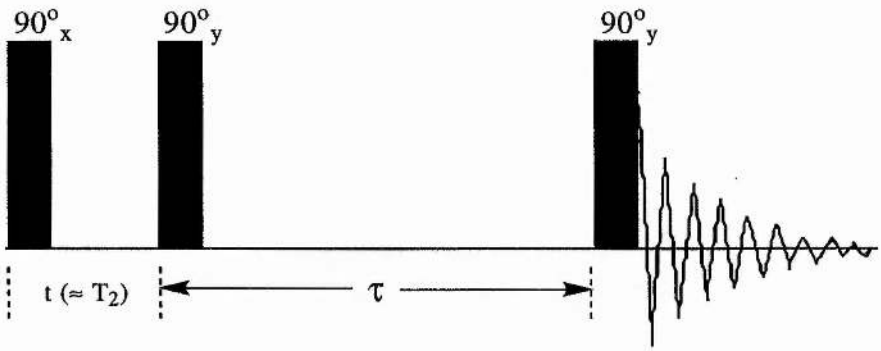

Fig. 1.13: Pulse sequence for measuring T_{1D}.

Measurements of T_{1D} values can give rates in a similar way to T_1, an example is given for cyclooctane showing that the range of rates measured for the diffusion are extended to much lower frequencies.[10]

1.3.1.4 Spin-spin relaxation and second moments

The spin-spin relaxation time (T_2) in solids is much shorter than T_1, whereas with rapid molecular motion (e.g. liquids) $T_1 \approx T_2$. In solids T_2, therefore, offers

extra information however, due to its dependence on magnetic field imperfections it is seldom used directly to study molecular motions. T_2 is measured by an echo pulse sequence (Fig. 1.14). There is an initial $90°_x$ pulse which places the magnetisation along the y' axis where it is allowed to spread out with time constant T_2 for a period τ. A refocussing $180°_y$ pulse is applied and the magnetisation is refocussed along the y' axis after a further interval τ. The decay of the magnetisation in the interval 2τ is a measure of the relaxation time T_2.

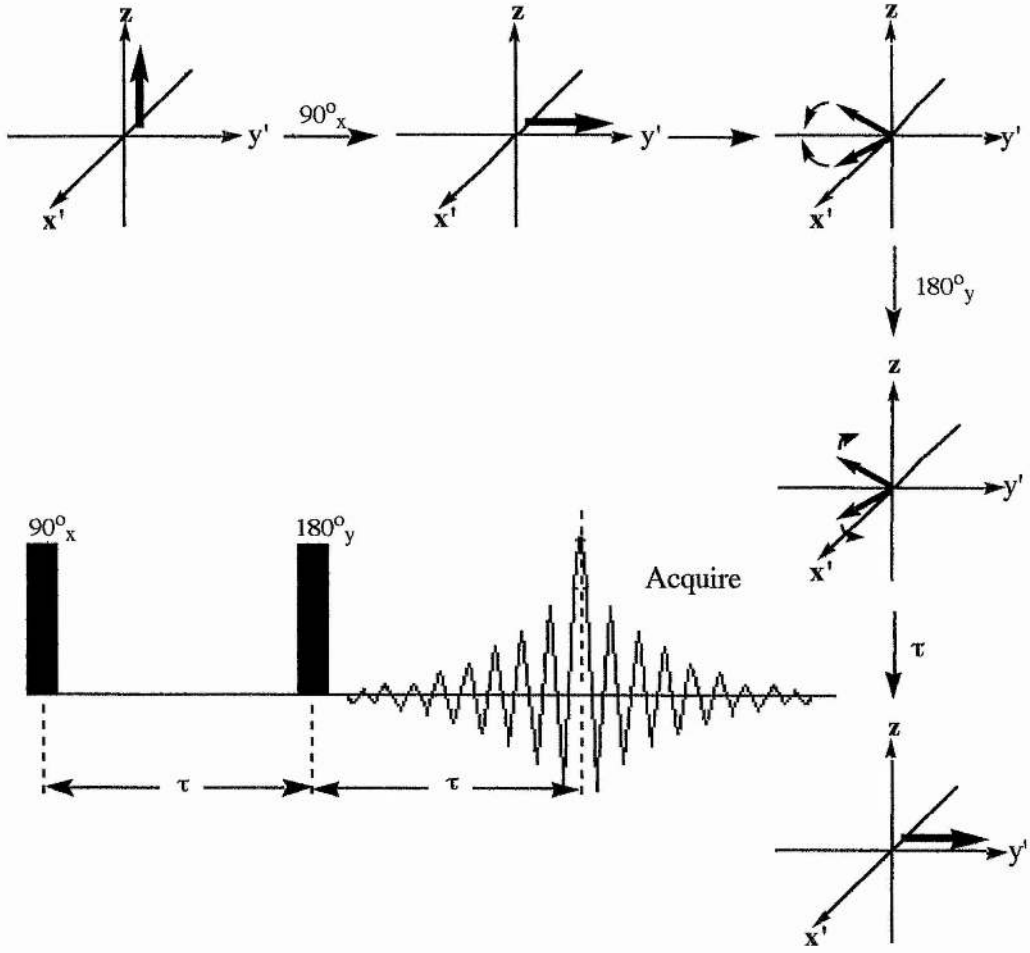

Fig. 1.14: The echo pulse sequence used for T_2 measurement.

Since $T_2 \propto 1/\Delta\nu$, changes in T_2 curves are replicated in changes in linewidths. T_2 is closely related to more useful term of second moment (ΔH^2), which is the mean square width of the curve in terms of the field (i.e. second moment, ΔH^2, is a measure of the mean square local dipolar field). This is defined mathematically as in:

$$\left(\Delta H^2\right) = \int_0^{\infty} (H - H_{av})\, f\,(H)\, dH \qquad \textbf{eqn.12}$$

Where eqn.12 refers to the parameters in Fig. 1.15.

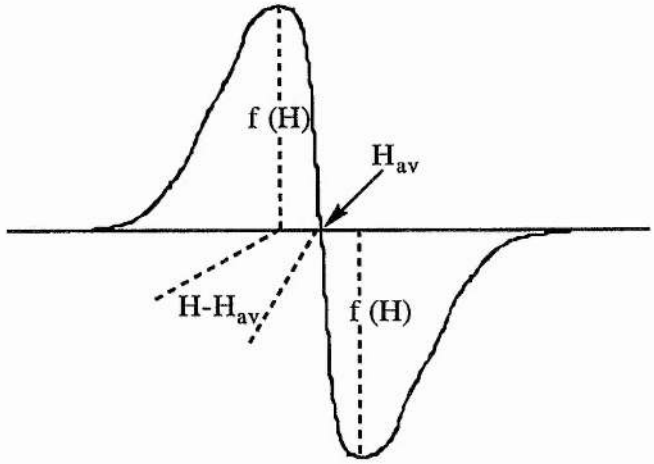

Fig. 1.15: A solid state ^1H NMR resonance giving the terms in **eqn.12**.

Second moments are very useful in characterising the broad featureless absorptions obtained from solid state ^1H NMR studies. The importance of second moments are that they can be calculated theoretically and are very sensitive to molecular motions.[3] The theoretical calculation of second moments is from:

$$(\Delta H^2) = K \,{}^1\!/_N \sum_{i,j} \frac{1}{r_{ij}^6}$$

eqn.13

K: constant.
N: no. of nuclei in the system whose interactions are considered.
r_{ij}: distance between two interacting nuclei.

Second moments contain line-broadening contributions only from pair wise interactions (multi spin correlations are contained in higher moments). The most interesting feature of second moments is their sensitivity to motion as seen by Andrew and Eades.[4,11]

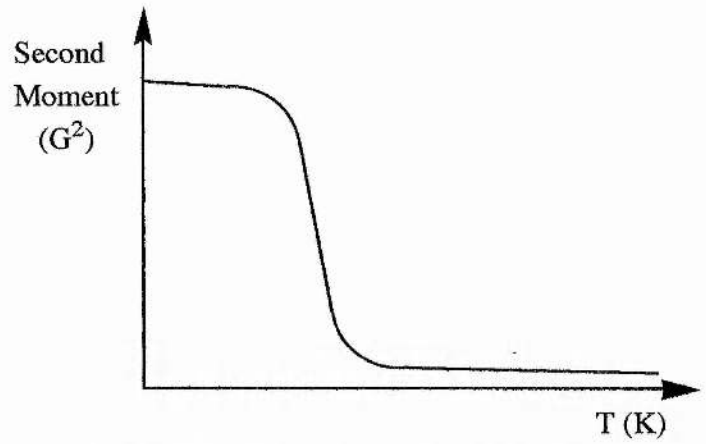

Fig. 1.16: Representation of the effect of rapid molecular motion on second moments.

In a rigid lattice the second moment is large, but with rapid motion the intramolecular dipole interaction is averaged and the second moment values fall sharply. The shape of second moments can be calculated by predicting the types of motion possible. Second moment lineshapes are, however, not sensitive enough to give reliable activation enthalpies. The transition temperature has proven to be a much more reliable measure, and produces the relationship $E_a \approx 166\ T_o$ kJ mol^{-1},[12] where T_o is the centre of the transition in K.

The motions in molecules studied by second moments are often distingished by selective deuteration. For example, in methylammonium chloride,[13] the effect on the second moment can be studied by observing $CH_3{}^+ND_3\ Cl^-$ and $CD_3{}^+NH_3\ Cl^-$ respectively. Therefore, the methyl group, $-NH_3$ group and whole cation molecular motions can be identified individually.

1.3.2 Quadrupolar nuclei

In the case where I>1/2 (e.g. ^2H, ^{14}N and ^{35}Cl) the spectrum is dominated by the quadrupolar interaction, characterised by the quadrupolar coupling constant (q.c.c.):

$$q.c.c. = \frac{e^2qQ}{h}$$

eQ = quadrupole moment
eq = field gradient
h = Planck's constant

eqn.14

Other interactions such as chemical shielding anisotropy (CSA), spin-spin couplings and dipolar interactions can be ignored although the latter may introduce some line broadening to the spectrum.

The measurement of spectra is thus dominated by the q.c.c., which is 170-200 kHz for deuterons attached to carbons, up to 5 MHz for ^{14}N and up to 80 MHz for ^{35}Cl. Deuterium has a relatively small quadrupole moment and therefore, is one of the simplest quadrupolar nuclei to observe, but even for deuterium a special pulse technique called quadrupole spin-echo is required (Fig. 1.17), which is analogous to the echo technique used for measuring T_2 (Fig. 1.14). The three spin states that quadrupolar nuclei can occupy mean that representation of this pulse sequence in the rotating frame using simple magnetisation vectors is not possible. The important aspect is that the second 90° pulse reverses the time dependence of the spins and they refocus to produce an echo from which the spectrum is obtained.

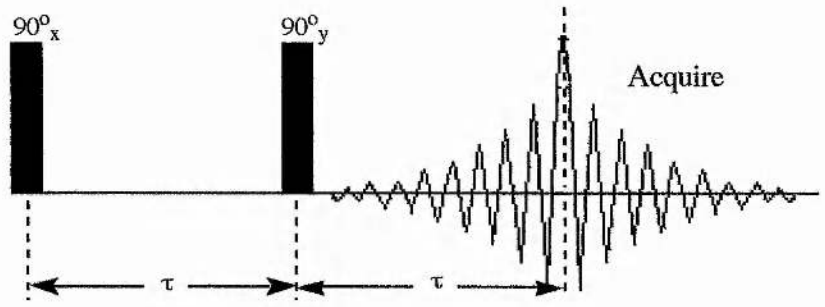

Fig. 1.17: Quadrupolar spin-echo pulse sequence.

This pulse sequence is needed because the nuclei relax so quickly and therefore, in a normal pulse sequence the pulse would need to be closely followed by acquisition of the signal. The high power required leads to pulse breakthrough and subsequent distortion of the spectrum, when simple one pulse techniques are attempted. This phenomenon sometimes known as acoustic ringing can be avoided by the use of an echo sequence.

The spectrum of a single deuteron is a doublet of the type described by Pake,[2] for the dipolar interaction of two I = 1/2 nuclei (section 1.12). The spectrum is, therefore, dependent on the orientation of the C-^{2}H vector in the magnetic field.

When motion is involved the spectral shape becomes dependent on the pulse interval used to produce the echo. The simulation of ^{2}H NMR lineshapes is possible with computer programmes which include various parameters, e.g. q.c.c., rate of

reorientation, reorientation axis or axes. Therefore, a successful simulation of an experimentally obtained spectrum gives details of the motion occurring. Selective deuteriation can, therefore, give the whole picture of motions in a molecule if the rate of molecular motion is of the order of the quadrupolar interaction, i.e. 10^{-5} to 10^{-6} s. Larmor frequency rates of motion can also be studied by relaxation time measurements giving a wide range of frequencies.[14]

1.3.3 Two dimensional spectroscopy

The application of two dimensional (2D) spectroscopy to solids is analogous to solution state NMR except for the introduction of cross polarisation to increase the ^{13}C signal to noise ratio. 2D-exchange spectroscopy with cross polarisation (2D CP/EXSY) can be used to study slow exchange processes of the order of the ^{13}C relaxation times i.e. 1-100s.[15] The pulse sequence (Fig. 1.18) shows the variable evolution time (t_1) which gives rise to the second dimension.

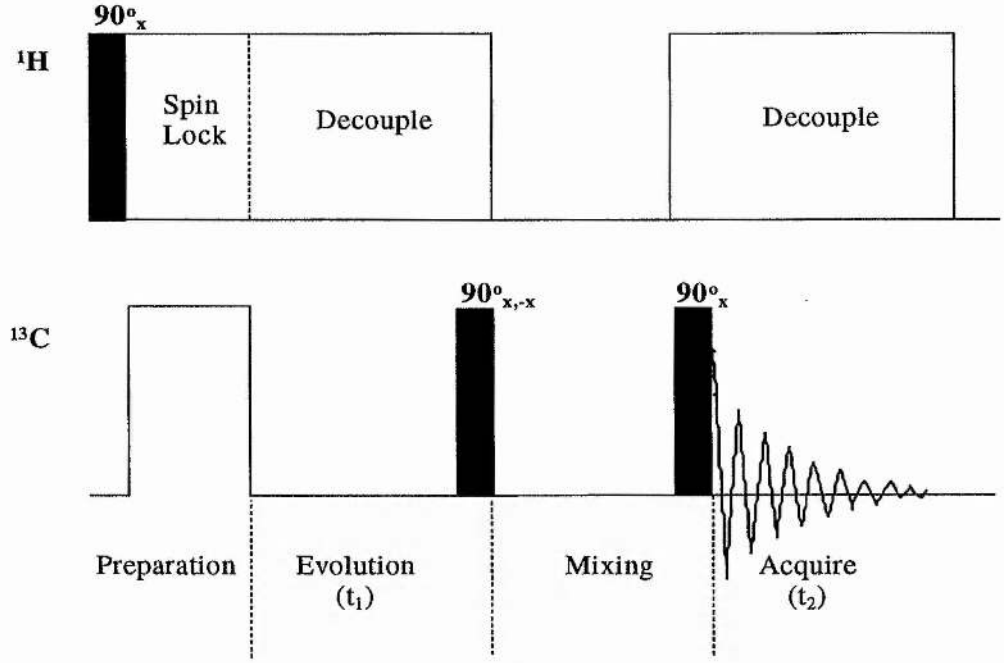

Fig. 1.18: 2D CP/EXSY pulse sequence.

The mixing time is when communication between spins can take place i.e. the time for a ^{13}C spin to change chemical shift. Therefore, the mixing time has to be of the correct length *ca* 1/k (where k is the rate constant for exchange) in order for the exchange to be observed.

1.3.4 Lineshape analysis

When a coalescence of resonances is observed, information about the energy of the process can be obtained from the coalescence temperature (T_c) and from the relation $k_c = \pi \Delta\nu/\sqrt{2}$, where $\Delta\nu$ is the splitting of the resonances in Hertz.[16] This gives rise to the equation:

$$\Delta G^{\ddagger} = 19.1\, T_c\left[10.3 + \log\left(T_c / \Delta\nu\right)\right] \quad \textbf{eqn.15}$$

This gives an idea of the free energy of activation required for processes occurring at a rate comparable to the chemical shift difference. With a ^{13}C frequency of 125.758 MHz, a 1 ppm chemical shift difference coalescence will occur when the process has a rate of the order of $10^2 s^{-1}$.

1.3.5 Maximum dipolar broadening

In the same rate range as the $T_{1\rho}$ effect is maximum dipolar broadening which is brought about by incoherent averaging caused by the intramolecular motion interfering with the coherent averaging of the decoupling radiofrequency field (50-100kHz).[17] The main benefit of this is that when maximum dipolar broadening is observed it is a good indication that $T_{1\rho}$ values can be measured. A rate of the rotation can also be obtained with the maximum linewidth occurring when the rate of molecular is equal to the decoupling field.

1.4 Activation parameters

As discussed in section 1.3.1.2 on $T_{1\rho}$ relaxation times it is possible to obtain values for both the free ensrgy of activation ($\Delta H^{\ddagger}$) and the entropy of activation ($\Delta S^{\ddagger}$). The concept of these parameters are relatively simple in isolated molecules with $\Delta H^{\ddagger}$ arising from the changes in intramolecular interactions between ground state and excited state. $\Delta S^{\ddagger}$ arises from the reorganisation of molecular vibrational modes as the molecule is goes from ground to transition state.

In the solid state these concepts become more complex. $\Delta H^{\ddagger}$ must now include both the intra- and intermolecular interactions. Close intermolecular approaches near

the site of the molecular motion now become important. For $\Delta S^{\ddagger}$ the allowed vibrational modes are now those of the entire lattice. The isolated molecule is, in principle, not involved in the $\Delta S^{\ddagger}$ in the solid state.

$\Delta S^{\ddagger}$ values for conformational motions in solution are generally small. Work by Dr Riddell *et al*.[7,18,19,20] has shown that $\Delta S^{\ddagger}$ values for intramolecular motions can be substantial in both a positive and negative sense.

1.5 Principle of Least Distress

One way of deciding whether a particular rotation is likely in the solid is to consider how much stress the lattice will be put under by that rotation. This is easily pictured by considering the case of a carbon-carbon bond rotation where one carbon is fixed and the other is bonded to three groups of differing size (Fig. 1.19).

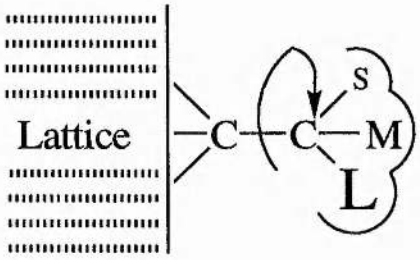

Fig. 1.19: A carbon bonded to three groups of varying size.

Any rotation about the C-C bond would require a larger group to go into a hole which is small and thus a distortion of the lattice would be required. For this reason the likelihood of group rotations in the solid state are greatest when the substituents are of similar size e.g. tertiary butyl, trimethyl ammonium will more readily rotate than isopropyl groups.

One well studied type of motion that fits the principle of least distress is the rotation of whole molecules that have high symmetry, about their position in the lattice. This is particularly common in plastic crystalline phases. Other types of molecular motion that should cause little distress to the lattice are pseudorotation of five- and seven-membered rings where the atomic displacements are small compared to the molecular dimensions.

This thesis examines examples of bond rotations, whole molecule rotation and pseudorotations in crystalline organic compounds. It also brings to light evidence for dynamic hydrogen bond exchange phenomenon not previously examined by NMR spectroscopy.

CHAPTER 2

2. Experimental

2.1 Symbols and Abbreviations

h., min.	hours, minutes
rb	roun bottomed
dil.	dilute
conc.	concentrated
t.l.c.	thin layer chromatography
G.C.	gas chromatography
mmol	mille moles
NMR	nuclear magnetic resonance
ppm	parts per million
Hz	hertz
s, d, t, q, m	singlet, doublet, triplet, quartet, multiplet
dd	doublet of doublets
AB_q	AB quartet
b	broad
m.p.	melting point
b.p.	boiling point
lit.	literature value
quat.	quaternary
Et	ethyl
Pr	propyl

2.2 Instrumentation

2.2.1 Solution NMR Spectroscopy

All ^{1}H and ^{13}C solution spectra were obtained on a Varian Gemini 200 operating at 200.052 and 50.303 MHz respectively and the ^{2}H solution spectra were obtained on a Bruker 300 operating at 46.02 MHz. The compounds were referenced to TMS (^{1}H and ^{13}C – 0 ppm) in $C^{2}HCl_3$ or to residual $CHCl_3$ (^{1}H-7.27 ppm and ^{13}C 77.01 ppm) in $C^{2}HCl_3$ and the deuterium spectra were referenced to $C^{2}HCl_3$ (^{2}H-7.27 ppm) in $CHCl_3$.

2.2.2 Elemental Analysis

Percentage carbon, hydrogen and nitrogen were obtained by Mrs S. Smith using a Carlo-Erba 1106 elemental analyser.

2.2.3 Melting points

All melting points were carried out on an Electrothermal melting point machine. The temperatures are uncorrected.

2.2.4 Solid–State Spectra

All solid–state NMR spectra were obtained on a Bruker MSL500 spectrometer in either high resolution or high power mode. Solid–state ^{13}C spectra were obtained at 125.758 MHz in the CP/MAS mode using 4 mm o.d. rotors spinning typically at 4–8 kHz. All solid–state spectra including $T_{1\rho}$ determinations were obtained by the cross polarisation pulse sequence. A cross polarisation contact time of 1-4 ms was commonly used.

Chemical shifts were referenced relative to the CH_2 group in adamantane at 38.56 ppm determined on a separate sample.

The ^{13}C spin locking frequency during the Hartmann–Hahn condition was determined using single carbon pulses and high power ^{1}H decoupling on adamantane and was found to be in the region 60–90 kHz. The same radio frequency power was used for the spin lock period in the $T_{1\rho}$ determinations.

The measurement of the 90° pulse is important as this gives the precessional frequency of the spin-lock field. The measurement is normally carried out on the reference sample (adamantane) by finding the two minima of one of the resonances corresponding to the 180° and 360° pulses. The 90° pulse (D_1) is, therefore, half the difference and $\omega_1 = 1/(4 \times D_1)$. This is then multiplied by 2π to convert it to radians s^{-1}. The value of ω_1 is, therefore, crucial to the measurement of activation parameters using $T_{1\rho}$ measurements.

All spinning side bands shown in the spectra are marked thus: ✳

2.3 Synthesis of 1,1-bis(hydroxymethyl)cyclopentane (BHMCP)[21]

(a) 1,1-bisethoxycarbonylcyclopentane

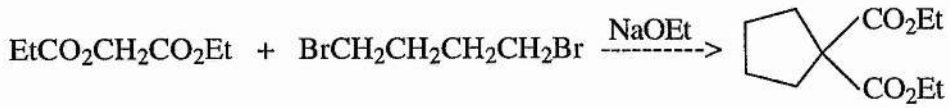

A 1l. three necked flask was set up with a dropping funnel, condenser with a $CaCl_2$ drying tube and a thermometer. Diethylmalonate (40.00 g, 0.25 moles) and 1,4-dibromobutane (56.14 g, 0.25 moles) were added and the mixture heated to *ca* 50 °C with stirring. A solution of Na (11.50 g, 0.5 moles) in ethanol (200 cm^3) was added slowly, temperature kept at about 60-65 °C with gentle heating. The mixture was left over the weekend with stirring and when tested was neutral and so further heating was not necessary. Water (450 cm^3) was added to dissolve the NaBr then the ethanol was removed by distillation. The product was then recovered by steam distillation with a little liquid being left in the flask probably being the polymerisation product. The ester layer was then separated off before the water layer was extracted with ether (250 cm^3). The ester and the extracts were combined and dried ($MgSO_4$) before the ether was removed to give the final clear liquid: yield (42.6 g, 79.5%); δ_H (200 MHz; C^2HCl_3) 1.15 (6H, t, 2 x $C\underline{H}_3$), 1.60 (4H, m, 2 x $CCH_2C\underline{H}_2$), 2.10 (4H, m, 2 x $CC\underline{H}_2CH_2$), 4.20 (4H, q, 2 x $C\underline{H}_2CH_3$).

(b) Conversion to BHMCP

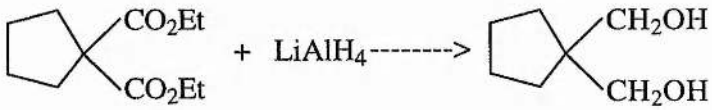

A 1l. three necked flask was set up with a dropping funnel, a double surface condenser with a $CaCl_2$ drying tube and a stopper. Placed in the flask was a solution of $LiAlH_4$ (8.90 g, 0.32 moles) and dry THF (210 cm^3). The ester (37.95 g, 0.18 moles) was then added dropwise to the stirred solution. The reaction mixture was stirred for a further hour at room temperature and then a 50% solution of NaOH (*ca* 50 cm^3) was added cautiously followed by addition of H_2O (*ca* 150 cm^3) until all the inorganic salts had coagulated. The THF layer and two ether washings (2 x 150 cm^3) of the inorganic residue were combined and dried ($MgSO_4$). The solvents were removed to leave an oily liquid which solidified overnight giving a yellow/white crystalline product. The product was recrystallised from petroleum ether to give a white crysatalline solid: yield (14.6 g, 62.4%), m.p. 94-95 °C (lit.,[14] m.p. 95-96

°C); δ_H (200 MHz; C^2HCl_3) 1.40 (4H, m, 2 x $CCH_2C\underline{H}_2$), 1.60 (4H, m, 2 x $CC\underline{H}_2CH_2$), 3.45 (4H, s, 2 x $C\underline{H}_2OH$), 4.90 (2H, s, 2 x OH); δ_C (50.13 MHz; C^2HCl_3), 26.77 (2 x $C\underline{C}H_2CH_2$), 32.87 (2 x $CCH_2\underline{C}H_2$), 50.60 ($\underline{C}(CH_2)_4$), 68.03 (2 x $\underline{C}H_2OH$).

2.4 Deuteriation of 2.3

Into a test tube was added BHMCP (0.42 g, 0.0032 moles) and ^2H_2O (*ca* 5 cm^3). The mixture was stirred overnight and then extracted with ether and dried ($MgSO_4$). The product was a white crystalline solid: yield (0.37 g, 87.5%); m.p. 91-92 °C, ^1H NMR showed the OH resonance had disappeared.

2.5 Synthesis of the bisbenzoate ester derivative of 2.3

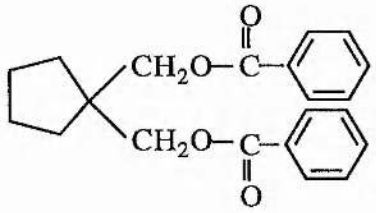

To a 50 cm^3 rb flask was added BHMCP (1.31g, 0.01 moles), 2.5 cm^3 of pyridine and freshly distilled benzoyl chloride (3.0 g, 0.02 moles). The mixture was then refluxed for an hour before a 5% solution of $NaHCO_3$ (12 cm^3) was added. The mixture was then extracted with ether and dried ($MgSO_4$). The resulting oily liquid was analysed by proton nmr to reveal that it was a mixture of the mono and di benzoate derivatives with perhaps a little starting material.

2.6 Synthesis of the bis (p-nitrobenzoate ester) derivative of 2.3

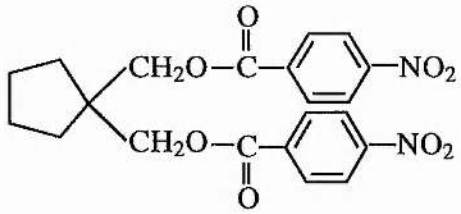

The p-nitrobenzoyl chloride was prepared freshly from p-nitrobenzoic acid and

thionyl chloride. The p-nitrobenzoyl chloride (1.80 g, 0.10 moles) was reacted with BHMCP (3.00 g, 0.023 moles) as in **2.3**. The product was recrystallised from petroleum ether 60/80 to give a pale yellow crystalline solid: yield (5.3 g, 53.6%), m.p. 161-162 °C (lit.,[14] m.p. 163 °C). Found: C, 59.22; H, 4.72; N, 6.56. Calc. for $C_{21}H_{20}N_2O_8$: C, 58.90; H, 4.68; N, 6.5%; δ_H (200 MHz; C^2HCl_3) 1.32 (4H, m, 2 x $CCH_2C\underline{H}_2$), 1.61 (4H, m, 2 x $CC\underline{H}_2CH_2$), 4.39 (4H, s, 2 x $C\underline{H}_2O$), 8.32 (8 H, AB_q, aromatic); δ_C (50.13 MHz; C^2HCl_3), 33.06 (2 x $C\underline{C}H_2CH_2$), 25.77 (2 x $CCH_2\underline{C}H_2$), 47.12 ($\underline{C}(CH_2)_4$), 124.16 (2 x $CH\underline{C}HCNO_2$, aromatic) and 131.20 (2 x $CH\underline{C}HCCO_2$, aromatic), the 3 other quaternaries did not come up, but were confirmed in the ^{13}C solid state NMR spectra; 134.3 ($CO_2\underline{C}(CH)_2$), 152.4 (C-NO_2) and 165.2 (CO_2).

2.7 Synthesis of the bis-methanesulphonate derivative of 2.3[22]

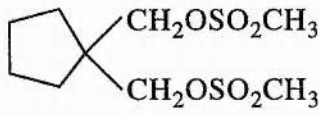

A solution of BHMCP (1.30 g, 0.01 moles) and pyridine (5 cm^3) in a 50 cm^3 rb flask was stirred at 5 °C and then methanesulphonylchloride was added over 30 min. with the temperature maintained at 5 °C. After *ca* 3 h. stirring at 5 °C ice water (20 cm^3) was poured onto the reaction mixture and the it was acidified with 5 cm^3 of dilute HCl. The product was filtered off and washed with a little water before being recrystallsed from water to give a white crystalline solid: yield (2.77 g, 96.9%), m.p. 91-92 °C (lit.,[15] m.p. 90-91 °C). Found C, 37.39; H, 6.36. Calc. for $C_9H_{18}O_6S_2$ C, 37.75; H, 6.34%; δ_H (200 MHz; C^2HCl_3) 1.55 (4H, m, 2 x $CCH_2C\underline{H}_2$), 1.70 (4H, m, 2 x $CC\underline{H}_2CH_2$), 4.10 (4H, s, 2 x $C\underline{H}_2O$), 3.05 (2 x CH_3); δ_C (50.13 MHz; C^2HCl_3), 33.06 (2 x $C\underline{C}H_2CH_2$), 25.48 (2 x $CCH_2\underline{C}H_2$), 37.67 (2 x CH_3), 46.76 ($\underline{C}(CH_2)_4$), 72.00 (CH_2O).

2.8 Synthesis of p-toluenesulphonate derivative of 2.3

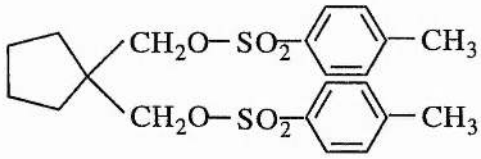

BHMCP (0.59 g, 4.56 mmol) and p-toluenesulphonylchloride (1.74 g, 4.56

mmol) were added to pyridine (10 cm^3) and stirred at 0 °C for 30 min. in an rb flask (25 cm^3). Pyridine hydrochloride came out of solution and then a 5% solution of $NaHCO_3$ (10 cm^3) was added. The mixture was extracted with diethyl ether (2 x 30 cm^3) and the combined extracts were then dried ($MgSO_4$). The solvent was removed under reduced pressure to give white crystals which were recrytallised from ethanol to give: yield (1.75 g, 86.6%); m.p. 111-112 °C (lit.,[23] 113 °C); δ_H (200 MHz; C^2HCl_3) 1.40 (4H, m, 2 x $CCH_2C\underline{H}_2$), 1.55 (4H, m, 2 x $CC\underline{H}_2CH_2$), 2.47 (6H, s, 2 x CH_3), 3.80 (4H, s, 2 x $C\underline{H}_2O$), 3.05 (2 x CH_3) 7.36 and 7.75 (8H, m, aromatic); δ_C (50.13 MHz; C^2HCl_3), 22.17 (2 x CH_3), 25.36 (2 x $CCH_2\underline{C}H_2$), 32.30 (2 x $C\underline{C}H_2CH_2$), 46.74 ($\underline{C}(CH_2)_4$), 72.42 (CH_2O), 128.58 (4 x CH, aromatic), 130.44 ($\underline{C}CH_3$, aromatic), 145.83 (CS, aromatic).

2.9 Synthesis of carbamate derivative of 2.3

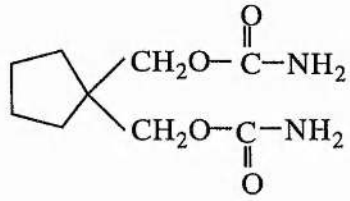

A solution of BHMCP (0.76 g, 6 mmol) and quinoline (1.50 g, 0.012 moles) and ether (30 cm^3) was added to phosgene (6.2 cm^3, 0.12 moles of a 20% solution) in a rb flask (50 cm^3). The mixture was stirred at room temperature for 6 h.. The mixture was then washed with dilute hydrochloric acid (30 cm^3), water (30 cm^3), sodium carbonate (30 cm^3 of a 10% solution) and finally with water (30 cm^3). The ether was removed under reduced pressure leaving a pale yellow liquid. The liquid (*ca* 6 cm^3) was added to ice cold aqueous ammonia (33% w/w) with rapid stirring. The product was then filtered off and washed with a little cold water before being recrystallised from ethanol/water to give a white crystalline solid: yield (0.93 g, 71.7%), m.p. 164-165 °C (lit.,[24] 167 °C); δ_H (200 MHz; C^2HCl_3) 1.40 (4H, m, 2 x $CCH_2C\underline{H}_2$), 1.62 (4H, m, 2 x $CC\underline{H}_2CH_2$), 3.92 (4H, s, 2 x CH_20), 5.15 (4H, s, NH_2).

2.10 Synthesis of 2,4-dioxaspiro[5.4]decane

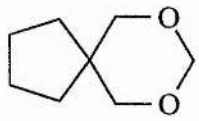

BHMCP (5.20 g, 0.04 moles) and p-formaldehyde (1.16 g, 0.04 moles of CH_2O-), p-toluenesulphonic acid (*ca* 0.1 g) and benzene (100 cm^3) were added to a rb flask (250 cm^3) and refluxed under Dean/Stark conditions 6h.. The reaction mixture was washed with dilute sodium hydroxide (50 cm^3 of a 10% solution) and with water (2 x 50 cm^3) and dried ($MgSO_4$) before the solvent was removed under reduced pressure to give a colurless liquid: yield (0.95 g, 16.7%); b.p. 58-60 °C 35 mmHg; ν_{max} (cm^{-1}) 2953 & 2858 (CH_2), 2764 (O-CH_2-O) 1455 (CH_2) and 1122 & 1077 (C-O); δ_H (200 MHz; C^2HCl_3) 1.43-1.73 (8H, m, CC$\underline{H}_2$C$\underline{H}_2$), 3.60 (4H, s, 2 x C$\underline{H}_2$O), 4.85 (2H, s, OC$\underline{H}_2$O); δ_C (50.13 MHz; C^2HCl_3), 24.97 (2 x CC$H_2\underline{C}H_2$), 33.51 (2 x C$\underline{C}H_2CH_2$), 75.95 (2 x CH_2O), 94.01 (OCH_2O); *m/z* (EI) 142 (1.4%, M^+), 95 (16, $[C_7H_{11}]^+$) and 82 (100, $[C_6H_{10}]^+$).

2.11 Synthesis of 3,3-diethyl-2,4-dioxaspiro[5.4]decane

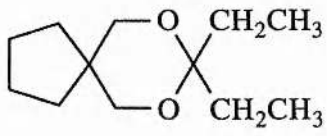

This compound was prepared in an identical way as (2.10) using BHMCP (2.6 g, 0.02 moles), pentan-3-one (1.7 g, 0.02 moles) and benzene (50 cm^3)to give a colourless liquid: yield (1.25 g, 31.6%), b.p. 88-90 °C / 2 mmHg; ν_{max} (cm^{-1}) 2950 & 2859 (CH_2, CH_3), 1462 (CH_2), 1378 (CH_3) and 1117 & 1084 (C-O); δ_H (200 MHz; C^2HCl_3) 0.90 (6H, t, 2 x CH_3), 1.43-1.66 (8H, m, CC$\underline{H}_2$C$\underline{H}_2$), 1.73 (4H, q, 2 x CH_2), 3.58 (4H, s, 2 x C$\underline{H}_2$O); δ_C (50.13 MHz; C^2HCl_3), 7.52 (2 x $CH_2\underline{C}H_3$), 24.93 (2 x $CCH_2\underline{C}H_2$), 25.93 (2 x $\underline{C}H_2CH_3$), 33.50 (2 x C$\underline{C}H_2CH_2$), 41.63 ($\underline{C}(CH_2)_4$), 68.83 (2 x CH_2O), 100.71 (OCH_2O); *m/z* (EI) 199 (1.0%, $[M + H]^+$), 169 (82.4, $[M - Et]^+$), 95 (100, $[C_7H_{11}]^+$) and 45 (9.5, $[EtO]^+$).

2.12 Synthesis of 3,3-dipropyl-2,4-dioxaspiro[5.4]decane

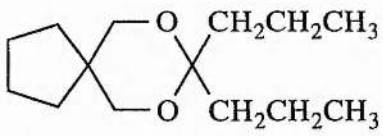

This compound was prepared in an identical way as (2.10) using BHMCP (2.6 g, 0.02 moles), heptan-4-one (2.28 g, 0.02 moles) and benzene (50 cm^3) to give a colourless liquid: yield (1.86 g, 41.2%); b.p. 100-110 °C / 2mmHg; ν_{max} (cm^{-1})

2958 & 2871 (CH_2, CH_3), 1454 & 1459 (CH_2), 1378 (CH_3) and 1119 & 1086 (C-O); δ_H (200 MHz; C^2HCl_3) 0.91 (6H, t, 2 x CH_3), 1.24-1.73 (16H, m, $CC\underline{H}_2C\underline{H}_2$ and $C\underline{H}_2C\underline{H}_2CH_3$), 3.55 (4H, s, 2 x $C\underline{H}_2O$); δ_C (50.13 MHz; C^2HCl_3), 14.43 (2 x $CH_2\underline{C}H_3$), 16.52 ($CH_2\underline{C}H_2CH_3$), 24.93 (2 x $CCH_2\underline{C}H_2$), 33.50 (2 x $C\underline{C}H_2CH_2$), 36.20 ($CH_2\underline{C}H_2CH_3$), 41.62 ($\underline{C}(CH_2)_4$), 68.86 (2 x CH_2O), 100.24 (OCH_2O);*m/z* (CI) 227 (16.2%, $[M + H]^+$), 141 (84, $[M + H - 2Pr]^+$) and 95 (100, $[C_7H_{11}]^+$).

2.13 Synthesis of 1,4-dioxaspiro[4.4]nonane

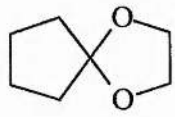

This compound was prepared in an identical way as (2.10) using cyclopentanone (8.41 g, 0.1 moles), ethylene glycol (6.20 g, 0.1 moles) and benzene (100 cm^3) to give a colourless liquid: yield (1.41 g, 0.1%), b.p. 56-60 °C / 40 mmHg, (lit.,[25] 54-55 °C / 35 mmHg); δ_H (200 MHz; C^2HCl_3) 1.60-1.75 (8H, m, $CC\underline{H}_2C\underline{H}_2$), 3.90 (4H, s, 2 x CH_2O); δ_C (50.13 MHz; C^2HCl_3), 23.51 (2 x $CCH_2\underline{C}H_2$), 35.87 (2 x $C\underline{C}H_2CH_2$), 64.17 (2 x CH_2O), 118.47 ($O_2\underline{C}(CH_2)_2$).

2.14 Synthesis of 2-chloromethyl-1,4-dioxaspiro[4.4]nonane

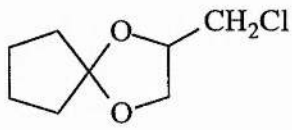

This compound was prepared in an identical way as (2.10) using cyclopentanone (4.21 g, 0.05 moles) and 3-chloropropane-1,2-diol (5.53 g, 0.05 moles) to give a colourless liquid which was distilled: yield (2.45g, 27.74 %); b.p. 66-69 °C / 1 mmHg; *m/z* (Found: M^+, 176.0612. Requires for $C_8H_{13}O_2Cl$; *m/z* 176.0604); ν_{max} (cm^{-1}) 2961 & 2876 (CH_2), 1454 & 1434, 1474 (CH_2), 1170 - 1050 (C-O) and 746 (C-Cl); δ_H (200 MHz; C^2HCl_3) 1.55-2.00 (8H, m, $CC\underline{H}_2C\underline{H}_2$), 3.38-3.68 (2H, dd, CH_2Cl), 3.81-4.14 (2H, dd, $CHC\underline{H}_2O$), 4.18-4.38 (1H, m, CH); δ_C (50.13 MHz; C^2HCl_3), 23.35 and 23.62 (2 x $CCH_2\underline{C}H_2$), 36.14 and 36.70 (2 x $C\underline{C}H_2CH_2$), 44.41 (CH_2Cl), 67.76 (CH_2O), 75.04 (CH), 119.95 ($O_2\underline{C}(CH_2)_2$); *m/z* (EI) 178, (7.0%, $M^+[^{37}Cl]$), 176 (21.4, $M^+[^{35}Cl]$), 149 (73.2, $[C_7H_{12}{}^{37}ClO]^+$), 147 (100, $[C_7H_{12}{}^{35}ClO]^+$), 127 (16.3, $[C_7H_{11}O_2]^+$), 55 (68.3, $[C_4H_7]^+$)

2.15 Synthesis of 3-bromo-3-nitro-1,5-dioxaspiro[5.4]decane

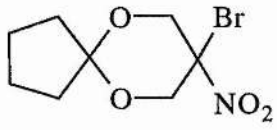

This compound was prepared in an identical way as (2.10) using cyclopentanone (2.10 g 0.025 moles) and 2-bromo-2-nitro-propane-1,3-diol (5 g, 0.025 moles) to give a dark brown solid which was recrystallised from ethanol to give a white solid m.p. 76-80 °C. Recrystallised again from ethanol/water mixture to give a white solid: yield (3.62 g, 55.02%); m.p. 80-82 °C; found: C, 36.11; H, 4.55; N, 5.26. Requires for $C_8H_{12}BrNO_2$: C, 36.34;H, 4.68; N, 5.20%; ν_{max} (Nujol)/cm^{-1} 1553 & 1377 (C-NO_2) and 1051 (C-O); δ_H (200 MHz; C^2HCl_3) 1.50-2.15 (8H, m, $CC\underline{H}_2C\underline{H}_2$), 4.22 and 4.84 (4H, dd, CH_2O); δ_C (50.13 MHz; C^2HCl_3), 22.15 and 24.15 (2 x $CCH_2\underline{C}H_2$), 30.21 and 38.76 (2 x $C\underline{C}H_2CH_2$), 67.63 (CH_2O), 81.66 ($(CH_2)\underline{C}BrNO_2$), 111.37 ($O_2\underline{C}(CH_2)_2$).

2.16 Synthesis of 4,4-dimethyl-*trans*-1,2-cyclopentanediol

(a) Preperation of the piperidone

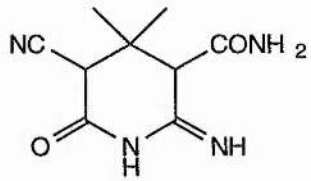

To a standard flask (250 cm^3) was added cyanoacetamide (29.88 g, 0.36 moles), water (120 cm^3), acetone (14.94 g, 0.26 moles) and piperidine (6 cm^3). The mixture was stirred and shaken vigorously until the cyanoacetamide had dissolved. The flask was stoppered and left overnight (product started to crystallise after *ca* 2 hours). The reaction mixture was filtered and washed with cold water (*ca* 100cm3) and dried in a desiccater. The filtrate was collected and put on an ice/water bath whereupon further product crystallised. This was filtered after 1h. and added to the main product in the desiccater and gave a white powdery solid: yield (24.54 g, 66.29%), m.p. 202-205 °C, (lit.,[26] 234 °C). The product, however appeared pure on t.l.c. so the next step was carried out.

(b) Conversion to ßß-dimethylglutaric acid

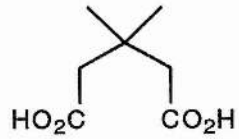

Piperidone (24.54g, 0.11 moles) and conc. H_2SO_4 (36.81 g, 0.38 moles) added to a 3 necked flask (250 cm^3) which was fitted with a thermometer, dropping funnel (100 cm^3) and a condenser. The mixture was heated to 180 °C and water (7.0 cm^3) added which produced vigorous evolution of CO_2 and a drop in temperature to 160 °C. After 1h. the mixture was not a solution as expected, but addition of remaining water (6 cm^3) was carried out slowly resulting in temperature falling to 130 °C. There remained a white precipitate which should be the di-imide,[19] which should dissolve at 150°C if the acid is strong enough. Further heated for 2 h., temperature increased to 150°C, but still the di-imide did not completely disslove. On addition of more water (2 cm^3), T -> 142 °C then back to 147 °C after 1h.. Mixture heated for further 3 h. at 150 °C, but the di-imide did not dissolve completely. Water (500 cm^3) added and the mixture filtered before extaction with ether (2 x 200 cm^3). The ether was dried (Na_2SO_4) and the ether removed under reduced pressure to give a white solid: yield (9.23 g, 51.5%), m.p. 95-97 °C, (lit.,[19] 101 °C).

(c) Esterification of ßß-dimethylglutaric acid

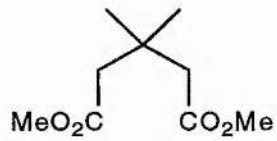

To a rb flask (250 cm^3) fitted with a condenser was added the acid (9.23 g, 0.058 moles) and methanol (100 cm^3) and conc. H_2SO_4 (1 cm^3). The mixture was refluxed for 4 h. and then the methanol was removed under reduced pressure. A 5% solution of $NaHCO_3$ (50 cm^3) was added and then the mixture was extracted with ether (2 x 35 cm^3), which was then removed under reduced pressure and dried (Na_2SO_4). The ester was then distilled to give a clear liquid (9.70 g, 80.7%), b.p. 116-119 °C / 30 mmHg (lit.,[27] 103-104 °C / 15 mmHg).

(d) Preparation of 4,4-dimethylglutaroin

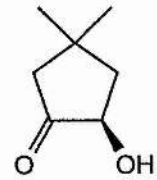

To a flame dried 3-necked flask (250 cm^3) was placed dry ether (50 cm^3) and then ammonia was condensed (*ca* 120 cm^3) using a dry ice/acetone bath. To the solution was added sodium (5.20 g, 0.23 moles) in pieces over 10 min., and then a solution of the ester (9.70g, 0.052 moles) in ether (50 cm^3) was added over 25 min.. The mixture was allowed to warm to *ca* -33 °C and stirred for 1 h.. The mixture was a thick blue sludge with some yellow solid on the bottom of the flask. The mixture was allowed to warm to RT and to the resulting solid was added ether (50 cm^3) and then it was left overnight for the ammonia to completely evaporate. A solution of methanol (20 cm^3) and ether (40 cm^3) was added slowly and produced vigorous bubbling and gave an orange/yellow solution. The mixture was acidified with 3M HCl (*ca* 220 cm^3) and the mixture became pale lemon yellow in colour. The ether layer was then separated and the aqueous layer extracted with ether (3 x 30 cm^3). The ether layers were combined and dried (Na_2SO_4) before the ether was removed under reduced pressure to give a yellow liquid: yield (2.71 g, 41.06%), b.p. 68-72 °C / 3 mmHg, (lit.,[28] 68-70 / 2 mmHg).

(e) Reduction of 4,4-dimethylglutaroin to give the diol

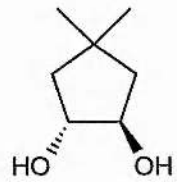

Into a 3 necked flask (100 cm^3) fitted with a condenser and a dropping funnel was added a solution of $NaBH_4$ (0.70 g, 0.018 moles) in absolute ethanol (20 cm^3). A solution of glutaroin (2.71 g, 0.027 moles) in absolute ethanol (5 cm^3) was added over 20 min. with stirring and the mixture was refluxed for 3 h.. After cooling a solution of 3M H_2SO_4 (30 cm^3) was added and then the ethanol was removed under reduced pressure. The solution was then extacted with ether (4 x 20 cm^3) and dried (Na_2SO_4). The ether was removed under reduced pressure to give a yellow/orange liquid which solidified on cooling. The solid was recrystallised from benzene to give white crystals: yield (1.21 g, 44.00%), m.p. 94-95 °C, (lit.,[21] 96-97 °C); δ_H (200

MHz; C^2HCl_3) 1.09 (6H, s, 2 x CH_3), 1.42 and 1.91 (4H, 2 x dd, CH_2), 2.10 (2H, s, OH), 4.08 (2H, m, CH); δ_C (50.13 MHz; C^2HCl_3), 31.98 (2 x CH_3), 33.72 (quat. C), 45.96 (CH_2), 78.85 (CH).

2.17 Deuteriation of alcohol groups of 2.16

To a rb flask (50cm^3) was added a solution of 4,4-dimethyl-*trans*-cyclopentane-1,2-diol (0.4 g, 0.0031 moles) and ^2H_2O (10 cm^3). The mixture was stirred for 1h. and then the solution was placed in a desiccater at reduced pressure. A white solid was recovered and the proton nmr shows no OH resonance: yield (0.34 g, 84%), m.p. 94-95 °C.

2.18 Synthesis of 1,1-diethylcyclopentane

(a) Preparation of 1-ethylcyclopentanol

A 3 necked flask (500 cm^3) was fitted with a condenser with a drying tube, a dropping funnel with a drying tube and a stopper. Mg (14.09 g, 0.58 moles) and dry ether (100 cm^3) were added and then a solution of ethyl bromide (63.22 g, 0.58 moles) and dry ether (100 cm^3) was added in order to make the Grignard reagent. After 15 min. stirring, a solution of cyclopentanone (44.00 g, 0.52 moles) in dry ether (150 cm^3) was added dropwise keeping the reaction gently refluxing. The solution was stirred and gently heated for a further 20 min. after addition was complete and then allowed to cool. It was then added to a saturated solution of NH_4Cl (500 cm^3) and the ether layer separated. The water layer was then extracted with ether (2 x 100 cm^3) and then the ether layers were washed with saturated NH_4Cl solution (300 cm^3) and water (300 cm^3) before being dried ($MgSO_4$). The ether was removed under reduced pressure giving a clear liquid: crude yield (51.03 g, 86.1%).

(b) Conversion to 1-ethyl-1-chlorocyclopentane

The alcohol (51.03 g, 0.45 moles) was added to a rb flask (500 cm^3) which contained hexane (80 cm^3) and conc. HCl (100 cm^3) at 0 °C. The mixture was stirred at 0 °C for 18 h. and then the organic layer was separated and washed consecutively with water (100 cm^3), 5% $NaHCO_3$ solution (100 cm^3) and water (100 cm^3). The organic layer was dried ($MgSO_4$) and then the hexane was removed under reduced

pressure to give a clear liquid: crude yield (34.50 g, 50.1%), b.p. 45-50 °C / 25 mmHg, (lit.,[29] 53 °C / 35 mmHg); δ_H (200 MHz; C^2HCl_3) 0.90 (3H, t, CH_3), 1.4 -2.0 (10H, b, 5 x CH_2); δ_C (50.13 MHz; C^2HCl_3), 10.75 (CH_3), 23.64 (2 x $\underline{C}H_2CH_2C$) 36.68 (2 x $CH_2\underline{C}H_2C$) and 84.72 (quat. C).

(c) Reaction of chloride with ethyl Grignard reagent

A 3 necked flask (500 cm^3) was fitted with a condenser with a drying tube, a dropping funnel with a drying tube and a stopper. Mg (8.02 g, 0.33 moles) and dry ether (50 cm^3) were added and then the ethyl bromide (38.12 g, 0.35 moles) was added to make the Grignard reagent. To the mixture was added a solution of 1-chloro-1-ethyl-cyclopentane (34.50g, 0.26 moles) in dry ether (50 cm^3) over 1.5 h. The reaction was refluxed gently for 10 h. and then the ether removed by distillation and replaced by toluene (250 cm^3) for a further 8 h. refluxing. The toluene was removed under reduced pressure and the resulting residue of liquid and solid was refluxed with Na (2.4 g, 0.10 moles) for 1h.. Attempted distillation gave a mixture with no sign of the desired product.

The toluene, which had been distilled off earlier was checked for any sign of the product. After distillation a clear liquid was obtained: yield (1.03 g, 3.1%), b.p. 35-40 °C / 25mmHg (lit.,[22] 149 °C / 731 mmHg), δ_H (200 MHz; C^2HCl_3) 0.82 (6H, t, 2 x CH_3), 1.31 (4H, q, 2 x $C\underline{H}_2CH_3$), 1.56 (8H, m, 2 x $C\underline{H}_2C\underline{H}_2$); δ_C (50.13 MHz; C^2HCl_3), 9.01 (2 x CH_3), 24.91 (2 x $C\underline{H}_2CH_3$), 30.24 (2 x $CCH_2\underline{C}H_2$), 36.98 (2 x $C\underline{C}H_2CH_2$) and 45.21 (quat. C).

2.19 Synthesis of perdeuterio 3,3-diethylpentane[30]

(a) Preparation of ethylbromide ($^2H_5$)

In a 3 necked flask (250 cm^3) fitted with a stillhead and condenser, dropping funnel and stopper was placed 48% HBr (65.4 cm^3) and to it was added conc. H_2SO_4 (15.1 cm^3) in portions with shaking. After *ca* 30 min. the mixture had cooled suffiently to add ethanol ($^2H_6$) (25 g, 0.48 moles). The receiver flask on the condenser was placed in an ice bath to prevent loss of EtBr due to evaporation. To the mixture was added conc. H_2SO_4 (25.4 cm^3) very slowly and the EtBr was distilled over 3 h.. The EtBr as then washed successively with an equal volume of conc. HCl, water, 5% $NaHCO_3$ solution and water before drying ($CaCl_2$). It was then distilled at atmospheric pressure to give a clear liquid; yield (40.35 g, 73.7%), b.p. 38 °C; $\delta 2_H$

(46.1 MHz; $CHCl_3$) 1.64 (3H, s, C^2H_3), 3.41 (2H, s, C^2H_2).

(b) (i) Preparation of 3-ethyl-3-chloropentane ($^2H_{15}$)

In a 3-necked flask (500 cm^3) fitted with a condenser fitted with a drying tube, dropping funnel fitted with a drying tube and stopper was placed Mg (5.25 g, 0.22 moles) and dry ether (100 cm^3). EtBr ($^2H_5$) (25.00 g, 0.22 moles) in dry ether (100 cm^3) was added to make the Grignard reagent. A solution of $(EtO)_2CO$ (8.26 g, 0.07 moles) in dry ether (100 cm^3) was added over 40 min. to keep the reaction gently refluxing. The mixture was then stirred and heated to reflux the ether gently for a further 20 min.. The reaction mixture was added to a saturated solution of NH_4Cl (200 cm^3) and then the ether layer was separated and the salt solution was extracted with ether (2 x 50 cm^3). The ether layers were combined and washed succesively with water (100 cm^3), a saturated solution of NH_4Cl (100 cm^3) and water (100 cm^3) before drying ($MgSO_4$). The ether was then removed under reduced pressure to give a clear liquid. This was then added straight to a rb flask (500 cm^3) containing pentane (70 cm^3) and conc. HCl (100 cm^3) and stirred vigorously for 12 hours in the stoppered flask. The organic layer was separated and washed succesively with water (100 cm^3), 5% $NaHCO_3$ solution (50 cm^3) and water (100 cm^3) before the pentane was removed under reduced pressure to give a clear liquid: yield (4.97 g, 47.5%), b.p. 90-95 °C / 22 mmHg, (lit.,[31] 71.2 °C / 16 mmHg); δ_{2H} (46.1 MHz; $CHCl_3$) 0.92 (9^2H, s, C^2H_3), 1.74 (6^2H, s, C^2H_2).

(b) (ii) Repeat preparation of 3-ethyl-3-chloropentane ($^2H_{15}$)

Same procedure as (i) by first preparing Grignard reagent, Mg (6.3 g) EtBr (25.68 g) and then reacting 90 cm^3 of a 1.43 M solution in Et_2O (0.13 moles) with $(EtO)_2CO$ (0.04 moles) to give: yield (5.04 g, 84%). This was then added to the product form (i) for the next step.

The last two steps were carried out by **Dr. D. Foster** because of his experience in the synthesis and use of Et_2Zn. Much gratitude is expressed to Doug for the time and effort to prepare such a pure product. The method is included here for completeness.

(c) Preparation of Et_2Zn ($^2H_5$)

To a 3 necked flask (250 cm3) equipped with dropping funnel, reflux condenser and flee was added ZnCl2 (5.80 g, 0.043 moles) and then flushed thoroughly with Argon. Ether (50 cm^3) was added and stirred to dissolve $ZnCl_2$.

A 1.43M solution of EtMgBr in ether (60 cm3, 0.086 moles) was added dropwise to colourless $ZnCl_2$ solution over 15-20 min.. There was an almost immediate formation of white precipitate. The reaction mixture was refluxed over an oil bath for 15 min.. The volatiles were removed the next day using trap to trap *in vacuo*. The product was distilled at atmespheric pressure with oil bath kept at 85 °C. Last traces of ether removed by warming column with hair dryer. The product was collected by trap to trap *in vacuo*: yield (5.55 g, 97.5%)

(d) Reaction of 3-ethyl-3-chloropentane with diethyl zinc ($^2H_5$)

To a 3 necked flask (500 cm^3) fitted with a reflux condenser, dropping funnel and a large flee was added $ZnCl_2$ (*ca* 100mg) and then the system was thoroughly degassed. Et_3CCl ($^2H_{15}$) (10.01 g, 0.67 moles) and CH_2Cl_2 (100 cm^3) were added and the mixture cooled to *ca* -25 °C with an acetone and dry ice bath. Et_2Zn ($^2H_{10}$) (5.53 g, 0.41 moles) was run into the flask via small bore connector but no immediate reaction observed. The mixture was warmed to +8 °C and when it suddenly reacted very exothermically. The mixture was refluxed with heat gun to ensure complete reaction. The reaction mixture was cooled and then hydrolysed with dil. HCl (*ca* 50 cm^3). The mixture was then separated and then washed with 5% $NaHCO_3$ solution (50 cm^3) and water (50 cm^3) and dried (Na_2SO_4). The CH_2Cl_2 was removed by distillation with the oil bath at *ca* 100 °C. This left *ca* 10 cm^3 of a pale yellow liquid which when collected by trap to trap *in vacuo* gave a clear colourless liquid: yield (9.72 g). Analysis by G.C. showed a small trace of CH_2Cl_2 and then:

side products	27%
product	64%
unreacted chloride	9%

The unreacted chloride was then removed by reaction with more Et_2Zn ($^2H_{10}$).

(d) (ii) Further reaction of 3-ethyl-3-chloropentane with diethyl zinc ($^2H_5$)

The reaction was carried out as in **(i)** using Et_2Zn (*ca* 1.1 g) and a solution of crude product in CH_2Cl_2 (20 cm^3). The reaction was refluxed for 2-3 h. to give a yellow solution and then hydrolysed with dil. HCl (16 cm^3). Resulting G.C. analysis showed unreacted chloride was gone and one of the other impurites was greatly reduced. The mixture was then distilled very carefully many times to get rid of impurities using a long vigreux column. The resulting pure product was observed by G.C. and dried (CaH_2): yield (1.86 g, 18.7%), b.p. 140 °C (lit.[30] 145-147 °C)

2.21 Synthesis of mono deuterio 3,3-diethylpentane

(a) Preparation of labelled ethanol

Acetaldehyde was added to a rb flask (50 cm^3) fitted with a stillhead and a condenser fitted with a reciever adaptor leading to a cardice condenser with a rb flask (50 cm^3) attached and immersed in an ice bath. The acetaldehyde was distilled to get it dry. The ether used subsequently was dried over sodium and $LiAlH_4$ added to it and then distilled. A 3 necked flask was fitted with a dropping funnel, condenser and drying tube and a stopper and a 1M solution in ether of $LiAl^2H_4$ (50 cm^3, 0.05 moles) was added. The acetaldehyde (8.81 g, 0.2 moles) in dry ether (50 cm^3) was added slowly over 2 h. with stirring. The resultant LiAl ethoxide salts were destroyed with a solution of NaOH (8.00 g, 0.20 moles) in 10 cm^3 of water. The mixure was filtered and the inorganic salts washed with ether (50 cm^3). The ether was then distilled off slowly to give a colourless liquid: yield (*ca* 5 g, 50%); $\delta 2_H$ (46.1 MHz; $CHCl_3$) 3.69 (1^2H, s, CH^2H).

(b) Conversion to the monodeuterio ethylbromide

This procedure was identical to **2.19 (a)** using ethanol (*ca* 5 g, 0.11 moles), 48% HBr (30 cm^3), conc. H_2SO_4 (7cm^3 and 11.8 cm^3). The resulting clear liquid, yield (*ca* 7 cm^3) was distilled and dried ($CaCl_2$).

(c) Preparation of labelled 3-ethyl-3-chloropentane

In a 3-necked flask (500 cm^3) fitted with a condenser fitted with a drying tube, dropping funnel fitted with a drying tube and stopper was placed Mg (4.86g, 0.20

moles) and dry ether (100 cm^3). EtBr (*ca* 7 cm^3, 0.09 moles) in dry ether (50 cm^3) was added to make the grignard reagent. A solution of pentan-3-one (11.43 g, 0.13 moles) in dry ether (100 cm^3) was added over 30 min.. The reaction mixture was gently refluxed for a further 20 min. and allowed to cool. The solution was then added to an ice cold saturated solution of NH_4Cl (200 cm^3) and then the ether layer was separated. The salt solution was then washed with ether (2 x 50 cm^3) and the ether layers were combined and washed successively with water (100 cm^3), saturated NH_4Cl solution (100 cm^3) and water (100 cm^3). The ether was dried ($MgSO_4$) and then removed under reduced pressure to give a clear liquid. This was then added straight to a rb flask (500 cm^3) containing pentane (100 cm^3) and conc. HCl (120 cm^3) and stirred vigorously for 12 hours in the stoppered flask. The organic layer was separated and washed succesively with water (120 cm^3), 5% $NaHCO_3$ solution (80 cm^3) and water (120 cm^3) before the pentane was removed under reduced pressure to give a clear liquid: yield (7.45 g, 0.055 moles); $\delta 2_H$ (46.1 MHz, $CHCl_3$) 1.46 (1^2H, s, CH^2H).

(c) Reaction of 3-ethyl-3-chloropentane with diethyl zinc

The reaction was carried out as for 2.19 (d) using Et_3CCl (7.45 g, 0.055 moles) and Et_2Zn (4.27 g, 0.035 moles). The pure product was a clear colourless liquid after distillation using a spinning band micro distillation apparatus: yield (3 cm^3), b.p. 140 - 160°C (lit.,[30] 145-147°C) note b.p. high because a heat gun was used to get all the product over.

Many thanks again to **Dr. D. Foster** for carrying out this last step and obtaining such a pure product.

2.21 Preparation of 4,4-dipropylheptane

(a) Synthesis of 4-propylheptanol

A three-necked flask (1l.) was set up with a dropping funnel with a drying tube, a double surface condenser with a drying tube and a stopper. Magnesium was added (9.60 g, 0.4 moles) and dry ether (200 cm^3) and then a solution of 1-bromopropane (55.35 g, 0.45 moles) in 50 cm^3 of dry ether was added dropwise over 30 minutes. The reaction was initiated by adding a 2 cm^3 of the propyl bromide with stirring before the rest of the solution was added. The reaction mixture was stirred for a

further 30 minutes with gentle heating and allowed to cool. A solution of heptan-4-one (41.12 g, 0.36 moles) in ether (50 cm^3) was added dropwise over 20 minutes and the was reaction stirred for a further hour. The reaction mixture was then washed with 200 cm^3 of saturated ammonium chloride solution which was then washed with 100 $cm^3$of ether. The ether extracts were combined and dried ($MgSO_4$) and then the ether was removed to give the yellow liquid product: yield (52.31 g, 92.0%); δ_H (200 MHz; C^2HCl_3) 0.93 (9H, t, 3 x CH_3), 1.14-1.53 (12H, m, 6 x CH_2), 1.60 (1H, s, OH); δ_C (50.13 MHz; C^2HCl_3), 14.61 (3 x CH_3), 16.64 (3 x $CH_2\underline{C}H_2CH_3$), 41.60 (3 x $\underline{C}H_2CH_2CH_3$), 74.35 (quat. C).

(b) Conversion to the chloride

The alcohol (52.31 g, 0.31 moles) were added to a three-necked flask (250 cm^3) fitted with a condenser and heated to *ca* 70 °C. HCl was then bubbled through the alcohol by the action of conc. sulphuric acid on conc. HCl acid. The HCl was also bubbled through a conc. sulphuric trap to dry the gas evolved. After *ca* 2 hours the mixture was removed and washed with water (100 cm^3) and then $NaHCO_3$ (100 cm^3) before it was distilled to give a clear liquid: yield (23.79g, 40.7%) b.p. 75-80 °C / 20 mmHg (lit.,[32] 54-56 °C / 7 mmHg); δ_H (200 MHz; C^2HCl_3) 0.93 (9H, t, 3 x CH_3), 2.15 (6H, m, 3 x $CH_2C\underline{H}_2CH_3$), 2.42 (6H, t, 3 x $C\underline{H}_2CH_2CH_3$); δ_C (50.13 MHz; C^2HCl_3), 14.07 (3 x CH_3), 17.41 (3 x $CH_2\underline{C}H_2CH_3$), 43.46 (3 x $\underline{C}H_2CH_2CH_3$), 78.11 (quat. C).

(c) Final conversion to the tetrapropyl alkane

A standard Grignard reaction was carried out as in 2.19 (a) using; Mg (6.30 g, 0.26 moles), propylbromide (34.44 g, 0.28 moles) and 4-chloro-4-propyl-heptane (23.79 g, 0.13 moles). The excess Grignard was destroyed with water (200 cm^3) and dilute sulphuric acid (100 cm^3). The ether layer was then removed and washed with water (100 cm^3) and then dried ($MgSO_4$) and finally a small amount of clear liquid was obtained: yield (1.67 g, 6.7%), b.p. 130-133 °C / 30 mmHg (lit.,[24] 60-61 / 6 mmHg); δ_H (200 MHz; C^2HCl_3) 0.86 (12H, t, 4 x CH_3), 1.02-1.28 (16H, m, 8 x CH_2); δ_C (50.13 MHz; C^2HCl_3), 15.50 (4 x CH_3), 16.70 (4 x $CH_2\underline{C}H_2CH_3$), 39.82 (4 x $\underline{C}H_2CH_2CH_3$), 37.80 (quat. C).

2.22 Synthesis of 5,5-dibutylnonane

(a) Preparation of 5-butlynonanol

This compound was prepared using the same method as 2.21 (a) using: Mg (8.51 g, 0.35 moles), BuBr (47.96 g, 0.35 moles), nonan-5-one (42.67 g, 0.30 moles) and ether (350 cm^3). The crude product was a clear liquid: yield (51.38 g, 85.5%);

(b) Conversion to 5-butyl-5-chlorononane

This compound was prepared using the same method as 2.21 (b) using: 5-chlorononanol (51.38 g, 0.26 moles), conc. HCl (150 cm^3) and hexane (100 cm^3). The product was a clear liquid: yield (42.62, 75.9%), b.p. 65-70 °C / 2 mmHg (lit.,[24] 102-103 °C / 7 mmHg);

(c) Reaction of (b) with BuMgBr

This reaction was carried out using the method for 2.21 (c) by first making the butyl Grignard with Mg (6.1 g ,0.25 moles) and BuBr (34.25 g, 0.25 moles) in dry ether (50 cm^3)and reacting it with 5-chloro-5-butylnonane (42.62 g, 0.20 moles) in dry ether (150 cm^3). The product when analysed by ^1H NMR showed no sign of the 5,5-butylnonane only the expected major product of 5-butylnon-4-ene.

2.23 Conversion of tetrabromoerythritol to tetraiodoerythritol

Tetrabromoerythritol (10.00 g, 0.026 moles) and sodium iodide (20.00 g, 0.13 moles) added to butan-2-one (60 cm^3) and refluxed for 48 h. The solvent was then removed under reduced pressure to give a pink solid. The solid was then Soxhlet extracted with ethanol for 24 h. The product was a pink solid: yield 13.85 g, 92.5%); m.p. 233-234 °C (lit.,[33] 233-234 °C)

CHAPTER 3

3. Tetraalkylalkanes

The most commonly studied tetraalkylalkane by solid state NMR is neopentane (2,2-dimethylpropane). The literature shows that neopentane has rotational freedom even at 78 K and that the phase transition at 140 K has no effect on the ^1H linewidth.[34] In a later paper the ^1H T_1 is shown to be dominated by methyl rotation (78-140 K) with an estimated E_a of 12.6 kJ mol^{-1}, although whole molecule tumbling is also significant. After the transition at 140 K cation tumbling governs the ^1H T_1 values (E_a = 4.2 kJ mol^{-1}) until 200 K where self diffusion becomes significant (E_a = 25.1 kJ mol^{-1}). ^1H $T_{1\rho}$ measurements were shown to be useful for measuring molecular motions in asymmetric tetraalkylalkanes.[6] No use of ^{13}C $T_{1\rho}$ measurements on tetraalkylalkanes have been reported in the literature.

3.1 3,3-diethylpentane (tetraethylmethane)

The interest in 3,3-diethylpentane was initiated by Roger Alder of the University of Bristol. In a paper in 1990 titled "The conformational effects of quaternary centres" by Alder *et al.*[35] it was shown by force field calculations that quaternary centres (Q) controlled both C-Q-C-C and Q-C-C-C torsion angles. The work was followed up with low temperature solution NMR studies, but these elucidated little due to freedom of movement. Alder then sent the sample to Dr Riddell for studies in the solid state. The sample is a liquid at room temperature with a melting point of 240 K[36] and so the temperature range for studying this compound in the solid state is limited. The probe set-up using liquid nitrogen as coolant allows a minimum temperature of *ca* 190 K, but even this temperature cannot always be obtained.

The ^{13}C CP/MAS NMR spectrum at 231 K (Fig. 3.1) shows the resonances for the methyls (7.9 ppm), the methylene groups (27.2 ppm) and the quaternary carbon (37.6 ppm). The spectrum at 210 K shows that the methylene signal has vanished and that the other two resonances have broadened. The methylene resonance then reappears when the sample is cooled to 203 K and the other two resonances are also sharpening. These changes are consistent with poor cross polarisation to the methylene carbon and seemed to us to indicate a short value of $T_{1\rho}$ at around 210K. This arises when the rate of molecular motion is similar to the precessional frequency of the spin locking field (*ca* 60 kHz).

Fig. 3.1: ^{13}C CP/MAS NMR spectra of 3,3-diethylpentane

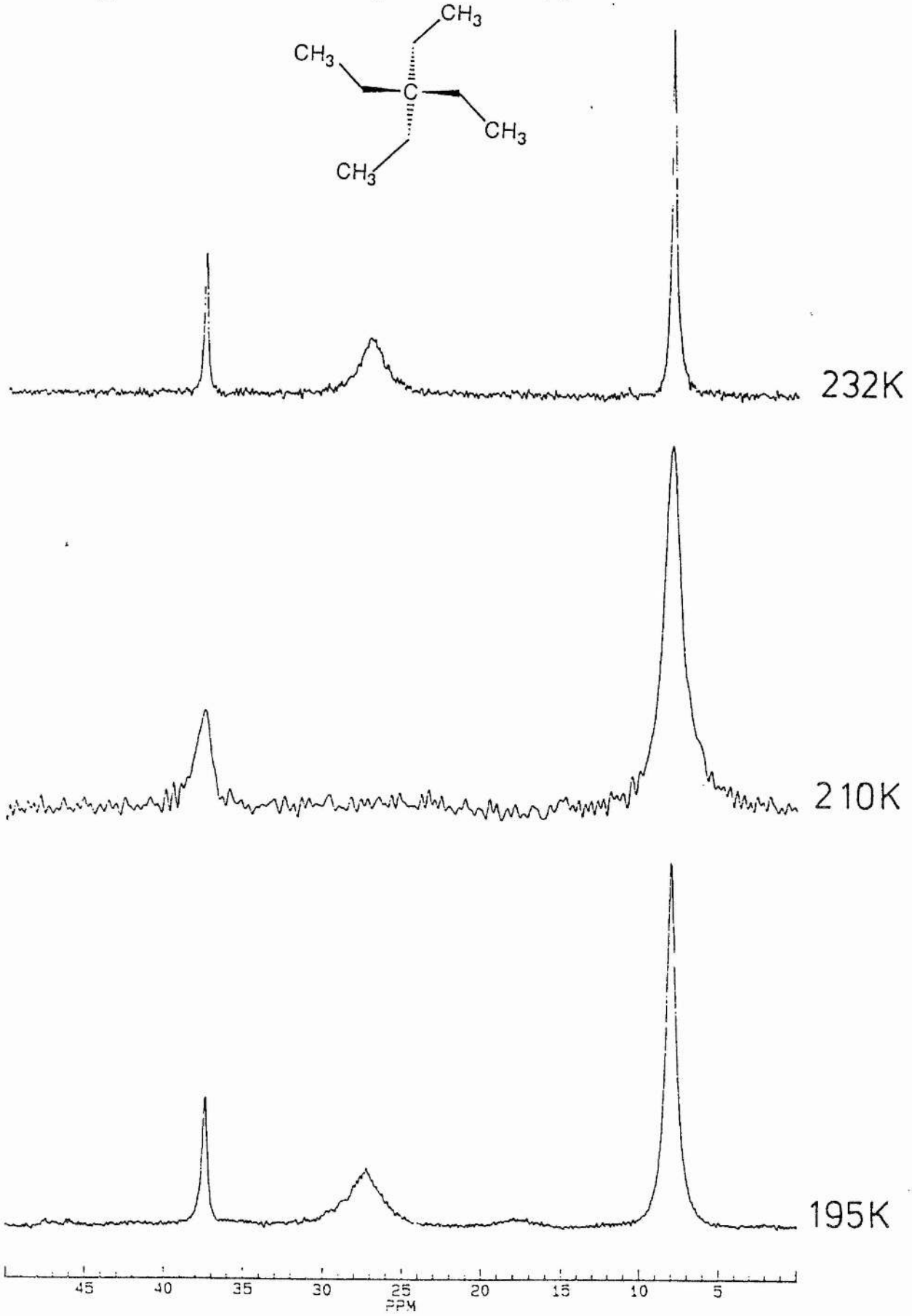

The line broadening of the resonances arises from the associated maximum dipolar broadening because the rate of the molecular process is of the same order as the proton decoupler.

The ^{13}C high powered decoupled (HPDEC) NMR spectra (Fig. 3.2) show that two phases are coexisting. The 'broad' phase seen in the ^{13}C CP/MAS NMR spectra (Fig. 3.1) dominates at low temperature and a 'sharp' phase is more prevalent at higher temperature. The 'sharp' phase visible in the HPDEC spectra (Fig. 3.2) is not seen in the ^{13}C CP/MAS spectra (Fig. 3.1) and, therefore, must arise from molecules with high mobility such that the ^{13}C-^{1}H dipolar interaction is decoupled. This phase persists throughout the temperature range studied although it decreases in intensity at lower temperature. This phase is referred to here as a metastable phase.

Phase changes in solid 3,3-diethylpentane have been investigated by thermodynamicists.[35] There are three stable solid phases: phase I (240K-210K), phase II (210K-208K) and phase III (< 208K). The entropy involved in the solid-solid phase changes (Table 3.1) is very small. Therefore, no large transition to a plastic crystal is evident. The paper makes no reference to a metastable phase which was, although one was found in 3,3-dimethylpentane.

T (K)	ΔS_{tr} (J K^{-1} mol^{-1})
240.1	42.1
210.4	3.85
208.3	2.34

Table 3.1: Data for the phase changes in 3,3-diethylpentane (ΔS_{tr} is the entropy change at the phase transition).[36]

The three solid phases and the liquid show only very small changes in ^{13}C chemical shifts (Table 3.2). The liquid and metastable phases are nearly identical as are phases I and III. No trace of phase II was found as might be expected given its very narrow temperature range. Therefore, the change in crystal structure between phases I and III is not very large as might be expected from the small size of the two ΔS_{tr}.

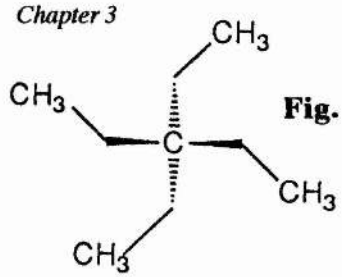

Fig. 3.2 (a): ^{13}C HPDEC NMR spectra of 3,3-diethylpentane

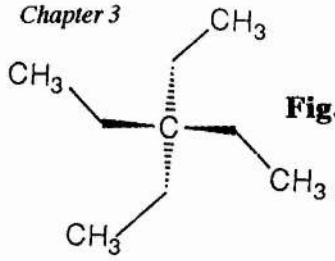

Fig. 3.2 (b): ^{13}C HPDEC NMR spectra of 3,3-diethylpentane

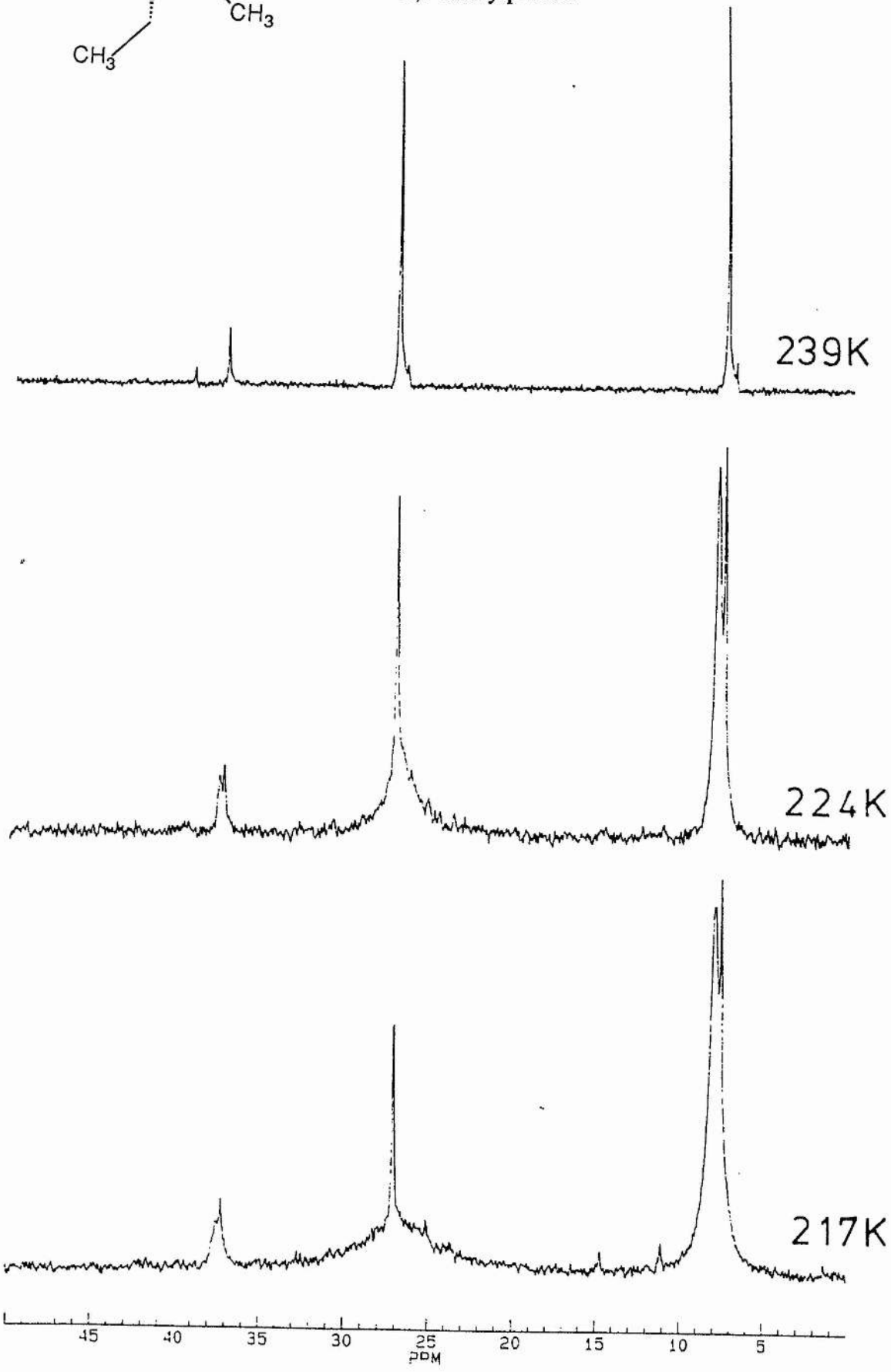

Resonance	phase III	phase I	metastable	liquid
methyl	8.03	7.96	7.46	7.45
methylene	27.2	27.1	27.0	27.0
quaternary	37.4	37.5	37.0	37.1

Table 3.2: ^{13}C chemical shifts (ppm) for the the different phases of 3,3-diethylpentane.

The metastable phase does not show up on the ^{13}C CP/MAS NMR spectra considered until now, but is clearly seen when a HPDEC pulse sequence (Fig. 3.2) is used. It is analogous to the single pulse sequences used in solution NMR, but requires much higher power, both for the pulse and for the decoupler. The 'new' resonances revealed by the HPDEC spectra (Fig. 3.2) have two possible sources. At first it was thought that they could be due to some residual liquid present below the melting point (i.e super-cooled liquid), because in a liquid it is not possible to satisfy the Hartmann-Hahn condition and so to cross polarise. The sample was therefore held at a constant temperature and the intensity of the 'new' resonances measured over time. There did seem to be a temperature dependence, but the resonances stabilised to a constant intensity in under 30 minutes. On cooling the 'new' phase decreased in intensity, but persisted right down to the lowest temperature (198 K) the sample was taken. The 'new' phase also increased in intensity again when the sample was heated and so it appears unlikely that it could be super cooled liquid. Therefore, if this phase is not a liquid it must be liquid like, i.e. have very fast molecular motions. The sharpness of the resonances suggests that this motion helps to average out the ^{1}H-^{13}C dipolar interactions. If the symmetry of the molecule is considered it is apparent there are three possible C_2 axes of the type shown (Fig. 3.3). If we imagine the molecule rotating about all of these axes at once this motion averages to the molecule rotating at the magic angle.

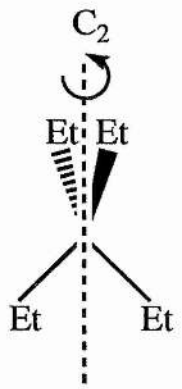

Fig. 3.3: Rotation in 3,3-diethylpentane about one possible C_2 axis.

This would therefore, explain the fact that this phase does not cross polarise. This isotropic motion also sharpens the resonances due to the lack of ^{13}C-^{1}H dipolar interactions. A similar phase is encountered in 2,3-dimethylbutane where two phases coexist and one phase is referred to as a supercooled rotating state.[6]

^{13}C $T_{1\rho}$ DATA

The ^{13}C $T_{1\rho}$ data (Table 3.3) gives the $T_{1\rho}$ plot (Fig. 3.4) which shows a sharp discontinuity at *ca* 210 K presumably as a result of the phase transition. The presence of this change at 210 K gives us a confidence in our temperature calibration of the probe set-up. A similar discontinuity was reported for 2,2-dimethylbutane for ^{1}H $T_{1\rho}$ data after a phase transition.[6] Above 210K phase I should be the stable phase. The lowest values of $T_{1\rho}$ for the three resonances are for the methylene carbon and so the motion is most likely to be about the qaternary to methylene carbon bond. The minimum value for the methylene is *ca* 1 msec (Table 3.3) and this is consistent with the rate of rotation of the ethyl groups being similar to the precessional frequency of ^{13}C in the spin lock field and with the poor cross polarisation. This is shown in the ^{13}C CP/MAS NMR spectra (Fig. 3.1) where the methylene resonance shows the largest effects of $T_{1\rho}$ relaxation and maximum dipolar broadening.

T (K)	C(1)	C(2)	C(3)
202	42.5	17.9	70.4
206	28.2	12.8	49.3
209	22.5	8.38	35.5
213	3.43		5.57
217	4.77	1.08	6.75
220	5.89	1.48	9.02
224	7.46	1.63	11.31
228	9.43	2.04	14.80
231	12.5	2.38	18.98
235	-	2.88	

Table 3.3: ^{13}C $T_{1\rho}$ values (msec) for 3,3-diethylpentane.

Phase III should be the stable phase below 208K. The $T_{1\rho}$ value for the methylene carbon immediately below the discontinuity is 8 msec (Fig. 3.4). This is consistent with the return of the methylene carbon at 203 K in the ^{13}C CP/MAS spectrum (Fig. 3.1). The quaternary and methyl resonances also display sharpening below 208 K but it is not as dramatic as the methylene. The variation of $T_{1\rho}$ values with temperature in Phase I indicates rates of ethyl group rotation greater than the spin

lock field (52.1 kHz). In the same way the rate of ethyl group rotation in phase III is less than 52.1 kHz (Fig. 3.4).

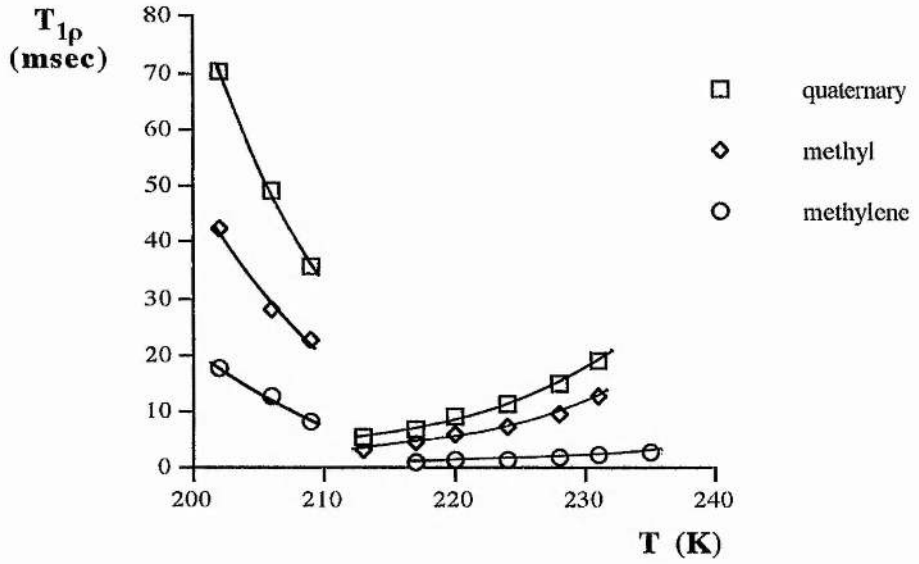

Fig. 3.4: $T_{1\rho}$ plot for all three carbons in 3,3-diethylpentane [ω_1 = 52.1 kHz]

The activation energies for the molecular motion in phase I are calculated for each resonance from an Arrhenius plot (Fig. 3.5).

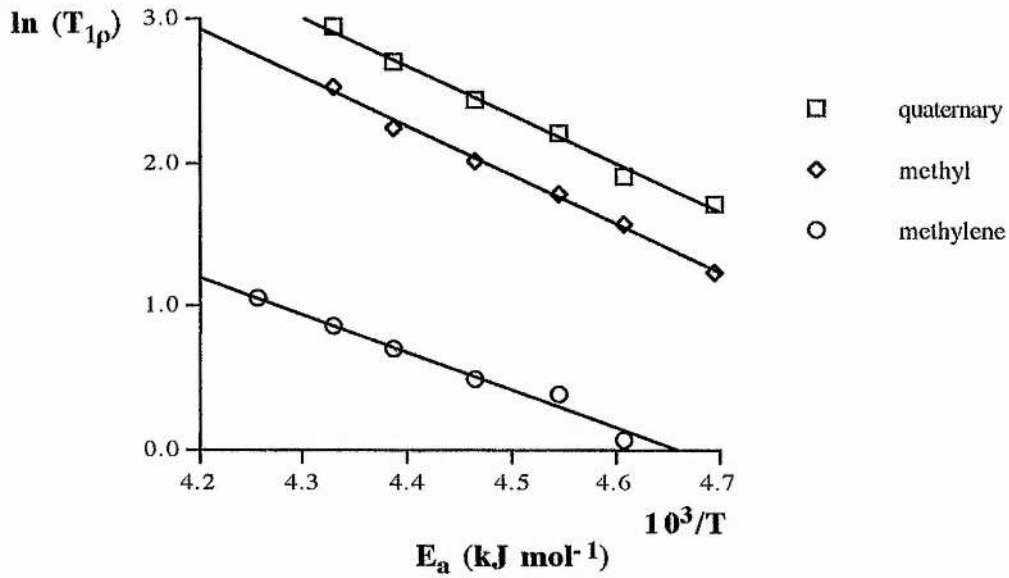

E_a (kJ mol^{-1})	
quaternary	28.0 ± 1.2
methyl	28.2 ± 1.6
methylene	21.8 ± 1.0

Fig. 3.5: Arrhenius plot of phase I (213 - 231 K) for all three carbons in 3,3-diethylpentane.

The activation energies from the data for the quaternary and methyl carbons are in good agreement, but the value for the methylene is low. The data for the methylene is not as good because the resonance is very broad and it has the shortest $T_{1\rho}$ values. Rotation of CH_3 about its C_3 axis is probably very much faster than ω_1 so it will not effect the $T_{1\rho}$ values measured. The activation energies for phase III are somewhat greater than in phase I (Fig. 3.6).

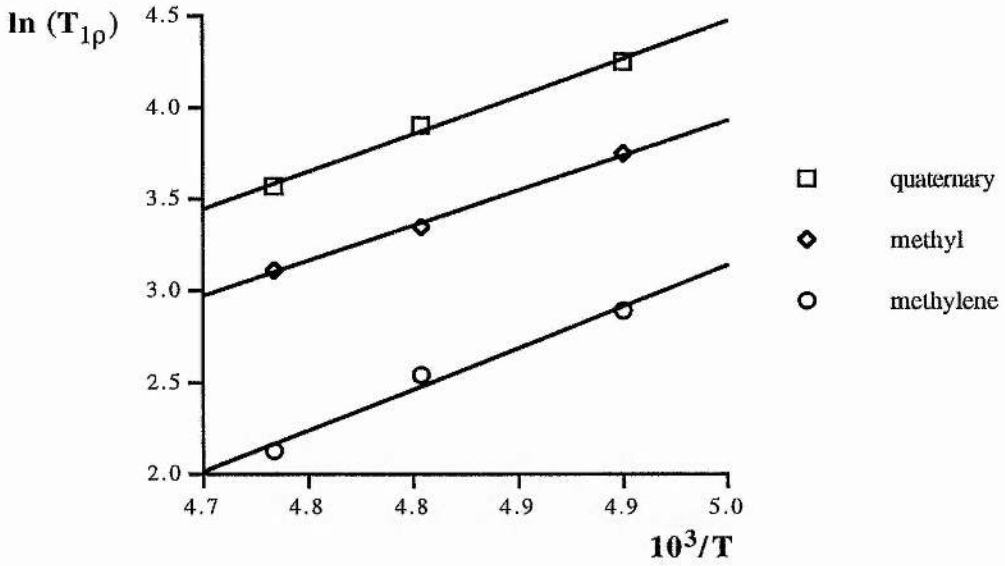

	E_a (kJ mol^{-1})
quaternary	34.2 ± 2.4
methyl	37.3 ± 5.9
methylene	32.1 ± 2.4

Fig. 3.6: Arrhenius plot of phase III (202 - 209 K) for all three carbons in 3,3-diethylpentane.

For phase III (below 208 K) a sudden discontinuity in the $T_{1\rho}$ values is observed resulting in a pronounced, but limited increase. The high values of $T_{1\rho}$ and the direction of the change with respect to temperature show that the rate of the process in phase III is < 52.1 kHz. The activation energy is only slightly larger than that of phase I but, the errors involved with only three points means that any conclusions are limited. The phase change presumably leads to a more compact structure that introduces greater hindrance to ethyl rotation as indicated by the sharp reduction in rate and the slight increase in activation energy. The solution of the crystal structure of the two phases was attempted by powder x-ray diffraction, but

proved very difficult to solve.

It was then suggested to synthesise the perdeuterio compound for neutron diffraction studies. The sample, however, now showed two new phase changes by DSC at 226 and 230 K with the melting point at 243 K (Appendix 1). The DSC of the undeuteriated sample was run and no phase changes other than the melting point (242 K) were found although theses would undoubtedly be occurring. This result is not surprising in view of the very small entropy changes observed for the I → II and II → III transitions in the earlier thermochemical work.[36] The entropy changes in the perdeuterio compound must, therefore, be correspondingly greater, but no attempt was made to estimate their magnitude. The perdeuterio sample, therefore, has three different phases as in unlabelled 3,3-diethylpentane. The phase changes occur at different temperatures in perdeuterio 3,3-diethylpentane and the neutron diffraction showed that phase I was not the same as that in the undeuteriated sample. The sample was however used to run some deuterium NMR.

In retrospect it is not surprising that the perdeuterio derivatrive has different phase changes. The C-^{2}H bond is shorter than the C-^{1}H bond and so the $C_9{}^2H_{20}$ molecules will pack more closely in the solid than $C_9{}^1H_{20}$. Closer packing will lead to stronger van der Waals interactions and hence to possible different phases.

3.1.1 Deuterium NMR

The ^{2}H NMR spectra (Fig. 3.7) show that at 238 K the high temperature phase and at 218 K the low temperature phase of 3,3-diethylpentane ($^2H_{20}$). Interestingly the spectrum at 228 K contains elements of both phase I and phase III and should in fact be phase II. The temperature gradient in the sample may be more than the 4° range of phase II so the spectrum is of all three phases. The spectra contain the two overlapping quadrupolar splitting patterns of the methyl and methylene carbons. From the quadrupolar coupling constant (q.c.c) the rates of motion can be estimated to be < 40 kHz for the methylene in phase III and > 40 kHz for the methylene in phase I. The deuterium NMR cannot distinguish for the methyl between its rotation about its C_3 axis and the ethyl rotation. The methylene spectrum, however, will only be modulated by the ethyl rotation and so the splitting will give the rate of rotation of the ethyl group.

Fig. 3.7: ^{2}H NMR spectrum of 3,3-diethylpentane ($^{2}H_{20}$)

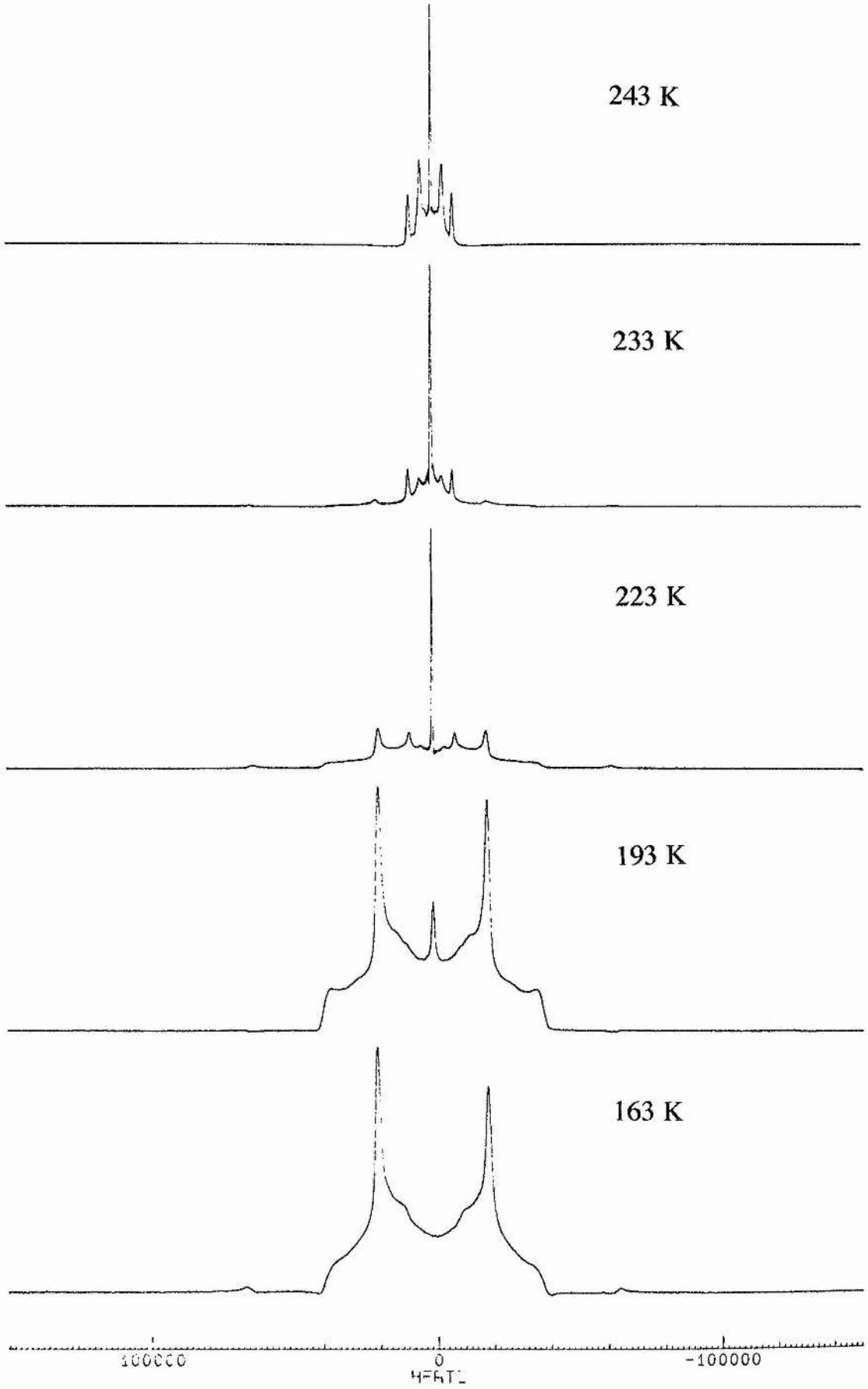

A mono deuterium labelled sample was prepared to obtain simplified spectra without the interference of the methyl group. The synthesis was done so that one deuterium atom was put onto one methylene group in any one molecule, but that only *ca* 75% of molecules would contain a deuterium atom. The compound would then not show any isotope effects. The ^{2}H NMR spectra of mono-^{2}H 3,3-diethylpentane (Fig. 3.8) show the quadrupolar splitting pattern of the methylene which was so difficult to see in the perdeuterio compound. The collapse of the splitting pattern at 203 K indicates that the rate of molecular motion is > 40 kHz even before the phase changes at 208 and 210 K. The spectra are quite poor as the sample needed a long relaxation delay (20 s) and many transients (*ca* 500). The large signal from the metastable phase (isotropic resonance) also provided added difficulties to the phasing of the spectra. The attempted simulation of the spectra using a computer programme and theories of Vold *et al.*[37] proved unsuccessful.

Fig. 3.8: ^2H NMR spectrum of 3,3-diethylpentane ($^2H_1$).

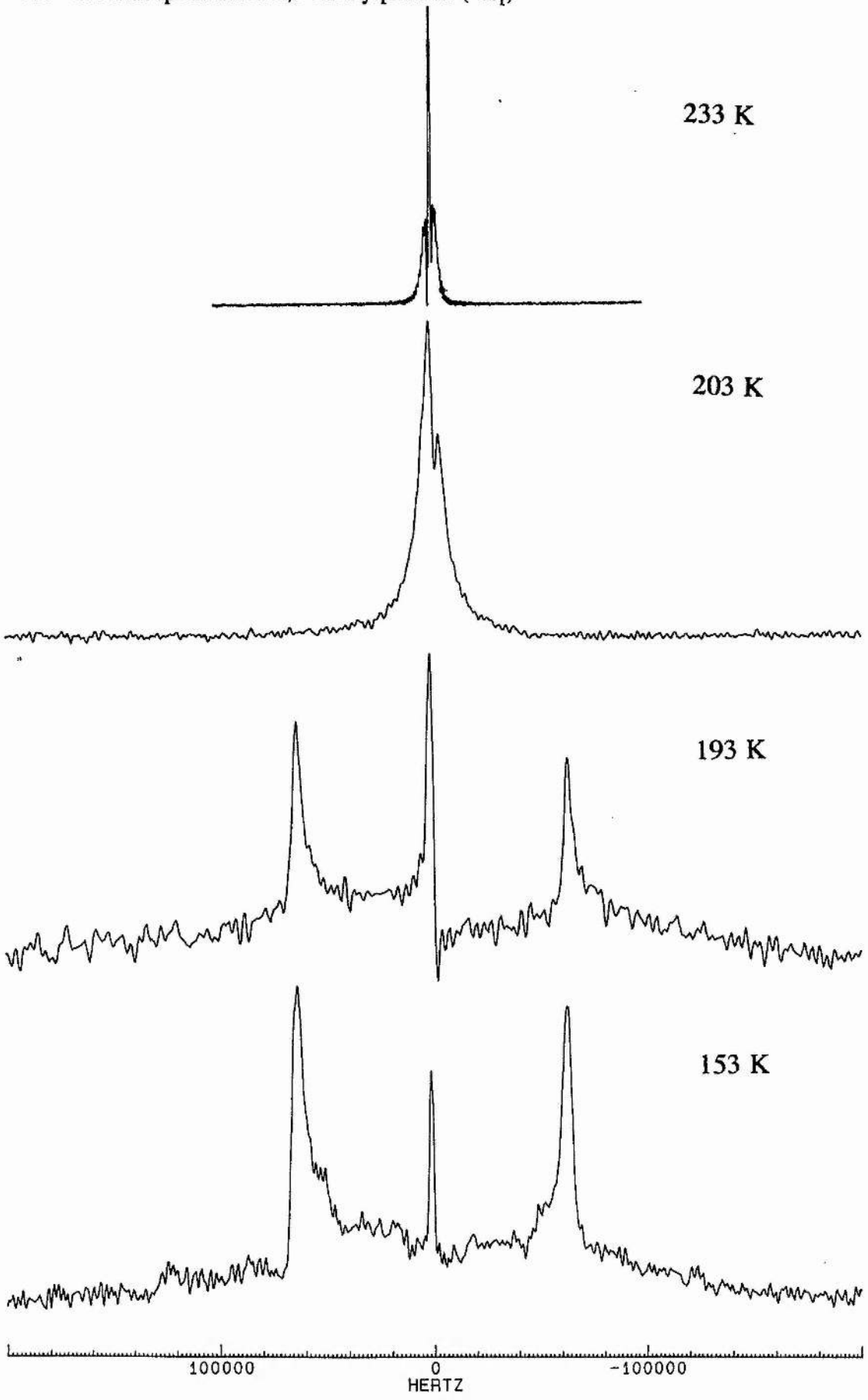

3.2 4,4-dipropylheptane (tetrapropylmethane)

As a result of the interesting discoveries made in 3,3-diethylpentane the synthesis of 4,4-dipropylheptane (Fig. 3.8) was carried out. No NMR or thermochemical studies have been reported in the literature. In the paper by Alder *et al.*[35] it is shown that there is two possible conformations with no g^+g^- interactions (Fig. 3.8).

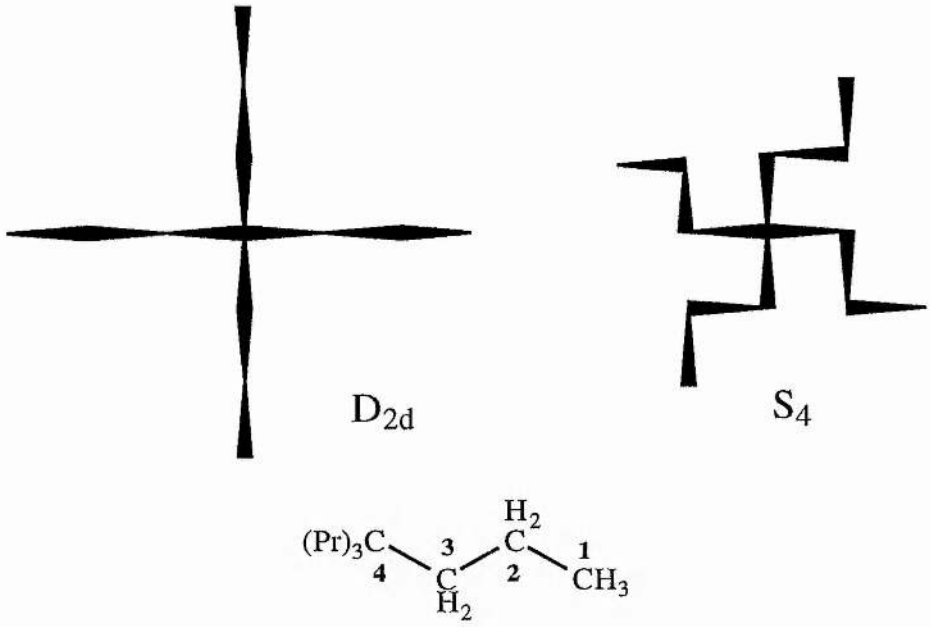

Fig. 3.8: The stable conformations of 4,4-dipropylheptane and the numbering scheme for the atoms.

The DSC plot (Appendix 1) shows that 4,4-dipropylheptane has two phases; phase I from the melting point at 252 K to *ca* 234 K and phase II (< 234 K). The ^{13}C CP/MAS NMR spectra (Fig. 3.10) show phase I as very sharp lines with the quaternary carbon only visible by using HPDEC because of the poor signal to noise using cross polarisation. The low temperature spectra show that phase II has broader lines and on closer inspection, slightly different chemical shifts (Table 3.3).

Carbon	Phase I	Phase II
1	15.6	15.3
2	16.7	16.4
3	39.6	40.9
4	37.7	37.2

Table 3.4: ^{13}C chemical shifts for the two phases of 4,4-dipropylheptane.

Fig. 3.10: ^{13}C CP/MAS NMR spectra of 4,4-dipropylheptane.

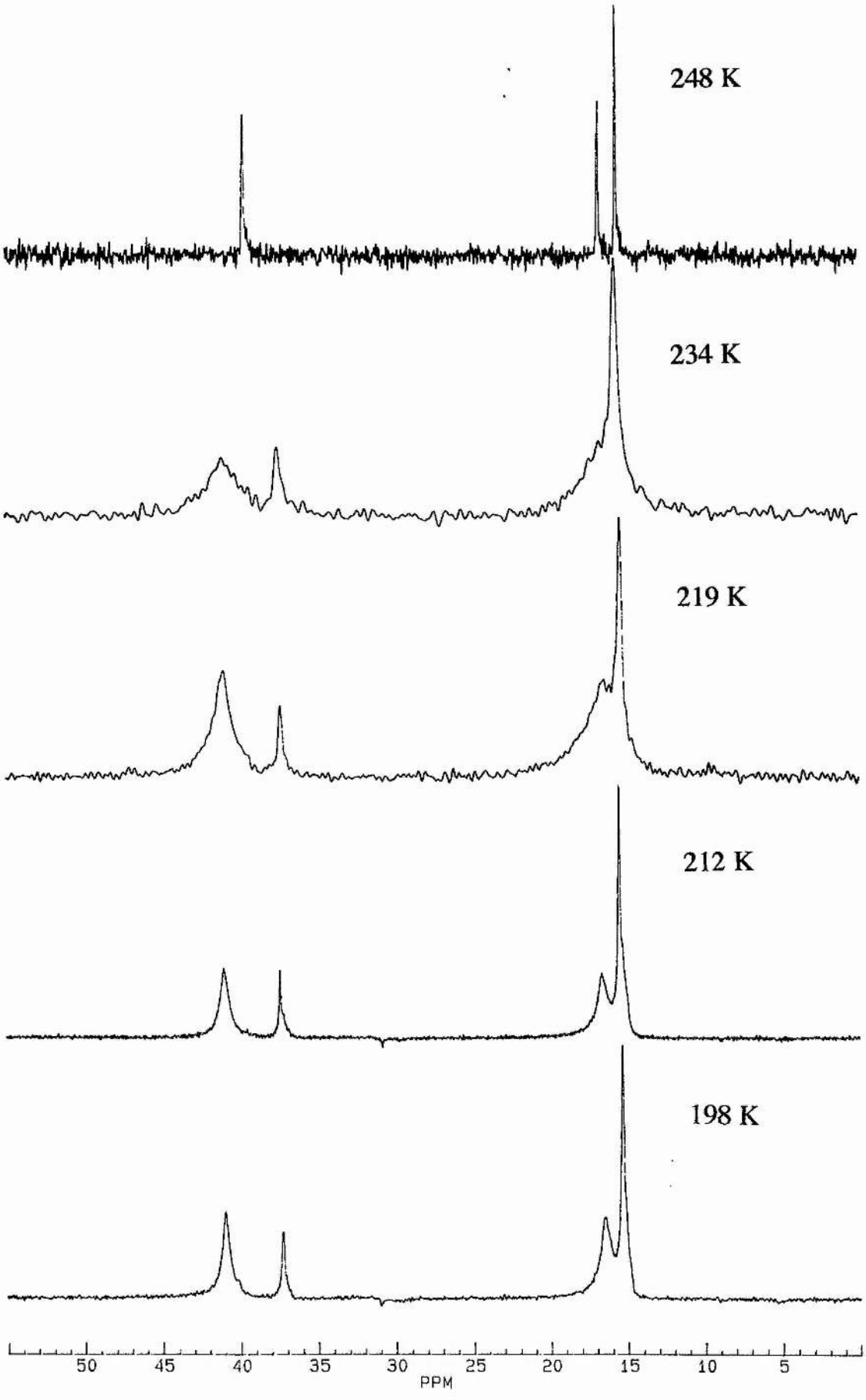

The spectra show maximum dipolar broadening as the phase transition is approached and then a sudden sharpening below 210 K. The resulting $T_{1\rho}$ plot (Fig. 3.11) from the measured $T_{1\rho}$ values (Table 3.5) shows another interesting result.

T (K)	C(1)	C(2)	C(3)
198	84.73	37.48	50.99
205	102.43	44.87	56.83
212		18.89	15.56
219	26.47	11.44	9.7
227	13.78	6.19	6.5
234	6.65	3.32	2.08

Table 3.5: ^{13}C $T_{1\rho}$ values (msec) for 4,4-dipropylheptane.

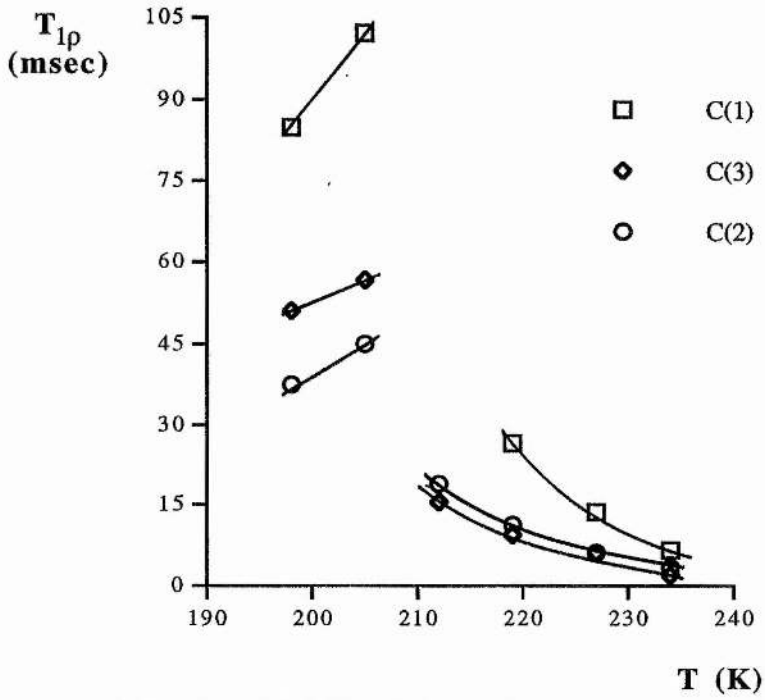

Fig. 3.11: ^{13}C $T_{1\rho}$ plot of the methyl resonance and the two methylene resonances [ω_1 = 54.3 kHz].

There appears to be a sharp discontinuity at *ca* 205 K as was seen for 3,3-diethylpentane at *ca* 210 K. The data for C(4) was unreliable because of its low intensity and so is not included. The resonances for C(2) and C(1) overlap, especially at higher temperature when the resonances broaden. This, therefore, could introduce extra errors to the $T_{1\rho}$ data. The data, however, show such a large reduction between 205 and 212 K that it suggests another phase change. The DSC (Appendix 1) does

show an anomaly at *ca* 220 K suggesting that a phase change takes place at low temperature as well. The $T_{1\rho}$ plot (Fig. 3.11) therefore, shows that the rate of the molecular motion < 54.3 kHz in the high temperature phase and > 54.3 kHz in the low temperature phase. This is in contrast to 3,3-diethylpentane where the opposite is true, i.e. the rate of motion decreases as the temperature is lowered. Only two points below the phase transition were measureable, but with all three carbons having the same trend the data must be believed. The fact that the rate of motion increases as the temperature is lowered suggests that it is not the same motion that is being measured below the transition. This is supported by the $T_{1\rho}$, data where C(2) values are lower than C(3) below 205 K and are slightly higher above 205 K.

The high temperature points (212 - 234 K) were used for an Arrhenius plot (Fig. 3.12), although with so few points the results are only a guide to the activation energies.

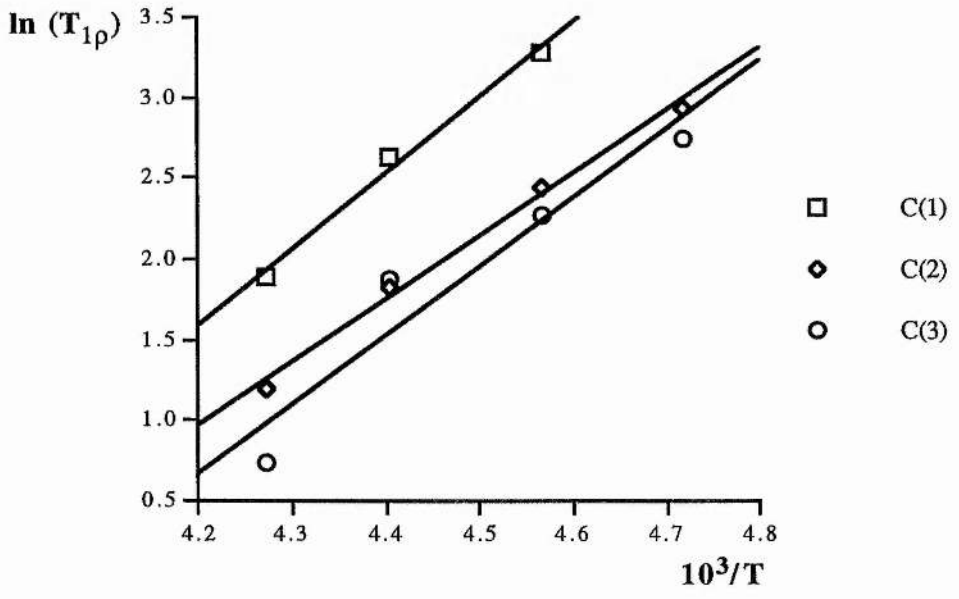

	E_a (kJ mol^{-1})
C(1)	39.0 ± 3.5
C(2)	32.4 ± 1.7
C(3)	35.7 ± 7.2

Fig. 3.12: Arrhenius plot for C(1-3) in 4,4-dipropylheptane.

The values for the activation energy are comparable to those seen for 3,3-diethylpentane (especially phase II where $E_a \approx 32$ - 37 kJ mol^{-1}). The likely motion appears to be a rotation about the C(2) - (3) bond as the $T_{1\rho}$ values for these two carbons are the lowest.

4. Tetraalkyl Ammonium Halides

The initial study of 3,3-diethylpentane lead to the study being extended to the tetraalkyl ammonium halides. The study of alkyl ammonium halides in the solid state has been carried out since the 1960's by a variety of NMR techniques. The interest in tetraalkyl ammonium halides was initiated by the results obtained by studying tetraalkyl alkanes. The early measurements were all carried out on tetramethyl ammonium halides using wide line ^1H NMR to measure the second moments and ^1H T_1 and relaxation times.[38] There was also a study on tetraalkyl ammonium halides which included ^1H $T_{1\rho}$ measurements[39] as well as ^1H T_1. A paper on tetramethyl ammonium chloride used ^1H T_1, $T_{1\rho}$ and T_2 to study molecular motions.[40] The more recent paper by Xenopoulos *et. al.*[41] on DSC, NMR and X-ray diffraction of Bu_4NCl, Bu_4NI and Hex_4NI triggered a series of papers on tetraalkyl ammonium halides (X = Br, I) : I [DSC of various tetraalkyl ammoniums];[42] II [tetramethyl, tetraethyl and tetrapropyl ammoniums][43] and III [tetrabutyl up to tetraheptyl ammoniums][44] covering all aspects of solid state ^{13}C NMR (CP, single pulse, CSA) and ^{13}C T_1 relaxation times. The series of papers is concerned with the thermal properties of the compounds based on the idea of conformational motion and disorder (condis crystals) and as such many long chain tetraalkyl ammoniums have been studied in later papers which are not as relevant to the present studies. Other relevant studies will be dealt with later in the chapter. The current study on tetraalkyl ammonium halides (X = Cl, Br and I) concentrates on the use of ^{13}C $T_{1\rho}$ measurements to investigate motions in the kilohertz range and so will give a useful comparison to the data obtained from the previous T_1 and second moment measurements.

4.1 Tetramethyl ammonium halides

As can be seen from the references already given tetramethyl ammonium halides have been the most extensively studied of the tetraalkyl ammonium salts. The two motions possible are the reorientation of the methyl about its C_3 axis and the molecular tumbling of the cation. In general the barrier to reorientation of methyls is low ($E_a \approx$ 12 kJ mol^{-1}) and so methyl reorientation will be rapid on the time scale of the spin lock field (*ca.* 50 kHz) used in ^{13}C $T_{1\rho}$ measurements in our temperature range. The case of restricted motion of a methyl group has been reported,[20,45,46] where the approach of a counter ion has lead to an increase in the barrier to rotation ($E_a \approx 30$ kJ mol^{-1}), obtained from ^{13}C $T_{1\rho}$ data. The activation energies for methyl rotation and

cation tumbling in tetramethyl ammonium halides are given (Table 4.1) from the paper by Albert *et al.*[39] as this is the most complete study.

Motion	E_a (kJ mol^{-1})
$(CH_3)_4NCl$ (phase III)	
C_3 rotation of CH_3	28.5 ± 1.7
Cation tumbling	54.4 ± 3.3
$(CH_3)_4NCl$ (phase II)	
C_3 rotation of CH_3	28.0 ± 1.7
Cation tumbling	36.8 ± 2.1
$(CH_3)_4NBr$	
C_3 rotation of CH_3	26.8 ± 1.7
Cation tumbling	48.1 ± 2.9
$(CH_3)_4NI$	
C_3 rotation of CH_3	23.0 ± 1.3
Cation tumbling	46.0 ± 2.9

Table 4.1: Activation energies for molecular motions in tetramethyl ammonium halides.[39]

The activation energies in Table 4.1 indicate that both the methyl rotation and cation tumbling could have an effect on the relaxation time $T_{1\rho}$ when they are compared to the values in the literature. The relatively large activation energy for methyl rotation is presumably due to the steric hindrance of the four methyls bonded to the nitrogen.

4.1.1 Tetramethyl ammonium chloride (TMACl)

TMACl has five phases,[39] although with phase III between 185 K and 400K this is the only phase that can be recorded on our instrument because the probe is limited to temperatures in the range 183 to 373 K.

The attempt to record a ^{13}C CP/MAS spectrum of this sample at room temperature (RT) proved impossible as no signal could be detected. The sample was heated to 312 K and a broad resonance ($w_{1/2}$ = 510 Hz) was obtained (Fig. 4.1). On further heating the resonance sharpened ($w_{1/2}$ = 96 Hz at 363 K) and the signal to noise ratio improved. The reason for the lack of signal at RT is attributed to a

Fig. 4.1: ^{13}C CP/MAS NMR spectra of $N(CH_3)_4Cl$.

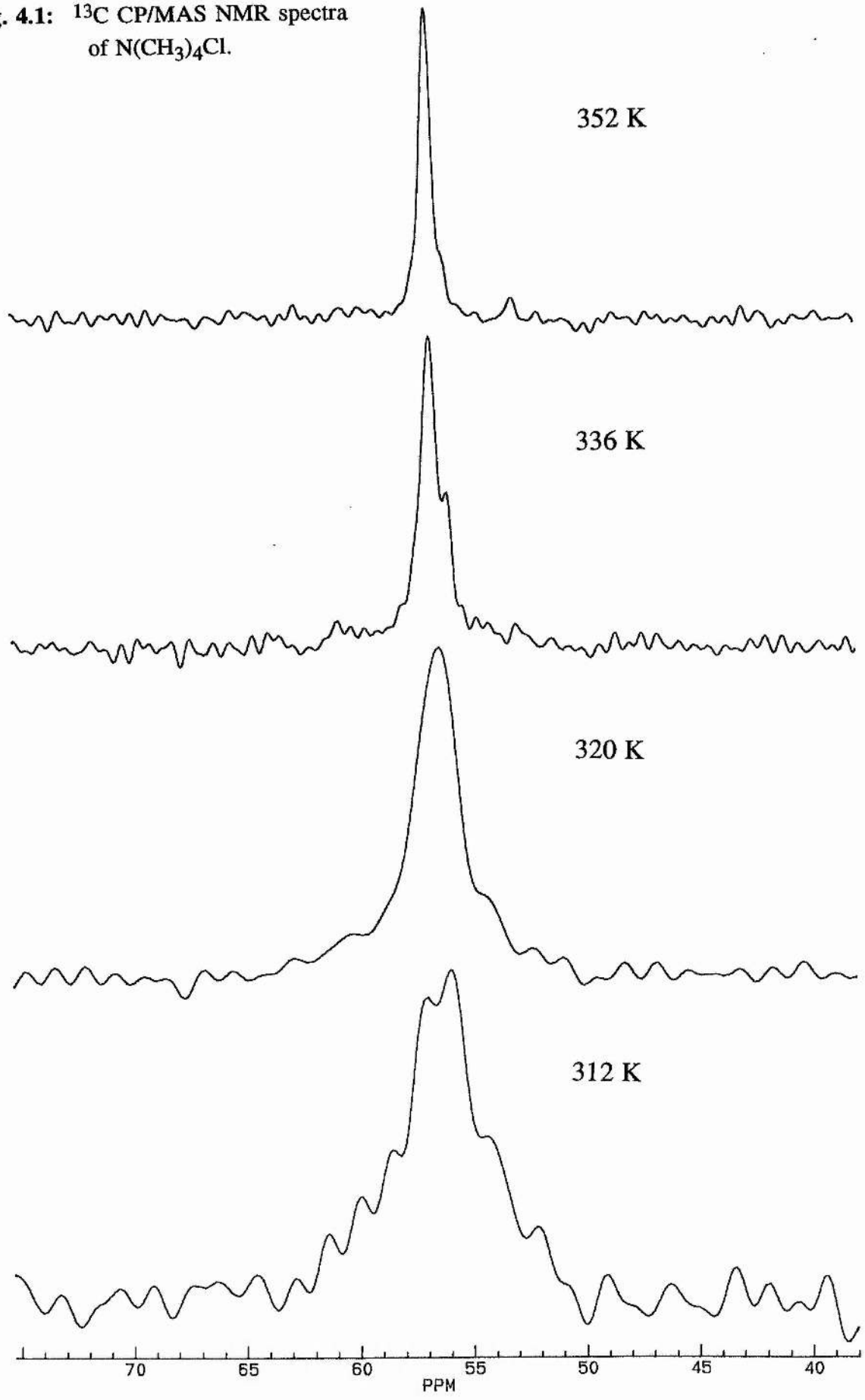

combination of short $T_{1\rho}$ and maximum dipolar broadening with the former being the most important. Therefore, the measurement of $T_{1\rho}$ values (Table 4.2) was undertaken and plotted against temperature (Fig. 4.2).

T (K)	$T_{1\rho}$ (msec)
368.2	11.8
360.2	7.89
352.2	6.69
344.3	5.18
336.3	5.50
328.3	3.60
320.3	2.22

Table 4.2: ^{13}C $T_{1\rho}$ values for TMACl.

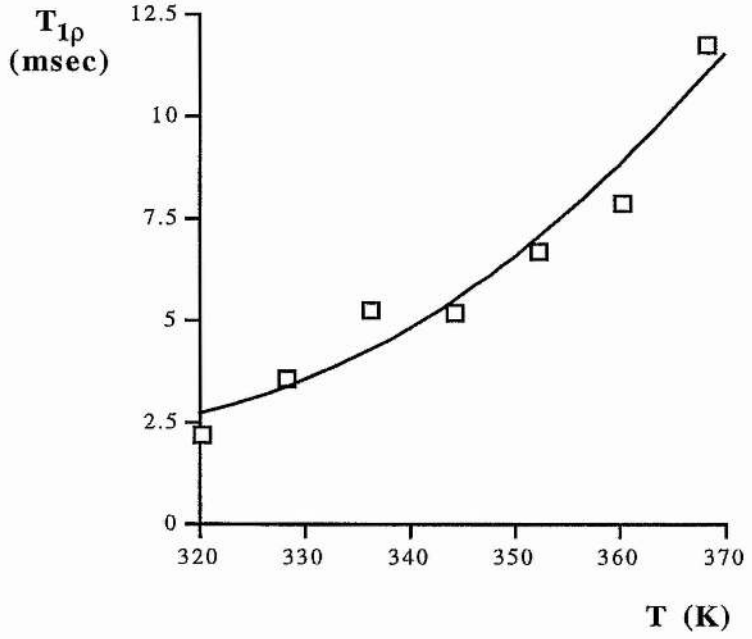

Fig. 4.2: $T_{1\rho}$ plot for TMACl [ω_1 = 49.5 kHz].

The temperature range that data could be recorded over was from 320 to 368 K, the upper temperature being due to the probe limits. Below 320 K, however, the signal deteriorates rapidly and no data could be recorded even when the temperature was lowered to 192 K. The ^1H T_1 data shows that the the minima for the two motions are only separated by *ca.* 100 K.[39] Therefore, this motion may initially be cation tumbling and then methyl rotation in addition results in the complete lack of signal.

The fact that the NMR signal does not return down to 192 K suggests it is not just one motion that is modulating the $T_{1\rho}$ relaxation over the temperature range of 192-370 K. The rate of methyl rotation can be calculated at different temperatures from the data in the literature,[39] and by substituting $1/\omega_1$ for τ_c in the equation:

$$\tau_c = \tau_o \exp(E_a/RT)$$

The $T_{1\rho}$ minimum for, methyl rotation is 192 K and for methyl reorientation 299 K. This indicates that it is the cation reorientation that is modulating the $T_{1\rho}$ values at high temperature, but as the temperature is lowered the methyl rotation increasingly contributes to the $T_{1\rho}$ relaxation. The activation energy measured for the process could be affected by this overlapping of effects.

The Arrhenius plot of ln ($T_{1\rho}$) vs. $10^3/T$ (Fig. 4.3) gives the activation energy (E_a) from the gradient.

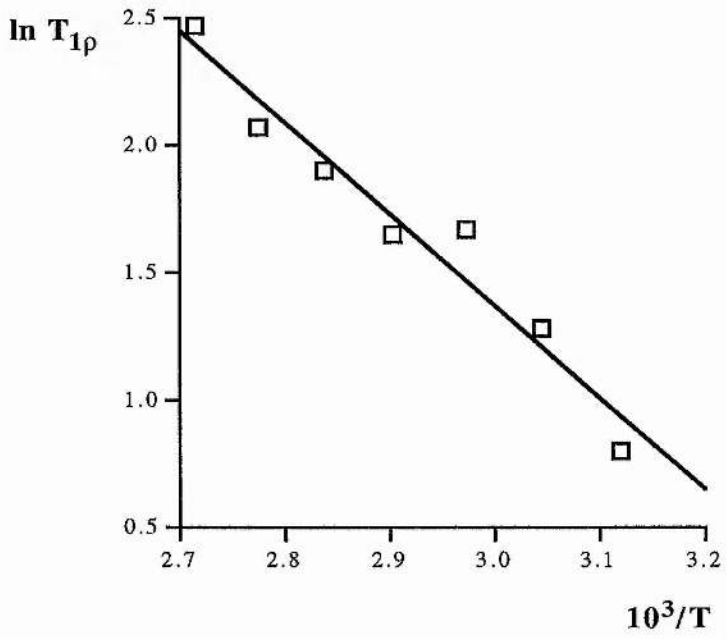

$E_a = 30.0 \pm 3.1$ kJ mol^{-1}

Fig. 4.3: Arrhenius plot for TMACl.

The methyl reorientation and cation tumbling have been studied by second moments (E_a = 27.2 and 35.6 kJ mol^{-1} respectively)[38(a)] and by ^1H T_1 measurements ($E_a = 28.5 \pm 1.7$ and 54.4 ± 3.3 kJ mol^{-1} respectively)[39]. The errors from the second moment calculations are quite large (*ca* 20%) due to the use of the

approximation $E_a = 166\ T_c$ kJ mol^{-1},[17] where T_c is the temperature at which the spectrum narrows (section 1.3.1.4). The comparison of ^{13}C $T_{1\rho}$ measurements with the second moment calculations indicates that the motion we are observing could be either methyl rotation or cation reorientation. The T_1 data, however, indicates that it is probably the methyl reorientation that is giving the $T_{1\rho}$ effect. The low value of activation energy reported for cation tumbling (35.6 kJ mol^{-1}) can be attributed to the fact that the phase change at *ca.* 400 K is only reversible with traces of solvent.[38(a)] The sample was heated to over 400 K to remove traces of solvent and water and so it will have remained in phase II after subsequent cooling. It is also reported in the paper by Albert *et al.*[39] that there is a phase change at 418 K as observed from T_1 data and on supercooling of the sample it stays in phase II and gives $E_a = 28.0 \pm 1.7$ and 36.8 ± 2.1 kJ mol^{-1} for methyl reorientation and cation tumbling respectively. Phase II is reported to be slightly less dense than phase III and to have a small difference in the ionic packing that could lead to the different barriers to rotation being observed. Our sample of TMACl used was heated under vacuum to about 100 °C and so should never have got into phase II. The sample was subsequently packed into the rotor for solid state NMR analysis on the open bench and so a possible explanation is that the sample retained some moisture or picked it up on packing and even while data was being recorded. It is, therefore, possible that some water remained in the lattice (tetraalkyl halides are generally hygroscopic, especially the chlorides) or that the sample picked up some moisture in the probe. In the paper by Blears *et al.*[38(b)] low activation energies for cation tumbling in TMAB and TMAI is attributed to impurities in the later paper.[39] Therefore, the activation energies of TMAB and TMAI should give a better indication of the reason for the low activation energy recorded for TMACl.

4.1.2 Tetramethyl ammonium bromide (TMABr)

The analysis of TMABr was carried out in the same way as for TMACl. It was possible to obtain a ^{13}C CP/MAS NMR spectrum at RT (Fig. 4.4), although the signal to noise ratio was very poor and the resonance was very broad ($w_{1/2}$ = 502 Hz). The subsequent heating of the sample sharpened the resonance ($w_{1/2}$ = 132 Hz at 360 K) and the signal to noise ratio improved significantly. The NMR signal, therefore, appeared to be showing classic signs of maximum dipolar broadening coupled with $T_{1\rho}$ effects as for TMACl. The ^{13}C $T_{1\rho}$ plot shows a somewhat more elongated temperature range and not the expected bell shaped curve (Fig. 4.5).

Fig. 4.4: ^{13}C CP/MAS NMR spectra of $N(CH_3)_4Br$

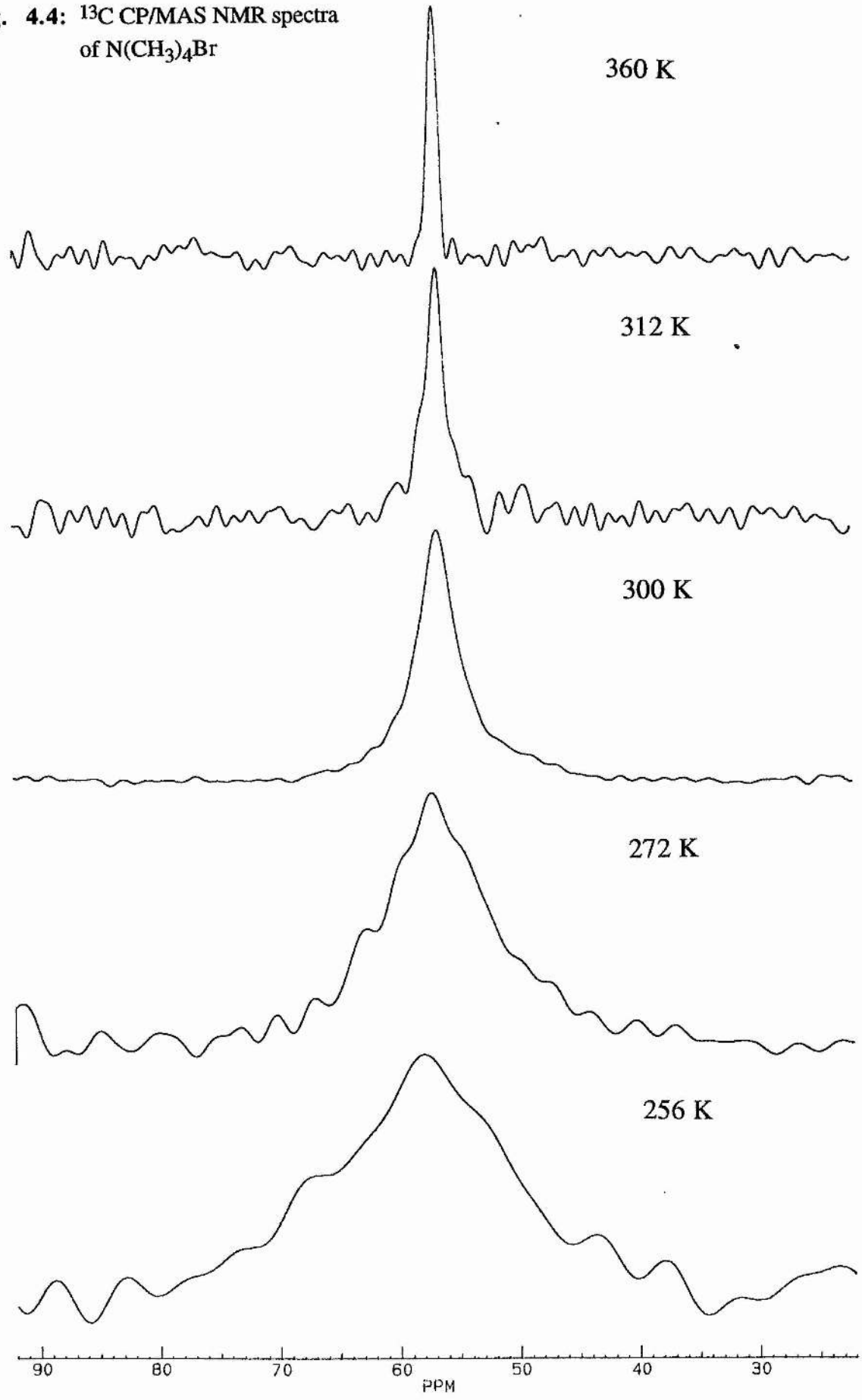

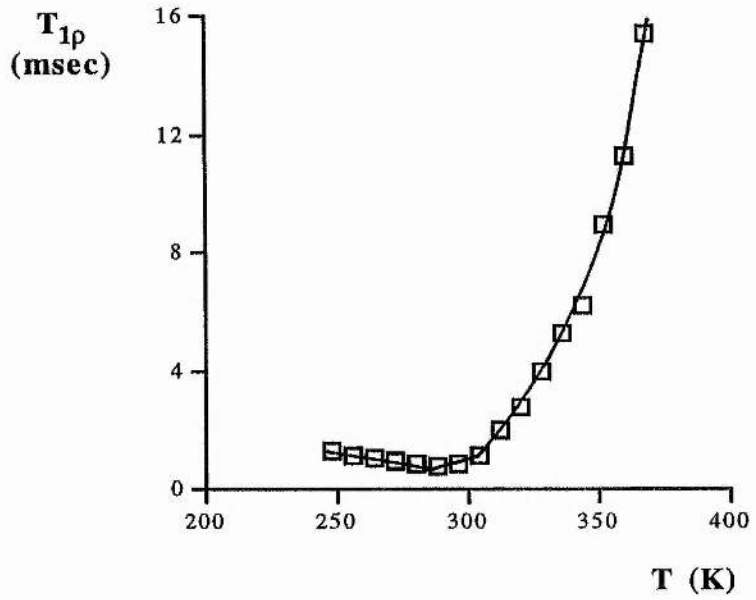

Fig. 4.5: $T_{1\rho}$ plot for TMABr

As the temperature is reduced the curve seems to reach a minimum, but as the temperature is lowered the $T_{1\rho}$ values increase very slowly indicating a secondary motion that is interfering with the spin-lock field. With only two motions possible that means the minimum is caused by cation tumbling and the continued low $T_{1\rho}$ values are caused by an overlap of effects due to cation tumbling and methyl reorientation. This can be shown diagramatically by calculating a second $T_{1\rho}$ plot for the methyl rotation and completing the cation tumbling $T_{1\rho}$ plot by mirroring the values from 368-288 K (Fig. 4.6).

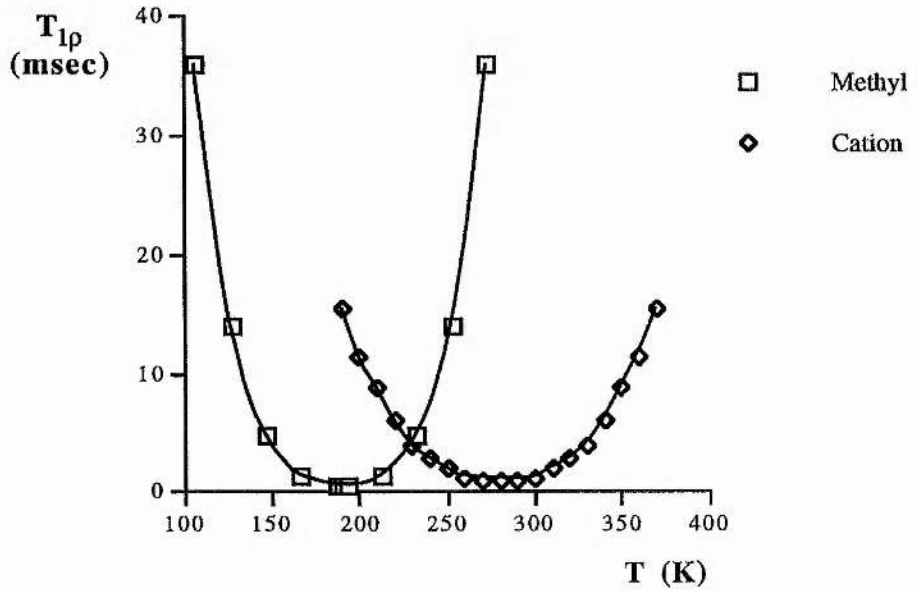

Fig. 4.6: Simulated $T_{1\rho}$ plots for the methyl rotation and cation tumbling.

The calculation of $T_{1\rho}$ was done by first calculating the $T_{1\rho}$ minimum temperature (section 4.1.1) and then the τ_c values from:

$$\tau_c = \tau_o \exp(E_a/RT)$$

τ_c was then substituted in the equation for $T_{1\rho}$:

$$1/T_{1\rho} = \frac{B^2\tau_c}{1+\omega_1^2\tau_c^2}$$

$T_{1\rho}$ values can then be calculated by assuming a reasonable value for B^2. A value of 1.5×10^8 s^{-2} was assumed because a value of thiis order is calculated for methylene carbons in TEPBr (section 5.2.2) and no B^2 values for methyls rotating at *ca.* 50 kHz has been calculated before.

The simulated $T_{1\rho}$ curves indicate that the methyl rotation should have little effect on the $T_{1\rho}$ values for cation tumbling above 280 K.

The activation energy is calculated between 368 and 312 K from the Arrhenius plot (Fig. 4.7).

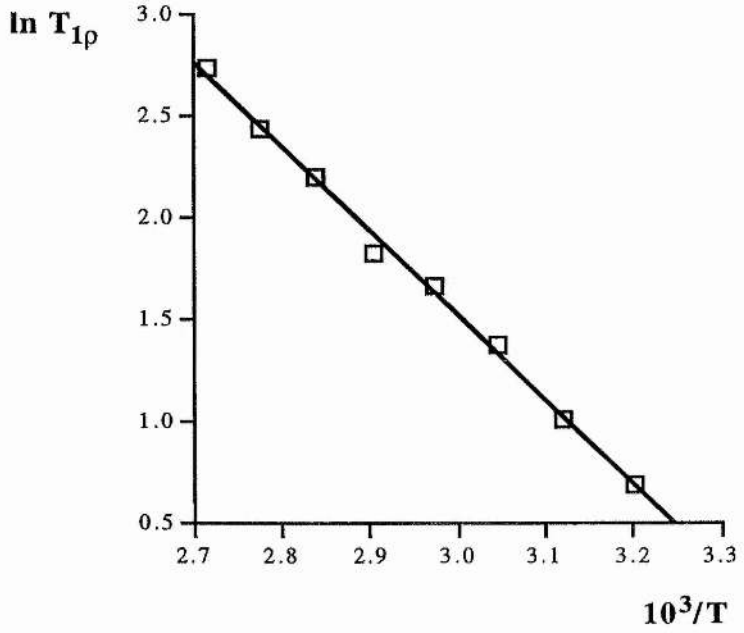

$E_a = 34.3 \pm 0.9$ kJ mol^{-1}

Fig. 4.7: Arrhenius plot for TMABr.

The calculation of activation energies for cation tumbling has again been carried out by second moment and T_1 measurements to give:

$E_a = 34.7 \pm 2.1$ kJ mol^{-1} second moment[37(b)]

$E_a = 50.7$ kJ mol^{-1} ln τ_c vs $1/T$[37(c)]

$E_a = 48.1$ kJ mol^{-1} T_1 and ^1H $T_{1\rho}$[39]

The data shows a similar disparity with high and low values as seen for TMACl. The explanation of the low value from the work by Blears *et al.*[38(b)] is attributed to impurities, in the later work by Albert *et al.*[39]

The low temperature $T_{1\rho}$ values (below 280 K) should give the same activation parameters as the high temperature values. This is obviously not going to be the case, because as can be seen the $T_{1\rho}$ curve does not give the bell shape associated with modulation of $T_{1\rho}$ by a single molecular motion. The $T_{1\rho}$ values are, therefore, modulated by the methyl reorientation with a second minimum for this motion at 192 K. The data below 280 K, therefore, is from a combination of the two motions and could not give any meaningful activation parameters.

If, however, it is assumed that the minimum reached at 288 K is purely from the cation tumbling then values for $\Delta H^{\ddagger}$ and $\Delta S^{\ddagger}$ can be derived (Section 1.3.1.2) using the data in Table 4.2. This seems a reasonable assumption on observing the simulation of $T_{1\rho}$ curves (Fig. 4.6).

The $T_{1\rho}$ and rate data calculated from the $T_{1\rho}$ minimum of 0.82 msec at 288 K is given in Table 4.3.

Temp. (K)	$T_{1\rho}$ (msec)	k (x 10^6 s^{-1})
368	15.5	11.7
360	11.3	8.55
352	9.01	6.80
344	6.20	4.67
336	5.28	3.98
328	3.96	2.97
320	2.75	2.04
312	1.99	1.44
304	1.10	0.69
296	0.91	0.50
288	0.82	0.31
280	0.92	0.19
272	1.01	0.16
264	1.04	0.15
256	1.15	0.13
248	1.31	0.11

Table 4.3: $T_{1\rho}$ data for TMABr [ω_1 = 49.5 kHz and $B^2 = 7.59 \times 10^8$ s^{-2}].

The resulting Eyring plot (Fig. 4.8) does not use the last five values (248 - 280 K) because these do not fit the line, due to the influence of the methyl rotation as has been discussed.

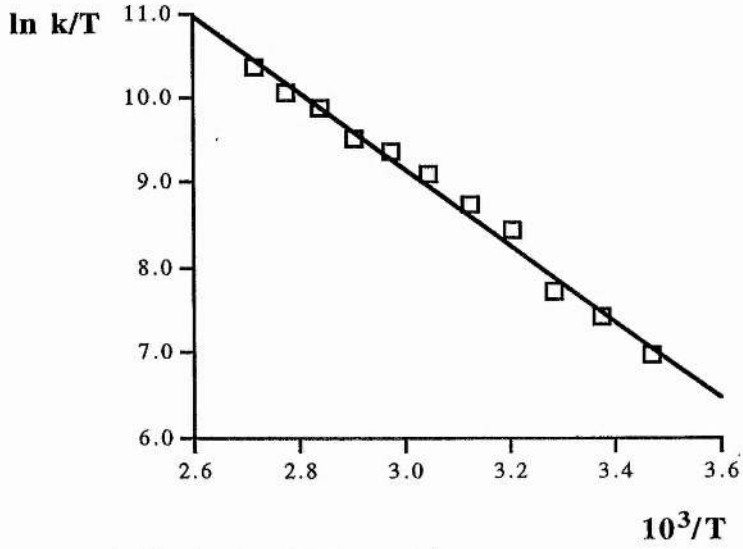

$\Delta H^{\ddagger} = 37.2 \pm 1.3$ kJ mol^{-1}

$\Delta S^{\ddagger} = -9.64 \pm 4.0$ J K^{-1} mol^{-1}

Fig. 4.8: Eyring plot and parameters for TMABr.

Calculation of the activation energy using the correlation times (τ) gives E_a = 39.9 ± 1.3 kJ mol^{-1}. This activation energy is higher than the value calculated earlier from ln $T_{1\rho}$ vs. 1/T (E_a = 34.3 ± 0.9 kJ mol^{-1}). This suggests that the assumption that the minimum is slightly lowered by methyl rotation. The true minimum is slightly higher and this would in turn decrease the value of the activation energy. The errors on the activation parameters should, therefore, be larger (especially for $\Delta S^{\ddagger}$).

4.1.3 Tetramethyl ammonium iodide (TMAI)

The ^{13}C CP/MAS NMR spectra of TMAI (Fig. 4.9) show that the spectra do not show any noticeable maximum dipolar broadening. The $T_{1\rho}$ data show, however, (Fig. 4.10) that at RT the signal is again decaying quickly ($T_{1\rho}$ = 6.55 msec), although the minimum value recorded is 4.03 msec at 288 K. The spectra, however, (Fig. 4.9) show that the iodide has much better signal to noise than previously seen for the other two halides where the minimum $T_{1\rho}$ values recorded are 2.22 msec at 323 K for TMACl and 0.82 msec at 288 K for TMABr. The signal then decays rapidly below 288 K with no spectra able to be recorded due to lack of signal which is presumably as a result of methyl rotation interfering with cross polarisation. The calculated $T_{1\rho}$ minima for methyl rotation (170 K) and cation tumbling (249 K), from the data in the paper by Albert *et al.*,[39] indicate this is possible.

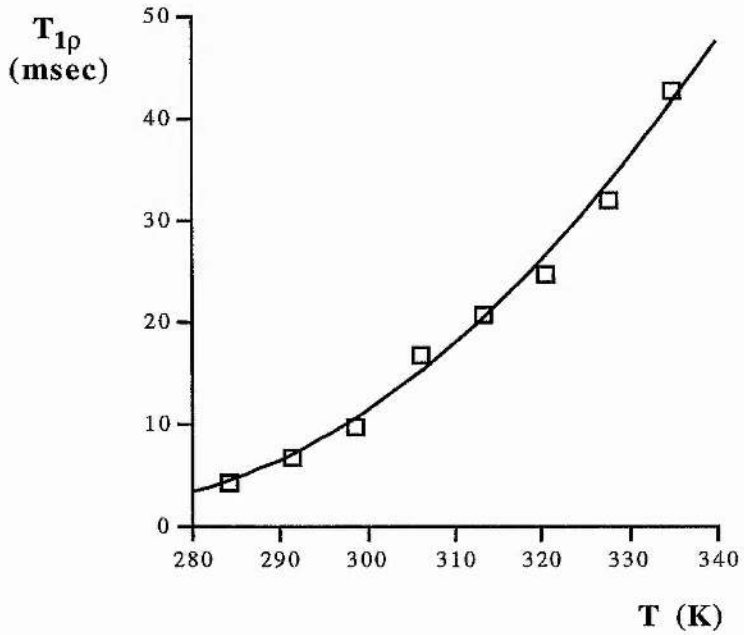

Fig. 4.10: $T_{1\rho}$ plot for TMAI.

Fig. 4.9: ^{13}C CP/MAS NMR spectra of $N(CH_3)_4I$

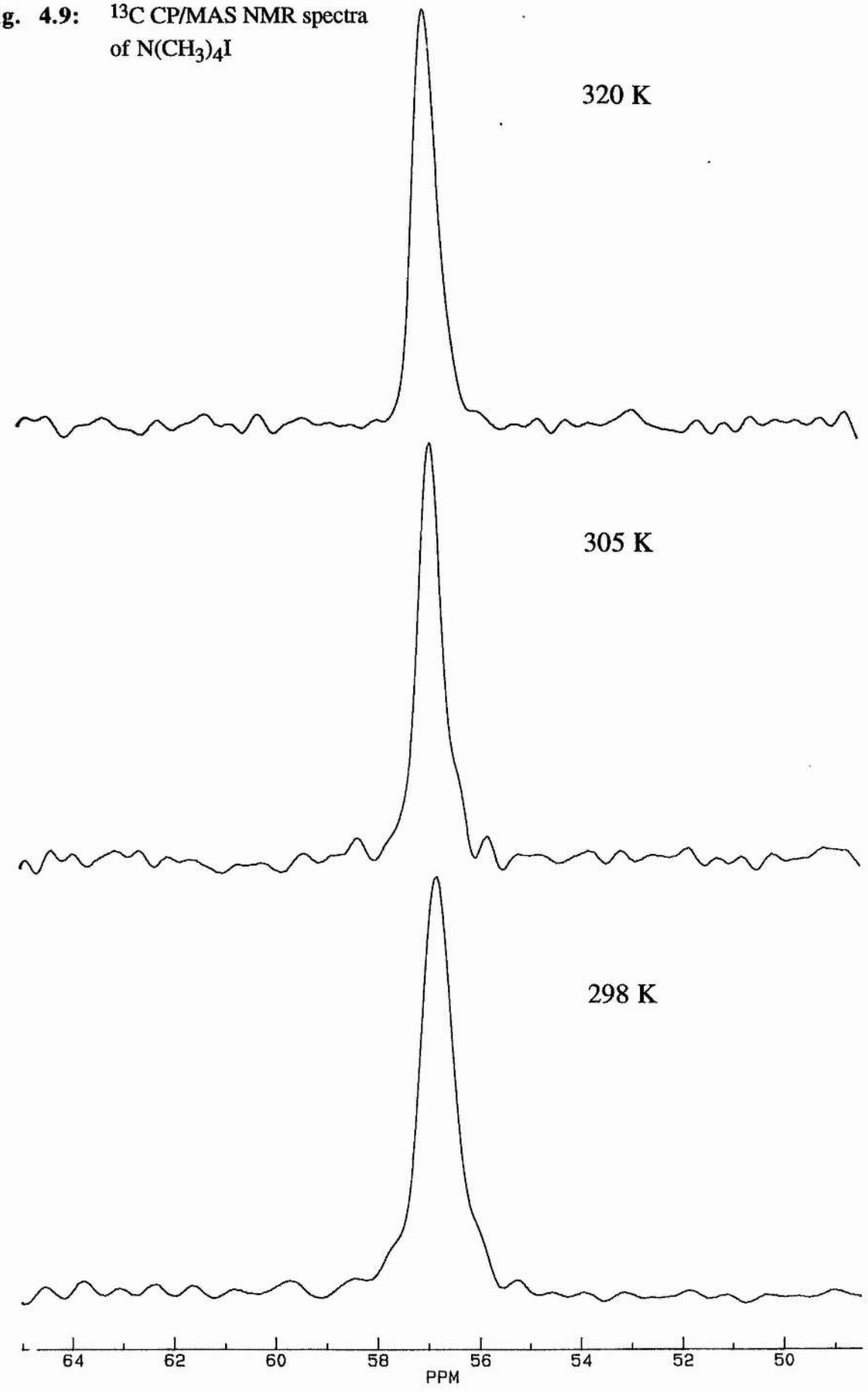

This improvement in signal to noise ratio is because this compound does not show a large maximum dipolar broadening (max. linewidth = 93.1 Hz at 293 K, min. linewidth = 67.9 Hz at 352 K). The $T_{1\rho}$ data (Table 4.4) allows the calculation of activation energy from the Arrhenius plot (Fig. 4.11).

T (K)	$T_{1\rho}$ (msec)
284	4.0
292	6.6
299	9.7
306	16.7
313	20.6
320	24.6
328	32.0
335	42.5

Table 4.4: ^{13}C $T_{1\rho}$ data for TMAI.

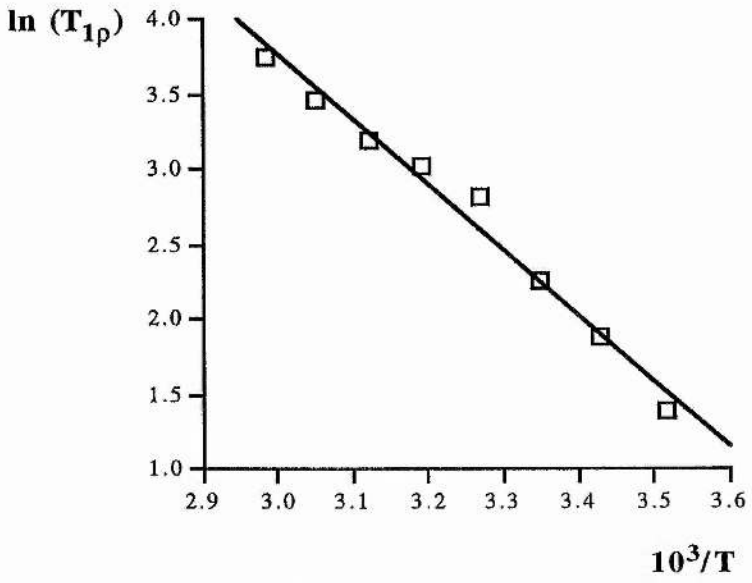

$E_a = 36.0 \pm 1.9$ kJ mol^{-1}

Fig. 4.11: Arrhenius plot for TMAI.

The trend for activation energies for both methyl rotation and cation tumbling, in tetramethyl ammonium halides is that they decrease as the halide increases in size.[39] The inhibition of cation tumbling is by interionic (intermolecular) forces whereas for the methyl rotation it is from intramolecular interactions. The methyls are assumed to be distorted in proportion with the elecrostatic interaction of the cation with the anion. The activation energy for the iodide, however, is the highest value

that has been recorded in the present work. The data is summarised in Table 4.5 along with the literature values.[39]

	Literature	*Present work*
Compound	**E_a (kJ mol^{-1})**	**E_a (kJ mol^{-1})**
$(CH_3)_4NCl$	54.4 ± 3.3	30.0 ± 3.1
$(CH_3)_4NBr$	48.1 ± 2.9	34.3 ± 0.9
$(CH_3)_4NI$	46.0 ± 2.9	36.0 ± 1.9
$(CH_3)_4NCl$ (phase II)	36.8 ± 2.1	-

Table 4.5: A comparison of the activation energies for cation tumbling from the literature,[39] and the present work.

The activation parameters from ^{13}C $T_{1\rho}$ values are consistently lower than the literature values, but this can be attributed to the purity of the samples. The opposite trend seen in the present work (E_a increases with increasing anion size) can be explained by assuming that the iodide sample contains less impurities than the bromide which in turn contains less impurities than the chloride. This seems reasonable since the chlorides of tetraalkyl ammonium salts are generally more hygroscopic than the bromides and iodides.

In general the chlorides are much more hygroscopic than either the bromide or iodide for all tetraalkyl ammonium halides. The samples were prepared for use as described in the experimental but even then there is still some moisture that can get into the probe in the spinning gases even though the gas is dried.

4.2 Tetraethyl ammonium halides

The analysis of all the tetraethyl ammonium halides (X = F, Cl, Br and I), by ^1H solid state NMR, has been carried out by Szafranska and Pajak,[47] and the bromide and iodide have been analysed by ^{13}C NMR in paper II of the series by Cheng *et al.*[43] The differential thermal analysis carried out in these two references show the solid-solid phase transitions (Table 4.6):

Compound	T_{tr} (K)[a]	ΔS_{tr} ($JK^{-1}mol^{-1}$)	T_{tr} (K)[b]	ΔS_{tr} ($JK^{-1}mol^{-1}$)
TEAF	308	16.6	-	-
TEACl	346, 368	7.6 + 16.2	-	-
TEABr	437, 460	40.3 + 3.1	448, 463	44.6, 3.2
TEAI	467	44.0	471	44.3

Table 4.6: DSC data for the tetraalkyl ammonium halides (a: Szafranska *et al.*.[47], b: Cheng *et al.*.[43]) and T_{tr} and ΔS_{tr} are the temperature and entropy at the phase change respectively.

The phase changes of higher entropy are reported,[47] to result in isotropic cation tumbling above the phase change i.e. the compound is in a plastic phase. The T_1 measurements show single minima for the bromide and iodide (32 ms at 148 K for both) which is from the reorientation of the methyl groups. The chloride has two minima (30 ms at 125 K and 60 ms at 400 K) and these are attributed to methyl and ethyl reorientation respectively. The fluoride also has two minima (20 ms at 125 K and 46 ms at 270 K) and these are attributed to methyl and cation reorientation respectively. The methyl reorientation gives an $E_a \approx 12.6$ kJ mol^{-1} for all the compounds. The other activation energies calculated from second moments are given (Table 4.7):

Compound	Ethyl rotation ($kJ\ mol^{-1}$)	Cation tumbling ($kJ\ mol^{-1}$)
TEAF	-	42.7
TEACl	50.3	55.3
TEABr	65.0	68.7
TEAI	65.8	69.6

Table 4.7: Activation energies from second moments.[47]

4.2.1 Tetraethyl ammonium chloride (TEACl)

This compound was not analysed by Cheng *et al.* so first the ^{13}C CP/MAS NMR spectra will be considered (4.12). The spectra show clearly the signal to noise ratio decreasing markedly from 349 K until the just above the $T_{1\rho}$ minimum (320 K) and then improving at 299 K. The methyl resonance (8.97 ppm) at 320 K ($w_{1/2}$ = 160 Hz) also sharpens as the sample is warmed to 349 K ($w_{1/2}$ = 52 Hz).

Fig. 4.12: ^{13}C CP/MAS NMR spectra of $N(Et)_4Cl$

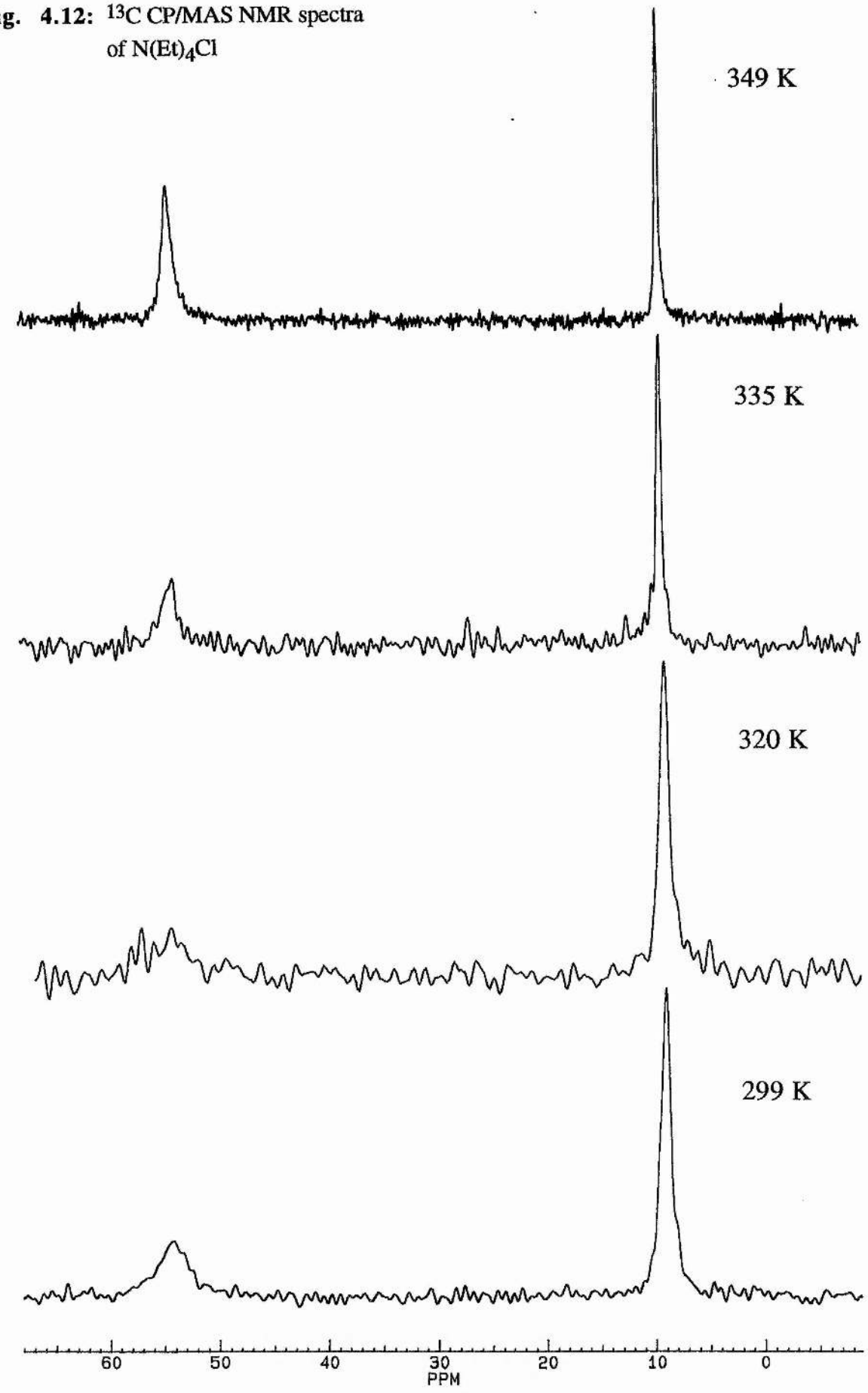

The methylene shows largest effects due to $T_{1\rho}$ and maximum dipolar broadening as is the case for 3,3-diethylpentane. This indicates that they are likely to be experiencing the same type of motion. The $T_{1\rho}$ effect is large and the $T_{1\rho}$ curve is narrow such that values for the methylene proved very difficult to obtain. Therefore, the $T_{1\rho}$ plot (Fig. 4.13) is for the methyl resonance only.

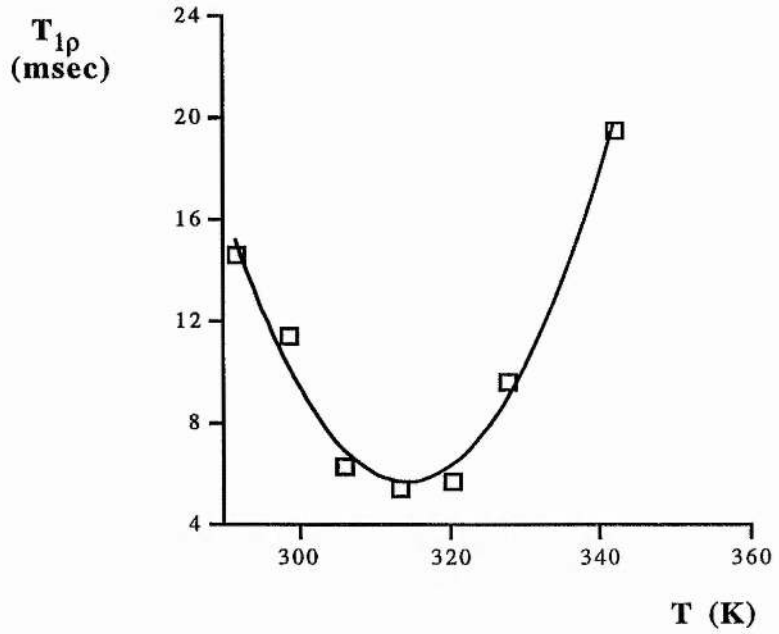

Fig. 4.13: $T_{1\rho}$ plot for TEACl [ω_1 = 61.0 kHz].

Therefore, from the $T_{1\rho}$ minimum of 5.5 ms at 314 K the calculation of rates for the molecular motion can be carried out (Table 4.8).

Temp (K)	$T_{1\rho}$ (msec)	k (x 10^5 s^{-1})
342	19.47	26.6
328	9.59	12.2
320	5.63	4.76
313	5.31	3.97
306	6.24	2.29
299	11.37	0.99
293	14.59	0.75

Table 4.8: $T_{1\rho}$ and rate data for TEACl [ω_1 = 61.0 kHz, $B^2 = 1.52 \times 10^8$ s^{-2}].

This data allows the calculation of activation parameters from the Eyring plot (Fig. 4.14).

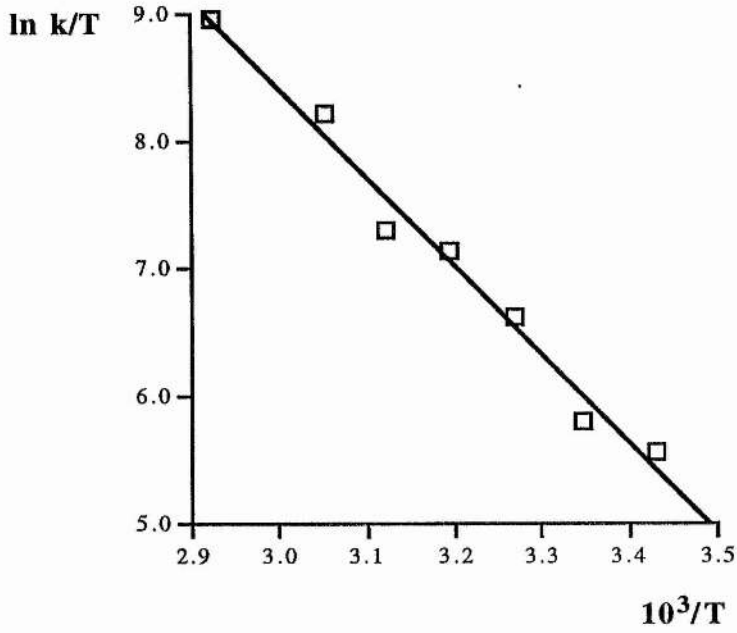

$\Delta H^{\ddagger} = +57.8 \pm 3.4$ kJ mol^{-1}
$\Delta S^{\ddagger} = +45.9 \pm 10.9$ J K^{-1} mol^{-1}

Fig. 4.14: Eyring plot and activation parameters for TEACl.

The calculation of the activation energy from an Arrhenius plot of ln τ vs 1/T ($E_a = 60.5 \pm 3.4$ kJ mol^{-1}) was also carried out for comparison with literature values and other compunds in the series where calculation of enthalpies and entropies is not possible.

The molecular motion occurring is the reorientation of the ethyl groups,[47] with cation tumbling not becoming significant until above the phase transition at 368 K. The activation energy is higher than that given by Szafranska and Pajak (50.3 kJ mol^{-1}) and although values calculated from second moments at rapid decreases in the derivative linewidths have only about 20% accuracy,[12] our results are somewhat higher.

4.2.2 Tetraethyl ammonium bromide and iodide (TEABr and TEAI)

The ^{13}C NMR spectra of these compounds are given in the literature.[43] The study of these compounds showed that ^{13}C $T_{1\rho}$ values did not change with temperature. The work by Szafranska and Pajak,[47] indicates that rapid reorientation

of the ethyl groups does not start until 390 K and 413 K for the TEABr and TEAI respectively. Cation tumbling starts just after the phase transition to the plastic phase (Table 4.6) at 437 K and 440 K for TEABr and TEAI respectively.

4.3 Tetrapropyl ammonium halides

Solid state ^{13}C NMR investigations of tetrapropyl ammonium bromide and iodide are also included in paper II of the series by Cheng *et al.*,[43] but no other NMR work has featured in the literature No references to any NMR work on tetrapropyl ammonium chloride could be found. The phase changes for the bromide and Iodide (Table 4.9) are taken from the literature, whereas the chloride was run in St. Andrews between 213 and 383 K and no phase changes were found.

Compound	T_{tr} (K)	ΔS_{tr} ($JK^{-1}mol^{-1}$)
TPACl	-	-
TPABr	382, 396	44.4, 0.9
TPAI	225, 419	6.4, 35.8

Table 4.9: DSC data for TPACl, TPABr and TPAI.[43]

4.3.1 Tetrapropyl ammonium chloride (TPACl)

The ^{13}C CP/MAS NMR spectra of TPACl (Fig. 4.15) show three resonances with the following chemical shifts:

	$\delta_c(ppm)$
CH_3	13.0
CH_2	15.9
CH_2-N	60.3

The chemical shifts do not change more than a few tenths of a ppm from 240 K up to 368 K. The resonances also do not show much sign of dipolar broadening which suggests that there is unlikely to be any $T_{1\rho}$ effect. The ^{13}C $T_{1\rho}$ plots [Fig. 4.16 (methyl) and Fig. 4.17 (methylenes)], however, show that there is a small $T_{1\rho}$ effect, and that at 368 K the $T_{1\rho}$ minimum is being approached.

Fig. 4.15: ^{13}C CP/MAS NMR spectra of $N(Pr)_4Cl$

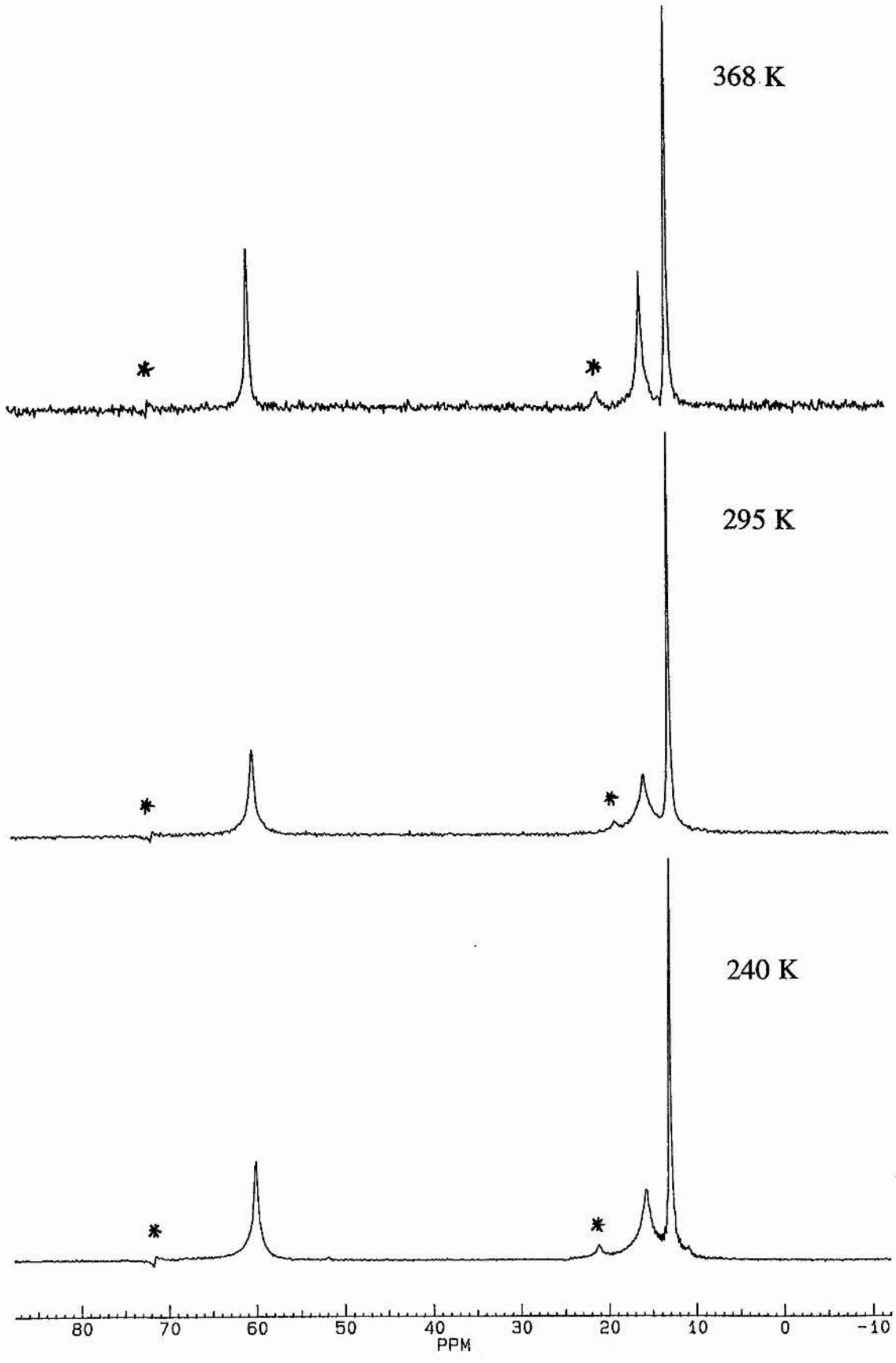

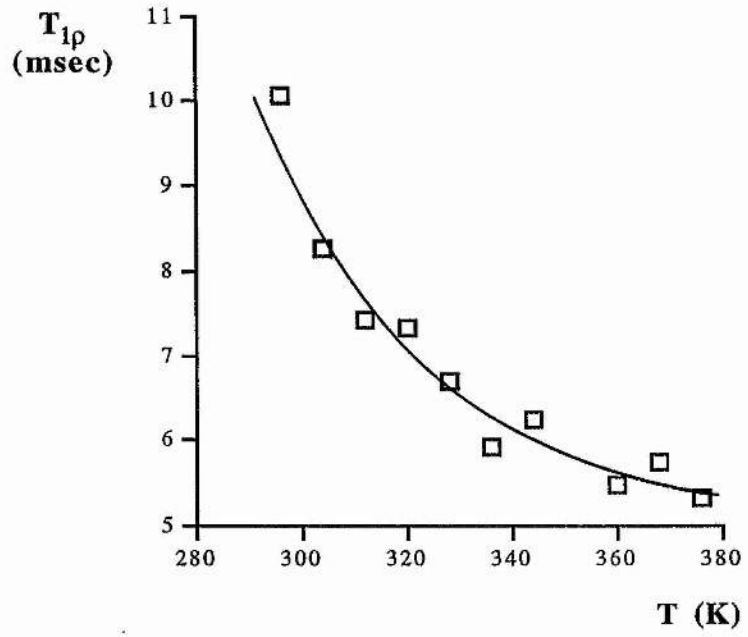

Fig. 4.16: ^{13}C $T_{1\rho}$ plot of methyl in TPACl.

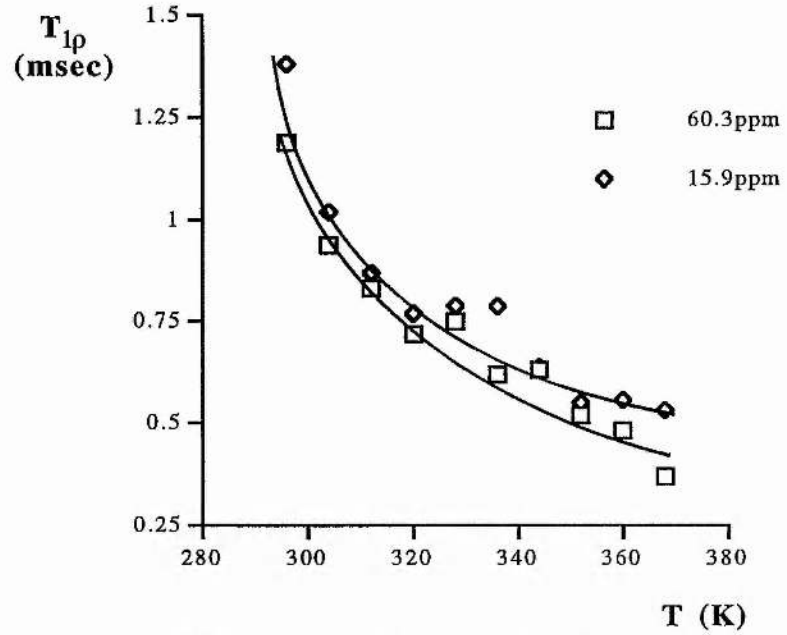

Fig. 4.17: ^{13}C $T_{1\rho}$ plot of the methylenes in TPACl.

The $T_{1\rho}$ values for the two methylenes are much lower than those for the methyl and so the motion must be a rotation about the bond between the two methylenes. The data is generally poor especially for the methylenes, mainly because the values are so low. This motion is very intriguing because the $T_{1\rho}$ values are very low and show only a very gradual change with temperature. The ^{13}C $T_{1\rho}$ values are used to calculate the activation energy of the motion from the Arrhenius plots (Figs. 4.18 and 4.19).

T (K)	CH_3	CH_2	CH_2-N
296.3	1.19	1.38	10.1
304.3	0.94	1.02	8.25
312.3	0.83	0.87	7.43
320.3	0.72	0.77	7.32
328.3	0.75	0.79	6.71
336.3	0.62	0.79	5.92
344.3	0.63	0.64	6.26
352.2	0.52	0.55	
360.2	0.48	0.56	5.47
368.2	0.37	0.53	5.75
376.2			5.31

Table 4.10: ^{13}C $T_{1\rho}$ values (msec) for the three carbons in TPACl.

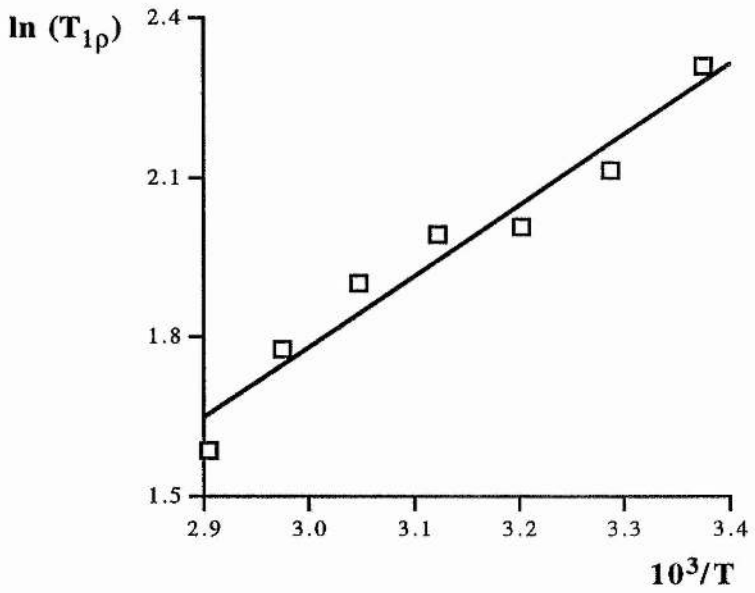

$E_a = 11.1 \pm 9.1$ kJ mol^{-1}

Fig. 4.18: Arrhenius plot for the methyl resonance in TPACl..

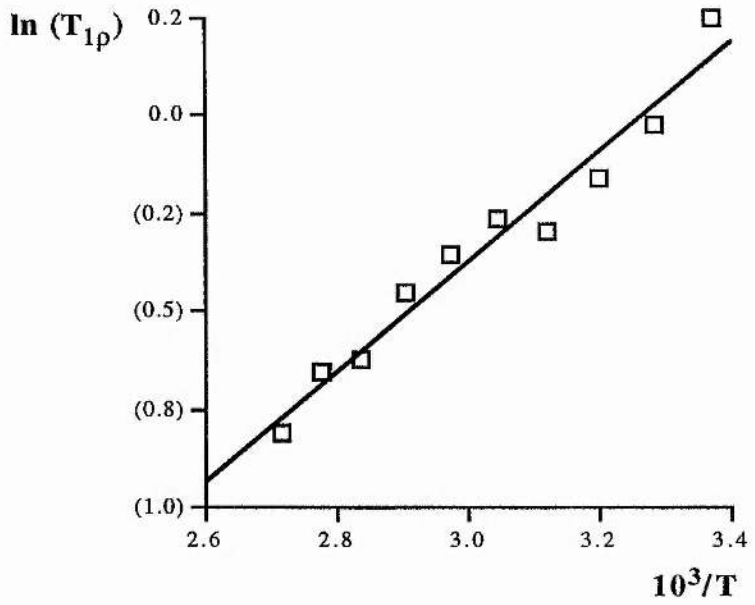

$E_a = 11.7 \pm 8.1$ kJ mol^{-1}.

Fig. 4.19: Arrhenius plot for the methylene resonances in TPACl.

The activation energies for the process causing the shortening of $T_{1\rho}$ values are very low compared to those expected for cation tumbling and alkyl group rotation. The ^{13}C CP/MAS NMR spectra (Fig. 4.15) also show that no appreciable maximum dipolar broadening is experienced by the resonances despite the very short $T_{1\rho}$ values. The rotation is centred on the first two bonds adjacent to the nitrogen, but these do not have rotational freedom due to steric repulsions,[42] and so the motion responsible for the changes in $T_{1\rho}$ may just be small librations in the propyl chain. These small vibrations, therefore, cause a change in $T_{1\rho}$ with temperature, but the change with temperature is so slow that it is not apparent in the spectra in terms of maximum dipolar broadening.

4.3.2 Tetrapropyl ammonium bromide (TPABr)

The ^{13}C CP/MAS NMR spectra are reported by Cheng *et al.*[43] and that no signal can be detected by CP after the phase change at 382.2 (Table 4.9). The transition gives τ_c values of *ca.* 10^{-10} s for C(1) and C(2) and so indicates a plastic crystal with rapid molecular motion and possibly diffusion and thus it does not cross polarise efficiently.

The fact that ethyl and propyl rotational freedom is not possible for steric reasons means that any $T_{1\rho}$ effects in this compound would be from librational motion or at just below the transition at 382.2 K where cation tumbling is becoming fast. Below the transition the ^{13}C T_1 values (20-30 s) for C(1) and C(2) are long and indicate a slow motion, $\tau_c \approx 10^{-5}$ s, which would effect $T_{1\rho}$ values. This motion is, therefore, a librational motion. The attempt to measure $T_{1\rho}$ values in the bromide showed a change in $T_{1\rho}$ values, but not one that varied consistently with temperature. Therefore, TPABr appears to have the same librational motion as TPACl except this time it has not been possible to show that it changes with temperature.

4.3.3 Tetrapropyl ammonium iodide (TPAI)

This compound shows a very interesting feature in the ^{13}C CP/MAS NMR spectra (Fig. 4.21) not previously seen in any of the tetraalkyl ammonium halides. Each carbon has four distinct resonances at low temperature (below 224 K). The four methyls are best resolved at 212 K and the C(2) carbon resonances at 190 K where one resonance has a distinct shoulder indicating the fourth chemical shift. The difference in chemical shifts would be much smaller if they were due to intermolecular inequivalencies especially for the inner carbons. The molecular structure, determined by X-ray,[43] shows that the four C-N bond lengths are different. The reason for this is shown to be that each of the four C(1)'s are in different proximity to the iodide. Therefore, the whole molecule is the asymmetric unit.

The spectra also show a marked $T_{1\rho}$ effect at RT and above, and also dipolar broadening. This effect is very strong between 262 and 320 K making the measurement of $T_{1\rho}$ values very difficult. An added difficulty is that there remains three methyl resonances up to 342 K and then two resonances up to 371 K, the high temperature limit of the probe. The methylene resonances do not significantly sharpen until 342 K with C(1) clearly showing two resonances at 364 K. The measurement of $T_{1\rho}$ values was very difficult and no positive results were obtained. Cheng *et al.* have reported,[43] that the motion of the cation detected at 232 K must be librational jumps about a preferred axis and so atomic coordinates can still be measured by X-ray. The colaescence of two of the methylene lines at 226 K and of two of the methyl lines gave free energy values (Table 4.11) from eqn. 15 (section 1.3.4).

Fig. 4.21(a): ^{13}C CP/MAS NMR spectra of $N(Pr)_4I$.

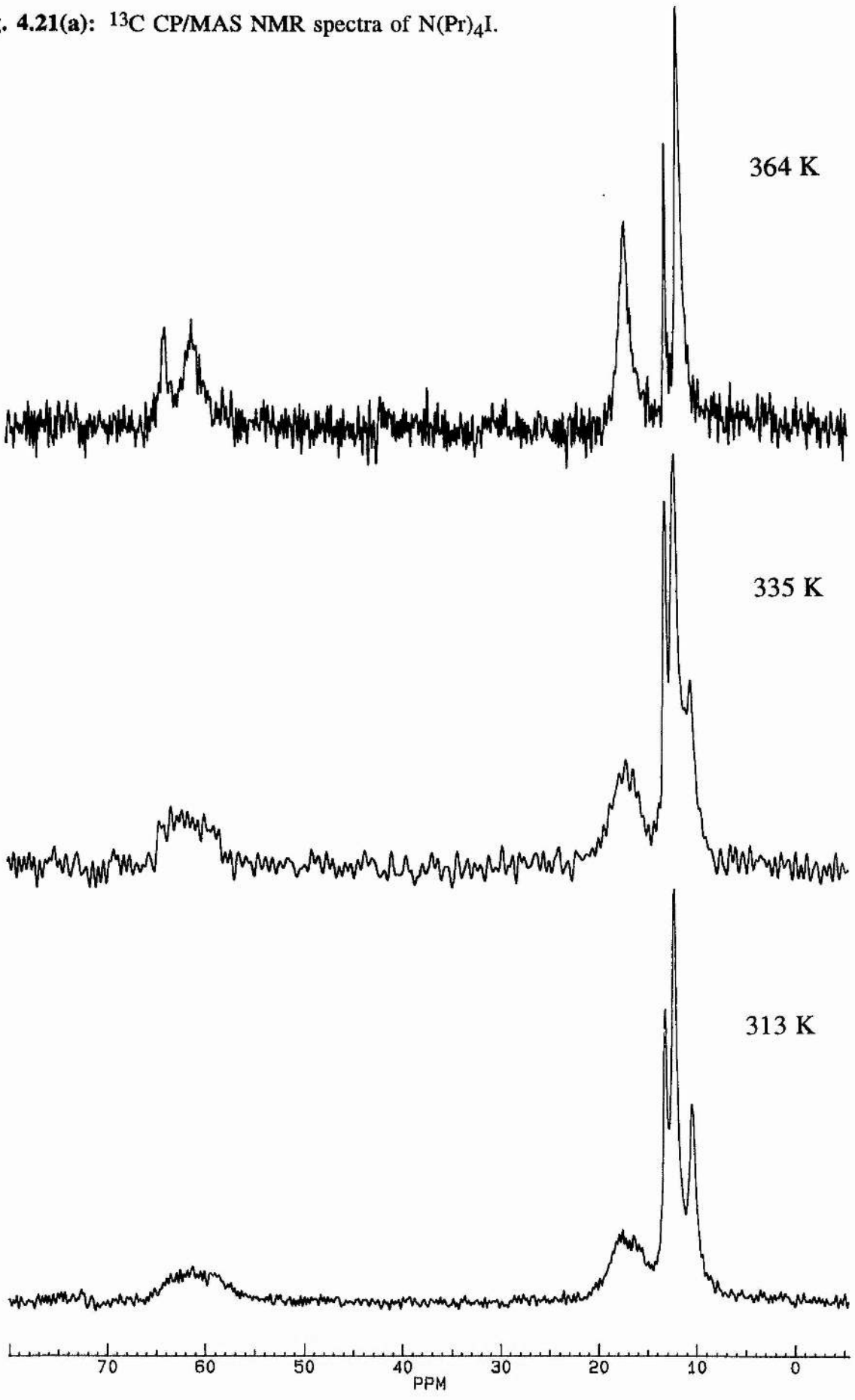

Fig. 4.21(b): ^{13}C CP/MAS NMR spectra of $N(Pr)_4I$.

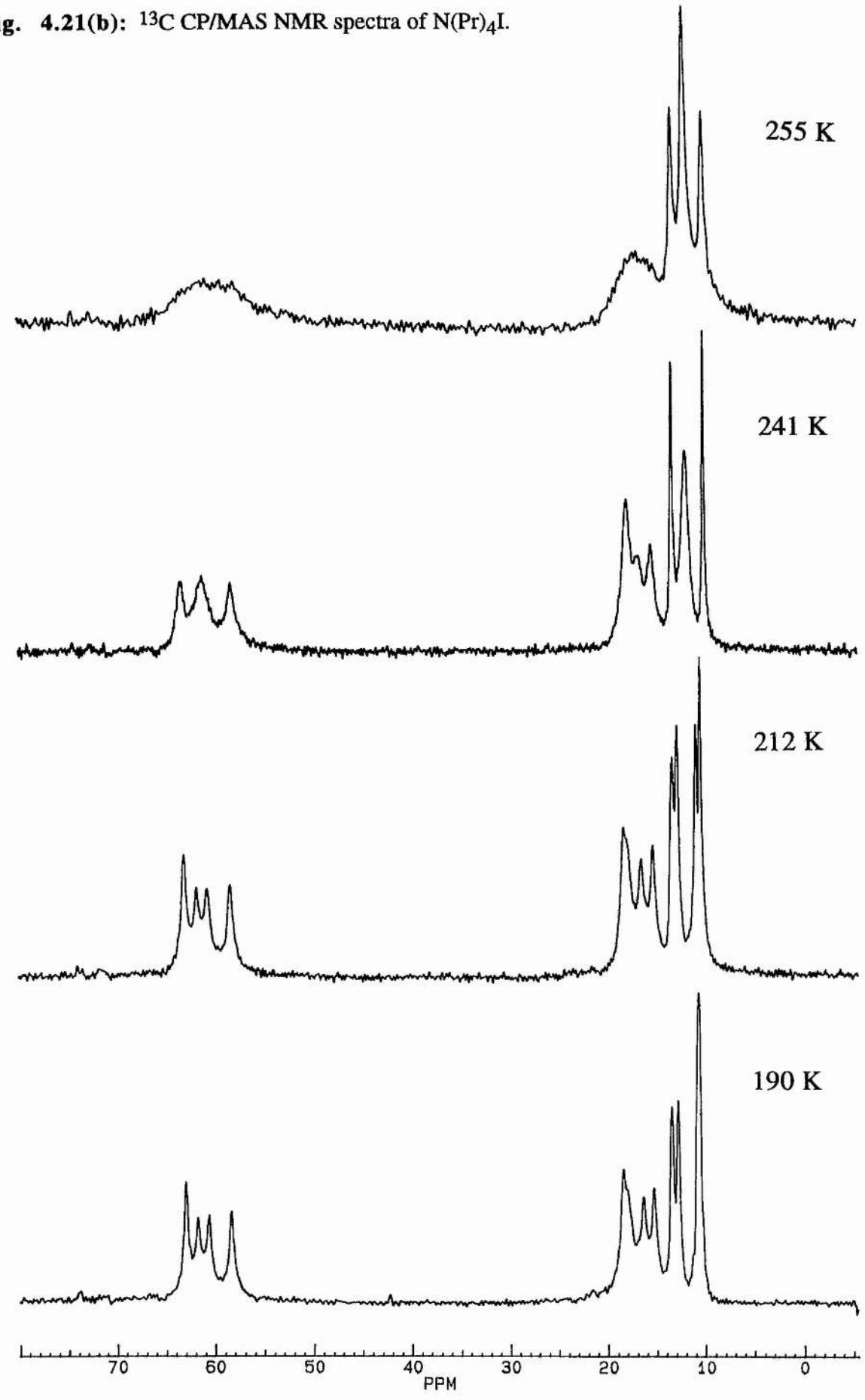

Carbon	T_c (K)	$\Delta\nu$ (Hz)	$\Delta G^{\ddagger}_c$ (kJ mol^{-1})
methyl	241	322	45.5
methylene	226	140	46.9

Table 4.11: Data for the coalescence in TPAI.

Even although there is a small phase change at 225 K the coalescence starts below this and for the methyls continues until 241 K. The molecular motion causing the coalescence is, therefore, independent of the phase change. The apparent coalesence at 262 K, however, is attributed to maximum dipolar broadening. The value for the possible molecular motion of the cation is low for such a large cation.

4.4 Tetrabutyl ammonium halides

The analysis of the bromide and iodide has been carried out by DSC and ^{13}C NMR, by Cheng *et al.* in paper III of their series.[44] The results of the DSC analysis (Table 4.12) show a lower temperature disordering transition and a high temperature isotropisation transition for the iodide and bromide. The bromide also has a minor transition at intermediate temperature. No references for the chloride could be found and so the DSC between 213 and 373 K was undertaken (Appendix 1).

Compound	T_{tr} (K)	ΔS_{tr} (JK^{-1}mol^{-1})
TBACl	284, 317, 343	-41.0, 9.3, 26.1
TBABr	367, 379, 394	41.2, 1.4, 37.6
TBAI	394, 421	71.2, 21.3

Table 4.12: DSC data for TBACl, TBABr and TBAI.

The negative value of entropy for the transition in TBACl at 284 K is possibly due to the formation of HCl as the sample is heated. TBACl is very hygroscopic and so the sample is likely to have contained some water. The DSC measurements were repeated and the same phase changes were recorded. The high temperature phase changes for all the compounds are their melting points.

4.4.1 Tetrabutyl ammonium chloride (TBACl)

The ^{13}C CP/MAS NMR spectra (Fig. 4.22) show four very sharp and distinct resonances ($w_{1/2} \approx 20$ Hz) for the methyls at RT. The three methylene resonances are somewhat broader ($w_{1/2} \approx 200$ Hz) with the C(2) and C(3) resonances split into two and three peaks respectively in the ratio of 1:1:1 and 3:1 whereas C(1) has a possible shoulder up field. The two central methyl resonances coalesce at 270 K. The spectra, therefore, indicate some kind of anion effect similar to that seen for TPAI, but centred on the methyl. The whole molecule, therefore, is the crystallographic asymmetric unit. No high temperature spectra were recorded because of the extreme hygroscopic nature of the sample which results in its melting point becoming reduced even when it is in the probe. No changes in $T_{1\rho}$ values were found over the temperature range.

4.4.2 Tetrabutyl ammonium bromide and iodide (TBABr and TBAI)

These compounds have very similar ^{13}C CP/MAS NMR spectra,[44] showing the methyl resonances in a 2:1:1 ratio at RT and above. The three methylene carbons, however, in TBAI have only one broad resonance apart from at 395 and 402 K where a downfield resonance appears and corresponds to the isotropic resonances at 409 K. In TBABr the ^{13}C T_1 values indicate that motion about the C(2)-C(3) bond becomes significant above the transition at 367 K to the mesophase and results in loss of signal due to $T_{1\rho}$ effects. TBAI, however, is in a plastic state above the transition at 394 K (therefore, cross polarisation becomes very difficult) with additional C(2)-C(3) motion. Therefore, no $T_{1\rho}$ effects can be measured in either compound since significant motion does not start until 367 K and 394 K for TBABr and TBAI respectively.

4.4.4 Tetrabutyl ammonium periodate (TBAP)

This compound is included because it provides a good example of the type of motions involved in the tetrapropyl and tetrabutyl ammonium halides except the motion can be studied by $T_{1\rho}$ measurements. The ^{13}C CP/MAS NMR spectra (Fig. 4.23) show that at 255 K there are four distinct methyl and methylene resonances [C(4) and C(1) respectively], two C(3) resonances (3:1 ratio) and a C(2) resonance with two shoulders. The resonances coalesce at *ca.* 260 K and immediately showing signs of dipolar broadening and a reduction in signal to noise due to $T_{1\rho}$ relaxation.

Fig. 4.22: ^{13}C CP/MAS NMR spectra of $N(Bu)_4Cl$.

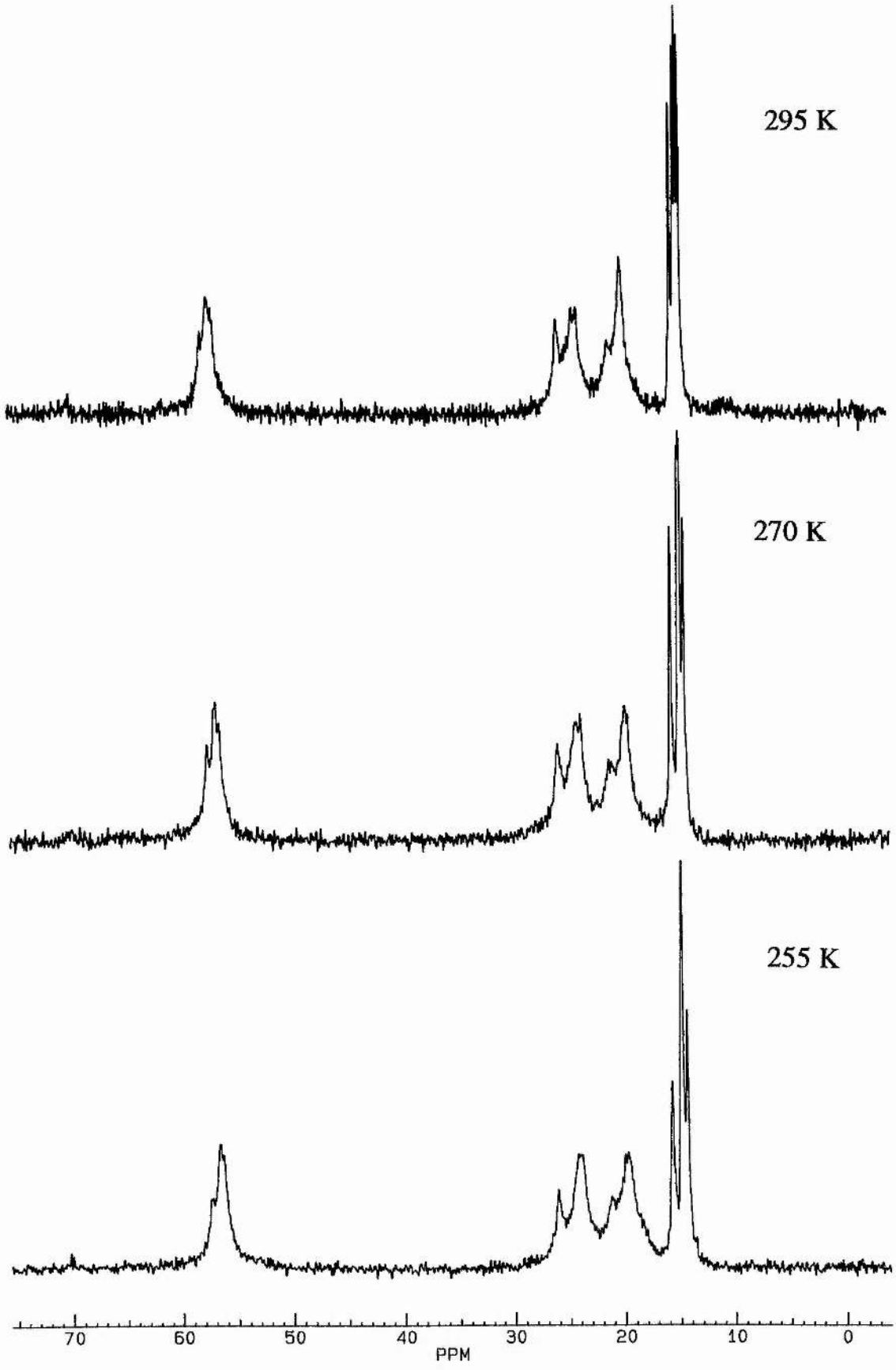

Fig. 4.23: ^{13}C CP/MAS NMR spectra of $N(Bu)_4IO_4$.

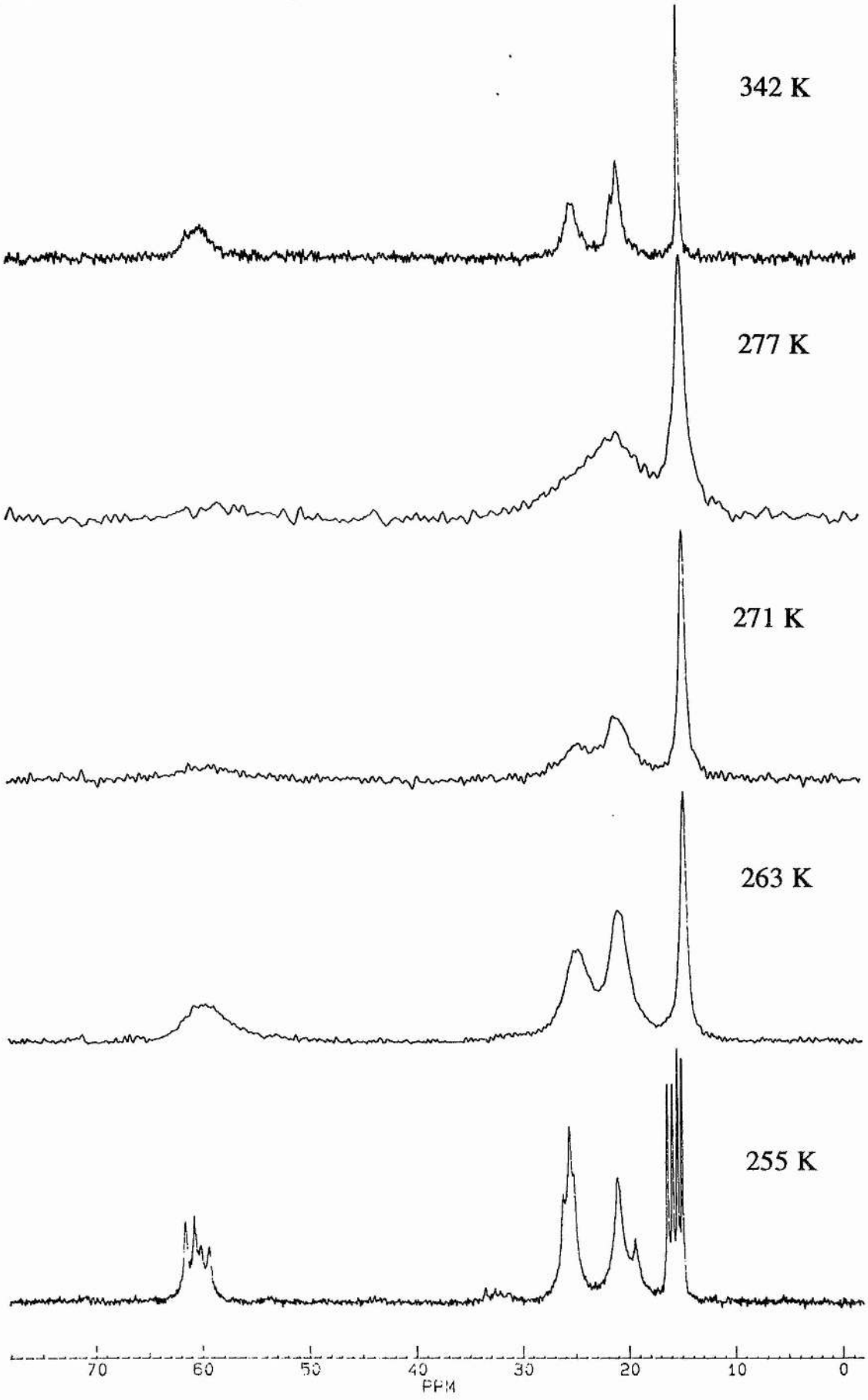

The coalescence of the methyl resonances is not at an average of the four chemical shifts, and so indicates a phase change. The resulting DSC (Appendix 1) showed two very small phase changes at *ca.* 254 K and 258 K and a much larger phase change at 276 K. Therefore, the two small phase changes appears to be responsible for the coalescence. Even although the temperature given for the spectrum at 255 K (Fig. 4.23) this is not completely accurate as there is a temperature gradient in the sample therefore, these two phase changes are taken together. The effect of the large phase change at 276 K is very hard to gauge because the spectra are so broad at this temperature, but no chemical shift change is evident. The apparent coalescence of the C(2) and C(3) resonances may be due to the phase change. It is more likely to be due to maximum dipolar broadening because the two resonances return at higher temperature (Fig. 4.23) when the resonances sharpen. The spectra are very similar to TPAI and to a lesser extent to the three tetrabutyl ammonium halides. The measurement of ^{13}C $T_{1\rho}$ values for the methyl resonance (Fig. 4.24) and methylene resonances [C(1-3)] (Fig.4.25) indicate a minimum is reached for C(4) and C(3).

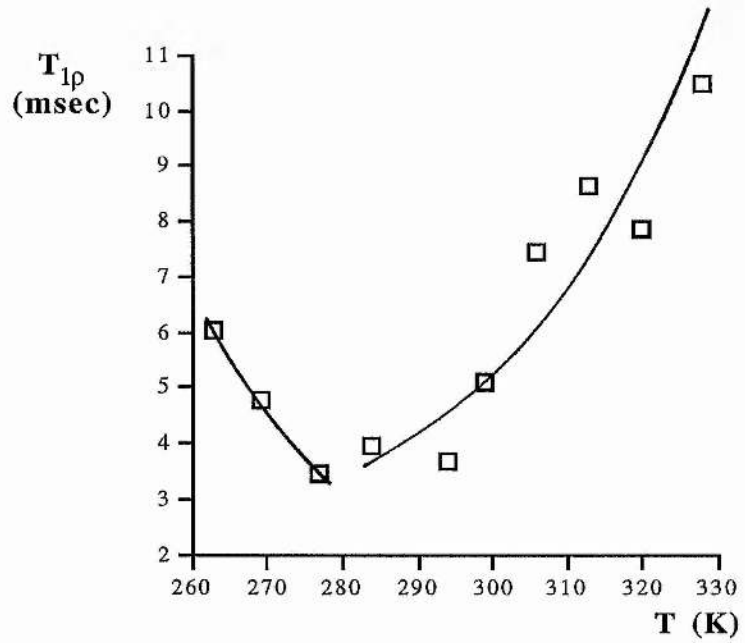

Fig. 4.24: ^{13}C $T_{1\rho}$ plot of the Methyl resonance for TBAP

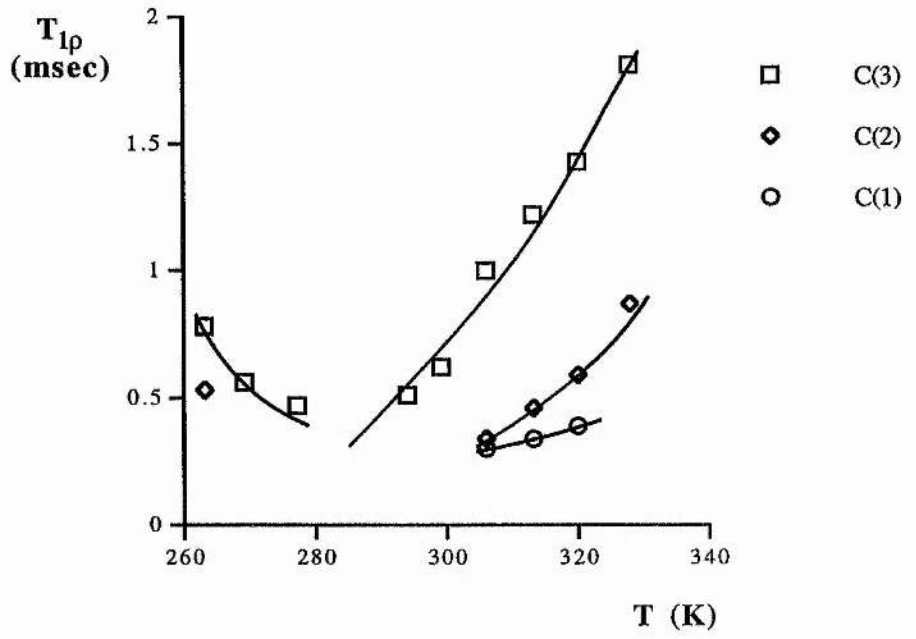

Fig.4.25: ^{13}C $T_{1\rho}$ plot of the Methylene resonances [C(1-3)] for TBAP.

The phase change at 276 K means that the curve cannot be considered as continuous. The $T_{1\rho}$ values must have a discontinuity, as seen in Chapter 3 for the tetraalkylalkanes, but it is difficult to observe because the $T_{1\rho}$ values are very low and are difficult to measure. The data does however, indicate that a minimum is being approached both above and below the transition and so there is not a large jump in the rate of molecular motion between the two phases. As for 3,3-diethylpentane it can be said that below the transition the molecular motion is slower than the spin-lock field and above the transition it is faster than the spin-lock field.

Another aspect of the $T_{1\rho}$ curve to be noted is that the first values that can be measured are at 263 K. This indicates that the two phase changes which initiate the coalescence of resonances also initiate rapid molecular motion.

$T_{1\rho}$ values for C(1) and C(2) could only be measured for a few temperatures because the resonances were of very low intensity and also were subject to extreme maximum dipolar broadening. The low values of T for all three methylenes suggest that the molecular motion is cation tumbling. The methyl T values are higher because of the methyl group rotation which reduces the effect of any motion producing shortening of T values.

The activation energies for the high temperature molecular motion are calculated from the $T_{1\rho}$ values (Table 4.13) from 294-328 K (Fig. 4.26).

Temp (K)	$T_{1\rho}$ [C(1)]	$T_{1\rho}$ [C(2)]	$T_{1\rho}$ [C(3)]	$T_{1\rho}$ [C(4)]
328		0.87	1.81	10.48
320	0.39	0.59	1.43	7.88
313	0.34	0.46	1.22	8.64
306	0.30	0.34	1.00	7.46
299			0.62	5.12
294			0.51	3.67
284			-	3.98
277			0.47	3.4
269			0.56	4.79
263		0.53	0.78	6.03

Table 4.13: $T_{1\rho}$ values (msec) for the four carbon resonances in TBAP. [ω_1 = 53.8 kHz]

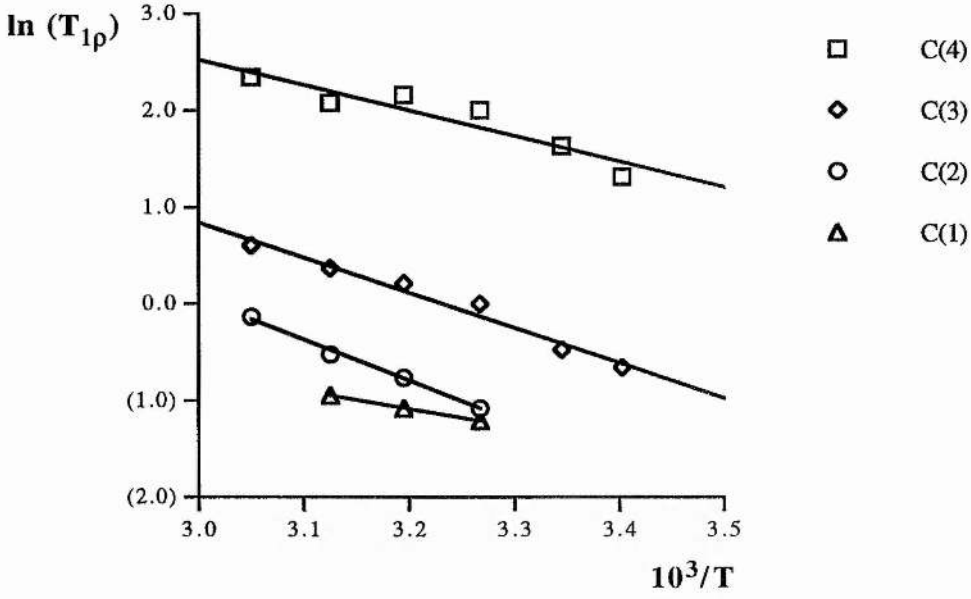

Carbon	E_a (kJ mol^{-1})
4	22.2 ± 3.2
3	30.1 ± 1.8
2	35.1 ± 1.5
1	15.3 ± 1.1

Fig. 4.26: Arrhenius plot and activation energies for the four resonances in TBAP.

The activation energies for the four resonances are in poor agreement with each other. The value for C(1) should be discounted because it is calculated from only three $T_{1\rho}$ values and these appear to be too close to the minimum and so are giving a very low activation energy. The reason for the disparity between the values for the methyl and the other two methylenes is not apparent. The activation energies are also somewhat lower than expected when compared to the TMAX and TEAX compounds studied. The much larger cation should require a larger activation energy as reported for the TEAX series of compounds (E_a = 43 - 70 kJ mol^{-1}),[47] where the low value is for the smallest anion (F^-) and the largest value is for the largest anion (I^-) this is the opposite trend to that for TMAX in the literature.[39] The large anion though may result in a structure such that the cation is placed in a large pocket in the lattice. The interionic forces with such a large anion are generally weak compared to halides for example. This could therefore, help to explain the rather unexpected motion in this large tetraalkyl ammonium salt.

CHAPTER 5

5. Tetraalkyl Phosphonium Halides

The study of tetraalkyl phosphonium halides should give an interesting comparison to the work done on the ammonium halides. In the literature there is only one reference for an NMR study of phosphonium salts and that is for the tetramethyl phosphonium halides (X = Cl, Br, I).[48] The paper uses ^{1}H NMR T_1 relaxation times to study molecular motions in these compounds and gives activation energies for the two motions (i.e. methyl rotation and cation tumbling). The data from the present study can therefore, be compared to this previous work and also to the work done on the tetramethyl ammonium halides in Chapter 4 and references therein.[38-40] The solid-state ^{13}C NMR spectra of tetraethyl and tetrabutyl phosphonium halides have not previously appeared in the literature and so initially a discussion of these will be undertaken. The ammonium salts discussed in Chapter 4 (and references therein),[41-44, 47] will also give an interesting comparison for the higher chain length compounds. In addition the ^{31}P nucleus should be able to provide NMR information to complement that from ^{13}C. Unfortunately ^{31}P NMR could not be undertaken for all the compounds because of a problem with the probe.

5.1 Tetramethyl phosphonium halides

In the paper by Ang and Dunell,[48] a plot of T_1 vs. temperature shows two minima for each of the three halides (X = Cl, Br and I) corresponding to methyl rotation and cation tumbling at low temperature (*ca* 150 - 200 K) and high temperature (*ca* 365-395 K) respectively. The activation energies (Table 5.1) for methyl rotation and cation tumbling are also reported.[48] The activation energies for both processes are much lower for tetramethyl phosphonium chloride and bromide than the corresponding tetramethyl ammonium compounds (Table 4.1). The iodide shows a comparable value for cation tumbling as observed for TMAI (Table 4.1). The activation energy for the methyl rotation in the iodide is higher than the other two halides, but is still about 10 kJ mol^{-1} less than the value observed for TMAI (Table 4.1). DSC was also carried out on the samples between 213 and 373 K and no phase changes were found. This is expected as the ^{1}H T_1 data shows no discontinuities.[48]

Motion	E_a (kJ mol^{-1})
$(CH_3)_4PCl$	
C_3 rotation of CH_3	10.8 ± 0.2
Cation tumbling	37.3 ± 0.8
$(CH_3)_4PBr$	
C_3 rotation of CH_3	10.0 ± 0.3
Cation tumbling	35.6 ± 1.3
$(CH_3)_4PI$	
C_3 rotation of CH_3	14.7 ± 0.17
Cation tumbling	45.2 ± 1.7

Table 5.1: Activation energies and correlation times for tetramethyl phosphonium halides.[48]

The temperature difference between the minima is close to 200 K (Table 5.2) compared to the 100 K separation seen for tetramethyl ammonium bromide and iodide.[39] This confirms that the ^{13}C $T_{1\rho}$ plots as predicted from the activation energies and correlation times should not show overlapping curves from the two molecular motions possible.

	T_1 minima (K)	
Compound	**Methyl rotation**	**Cation tumbling**
$(CH_3)_4PCl$	160	370
$(CH_3)_4PBr$	150	370
$(CH_3)_4PI$	200	390

Table 5.2: Approximate values for the temperature of the T_1 minima for tetramethyl phosphonium halides.[48]

The x-ray structures have also been determined,[48] and show that the chloride and bromide are hexagonal (as seen for $(CH_3)_4AsBr$) and that the iodide has lower symmetry as it could not be indexed to tetragonal (i.e. tetramethyl ammonium halides) or hexagonal. The difference in structure is assumed to be the reason that the iodide shows such different values of activation energies.

5.1.1 Tetramethyl phosphonium chloride (TMPCl)

The ^{13}C CP/MAS NMR spectra of tetramethyl phosphonium chloride (TMPCl) [Fig. 5.1] show at 360 K the phosphorous-carbon coupling (J_{PC} = 54.7 Hz). The resonances then broaden and coalesce at 288 K. The maximum dipolar broadening occurs at *ca* 224 K which is *ca* 20 K lower than the minimum seen for ^{13}C $T_{1\rho}$ (Fig. 5.2). The ^{13}C chemical shift of TMPCl decreases gradually from 10.2 ppm at 360 K to 8.9 ppm at 208 K. This and the fact that the resonance is much broader at low temperature, notwithstanding maximum dipolar broadening, suggests structural changes and reduction of influence from molecular motion.

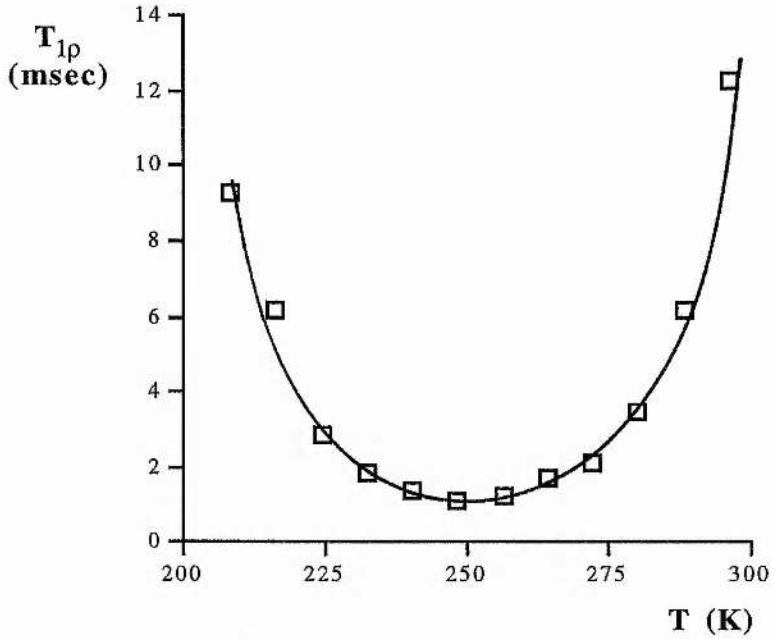

Fig. 5.2: ^{13}C $T_{1\rho}$ plot for TMPCl [49.0 kHz]

The $T_{1\rho}$ plot has a minimum of 1.10 ms at 248 K which is comparable to the minimum for TMABr (0.82 ms) which was lowered slightly by the influence of methyl rotation. The minimum can be used to obtain rate data (Table 5.3), which should confirm which process is causing the modulation of the ^{13}C $T_{1\rho}$ values.

Fig. 5.1: ^{13}C CP/MAS NMR spectra of $P(CH_3)_4Cl$.

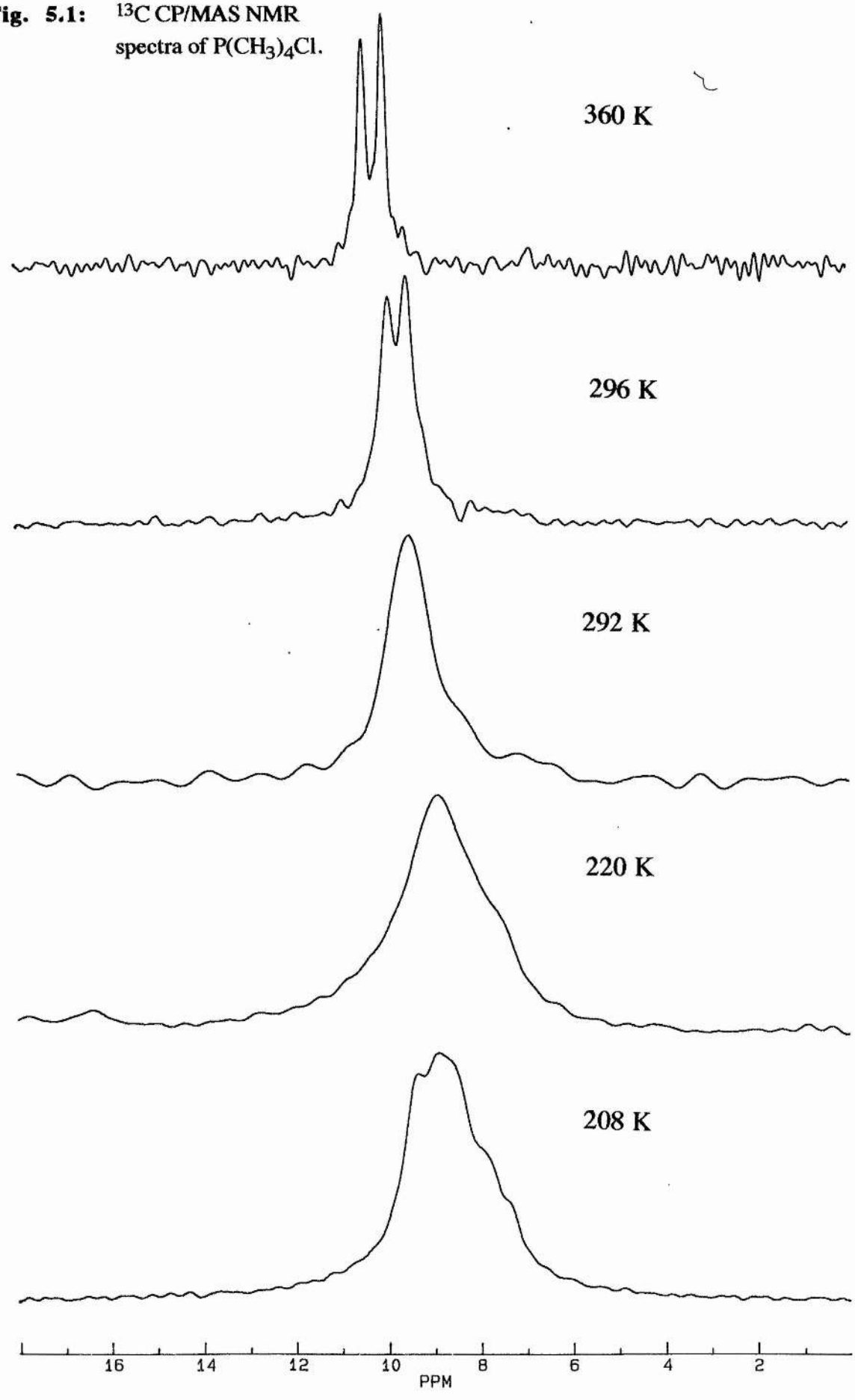

Temp (K)	$T_{1\rho}$ (msec)	k (s^{-1}) x10^6
296	12.2	68.5
288	6.18	34.3
280	3.46	18.9
272	2.13	11.1
264	1.72	8.55
256	1.24	5.08
248	1.10	3.08
240	1.34	1.61
232	1.87	1.00
224	2.84	0.62
216	6.19	0.28
208	9.25	0.18

Table 5.3: $T_{1\rho}$ values and rates for TMPCl [ω_1 = 49.0 kHz and B^2 = 5.60 x 10^8 s^{-2}].

The data from Table 5.3 can then be used to calculate the activation parameters from an Eyring plot (Fig. 5.3).

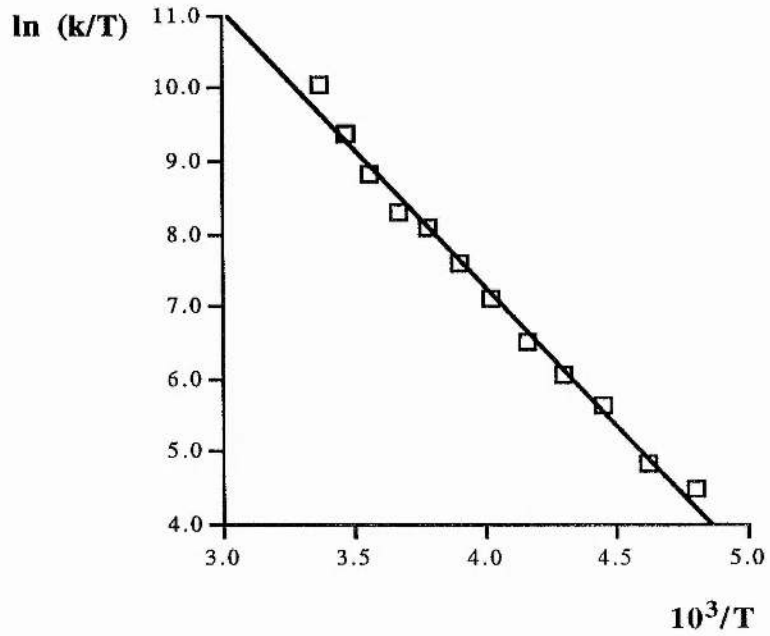

$\Delta H^{\ddagger}$ = +31.7 ± 1.0 kJ mol^{-1}

$\Delta S^{\ddagger}$ = -10.2 ± 3.9 J K^{-1} mol^{-1}

Fig. 5.3: Eyring plot for TMPCl.

The activation energy can also be calculated, from an Arrhenius plot of ln τ vs 1/T and gives E_a = 33.8 ± 1.0 kJ mol^{-1}. The molecular motion causing the interference with the spin lock field (i.e. $T_{1\rho}$ effect) is confirmed as being cation tumbling, because activation energy for methyl rotation is *ca* 11 kJ mol^{-1} (Table 5.1). The activation energy is slightly lower than the literature value for cation tumbling (E_a = 37.3 kJ mol^{-1}) which could be due to water contamination as seen for the tetramethyl ammonium salts (Chapter 4).

5.1.2 Tetramethyl phosphonium bromide (TMPBr)

The solid state ^{13}C CP/MAS NMR spectra (Fig. 5.4) show again the phosphorus-carbon coupling (J_{PC} = 54 Hz) at 360 K with a $w_{1/2} \approx$ 18 Hz for each resonance. The resonance then broadens on cooling as seen for TMPCl until at RT the two resonances are coalescing ($w_{1/2} \approx$ 44 Hz). The coalescence is complete at 272 K with the resonance broadening further ($w_{1/2}$ = 133 Hz) and showing a loss of signal to noise. The resonance continues to broaden until at 224 K it reaches a maximum ($w_{1/2}$ = 583 Hz). The resonance sharpens ($w_{1/2}$ = 377 Hz) and the signal to noise improves as the sample is cooled further to 200 K. The sample therefore, appears to go through a $T_{1\rho}$ minimum which is confirmed by the ^{13}C $T_{1\rho}$ plot for TMPBr (Fig. 5.5) which shows that the minimum is at slightly lower temperature than the chloride (232 K as opposed to 248 K respectively).

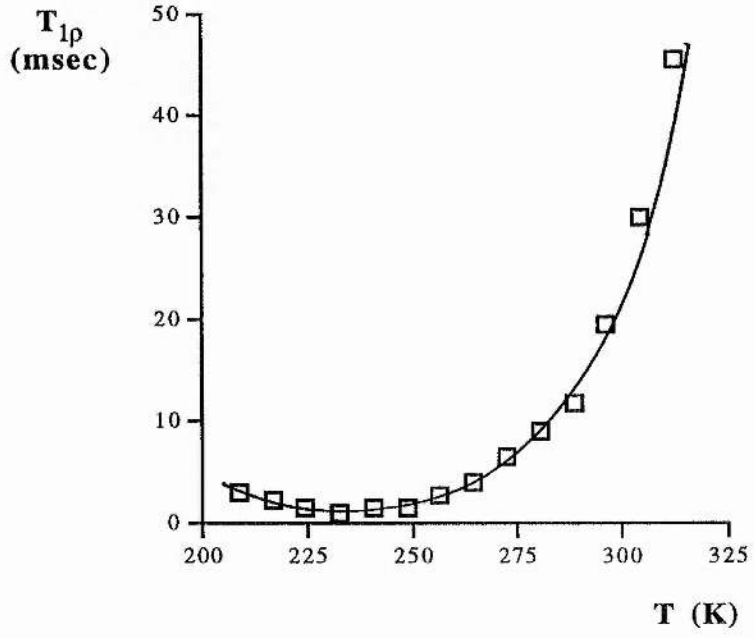

Fig. 5.5: $T_{1\rho}$ plot for TMPBr [ω_1 = 43.5 kHz].

Fig. 5.4: ^{13}C CP/MAS NMR spectra of $P(CH_3)_4Br$.

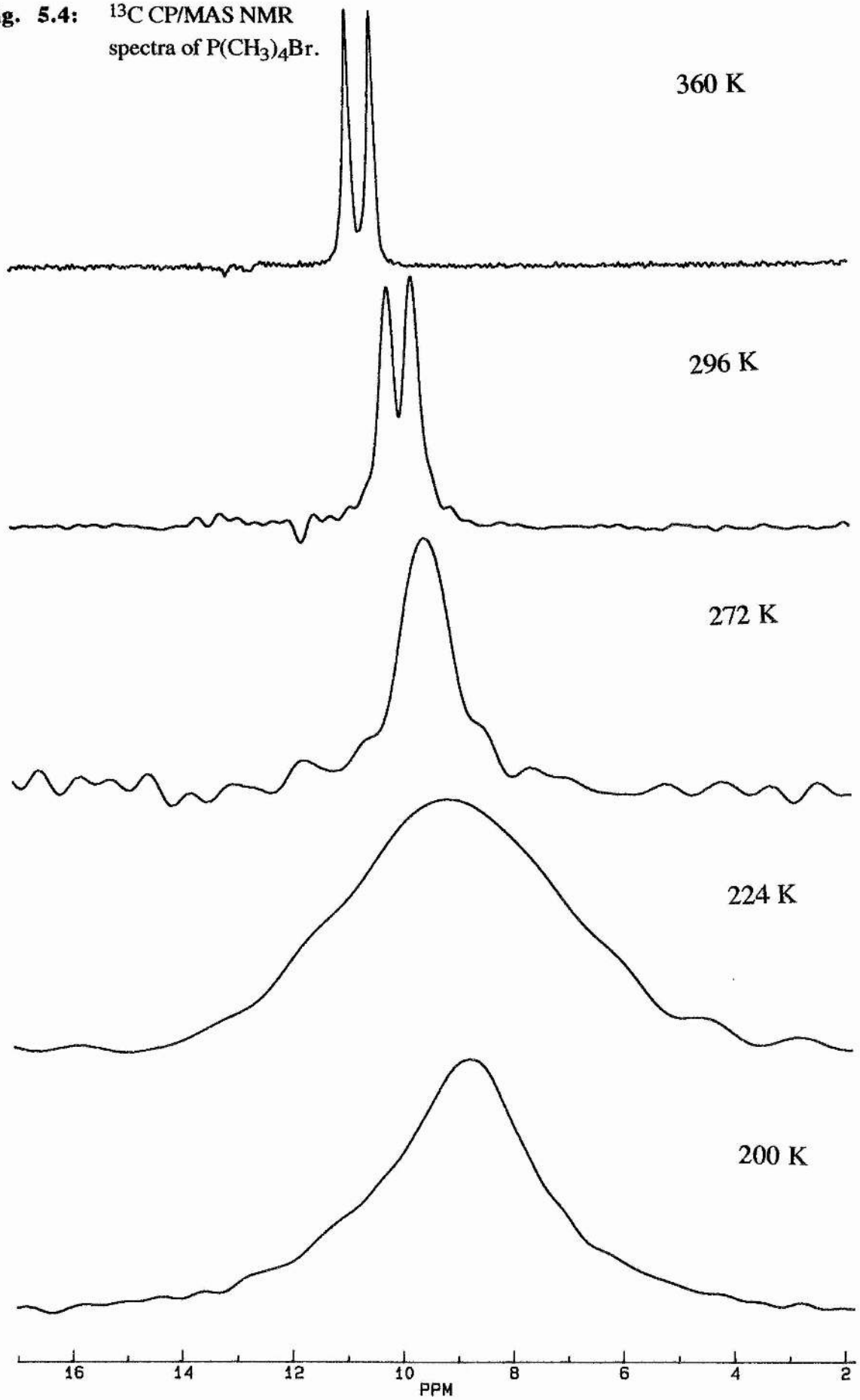

The ^{1}H T_1 minima for the chloride and bromide are both at *ca* 370 K (Table 5.2), therefore the ^{13}C $T_{1\rho}$ minimum would be expected to be at the same lower temperature as seen for TMPCl (Fig. 5.2). The slight difference is because the spin lock field was lower for the bromide, 43.5 kHz compared to 49.0 kHz for the chloride. The low temperature cut off is due to the temperature limitations of the probe set-up.

The $T_{1\rho}$ values can be used to obtain rate data (Table 5.4), because of the $T_{1\rho}$ minimum of 1.13 ms at 232 K. The minimum $T_{1\rho}$ value is comparable to that for TMPCl indicating as expected that cation tumbling is causing the $T_{1\rho}$ effect.

Temp. (K)	$T_{1\rho}$ (msec)	k (x 10^6 s^{-1})
312	45.6	22.02
304	30.0	14.51
296	19.5	9.43
288	11.9	5.75
280	9.20	4.42
272	6.66	3.19
264	4.18	1.98
256	2.71	1.25
248	1.64	0.68
240	1.61	0.67
232	1.13	0.27
224	1.54	0.12
216	2.24	0.074
208	2.96	0.054

Table 5.4: $T_{1\rho}$ values and rates for TMPBr [ω_1 = 43.5 kHz and $B^2 = 4.84 \times 10^8$ s^{-2}].

The activation parameters can then be calculated from an Eyring plot (Fig. 5.6).

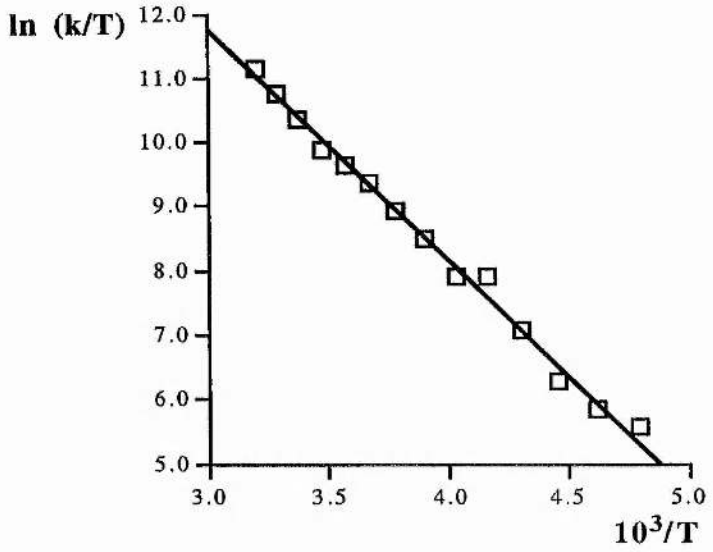

$\Delta H^{\ddagger} = +29.7 \pm 0.75$ kJ mol^{-1}

$\Delta S^{\ddagger} = -11.03 \pm 3.0$ J K^{-1} mol^{-1}

Fig. 5.6: Eyring plot and activation parameters for TMPBr

The activation energy calculated from an Arrhenius plot of ln τ vs 1/T (E_a = 31.8 ± 0.76 kJ mol^{-1}) is smaller than the literature value (E_a = 35.6 kJ mol^{-1}).[48] TMPCl and TMPBr follow the same trend as the literature with the values decreasing slightly.

5.1.3 Tetramethyl phosphonium iodide (TMPI)

The ^{13}C CP/MAS NMR spectra (Fig. 5.7) again shows the phosphorus-carbon coupling above ambient temperature (J_{PC} = 52.8 Hz at 376 K, $w_{1/2}$ = 27 Hz). The coalescence is at 328 K ($w_{1/2}$ = 105 Hz) due to dipolar broadening with the signal to noise also getting worse as the temperature is decreased (Fig. 5.7). The maximum dipolar broadening is at *ca* 256 K ($w_{1/2}$ = 303 Hz) and then the resonance sharpens slightly at 224 K ($w_{1/2}$ = 122 Hz). The ^{13}C chemical shift also decreases gradually from an average of 14.2 ppm at 376 K to 12.7 ppm at 224 K compared to the 10.6 ppm at 360 K to 8.9 ppm at 200 K for the bromide and 10.2 ppm at 360 K to 8.9 ppm at 208 K for the chloride. The difference in chemical shift for the iodide is presumably a result of the different crystal structure reported by Ang and Dunnell.[48] The ^{13}C $T_{1\rho}$ plot (Fig. 5.8) shows shows that the minimum is at higher temperature (272 K) than TMPCl and TMPBr.

Fig. 5.7: ^{13}C CP/MAS NMR spectra of $P(CH_3)_4I$.

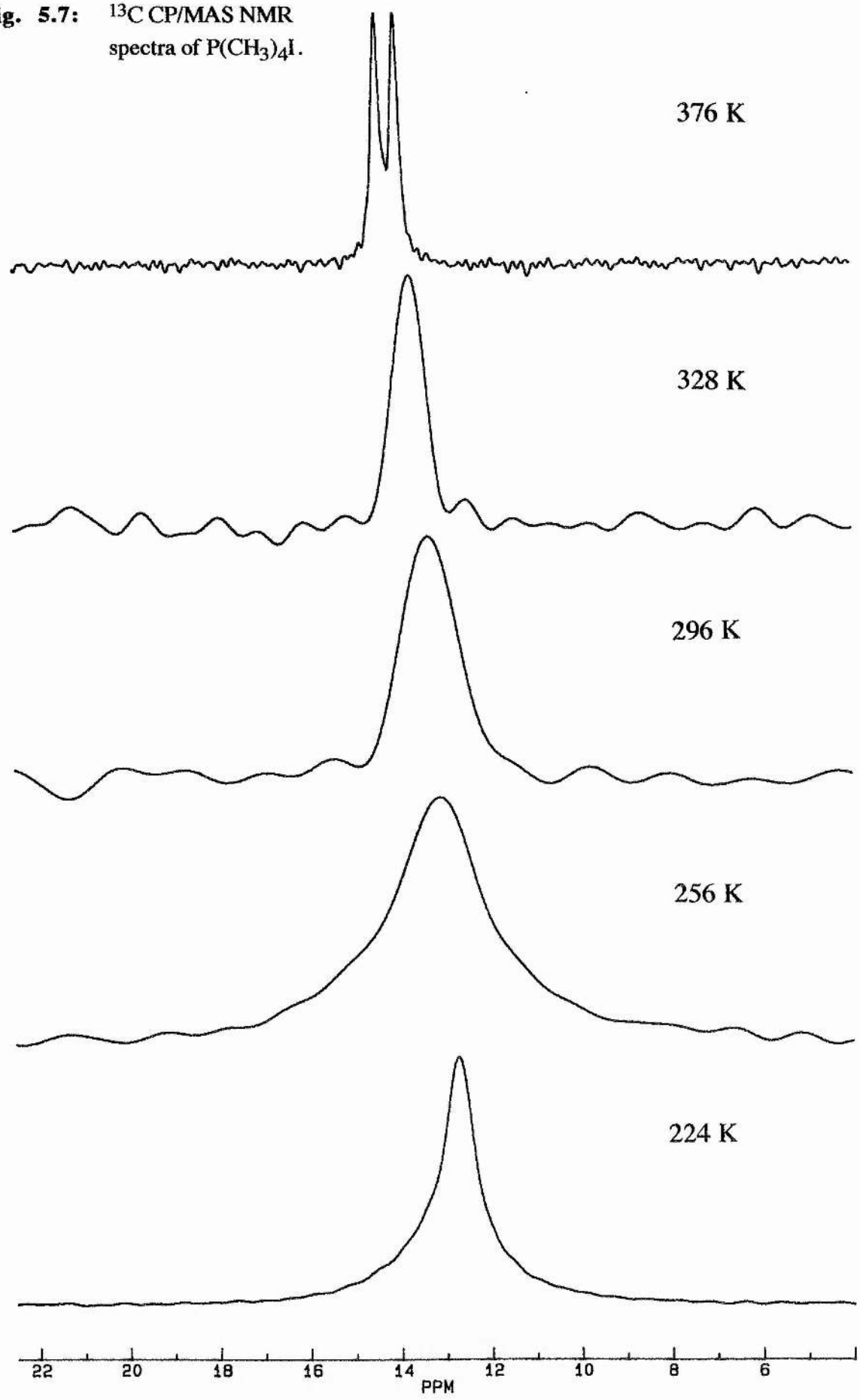

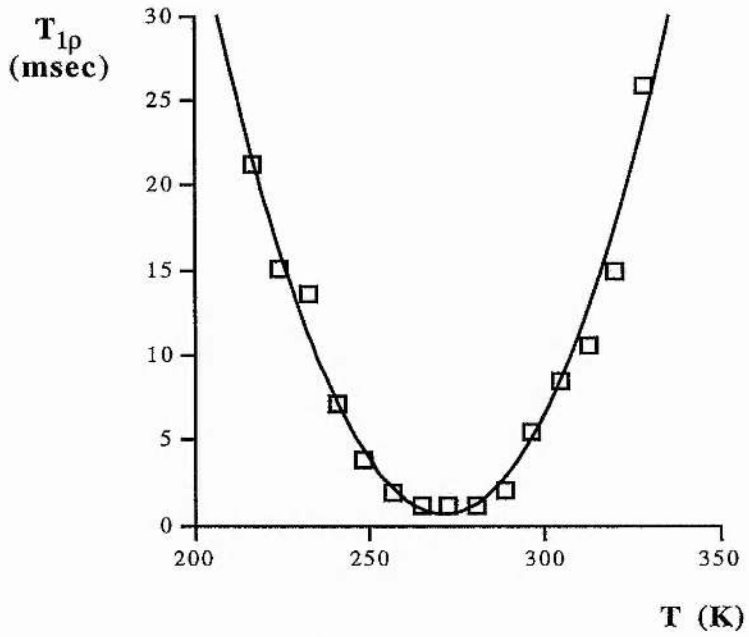

Fig. 5.8: ^{13}C $T_{1\rho}$ plot for TMPI [ω_1 = 48.1 kHz].

The minimum of the ^{13}C $T_{1\rho}$ plot at 272 K of 1.14 msec allows the calculation of rates (Table 5.5). The minimum is very similar to the previous two compounds (i.e. 1.10 msec for TMPCl and 1.13 msec for TMPBr).

Temp (K)	$T_{1\rho}$ (msec)	k (x 10^5 s^{-1})
328	25.9	137
320	15.0	79.4
312	10.7	56.5
304	8.51	44.8
296	5.46	28.7
288	2.01	9.71
280	1.19	4.07
272	1.14	3.02
264	1.18	2.32
256	1.95	0.97
248	3.84	0.46
240	7.22	0.24
232	13.6	0.13
228	15.1	0.12
220	21.2	0.081

Table 5.5: ^{13}C $T_{1\rho}$ values and rates for TMPI [ω_1 = 48.1 kHz and B^2 = 5.30 x 10^8 s^{-2}].

The rates are used in an Eyring plot to calculate activation parameters (Fig. 5.9).

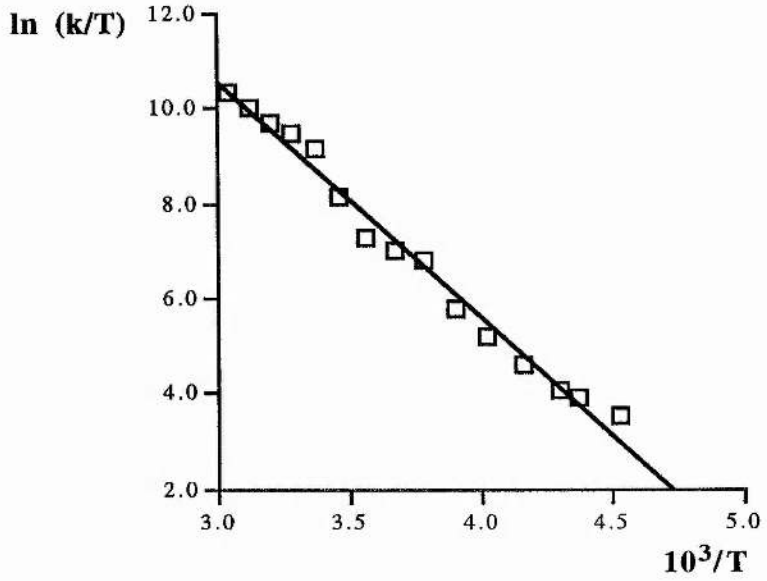

$\Delta H^{\ddagger} = +41.9 \pm 1.5$ kJ mol^{-1}.
$\Delta S^{\ddagger} = +17.1 \pm 5.8$ J K^{-1} mol^{-1}.

Fig. 5.9: Eyring plot for and activation parameters for TMPI.

The activation energy was also calculated from an Arrhenius plot ($E_a = 44.1 \pm 1.6$ kJ mol^{-1}) and is inside the confidence limits for the activation energy in the literature ($E_a = 45.2 \pm 1.7$ kJ mol^{-1}).[48] The iodide sample was presumably purer than the chloride and bromide i.e. contained less water. The entropy of activation of the iodide is positive, whereas the values for the chloride and bromide are both negative. This again is presumably due to the difference in crystal structure. The iodide presumably has a crystal structure of lower symmetry which leads to a higher activation energy for the cation tumbling. Any motion of the cation also causes more of a disturbance to the lattice whereas the molecular motion in TMPCl and TMPBr seems to be correlated. The structure of TMABr is tetragonal and this also has a negative entropy of activation for cation tumbling. Negative $\Delta S^{\ddagger}$ values have been reported before, [7,18-20,49] for t-butyl and -$N(Me)_3$ rotation where following the principle of least distress the rotation causes minimum lattice distortion.

5.2 Tetraethyl phosphonium halides

No references to dynamic NMR studies or DSC analysis of tetraethyl phosphonium halides could be found in the literature. The compounds were analysed by DSC (Appendix 1) to find the phase changes and entropies of transition (Table 5.6).

Compound	T_{tr} (K)	ΔS_{tr} (J K^{-1} mol^{-1})
TEPCl	341	10.9
TEPBr	339, 365	24.1 , 19.3
TEPI	368, ~383	20.9 , <10

Table 5.6: DSC data for the tetraethyl phosphonium halides.

On comparison to the DSC data for the tetraethyl ammonium bromide and iodide (Table 4.4) the entropies are smaller and at lower temperature. Tetraethyl ammonium chloride has a phase changes with similar entropy and at comparable temperatures. The size of the second phase change in TEPI is estimated to be small as it was not possible to calculate a value. The three phosphonium compounds are all slightly different to each other but all have phase changes which are likely to be associated with different molecular motion in the compounds.

5.2.1 Tetraethyl phosphonium chloride (TEPCl)

The ^{13}C CP/MAS NMR spectra for TEPC (Fig. 5.10) show the methylene resonance at *ca* 13.0 ppm and the methyl at *ca* 6.7 ppm. The ^{13}C chemical shift of the methylene undergoes a gradual change with temperature from 12.7 ppm at 208 K up to *ca* 13.3 ppm at 368 K while the methyl resonance (*ca* 6.7 ppm) does not show any change with temperature. The linewidths show no change from 208 K up to 296 K, the resonances then begin to broaden with the methylene ($w_{1/2}$ = 118 Hz) and the methyl ($w_{1/2}$ = 31 Hz) at 296 K to $w_{1/2}$ = 272 Hz and 46 Hz respectively at 368 K. This dipolar broadening again indicates that a variation of ^{13}C $T_{1\rho}$ with temperature can be measured (Fig. 5.11).

Fig. 5.10: ^{13}C CP/MAS NMR spectra of $P(Et)_4Cl$.

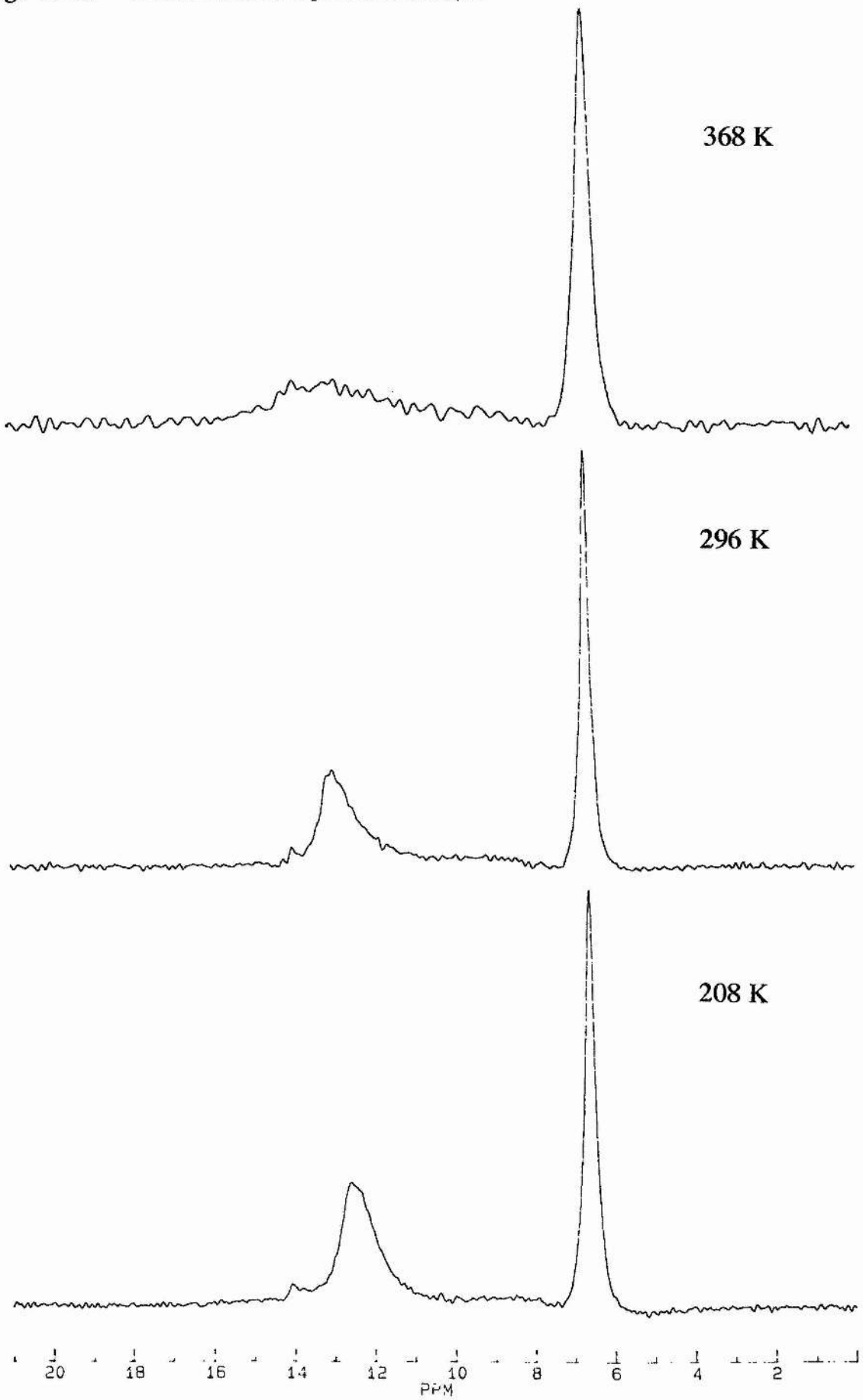

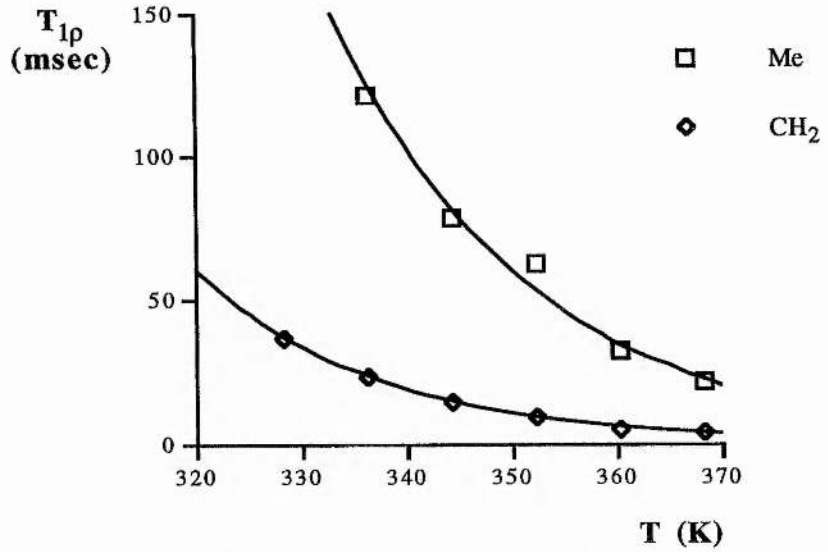

Fig. 5.11: ^{13}C $T_{1\rho}$ plot for TEPCl [ω_1 = 50.0 kHz].

The methyl $T_{1\rho}$ values are greater than the CH_2 $T_{1\rho}$ values suggesting the process is not methyl rotation. This leaves molecular reorientation in the solid or ethyl group rotation. The motion causing the interference with the spin lock field unfortunately is at the high temperature limit of the probe and so only five points could be obtained.

The ^{31}P $T_{1\rho}$ values were also measured (Fig. 5.12) and are much more accurate due to the difference in relative sensitivity of carbon and phosphorus (*ca* 1:4) and that ^{31}P is 100 % abundant and ^{13}C is 1.11 % abundant. The signal for phosphorus is very strong and therefore, the signal to noise ratio is very much better. This is very important at around the $T_{1\rho}$ minimum and where good signal to noise is still possible whereas for ^{13}C the signal becomes so poor that no data can be recorded.

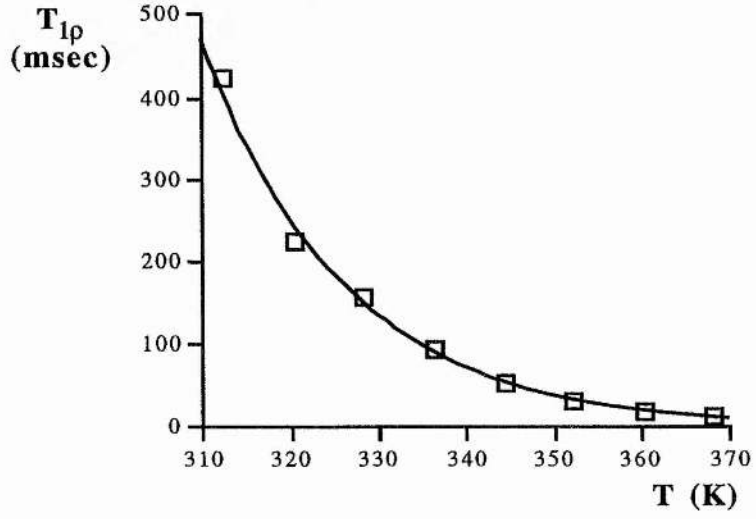

Fig. 5.12: ^{31}P $T_{1\rho}$ plot for TEPCl [ω_1= 51.0 kHz].

The $T_{1\rho}$ values (Table 5.7) were used to obtain activation energies for the process from the methyl, methylene and the central phosphorus. (Fig. 5.13).

T (K)	CH_3	CH_2	P
368	21.9	3.84	12.1
360	32.7	5.39	20.0
352	62.3	9.33	33.1
344	79	14.6	54.1
336	121	24	93.6
328		37.2	156
320			224
312			423

Table 5.7: ^{13}C and ^{31}P $T_{1\rho}$ values (msec) for TEPCl.

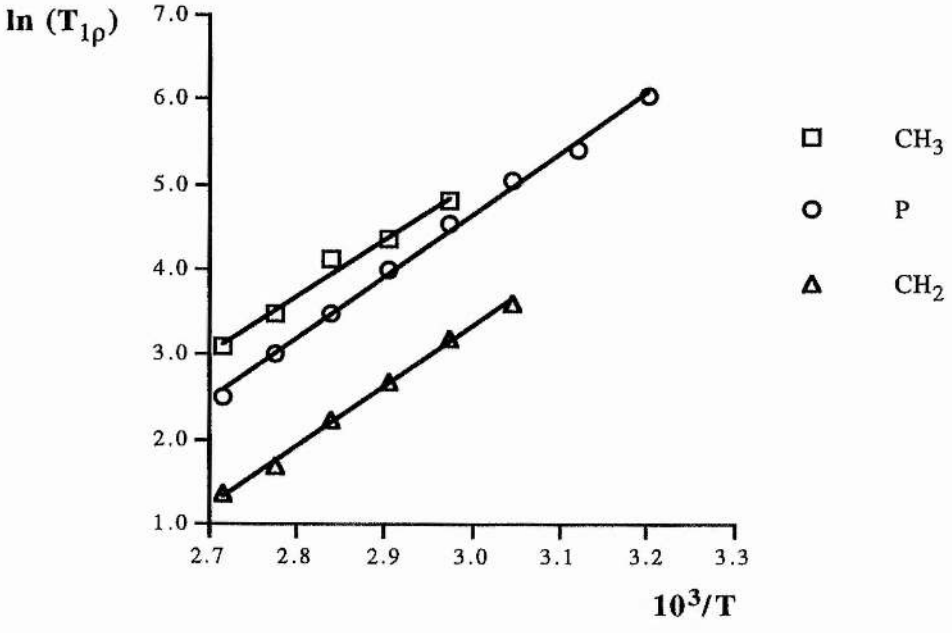

methyl: $E_a = 55.3 \pm 4.7$ kJ mol^{-1}
methylene: $E_a = 58.5 \pm 1.5$ kJ mol^{-1}
phosphorus: $E_a = 60.0 \pm 1.5$ kJ mol^{-1}

Fig. 5.13: Arhenius plot for TEPCl

The correlation between the three different activation energies is good. The methyl ^{13}C $T_{1\rho}$ values are somewhat unreliable because they are so large. The large

^{31}P $T_{1\rho}$ values are more reliable because of the very strong signal for phosphorus as has already been discussed.

Ethyl group rotation in the series TEAX (X = halogen) is restricted for steric reasons,[43] but an activation energy of 50.3 kJ mol^{-1} for TEACl,[47] was measured using second moments. In section 4.2.1 current results suggest a value of 60.5 kJ mol^{-1} which also fits in better with the results for the bromide and iodide in the literature (*ca* 65 kJ mol^{-1}). The activation energy obtained for TEPC, therefore, is in good agreement with these results considering that steric hindrance should be relieved to some extent by the larger phosphorus cation. The $T_{1\rho}$ values themselves with much higher values for the methyl group as opposed to the methylene also indicate that the motion is centred on the carbon phosphorus bond and not on the carbon-carbon bond. The possibility that the motion is cation tumbling cannot be discounted because these activation energies are *ca* 4-5 kJ mol^{-1} higher than the values for ethyl rotation,[47] for the TEAX compounds (Table 4.5). Another indication that the results are due to ethyl rotation is that no modulation of $T_{1\rho}$ could be found down to 208 K. The results of Szafranska show that the onset of significant motion of the ethyl groups and the cation are only separated by *ca* 30-45 K. Therefore, if it was cation tumbling causing the modulation then the effect of ethyl group rotation should be observed at lower temperatures.

5.2.2 Tetraethyl phosphonium bromide (TEPBr)

The ^{13}C CP/MAS NMR spectra (Fig. 5.14) of TEPBr show two resonances. The methylene resonance changes gradually from 11.9 ppm at 255 K to 13.2 ppm at 349 K. The methyl resonance changes gradually from 7.47 ppm at 255 K to 7.60 ppm at 373 K. The change in linewidths of the two resonances with temperature is given in Table 5.8.

	linewidth (Hz)	
Temp (K)	**CH_2**	**CH_3**
349	34, 42	33
320	137	31
294	258	57
277	599	100
255	236	43

Table 5.8: Change in linewidth ($w_{1/2}$) with temperature for TEPBr.

Fig. 5.14: ^{13}C CP/MAS NMR spectra of $P(Et)_4Br$.

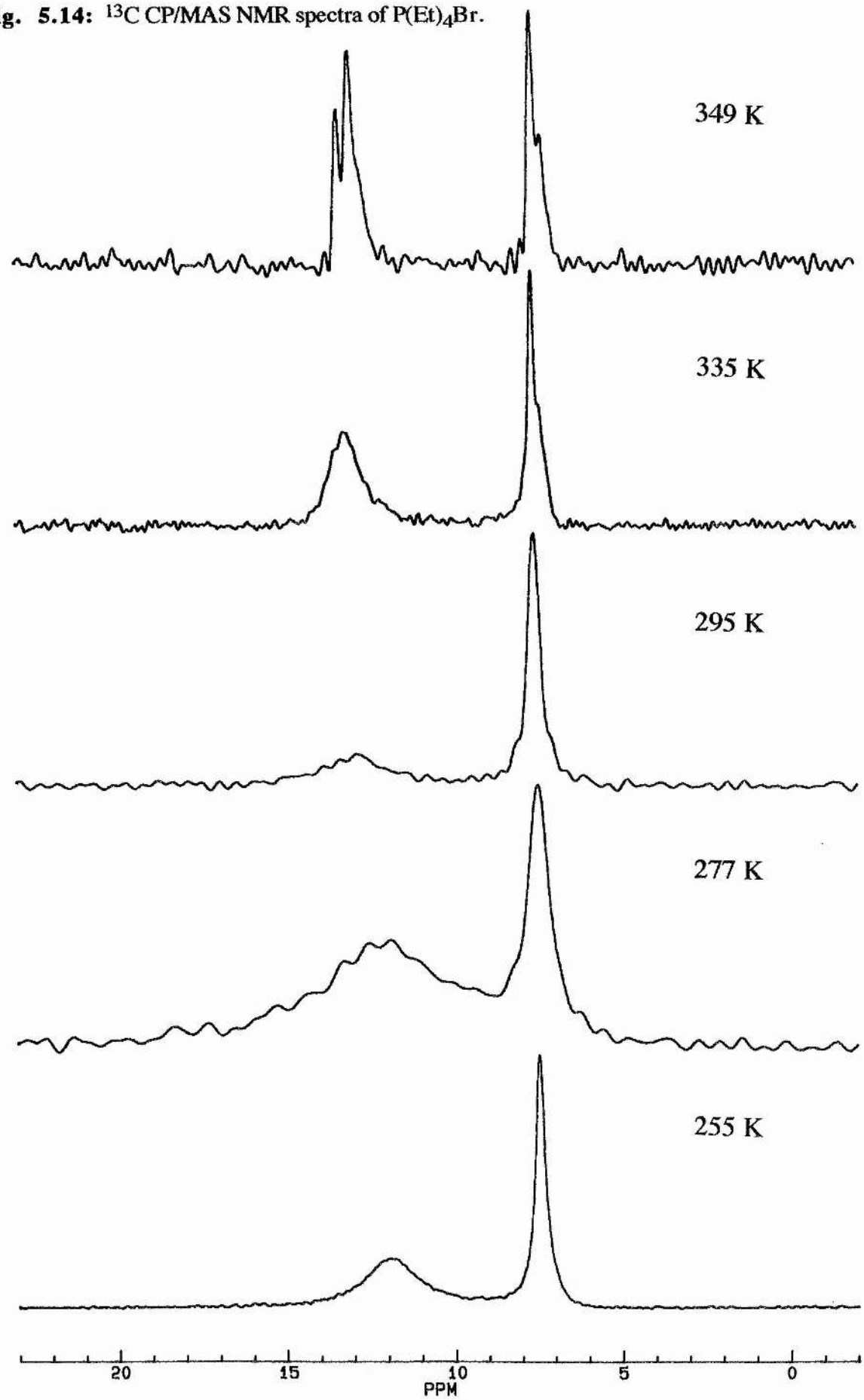

The largest linewidth recorded at 277 K is very close to the ^{13}C $T_{1\rho}$ minimum at 270 K (Fig. 5.16). The $T_{1\rho}$ plot shows that the minima for the methyl and methylene come at the same temperature. The lower values for the methylene indicate that the motion modulating the $T_{1\rho}$ relaxation is not methyl rotation. The motion is likely to be ethyl rotation as reported for 3,3-diethylpentane, TEACl and TEPCl.

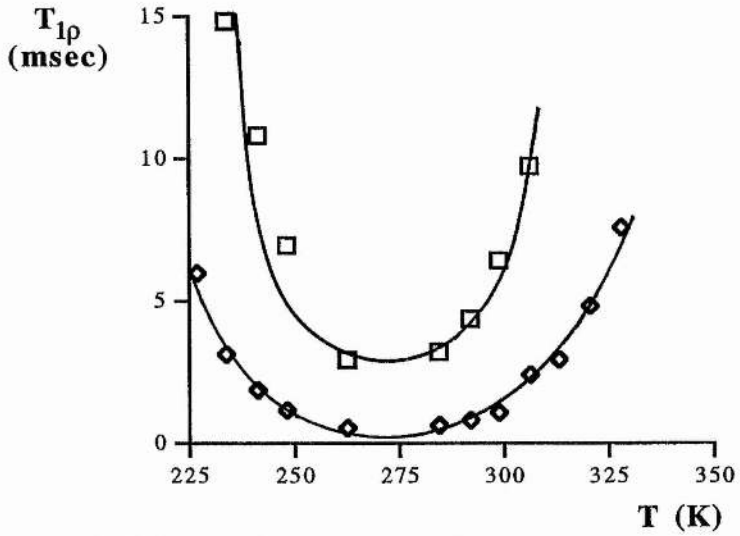

Fig. 5.15: ^{13}C $T_{1\rho}$ plot for methylene in TEPBr.

The minimum of 0.48 msec and 2.49 msec for the methylene and methyl carbons respectively allow the calculation of the rate data (Table 5.9).

	Methylene		*Methyl*	
Temp (K)	**$T_{1\rho}$ (msec)**	**k (x 10^5 s^{-1})**	**$T_{1\rho}$ (msec)**	**k (x10^5 s^{-1})**
327	7.59	103.4	-	-
320	4.86	66.2	-	-
313	2.94	39.8	-	-
306	2.46	33.2	9.79	25.32
299	1.13	14.7	6.44	16.23
293	0.86	10.7	4.41	10.58
277	0.68	7.94	3.27	7.09
263	0.6	1.64	2.95	1.80
248	1.15	0.71	7.00	0.60
241	1.89	0.42	10.8	0.38
233	3.11	0.25	14.9	0.28
227	6.04	0.13	-	-

Table 5.9: Data for the methylene and methyl carbons in TEPBr [ω_1= 52.1 kHz; B^2 =1.36 x 10^9 (methylene) and B^2 = 2.63 x 10^8 (methyl)].

The data for the methyl and methylene are of the same magnitude and so the rate values were combined for the Eyring plot (Fig. 5.16).

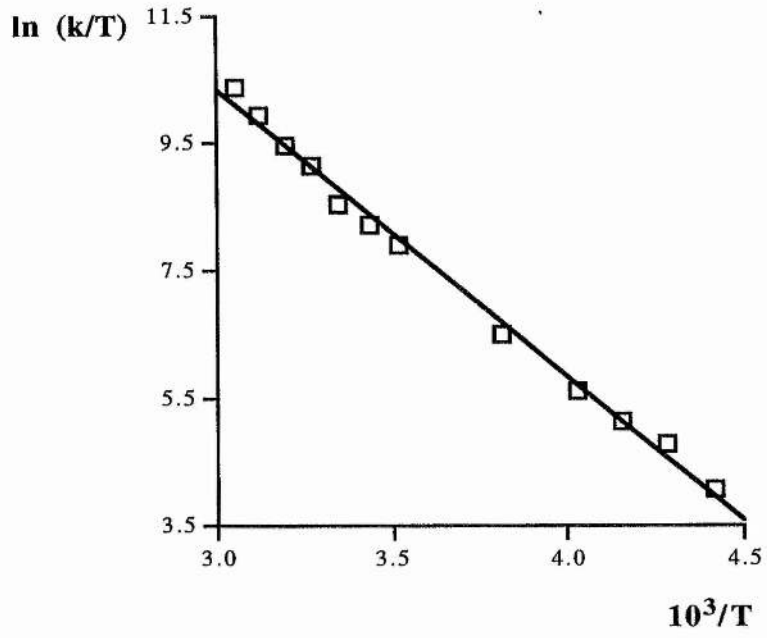

$\Delta H^{\ddagger} = +37.4 \pm 0.9$ kJ mol^{-1}
$\Delta S^{\ddagger} = +0.30 \pm 3.5$ J K^{-1} mol^{-1}

Fig. 5.16: Eyring plot for the combined data for the methyl and methylene in TEPBr.

The activation energy ($E_a = 39.5 \pm 1.0$ kJ mol^{-1}) calculated from an Arrhenius plot of ln τ vs 1/T is somewhat lower than the value for TEABr ($E_a = 65.0$ kJ mol^{-1}).[47] The value would be expected to be a lot lower because of the reduction in steric hindrance due to the larger phosphorus atom. A large drop in activation energy is seen for methyl rotation when going from nitrogen to phosphorus in the tetramethyl compounds (e.g. TMABr; $E_a = 27$ kJ mol^{-1},[39] and TMPBr; $E_a = 10$ kJ mol^{-1},[48]).

The ^{31}P $T_{1\rho}$ values were also recorded (Fig. 5.17) and show that the minimum is at higher temperature than the ^{13}C data. The spin-lock field is larger and this accounts for the difference.

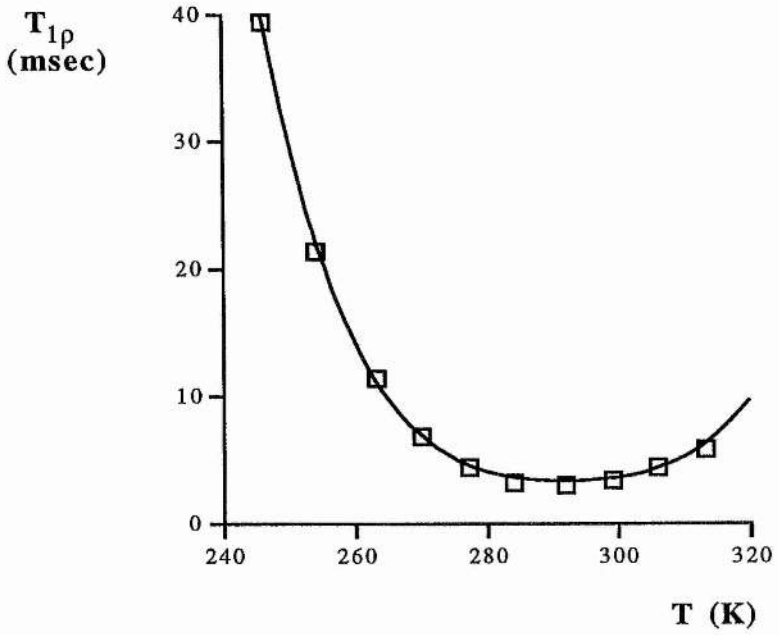

Fig. 5.17: ^{31}P $T_{1\rho}$ plot for TEPBr [ω_1 = 61.0 kHz].

The ^{31}P $T_{1\rho}$ minimum of 3.08 msec at 292 K allows the calculation of rates for the molecular motion (Table 5.10).

Temp (K)	$T_{1\rho}$ (msec)	k (x 10^5 s^{-1})
313	5.93	13.69
306	4.50	9.71
299	3.48	6.33
292	3.08	3.83
284	3.30	2.63
277	4.42	1.56
269	6.84	0.91
263	11.55	0.52
255	21.45	0.28
248	39.39	0.15

Table 5.10: ^{31}P $T_{1\rho}$ values and rate data for phosphorus in TEPBr [ω_1 = 61.0 kHz and $B^2 = 2.49 \times 10^8$]

The resulting Eyring plot (Fig. 5.18) shows that the data gives a very good fit.

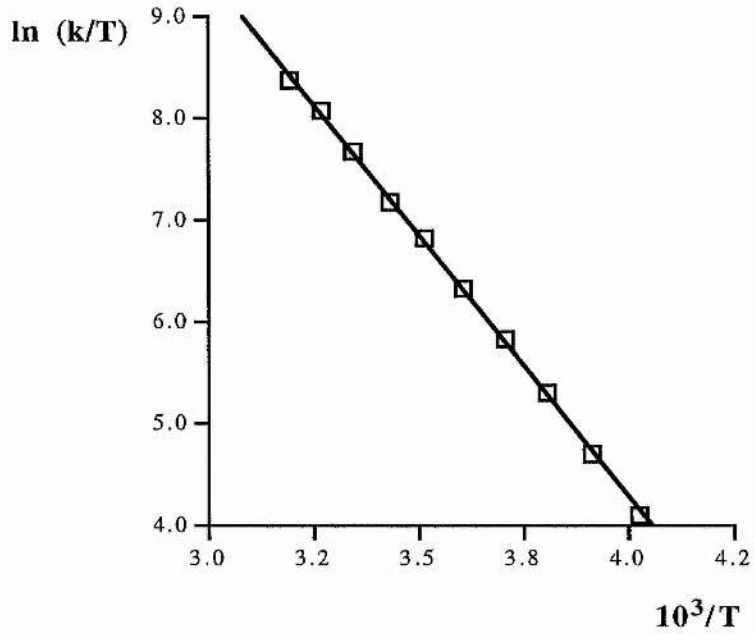

$\Delta H^{\ddagger} = +42.8 \pm 0.39$ kJ mol^{-1}
$\Delta S^{\ddagger} = +9.28 \pm 1.4$ J K^{-1} mol^{-1}

Fig. 5.18: Eyring plot for phosphorus in TEPBr.

The activation energy (E_a = 45.1 kJ mol^{-1}) was calculated from the Arrhenius plot of ln τ vs. 1/T. The activation energy calculated from ^{31}P $T_{1\rho}$ data is larger than that calculated from the ^{13}C $T_{1\rho}$ data. The drop of around 20 kJ mol^{-1} in activation energy from TEABr (E_a =65.0 kJ mol^{-1}) is comparable to the literature values for the TMAX,[39] and TMPX,[48] compounds. The entropy of activation is low indicating that the molecular motion does not cause too much stress on the structure as seen for TEACl.

5.2.3 Tetraethyl phosphonium iodide (TEPI)

The ^{13}C CP/MAS NMR spectra (Fig. 5.19) show that from 224 K up to *ca* 352 K the methyl resonance sits on top of the broad methylene resonance. The ^{13}C chemical shift of the methyl resonance changes between 8.40 ppm at 295 K and 7.89 ppm at 368 K [Fig. 5.19(a)]. The ^{13}C chemical shift of the methylene can only be given above 352 K and is 12.35 ppm at 360 K and 12.80 ppm at 368 K because it is underneath the methyl resonance at lower temperatures. The methyl resonance broadens slightly from, $w_{1/2}$ = 88 Hz at 224 K to 104 Hz from 296 - 352 K. At 360

K, $w_{1/2}$ = 61 Hz (methyl) and $w_{1/2}$ = 299 Hz (methylene) and then at 368 K they have sharpened, $w_{1/2}$ = 21 Hz and 109 Hz for the methyl and methylene resonances respectively. Above 368 K the sample seems to be in two phases with two methyl resonances at 7.88 ppm ($w_{1/2}$ = 15 Hz) and 8.25 ppm ($w_{1/2}$ = 33 Hz), with the downfield resonance *ca* 2/3 as intense as the upfield resonance. Take note the methyl is broadening now! The methylene shows a broad resonance at 12.96 ppm ($w_{1/2} \approx$ 110 Hz) and then sharp resonances at 14.09 ppm and 12.96 ppm ($w_{1/2} \approx$ 14 Hz) which are split by the phosphorus (J_{PC} = 49.05 Hz). The downfield methyl resonance at 384 K is now 1/3 as intense as the upfield resonance. The downfield resonance has $w_{1/2}$ = 18 Hz (i.e. sharpening again) and the upfield resonance has $w_{1/2}$ = 16 Hz.

The phase change recorded at 368 K (Table 5.6) results in the appearance of a sharp phase which coexists with the original phase right up to 384 K [Fig. 5.19(a)]

Inspection of the broad hump under the methyl resonance indicates that the methylene resonance also broadens somewhat from 224 K to 296 K [Fig. 5.19(b)] and at 352 K [Fog. 5.19(a)] it has all but disappeared due to presumably a combination of maximum dipolar broadening and shortening of the ^{13}C $T_{1\rho}$ relaxation time. The ^{13}C $T_{1\rho}$ plot (Fig. 5.20) however, shows that the $T_{1\rho}$ values are somewhat erratic. The main problem is that for most of the time the methylene is underneath the methyl resonance. This means that this is really a combined $T_{1\rho}$ plot for both the methylene and methyl resonances and so may not be very accurate

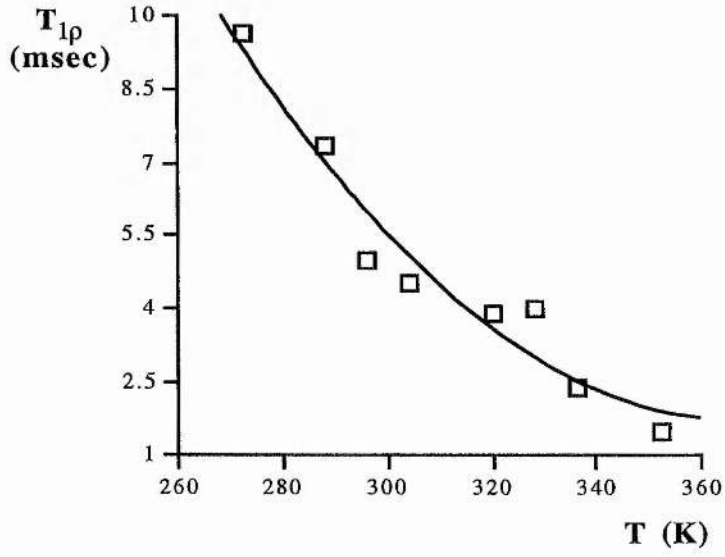

Fig. 5.21: ^{13}C $T_{1\rho}$ plot for the methyl in TEPI [ω_1 = 34.7 kHz].

Fig. 5.20(a): ^{13}C CP/MAS NMR spectra of $P(Et)_4I$.

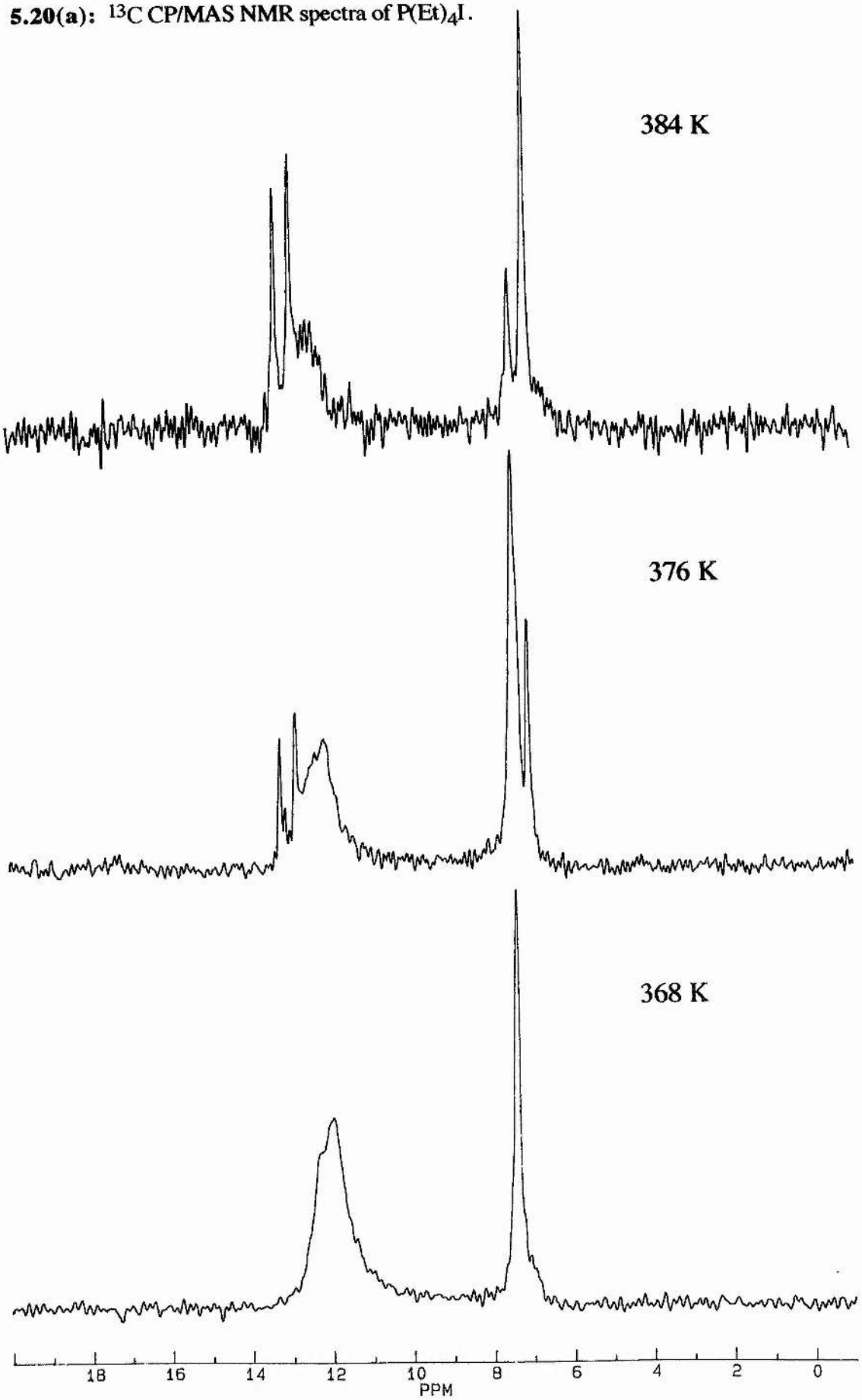

Fig. 5.20(b): ^{13}C CP/MAS NMR spectra of $P(Et)_4I$.

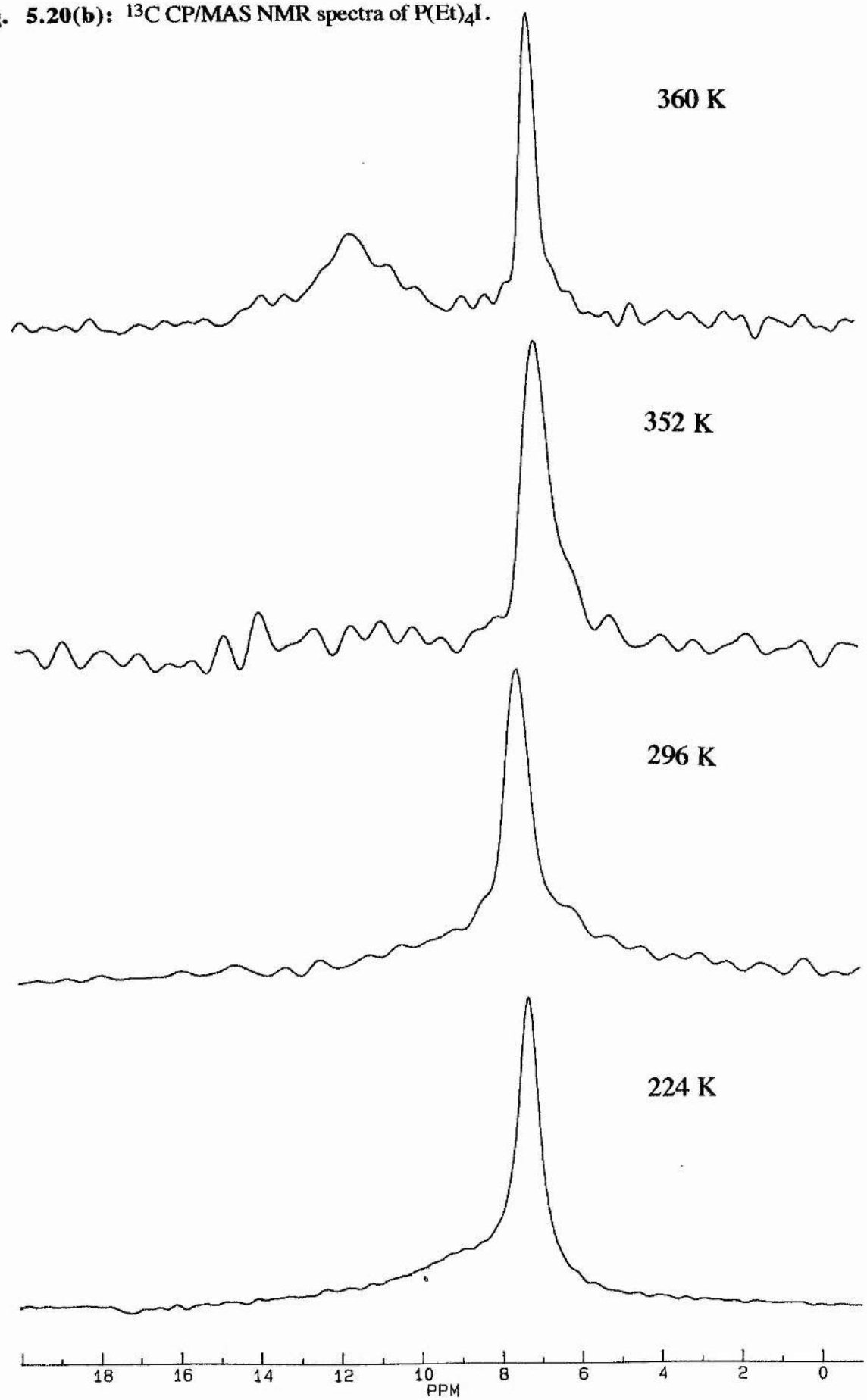

The $T_{1\rho}$ curve shows that the values are irregular due to the influence of the methylene carbon. The $T_{1\rho}$ values (Table 5.11) are used for an Arrhenius plot (Fig. 5.21) which gives a very low value for the activation energy.

T (K)	$T_{1\rho}$ (msec)
272	9.64
288	7.35
296	4.99
304	4.52
320	3.89
328	4.00
336	2.36
352	1.51

Table 5.11: ^{13}C $T_{1\rho}$ values for the methyl in TEPI.

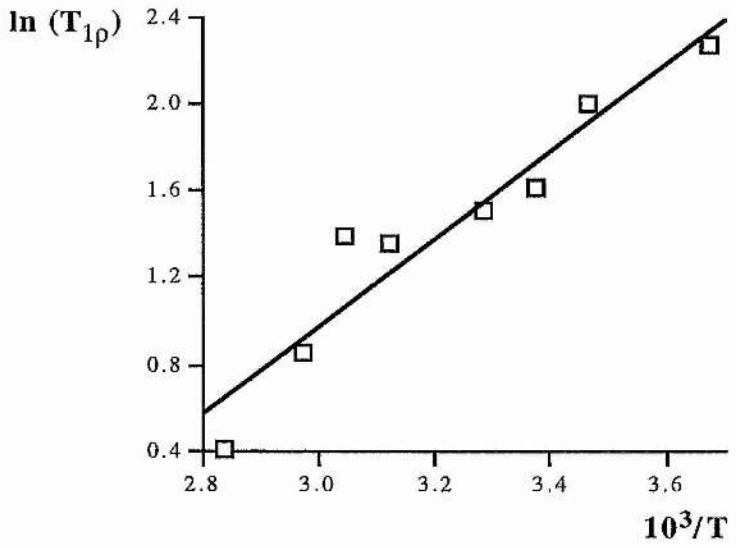

$E_a = 16.8 \pm 2.1$ kJ mol^{-1}.

Fig. 5.21: Arrhenius plot and activation energy for TEPI.

The low value for the activation energy suggests this is either methyl rotation or very low energy motions about the P-C bond. The broadness of the methylene resonance indicates that it is not just methyl rotation. The activation energy is unreliable because of the influence of the broad methylene resonance. For this reason not too much stress should be put on the actual value obtained for this compound. The motion is likely to be ethyl rotation as seen for the previous two tetraethyl

compounds. Additional errors in $T_{1\rho}$ values may come from a possible high temperature process (e.g. cation tumbling) whose occurrence is indicated by the re-broadening of the methyl resonance above 368 K [Fig. 5.19(a)].

5.3 Tetrabutyl phosphonium halides

The tetrabutyl phosphonium salts have not been studied before by dynamic NMR techniques and no references to DSC work were found. A study of the phase changes (213 - 393 K) was, therefore, carried out by DSC (Appendix 1) and the entropies calculated (Table 5.12).

Compound	T_{tr} (K)	ΔS_{tr} (J K^{-1} mol^{-1})
TBPCl	222, 257, 280, 311	1.7, -21.9, 26.3, 12.9
TBPBr	385	-
TBPI	379	-

Table 5.12: DSC data for the tetrabutyl phosphonium halides.

The three high temperature phase changes are the melting points of the three compounds. The low value for TBPCl is probably due to water impurities which also may give the exothermic reaction at 257 K by formation of HCl. The phosphonium bromide and iodide compounds do not have the multiple phase changes as seen in the TBABr and TBAI compounds.

5.3.1 Tetrabutyl phosphonium chloride (TBPCl)

The ^{13}C CP/MAS NMR spectra of TBPCl (Fig. 5.22) show a considerable change as the sample is cooled from 320 K. The spectrum at 320 K shows three resonances: methylene [C(1)]; δ_c = 20.12 ppm and $w_{1/2} \approx 355$ Hz; methylenes [C(2,3)] δ_c = 24.92, $w_{1/2}$ = 176 Hz and methyl [C(4)] δ_c = 14.41 ppm, $w_{1/2}$ = 65 Hz. On cooling to 296 K a decoalescing takes place giving a small shoulder on C(4) ($w_{1/2}$ = 60 Hz) at 15.6 ppm and C(2,3) splits unevenly to give two resonances (δ_c = 25.3 and 24.4 ppm). There may also be a new resonance at δ_c = 22.1 ppm to complete the splitting of the resonances. This resonance, however, is obscured somewhat by the resonance at δ_c = 24.4 ppm. The resonances all show a drift to

Fig. 5.22: ^{13}C CP/MAS NMR spectra of $P(Bu)_4Cl$.

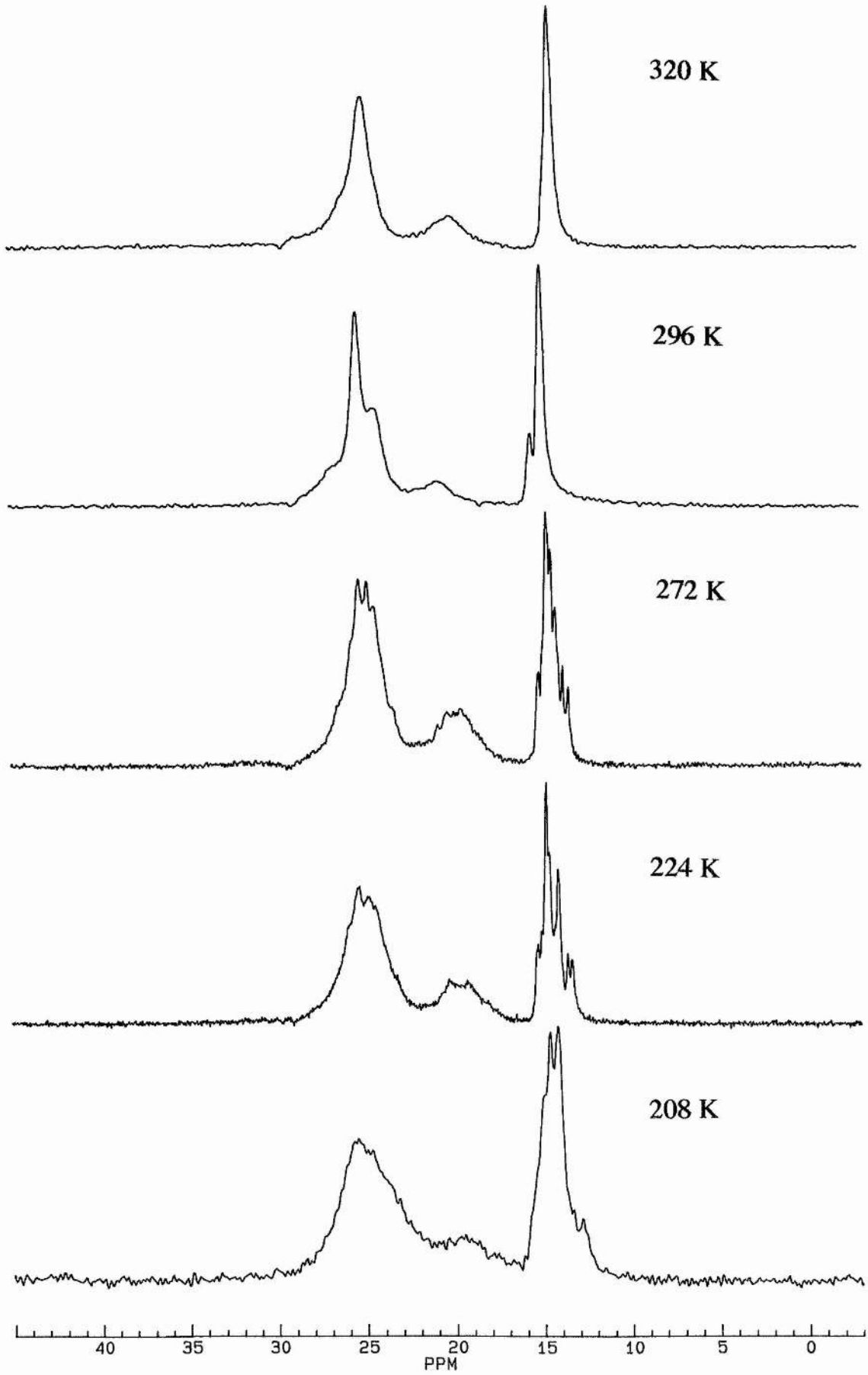

higher field of *ca* 0.5 ppm and a slight sharpening which is difficult to quantify because of the shoulders. The methyl resonance continues to decoalesce down to 224 K where *ca* 7 resonances between 13.0 and 15.5 ppm. The methylene resonance shifts back upfield to *ca* 19.8 ppm at 224 K and is still very broad ($w_{1/2} \approx 393$ Hz). The methylene carbons [C(2,3)] are all contained in a broad resonance ($w_{1/2} = 322$ Hz) at 224 K between 23 and 29 ppm. The resonances then all broaden [C(2,3): $w_{1/2} = 466$ Hz] which also results in the coalescence of some of the methyl resonances.

The explanation of this is difficult because from tetrabutyl ammonium halides it is only expected that some decoalescing into four lines for each carbon (one chemical shift for each of the carbons in each chain) takes place. In the ammonium compounds the resonances are, therefore, all of the same intensities. In TBPCl the methyl resonances are of varying intensities or perhaps there are numerous resonances with some overlapping. This compound may, therefore, have more than one molecule in the asymmetric unit which is frozen out at low temperature along with the same chain distortion seen in the ammonium compounds.

5.3.2 Tetrabutyl phosphonium bromide (TBPBr)

The ^{13}C CP/MAS NMR spectra of TBPBr (Fig. 5.23) show at 353 K five resonances. The resonances then undergo coalescence as the sample is cooled. The changes in chemical shifts and linewidth are given in Table 5.13.

	C(1)		*C(2,3)*		*C(4)*	
Temp (K)	**δ_c (ppm)**	**$w_{1/2}$ (Hz)**	**δ_c (ppm)**	**$w_{1/2}$ (Hz)**	**δ_c (ppm)**	**$w_{1/2}$ (Hz)**
353	20.5+20.2	15+15	24.8+24.6	39	14.3	15
349	*ca* 20.0	-	24.84	154	14.9	45
328	20.62	284	24.97	51	15.0	43
320	20.96	216	26.3 + 24.97	59	15.0	73

Table 5.13: ^{13}C chemical shifts and linewidths for TBPBr between 320 and 353 K.

The splitting of the methylene [C(1)] resonance is a result of ^{31}P-C coupling ($J_{PC} = 46.5$ Hz). The two methylene resonances [C(2,3)] are just starting to split and this is the only time the C(2,3) resonances have been resolved in the ammoniums or

Fig. 5.23(a): ^{13}C NMR spectra of $P(Bu)_4Br$.

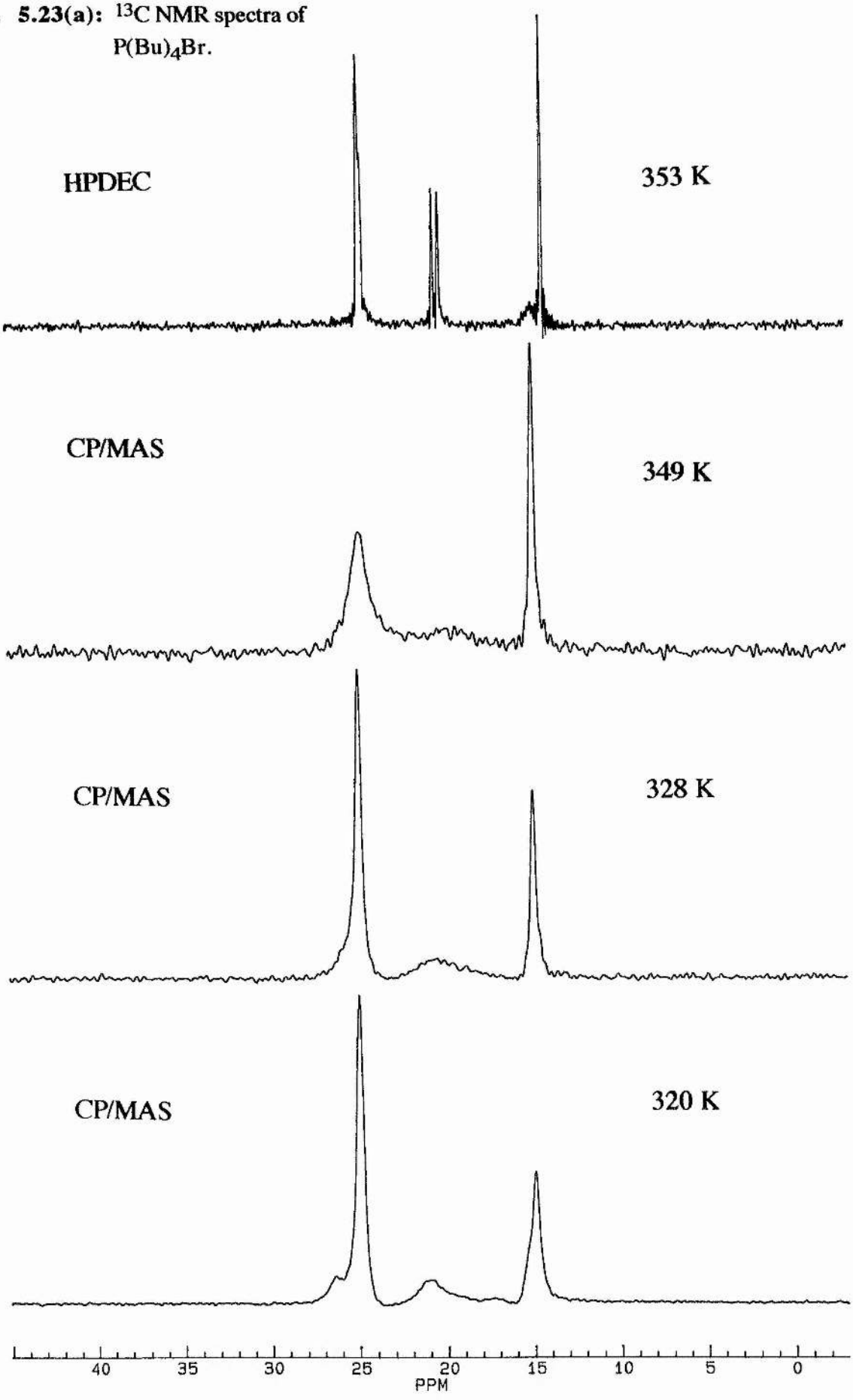

Fig. 5.23(b): ^{13}C CP/MAS NMR spectra of $P(Bu)_4Br$.

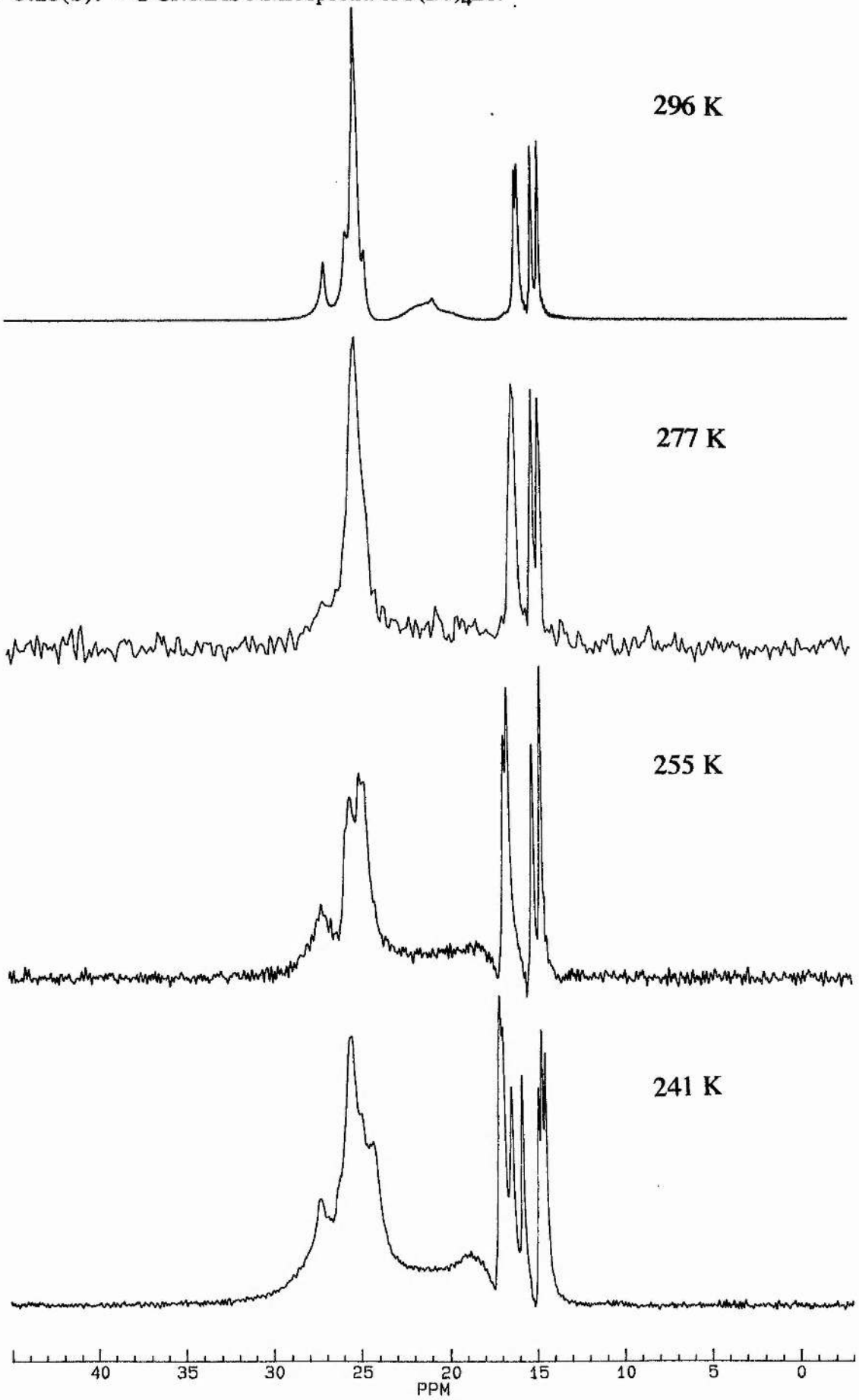

phosphoniums in the present work. This is due to the fact the linewidths are very narrow presumably because at this temperature TBPBr is in a plastic phase. The spectrum was recorded using a single pulse technique which possibly showed the plastic phase which is very difficult to record using CP/MAS. The CP/MAS spectrum at 349 K [Fig. 5.23(a)] shows a marked downfield shift and broadening of the methyl resonance (Table 5.13). The methylene resonances are considerably broader with C(1) almost gone completely due to maximum dipolar broadening and $T_{1\rho}$ effect. The resonances then sharpen as the sample is cooled to 328 K and then at 320 K C(4) and C(2,3) broaden slightly as they start to split [Fig. 5.23(a)]. On further cooling to 296 K the C(2,3) and C(4) resonances decoalesce [Fig. 5.23(b)] as previously seen for tetrapropyl ammonium iodide and tetrabutyl ammonium halide (X =Br and I). The low temperature chemical shifts are summarised in Table 5.14.

Temp (K)	C(1)	C(2,3)	C(4)
293	20.6	26.8, 25.5, 25.0, 24.5	15.9, 15.7, 15.0, 14.6
277	-	25.1	16.2, 15.1, 14.7
255	~17.5 - ~23	27.2, 25.5, 25.0, 24.8	16.8, 16.6, 15.2, 14.7
241	~18 - ~22.5	27.3, 25.5, 24.9, 24.3	17.1, 16.9, 16.4, 15.8, 14.9, 14.7, 14.5

Table 5.14: ^{13}C chemical shifts (ppm) from 295 - 241 K for TBPBr

The methyl [C(4)] clearly shows the four environments whereas the spectrum between 24 and 27 ppm for C(2) and C(3) must contain the eight possible resonances with most of them overlapping. The broad C(1) resonance ($\delta_c \approx 20.64$ ppm, $w_{1/2} =$ 206 Hz) must also contain four resonances. At 277 K the spectrum shows maximum dipolar broadening and loss of signal from shortening of $T_{1\rho}$. At 255 K the spectrum has sharpened again and the C(4) resonances have moved downfield (Table 5.13). The C(1) resonances appear to lie between *ca* 17.5 and 23.0 ppm and have merged into the C(2,3) resonances. Finally at 241 K C(4) has decoalesced further into *ca* 7 resonances. The furthest downfield peak may contain another resonance as it is more intense than the other resonances. This would indicate that the molecule has undergone a phase change resulting in a structure with two molecules in the asymmetric unit. The peak due to C(2,3) has broadened, presumably to contain the new resonances. The C(1) resonance is still very broad but is now more intense at the

high field end (δ_c = 18.80 ppm). The results for the bromide are similar to the those for TBPCl and TBAX (X= Br and I).

The various broadening and loss of signal, most noticeably at 277 and 349 K lead to some $T_{1\rho}$ measurements being made (Fig. 5.24).

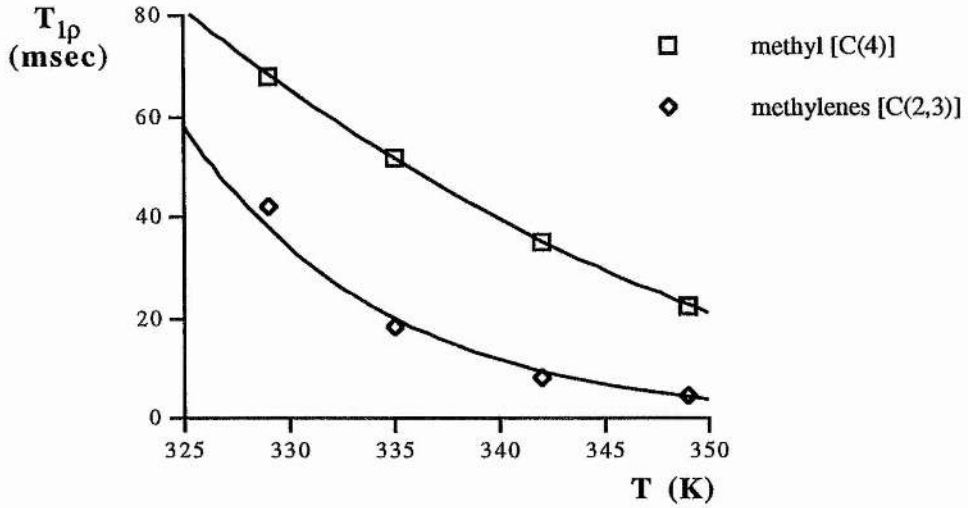

Fig. 5.24: ^{13}C $T_{1\rho}$ plot for the methyl (14.9 ppm) and methylenes (24.9 ppm) in TBPBr [ω_1 = 45.5 kHz].

At high temperature the results do seem to indicate that $T_{1\rho}$ values are changing with temperature. The problem is that only a narrow temperature range (22 K) could be measured. The attempt to measure data to correspond with the maximum dipolar broadening at *ca* 277 K gave very poor results, because the C(4) and C(2,3) resonances were spliting and coalescing. The measurement of ^{31}P $T_{1\rho}$ values was also carried out (Fig. 5.25).

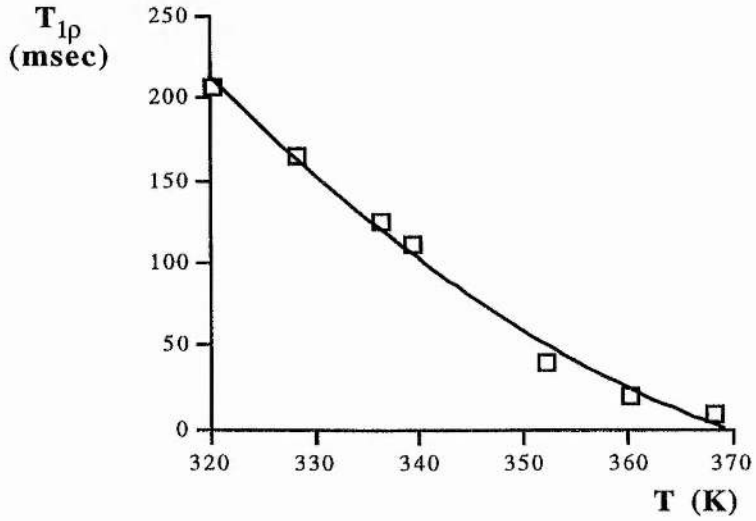

Fig. 5.25: ^{31}P $T_{1\rho}$ plot for TBPBr [ω_1 = 51.0 kHz].

The ^{13}C $T_{1\rho}$ and ^{31}P data (Table 5.15) gave the Arrhenius plots for C(4) and C(2,3) (Fig. 5.26).

T (K)	C(2,3)	C(4)	P
368	-	-	8.2
360	-	-	19.7
349	4.89	22.51	39.7
342	8.31	34.97	111
335	18.22	51.69	124
329	42.02	68.24	165
320	-	-	206

Table 5.15: ^{13}C and ^{31}P $T_{1\rho}$ values (msec) for TBPBr.

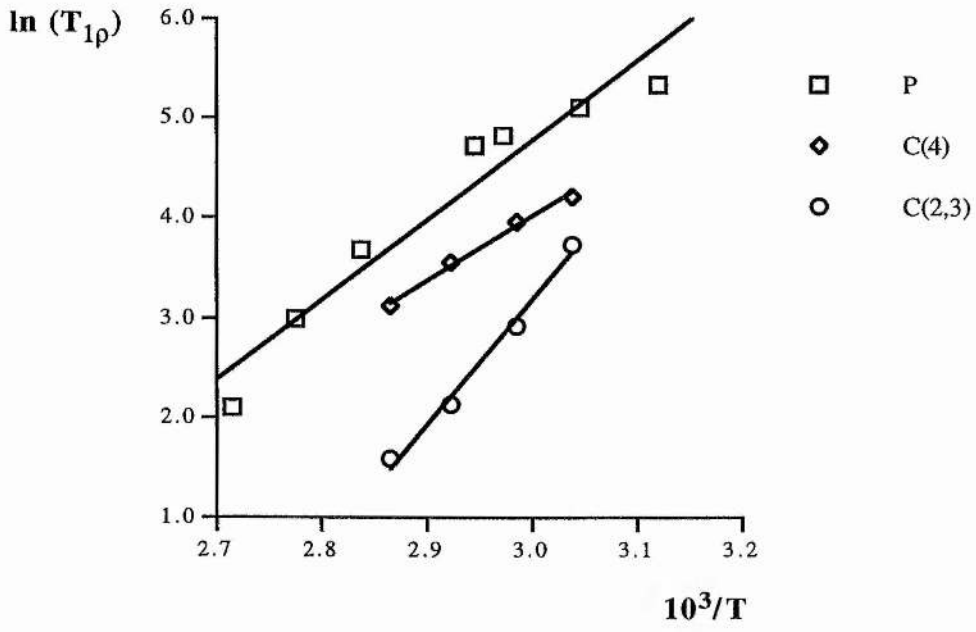

Methyl - C(4): $E_a = 53.0 \pm 3.1$ kJ mol^{-1}
Methylenes - C(2,3): $E_a = 103 \pm 8.1$ kJ mol^{-1}
Phosphorus: $E_a = 66.9 \pm 7.84$ kJ mol^{-1}

Fig. 5.26: Arrhenius plots for phosphorus, C(2,3) and C(4) of TBPBr

At high temperature the activation energies from the ^{13}C $T_{1\rho}$ data indicate that they either were not relaxing due to the same mechanism or that the errors were too large from the four points to give meaningful results. The activation energy for the

phosphorus data is closer to the value for the methyl resonance. The large error for the normally very accurate ^{31}P data indicates that there may well be more than one motion modulating the $T_{1\rho}$ values. The most likely explanation is that it is the molecular motion associated with the maximum dipolar broadening at *ca* 277 K that is causing the problems.

The possible motions are an initial rotation about the C(2)-C(3) bond and then subsequent rotation about C(1)-C(2) and cation tumbling. The activation energy for the proposed bond rotation is of the same order as seen in TEPCl (5.2.1) and in TBPI (5.3.3).

5.3.3 Tetrabutyl phosphonium iodide (TBPI)

The ^{13}C CP/MAS NMR spectra (Fig. 5.27) again show a marked change over a wide range of temperatures (208 - 360 K). The spectra show the same decoalescing of the methyl [C(4)] as seen for TBPBr, although it is a more gradual process and is finally complete at 224 K. No high temperature plastic crystal as in TBPBr is observed for TBPI [Fig. 5.27(a)]. The central methylenes [C(2,3)] therefore, both overlap at high temperature and any splitting at lower temperature cannot be attributed to either resonance. The decoalescence of C(2,3) observed at (328 K) also occurred in TBPBr, giving a downfield resonance (δ_c = 26.2 ppm). The C(2,3) resonance continues to decoalesce and at 208 K is broad with numerous shoulders [Fig. 5.27(b)] The C(1) resonance shows for the first time a splitting (328 K, δ_c = 20.9 and 19.3 ppm) which becomes three distinct resonances ($\delta_c \approx$ 16-22 ppm) between 296 and 248 K. The main changes in chemical shift are summarised in Table 5.16.

Temp (K)	C(1)	C(2,3)	C(4)
360	20.8	24.8	14.9
328	21.0 + 19.1	25.9 + 24.7	15.6 + 14.8
264	20.9 + 19.2	26.1 + 24.6	15.9 + 15.0
	+ 17.7	+ 25.1	+ 14.3
208	20.8	26.0 + 25.2 +	16.5 + 15.3 +
		24.5 + 23.9	14.5 + 14.0

Table 5.16: ^{13}C chemical shifts (ppm) for TBPI.

Fig. 5.27(a): ^{13}C NMR spectra of $P(Bu)_4I$.

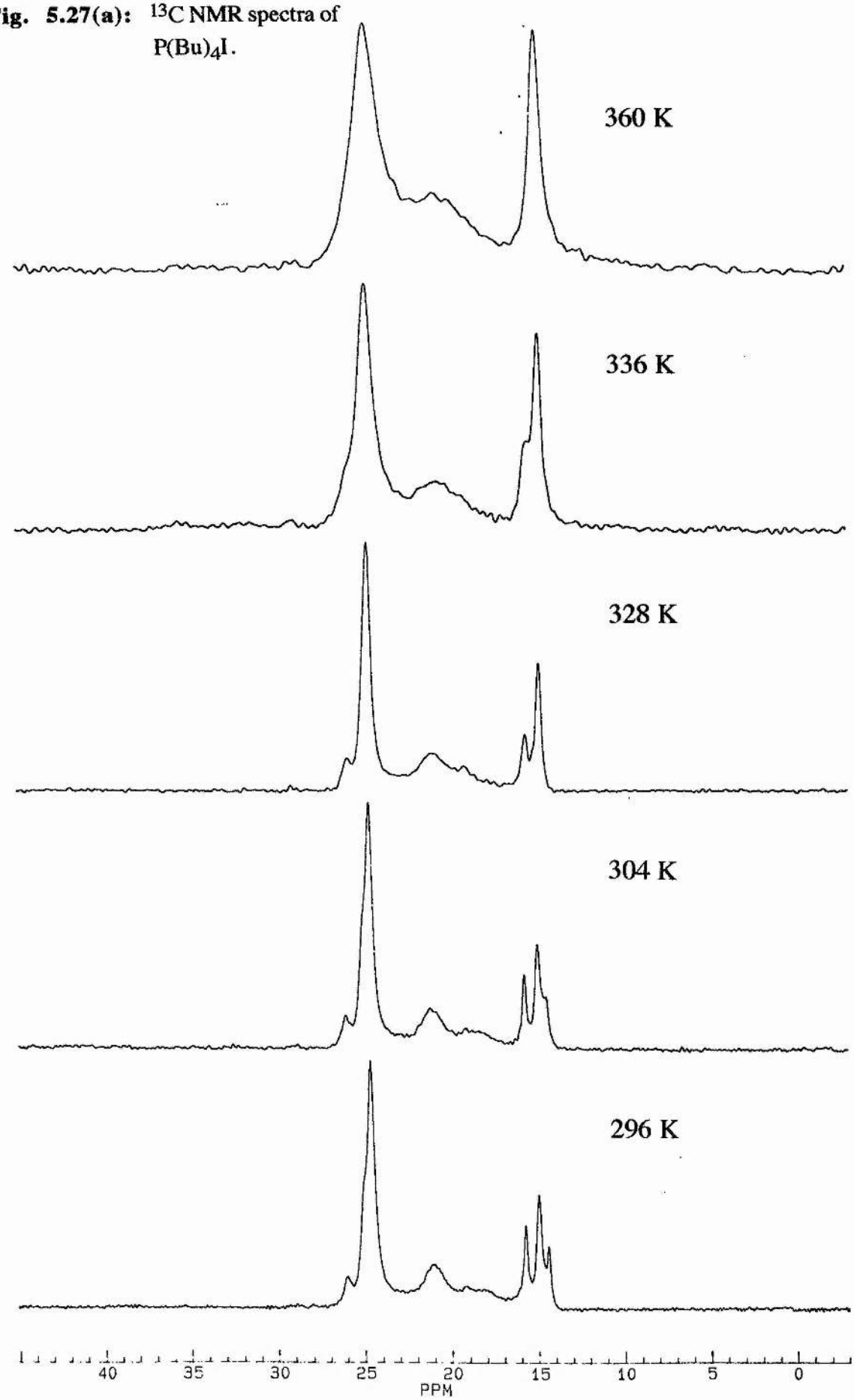

Fig. 5.27(b): ^{13}C NMR spectra of $P(Bu)_4I$.

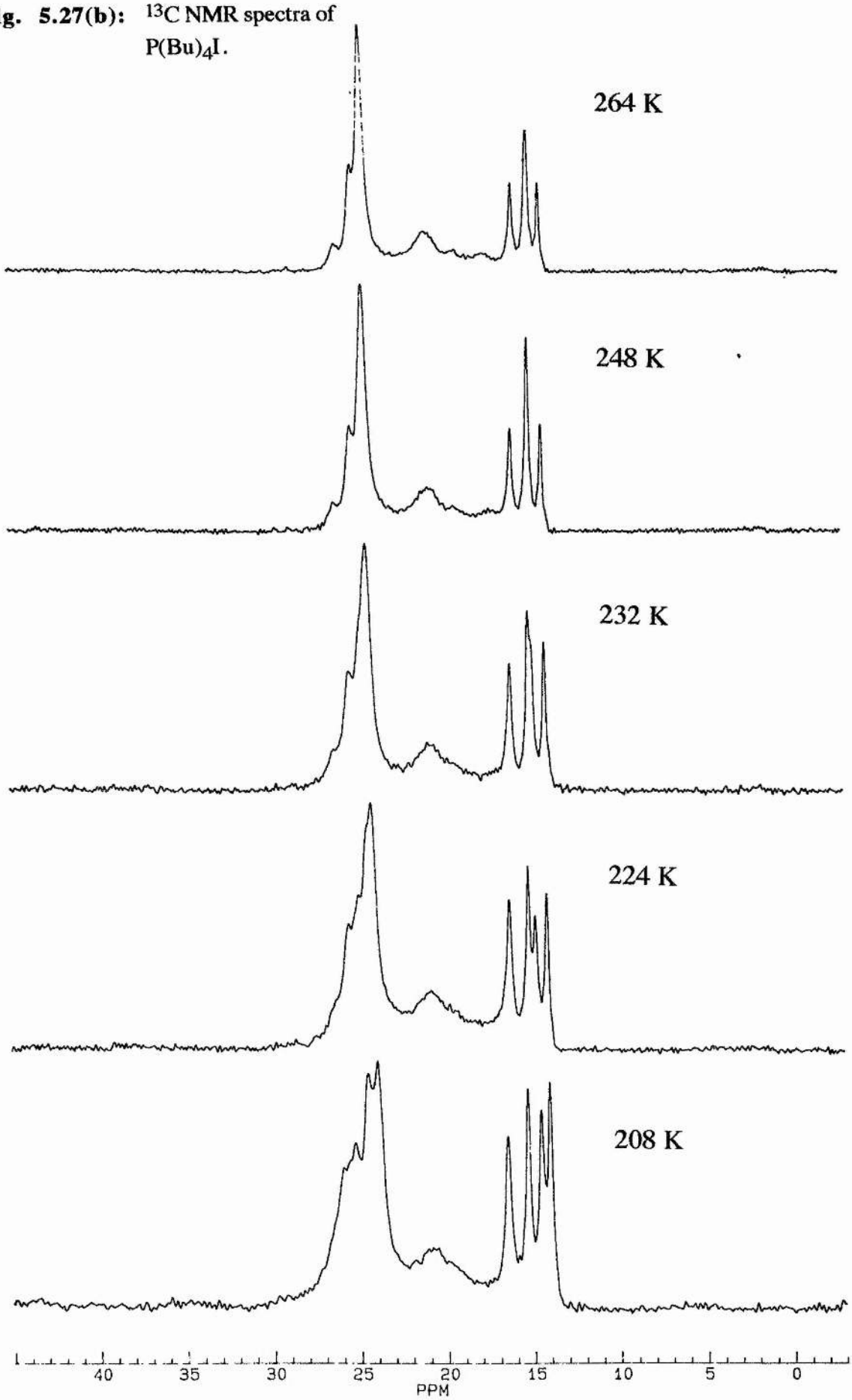

The presence of a process causing coalescence is confirmed by plotting the chemical shifts vs. temperature (Fig. 5.28).

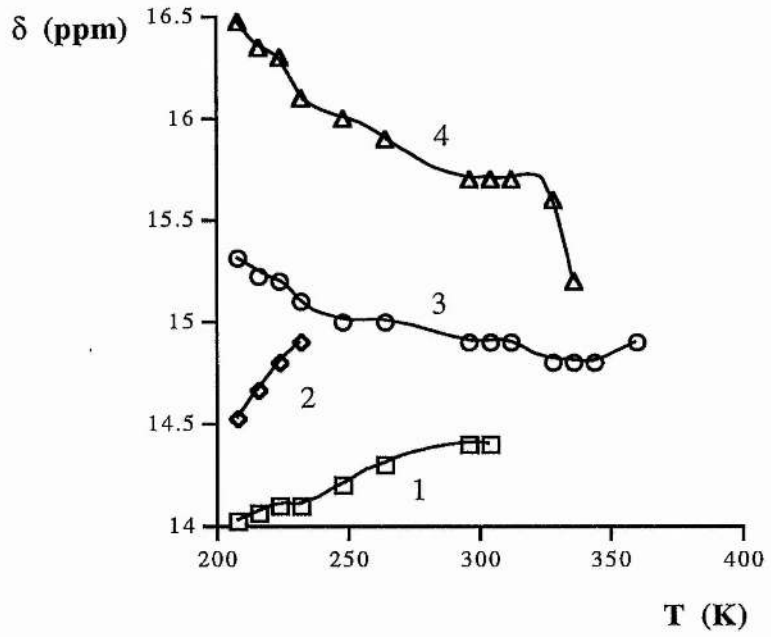

Fig. 5.28: Variation of the ^{13}C chemical shifts (ppm) of the four methyl resonances with temperature.

The plot shows that the arbitrarily named methyls 1 and 4 are coalescing with 3 and that 2 is just showing a gradual chemical shift change. This means that two $\Delta G_c^{\ddagger}$ values can be calculated for the coalescence (Table 5.17).

Methyls	T_c (K)	$\Delta\nu$ (Hz)	$\Delta G_c^{\ddagger}$ (kJ mol^{-1})
1 & 3	308	163	62.2
3 & 4	338	151	68.8

Table 5.17: Data for the coalescence phenomena of the methyl resonances.

The magnitude of the $\Delta G_c^{\ddagger}$ values are slightly larger than those measured for alkyl group rotations in other tetraalky phosphonium compounds.

The spectra also show broadening at high temperature as seen in TBPBr but not at *ca* 277 K as seen in TBPBr. The measurement of ^{13}C $T_{1\rho}$ values confirmed that at high temperature motion in the molecule was affecting cross polarisation (Fig. 5.29)

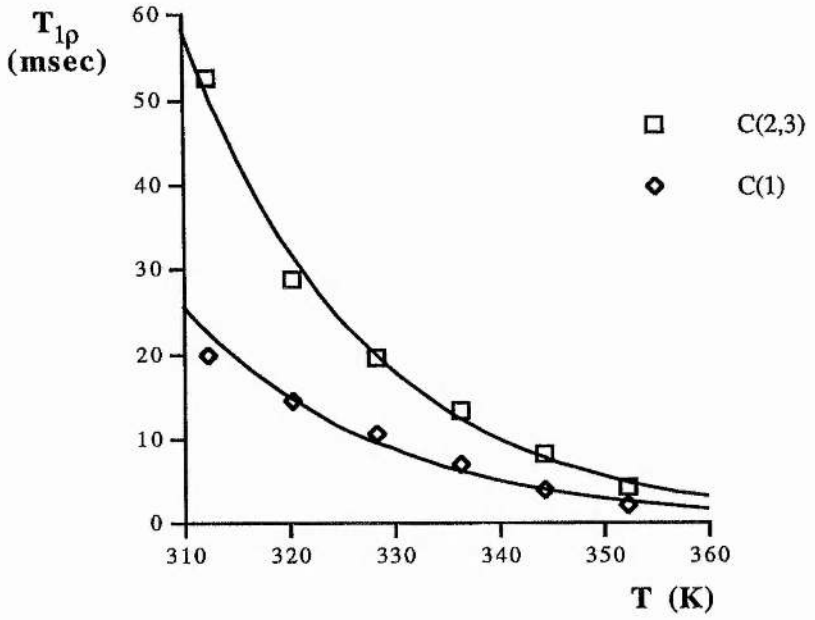

Fig. 5.29: ^{13}C $T_{1\rho}$ plot for the three methylenes [C(1) and C(2,3)] in TBPI.

The ^{13}C $T_{1\rho}$ data (Table 5.17) is used to calculate activation energies for the process from an Arrhenius plot (Fig. 5.30).

T (K)	C(1)	C(2,3)
352	4.39	2.16
344	8.33	4.08
336	13.2	7.12
328	19.7	10.5
320	28.8	14.6
312	52.6	19.8

Table 5.18: ^{13}C $T_{1\rho}$ values (msec) for TBPI.

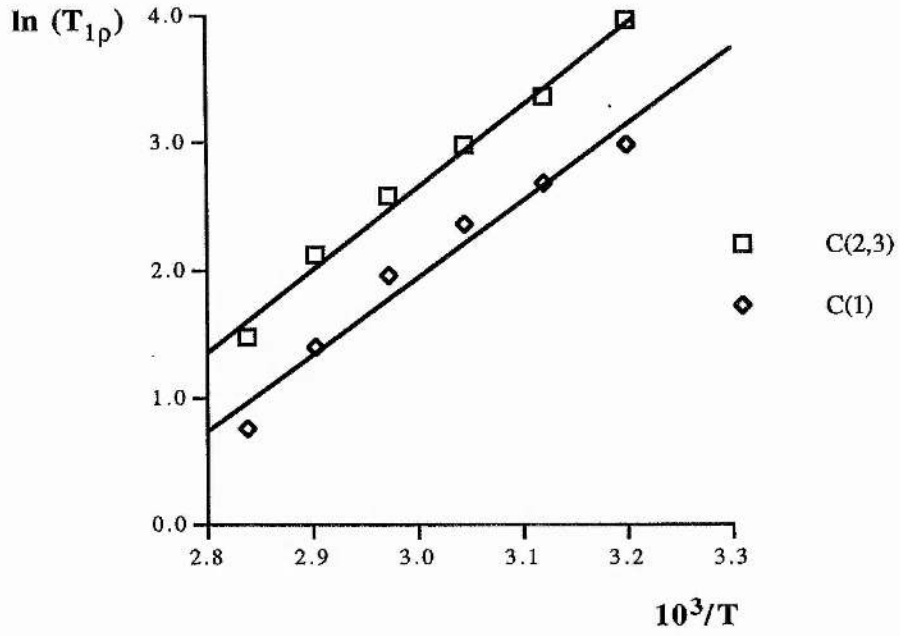

Methylenes - C(2,3) $E_a = 54.4 \pm 3.3$ kJ mol^{-1}.
Methylene - C(1) $E_a = 50.1 \pm 4.2$ kj mol^{-1}.

Fig. 5.29: Arrhenius plot for the three methylenes C(1) and C(2,3) in TBPI.

The activation energies are smaller than the $\Delta G^{\ddagger}_c$ values indicating they are not from the same process. The activation energies are of the same order as for ethyl rotation in TEPCl and for the data for the methyl in TBPBr. The data, however, is for the three methylenes as opposed to for C(2,3) and C(4) as seen in TBPBr. The fact that C(4) does not show a change of $T_{1\rho}$ with temperature indicates the motion may be about the C(1) - C(2) bond.

5.4.1 Ethyl-tri-butyl phosphonium bromide (ETBPBr)

This compound was supplied by Dr. R. A. Aitken and was run out of interest to see if different chain lengths lead to any new features in the solid state. The ^{13}C CP/MAS NMR spectra (5.30) has five resonances at 300 K. The numbering scheme for ETBPBr (Fig.5.31) is used for the assignments of the chemical shifts summarised in Table 5.12.

Fig. 5.30: ^{13}C CP/MAS NMR spectra of ETBPBr

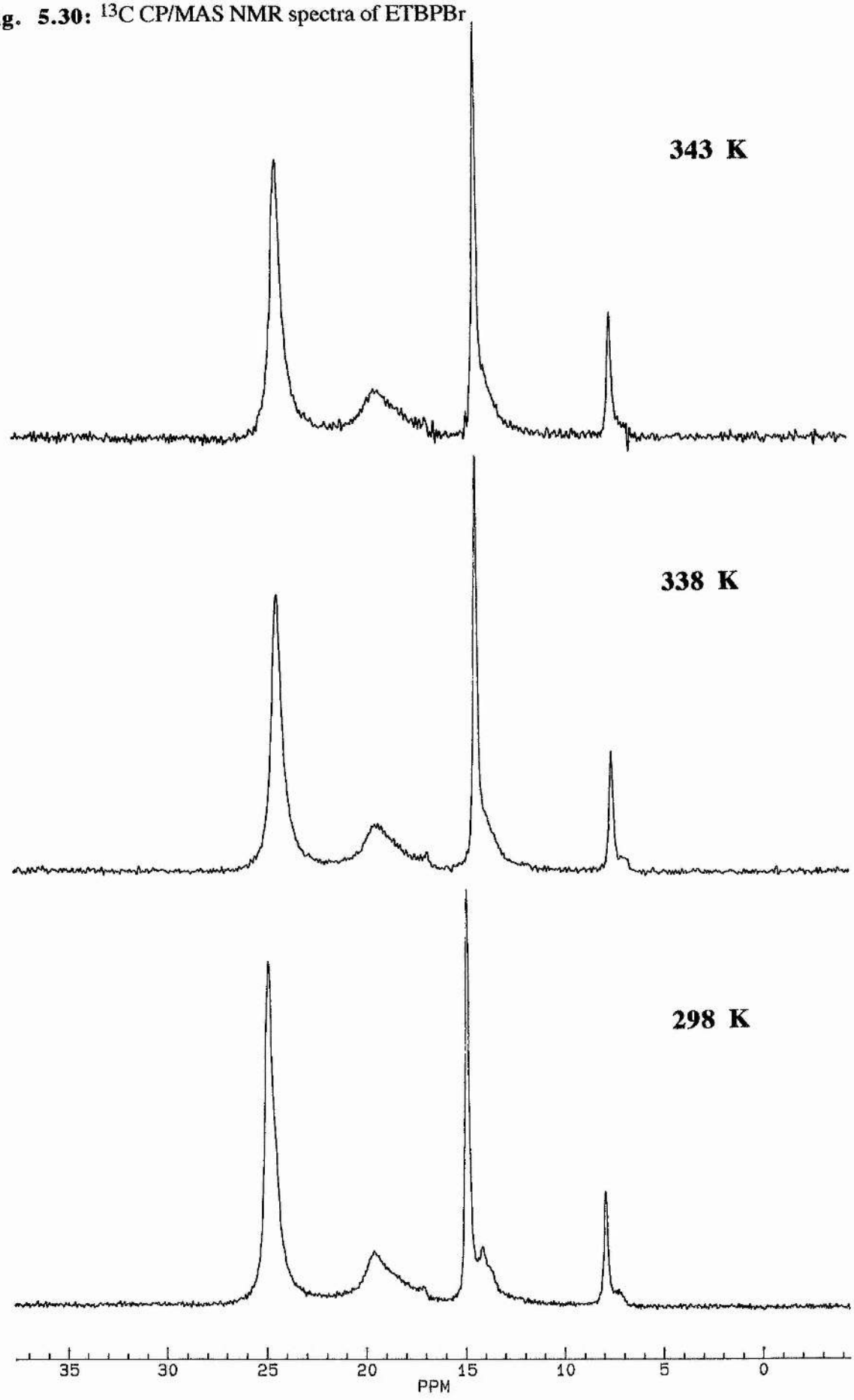

Carbon	δ_c (ppm)
1	19.6
2, 3	24.8
4	14.9
1'	14.1
2'	7.9

Table 5.12: ^{13}C Chemical shifts for ETBPBr

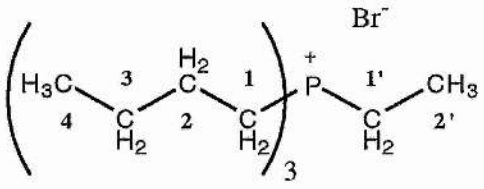

Fig. 5.31 Numbering scheme for ETBPBr

The methyl on the ethyl group [C(2')] has a low intensity upfield shoulder (*ca* 7.3 ppm) and the C(1) resonance has a similar anomaly (*ca* 17.1 ppm). These resonances are presumably due to a minor phase coexisting with the main phase. The only change in the spectra as the sample is warmed from 298 to 336 K is that the C(2,3) resonance broadens slightly and is slightly reduced in intensity relative to the methyl resonances. The measurement of ^{13}C $T_{1\rho}$ values showed a change with temperature (Fig. 5.32).

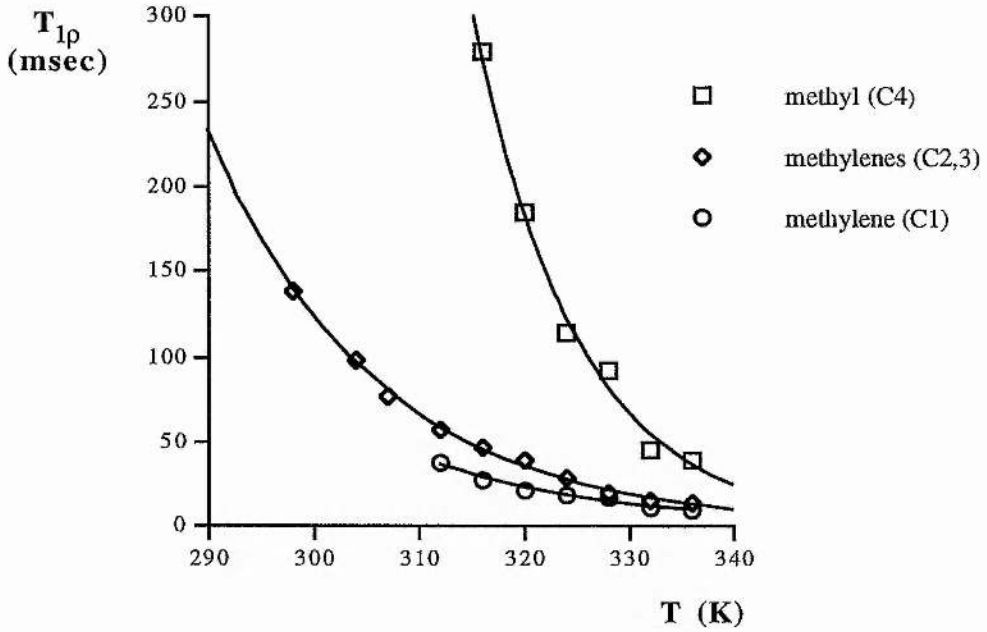

Fig. 5.32: ^{13}C $T_{1\rho}$ plot for ETBPBr [ω_1 = 52.6 kHz)

The $T_{1\rho}$ plot indicates that the motion effects C(1) the most with C(2,3) also showing a large effect. The $T_{1\rho}$ data (Table 5.20) gives an Arrhenius plot (Fig. 5.33)

that indicates the C(4) $T_{1\rho}$ values are not being modulated by the same motion as the other resonances.

T (K)	C(1)	C(2,3)	C(4)
336		13.6	
332		14.9	
358		20.5	
324	9.00	29.6	39.9
320	11.0	38.9	46.0
316	16.8	47.8	91.4
312	19.1	57.3	115
307	21.4	77.5	186
304	27.9	97.4	279
298	38.8	138	

Table 5.20: ^{13}C $T_{1\rho}$ values (msec) for ETBPBr.

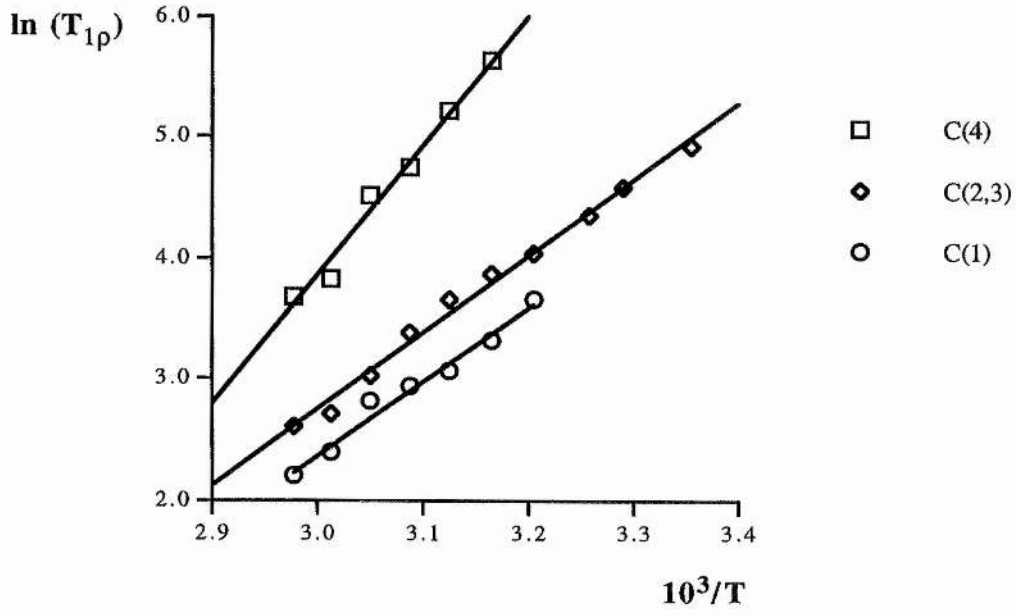

	E_a (kJ mol^{-1})
C(1)	50.5 ± 3.6
C(2,3)	52.2 ± 1.8
C(4)	89.2 ± 6.0

Fig. 5.34: Arrhenius plot for C(1) C2,3) and C(4) in ETBPBr.

The activation energies for C(1) and C(2,3) are comparable to the values for group rotation in TEACl [C(2)], TEPCl [C(1) and C(2)], TBPBr [C(4)] and TBPI [C(2,3) and C(4)]. The rotation in ETBPBr is about the P - C(1) bond.

CHAPTER 6

6. Solid-state dynamics in cyclopentane derivatives

In the introduction (section 1.5) it is stated in the principle of least distress that pseudorotation in five-membered rings might be observable in crystalline solids. Some indication that this might be correct was found in two papers by Lambert *et al.*[50,51] Accordingly it was decided to examine some cyclopentane and related heterocyclic derivatives.

The pseudorotation in cyclopentane between an envelope and a half-chair conformation (Fig. 6.1) allows the bond eclipsing strain in planar cyclopentane to be greatly reduced. The total strain in cyclopentane is reduced to 27 kJ mol^{-1} compared to a theoretical strain of 42 kJ mol^{-1} for the bond opposition torsional energy due to five eclipsed CH_2 groups.[52]

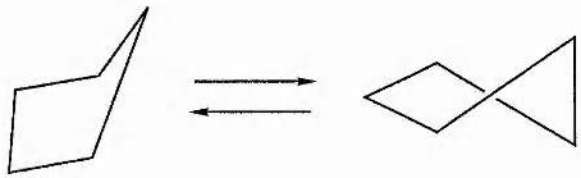

Fig. 6.1: Pseudorotation of cyclopentane

Pseudorotation has been defined by Hendrickson,[53] as the passage of a ring with a plane of symmetry through an atom to one with an axis of symmetry bisecting the bond adjacent to the carbon and vice versa. The pseudorotation can be envisaged as the displacement of one CH_2 element out of the ring plane which is then transmitted around the ring. Pseudorotation in cyclopentane itself is essentially free with a negligible barrier. An early study of solid cyclopentane by second moment and T_1 relaxation times shows that very little motion is observed below 120 K.[54] The phase transition in cyclopentane at 122 K then introduces significant molecular motion in the solid. The motions present in derivatives of cyclopentane may be different and furthermore any barriers to pseudorotation in free molecules of cyclopentane derivatives may be enhanced by inclusion in a solid matrix.

The interest in pseudorotation in solid cyclopentane derivatives came from a paper by Lambert *et al.*[50] where cyclopentanol showed peak broadening down to the phase change at -37 °C and then multiple decoalescing of the C(2) and C(3) resonances at lower temperatures. The broadening indicates that rapid molecular

motion may be occurring in the high temperature phase. The decoalescence has been attributed to hydrogen bonded aggregation,[51] because the spectra for cyclopentanol-O^2H give slightly different results. Deuteriation lowers the melting point and phase transition and the broadening occurs at lower temperatures also. The decoalescence of C(3) is the only one that occurs down to -90 °C. The change from ^1H to ^2H would be expected to contribute changes to the structure and dynamics of the hydrogen bonded aggregates. In the second paper by Lambert *et al.*,[51] a more extensive study of five- and six-membered rings was included. The compounds that showed maximum dipolar broadening and thus indicated that they could be studied using ^{13}C $T_{1\rho}$ were; cyclohexanol, *trans*-1,2-cyclopentanediol and sulpholane. After the first paper by Lambert *et al.* our idea was to study ring pseudorotations by synthesising molecules with groups attached that would form an interlocking lattice.

6.1 1,1-bis-(hydroxymethyl)cyclopentane (BHMCP)

One compound synthesised to investigate pseudorotation in the solid state was 1,1-bis-(hydroxymethyl)cyclopentane [Fig. 6.2].

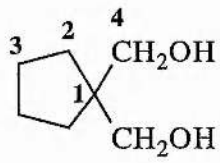

Fig. 6.2: 1,1-bis(hydroxymethyl)cyclopentane

The solid state ^{13}C CP/MAS spectrum for BHMCP at ambient temperature (Fig. 6.3) shows two resonances for the CH_2 groups at the C(2) position and for the two CH_2 [C(4)] groups attached to the ring. A coalescence is observed as the sample is warmed, the coalescence temperatures for the two sets of resonances are 313 K and 315 K respectively (Fig. 6.3). The compound shows only one phase by DSC between RT and the melting point at 94 °C. This means that the decoalescence is not, as seen for cyclopentanol, due to the plastic to non-plastic phase transition. There is, however, another possible explanation for this apart from ring pseudorotation and that is a dynamic change in H-bonding (Fig. 6.4). This process would involve a rotation about the C(1) - C(4) bond.

Fig. 6.3: ^{13}C CP/MAS NMR spectra of BHMCP.

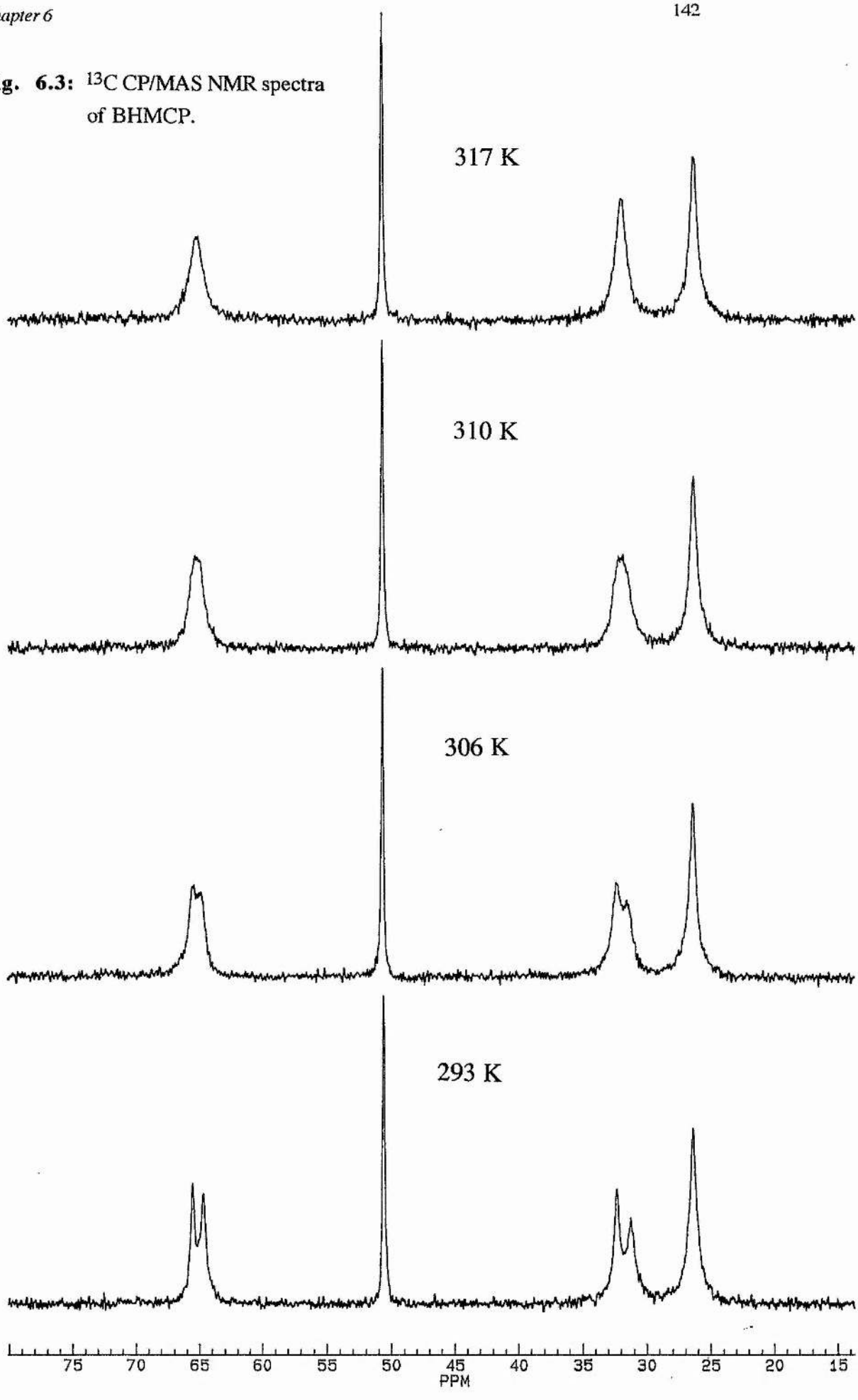

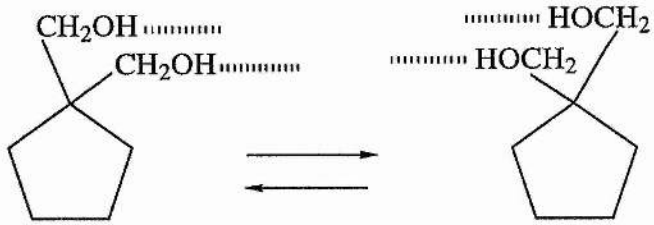

Fig. 6.4: Dynamic change in H-bonding in BHMCP

One way of checking is to compare the activation parameters for the OH and O^2H compounds. In practice this is done by looking for a change in the free energy of activation at the coalescence temperature ($\Delta G_c^{\ddagger}$). The calculation of $\Delta G_c^{\ddagger}$ from the coalescence of two resonances is achieved using equation 1 [T_c = coalescence temperature (K) and $\Delta\nu$ = peak separation (Hz)].

$$\Delta G_c^{\ddagger} = 19.13\ T_c\ [10.3 + \log (T_c/\Delta\nu)] \qquad \textbf{eqn.1}$$

The free energy value for CH_2OH is 62.8 kJ mol^{-1} and for the ring methylene groups is 62.2 kJ mol^{-1}.

The deuteriation of BHMCP should result in a different coalescence point if in fact the hydrogen bond flipping is involved in the process giving rise to the coalescence. The ^{13}C CP/MAS NMR spectra (Fig. 6.5) of the -O^2H derivative gave an unexpected result. The C(2) and C(4) resonances no longer show any splitting, but the C(3) resonance is split at 234 K and with the coalescence at 296 K. These are dramatic differences and upon changing from -O^1H to -O^2H and is presumably due to their different relative hydrogen bond strengths. This can lead to can lead to either a change in structure in the solid state or a change in activation energy of the process involving making and breaking of H-bonds.

Results elsewhere in the group on similar systems are consistent with the second explanation. 2,2-Dimethylpropane-1,3-diol and 1,1-(bishydroxymethyl)-cycloheptane both show small increases in $\Delta G_c^{\ddagger}$ on changing from O^1H to O^2H.[55] The much more substantial changes here suggest a change in structure or a change in mechanism or both. The ^{13}C chemical shifts of the two derivatives at different temperatures (Table 6.1) shows that C(1) and C(2) are the only resonances that show any change. The other resonances show very little change after they have coalesced.

Fig. 6.5: ^{13}C CP/MAS NMR spectra of BHMCP (-O^2H).

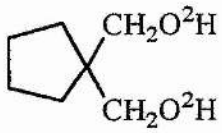

	O^1H		O^2H	
Carbon	**293 K**	**317 K**	**234 K**	**320 K**
1	50.6	50.8	49.7	49.9
2	32.3 +31.2	32.0	32.4	32.7
3	26.6	26.3	26.8 +25.7	26.2
4	65.5 + 64.6	65.3	65.4	65.5

Table 6.1: ^{13}C chemical shifts (ppm) for BHMCP with O^1H and O^2H.

The structure of the O^2H sample is, therefore, slightly different with the changes all coming in the ring and not at the H-bonded end of the molecule. There were some problems in obtaining spectra for the O^2H sample because very long runs were required to achieve good signal to noise due to long ^1H T_1. After a day or so the sample could be seen to deteriorate and signs of the O^1H containing compound could be seen in the ^{13}C CP/MAS NMR spectrum.

6.1.1 Ester derivatives of BHMCP

The presence of the hydroxyl groups in BHMCP allows its conversion to solid cyclopentane ester derivatives (Fig. 6.6). The room temperature ^{13}C CP/MAS NMR spectra of the ester derivatives (Fig. 6.7) show no splitting of the ring resonances.

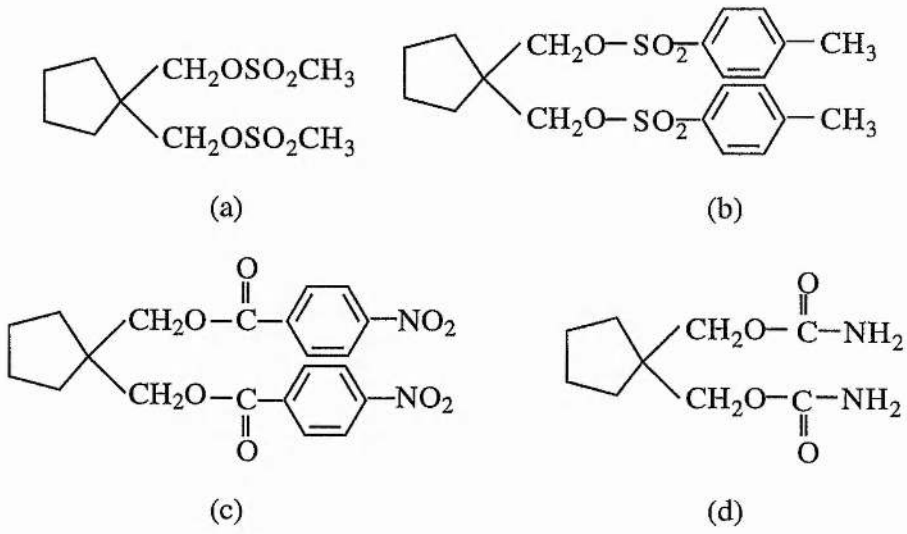

Fig. 6.6: Ester derivatives of BHMCP: (a) 1,1-bis-(methanesulphonatemethyl)-cyclopentane, (b) 1,1-bis-(p-toluenesulphonatemethyl)cyclopentane, (c) 1,1-bis-(p-nitrobenzoyloxymethyl)cyclopentane, (d) 1,1-bis-(carbamatemethyl)cyclopentane.

Fig. 6.7: ^{13}C CP/MAS NMR of Ester derivatives of BHMCP at RT.

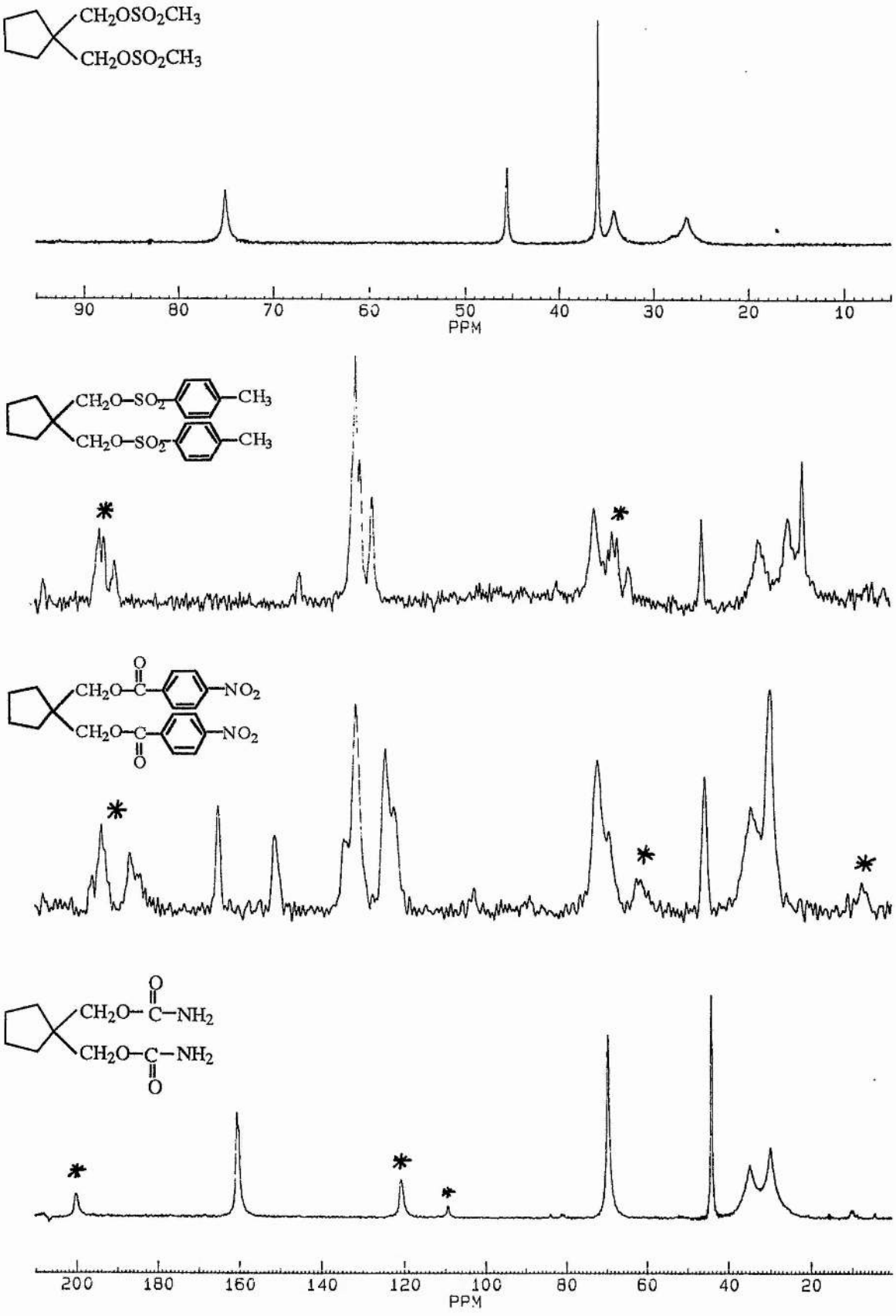

The spectra showed no changes on varying the temperature. This, therefore, supports the argument that the motion occurring in BHMCP is one of hydrogen bond exchange.

6.1.2 Bicyclic derivatives of BHMCP

The 2,4-dioxan derivatives showed some interesting variable temperature ^{13}C CP/MAS NMR spectra without any complications from hydrogen bonding.

6.1.2.1 2,4-dioxaspiro[5.4]decane (DOSD)

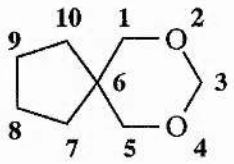

Fig. 6.8: Carbon numbering scheme for DOSD

This compound is a liquid at room temperature and appears to freeze into a plastic phase at 242 K. The ^{13}C HPDEC spectra of this compound from 295 K down to the freezing point (Fig. 6.9) show the broadening and subsequent decoalescing of the C(7,10) resonances into the axial and equatorial sites. The spectra of the plastic phase at 241 and 237 K (Fig. 6.9) show that the C(8,9) resonance is also decoalescing (*ca* 25 ppm). The recycle delay used for the plastic phase was 5 secs but, when it was increased to 40 secs the spectrum at 227 K showed there was another phase (phase II) coexisting with the plastic phase (phase I) with a much longer ^{1}H T_1. The resonances for the two phases (Table 6.2) show that it is only the chemical shifts for the C(7,10) resonances that are the same for the two phases.

Carbon	δ_c (phase I)	δ_c (phase II)
1,5	76.0 + 78.7	72.4 + 77.5
3	94.2	93.3
6	42.8	43.1
7,10	32.3 + 35.5	32.3 + 35.5
8,9	26.0 + 25.6	24.6

Table 6.2: ^{13}C chemical shifts (ppm) for the two phases of DOSD

Fig. 6.9(a): ^{13}C HPDEC NMR spectra of DOSD.

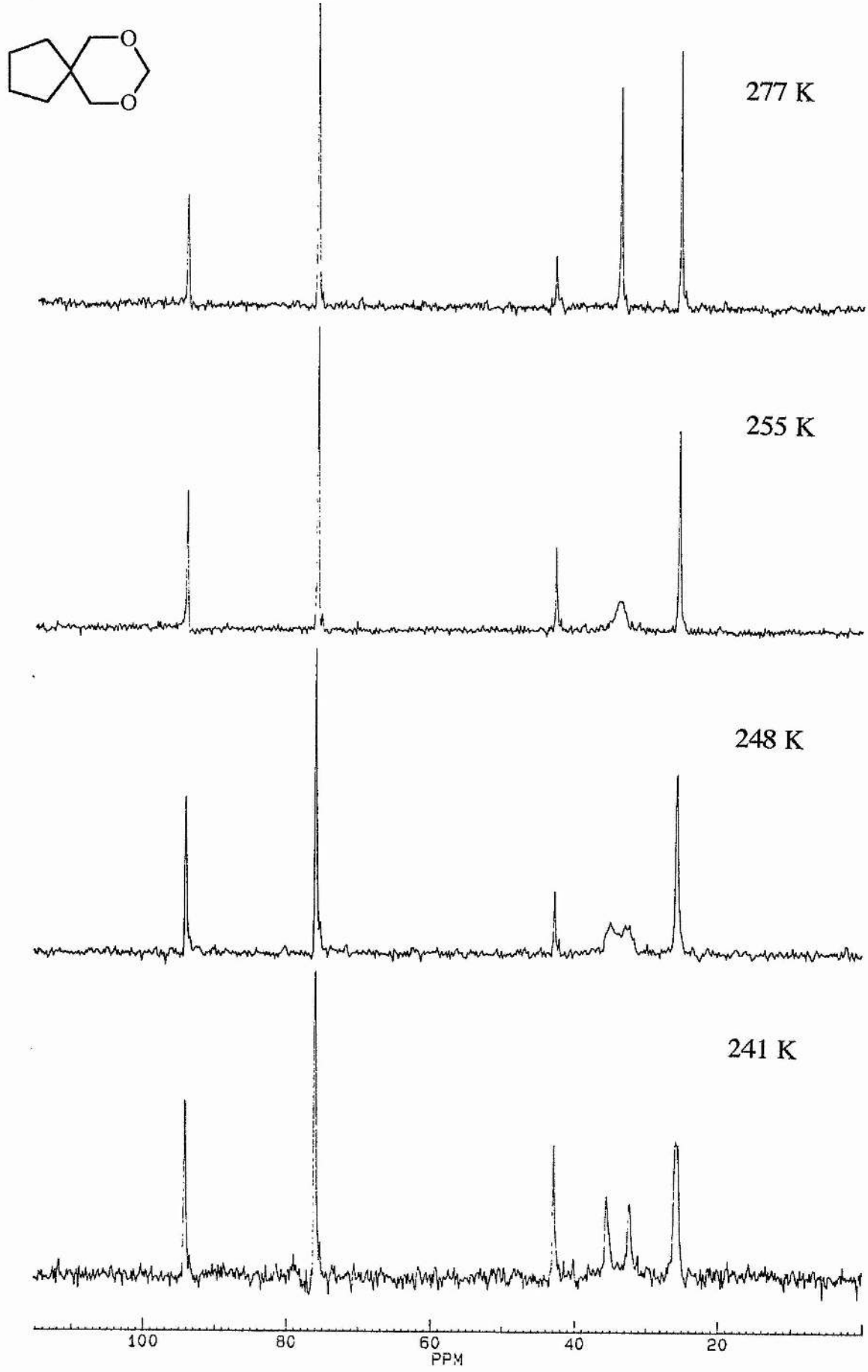

Fig. 6.9(b): ^{13}C HPDEC NMR spectra of DOSD.

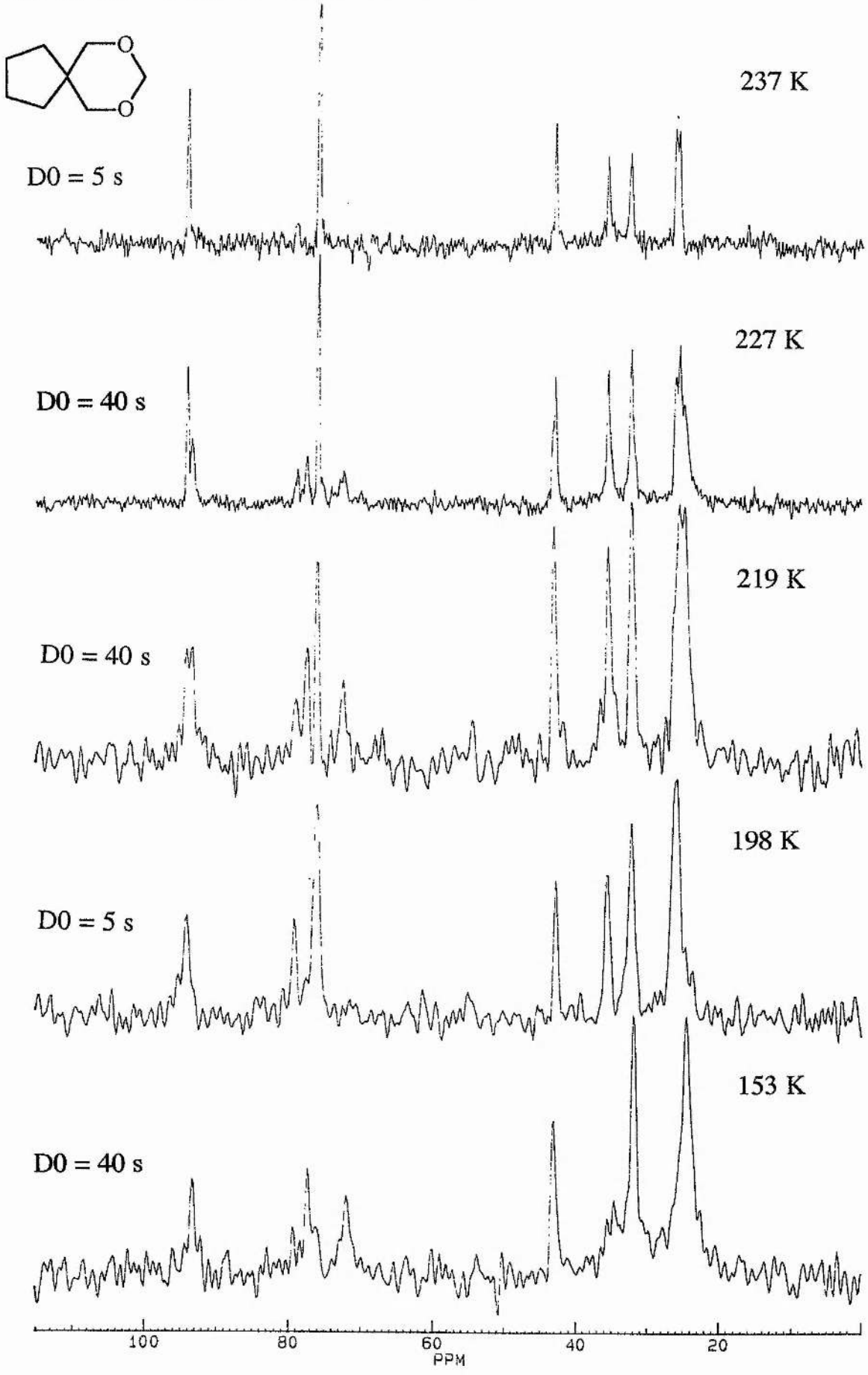

The ^{13}C CP/MAS NMR spectra of DOSD (Fig. 6.10) show that with a recycle delay of 40 secs the only resonances observable are those for phase II. The sample showed no change over the range 227 - 190 K. Above 227 K no spectrum could be obtained due to lack of signal. Therefore, the phase transition is *ca* 230 K with some of the plastic phase remaining in supercooled pockets as seen for 3, 3-diethylpentane. Using a delay of 5 secs, which decreases the signal of phase II and an increased number of transients phase I can be detected using cross polarisation. The phase I resonances for C(1,5) and C(3) can clearly be seen (Fig. 6.10).

The most intriguing feature of these spectra is the different resonances for C(1,5). In the plastic phase there is an intense resonance at 76.0 ppm and then a low intensity resonance at 78.7 ppm. Even at 241 K there is a small resonance just above the noise which increases in intensity until at 198 K the resonance is *ca* one third as intense as the resonance at 76.0 ppm. In phase II the C(1,5) resonance is split by *ca* 5 ppm, but the resonances are of a comparable intensity. The splitting is therefore induced by the effect of the frozen conformation of the ring or by the conformation of the six membered dioxan ring. The uneven intensities of the C(1,5) resonances in phase I suggests there are two conformations which only effect the C(1,5) resonance and that one conformation is preferred.

6.1.2.2 3,3-diethyl-2,4-dioxaspiro[5.4]decane (DEDD)

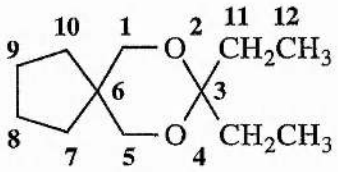

Fig. 6.11: Carbon numbering scheme for DEDD.

This compound is a liquid with a melting point *ca* 238 K. The ^{13}C HPDEC NMR spectrum of this compound at 234 K (phase I) (Fig. 6.12) shows it has very sharp resonances apart from C(7,10) at 26.4 ppm. The resonances then broaden as the sample is cooled to 227 K and at 218 K the signal has deteriorated (Fig. 6.12). At 212 K the compound goes through a phase change, with the resonances broadening and a new resonance for C(1,5) appearing (phase II). The ^{13}C CP/MAS NMR spectrum of the compound below the phase change has been lost, but the chemical

Fig. 6.10: ^{13}C CP/MAS NMR spectra of DOSD.

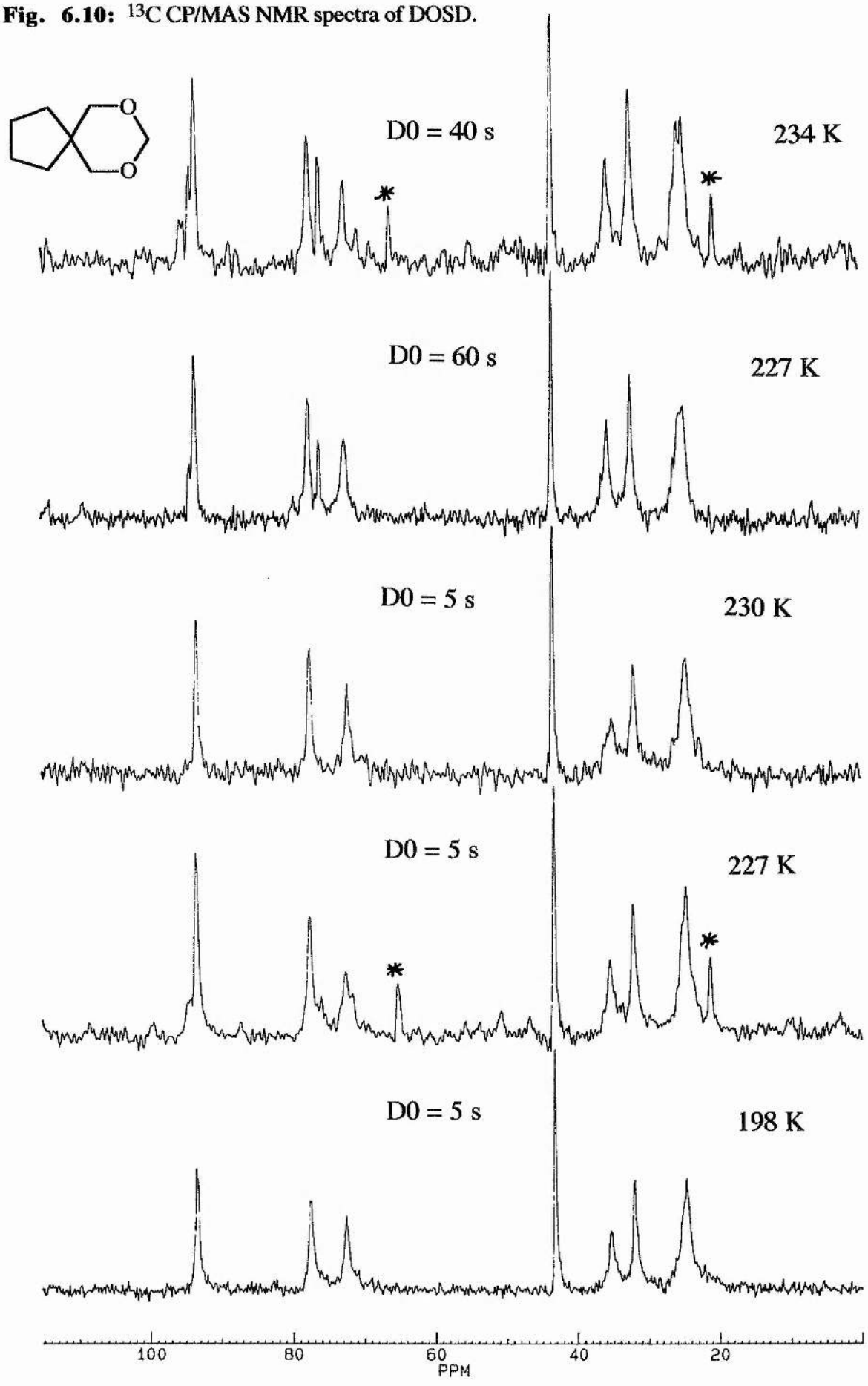

Fig. 6.12: ^{13}C HPDEC NMR spectra of DEDD.

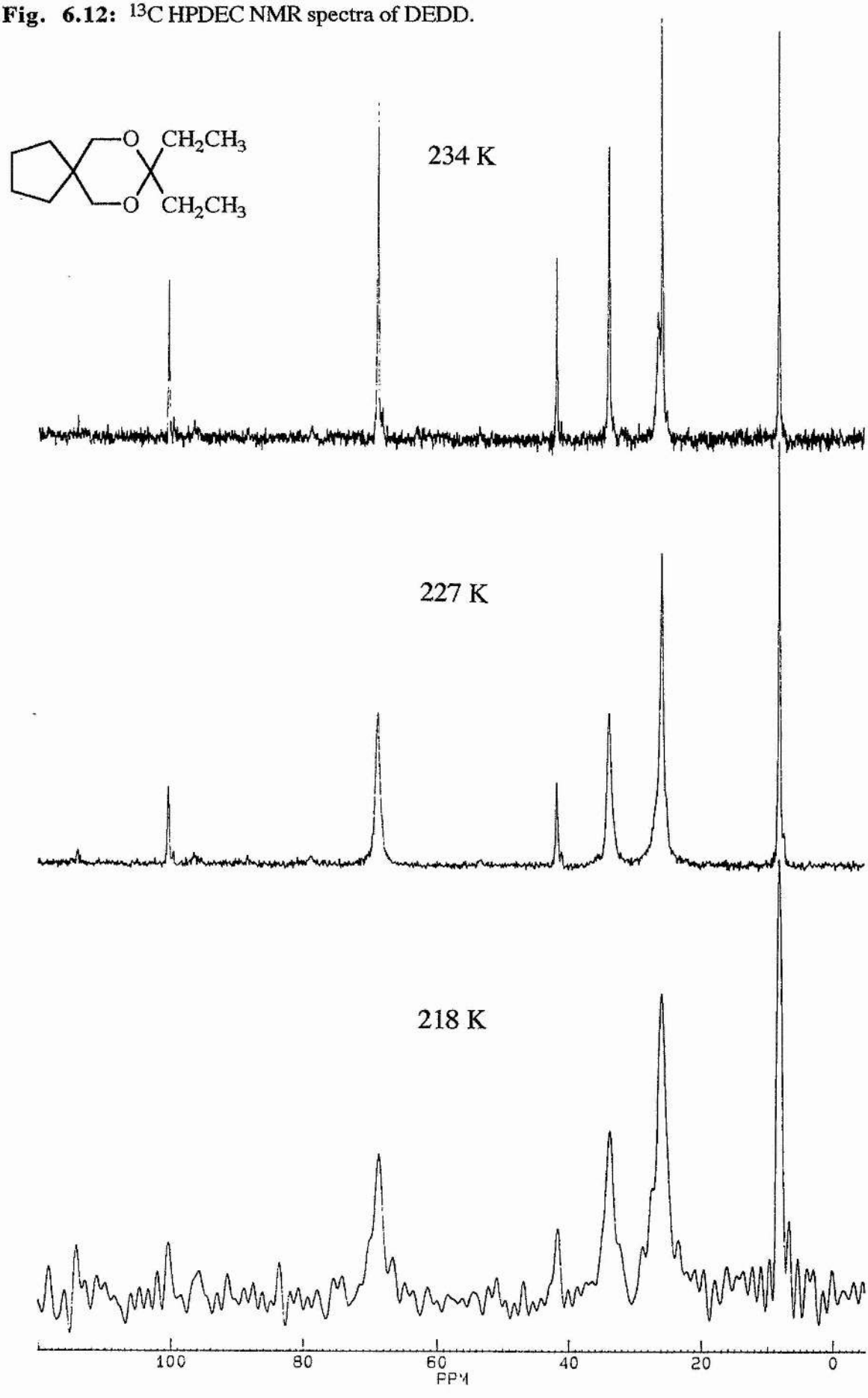

shifts for it are given (Table 6.3). The resonances for the two solid phases and the liquid phase (Table 6.3) show that the chemical shifts have not altered greatly.

Carbon	liquid	phase I	phase II
1,5	68.9	68.7	69.3 + 78.8
3	100.4	100.4	100.7
6	41.8	41.7	41.7
7,10	33.9	33.8	33.1
8,9	25.8	25.8	25.9
11	26.4	25.8	25.9
12	8.1	8.1	8.2

Table 6.3: ^{13}C NMR chemical shifts (ppm) for DEDD.

Phase II shows the same splitting of C(1,5) as seen in DOSP and it is also observed in the next compound, the di-propyl derivative. The C(7,10) resonance is also very broad indicating a decoalescence.

6.1.2.3 3,3-dipropyl-2,4-dioxaspiro[5.4]decane (DPDD)

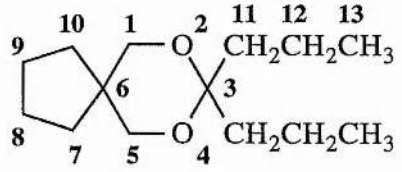

Fig. 6.13: Carbon numbering scheme for DPDD.

This compound is a liquid which freezes at *ca* 243 K into a plastic phase which then undergoes a transition at *ca* 204 K. The ^{13}C HPDEC NMR spectra (Fig. 6.14) show that the resonances broaden considerably as the temperature is lowered further. The chemical shifts of the resonances are similar for both phases apart from C(11) and C(7,10) (Table 6.4). Below the transition cross polarisation becomes possible (Fig. 6.14) and the chemical shifts correspond to phase II.

Fig. 6.14: ^{13}C NMR spectra of DPDD.

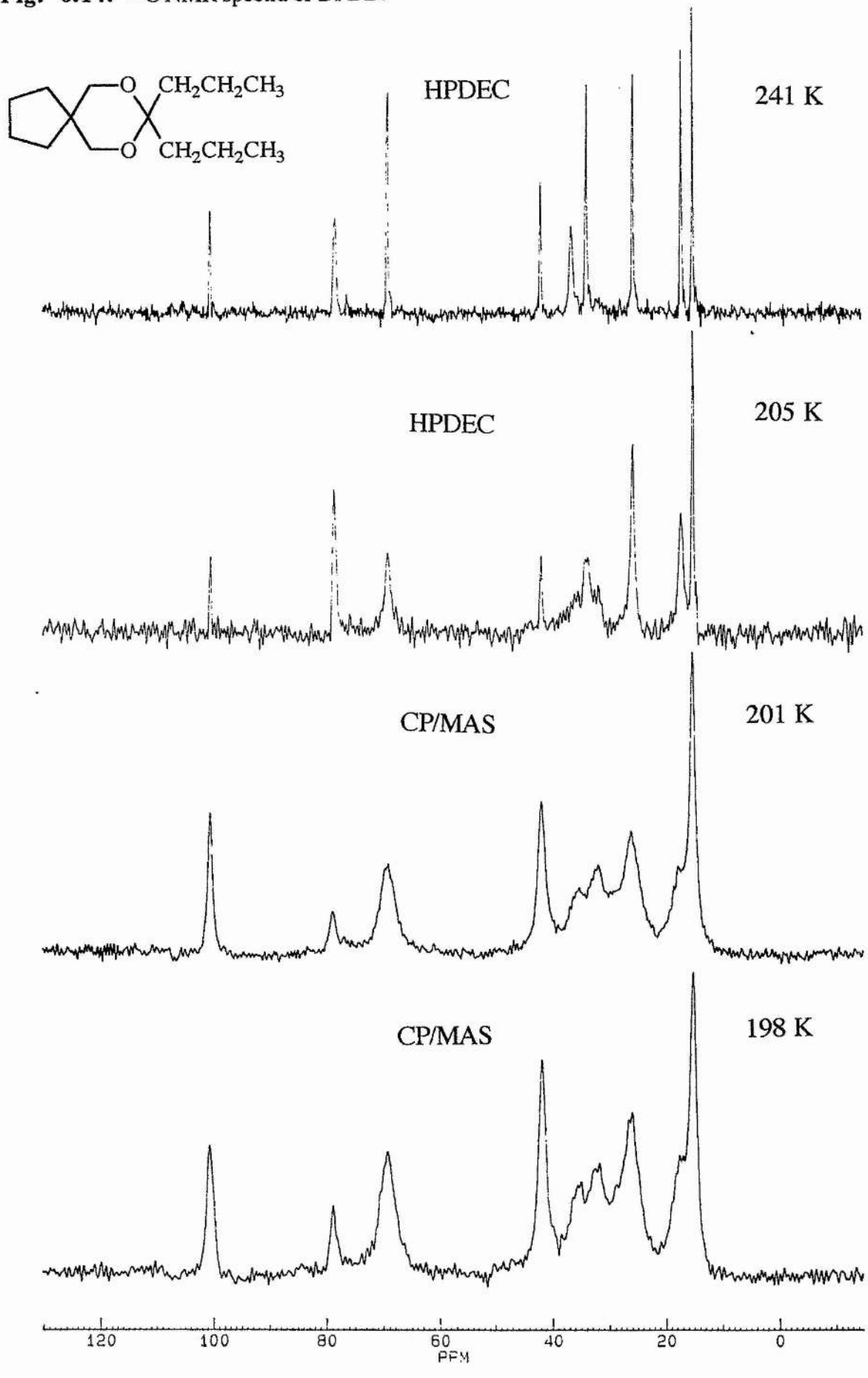

Carbon	phase I	phase II
1,5	69.3 & 78.4	69.0 & 78.8
3	100.5	100.5
6	42.0	41.8
7,10	36.6	35.0
8,9	25.8	26.0
11	34.0	31.9
12	17.2	17.0
13	15.1	15.2

Table 6.4: ^{13}C NMR chemical shifts (ppm) for DPDD

This compound again shows a splitting of C(1,5) in the ratio of *ca* 3:1 as seen for the two previous dioxaspiro compounds. The most surprising difference between phase I and II is the proposed 1.6 and 2.1 ppm upfield shifts of the C(7,10) and C(11) resonances. This may not be the case as the C(7,10) may have split as observed in DOSP and the C(11) resonance then overlaps with one of the resonates.

6.2 Bicyclic derivatives of cyclopentanone

For a comparison a related series of bicyclic dioxaspiro compounds were synthesised from cyclopentanone and examined by NMR.

6.2.1 1,4-dioxaspiro[4.4]nonce (DOSN)

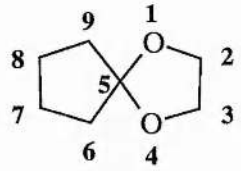

Fig. 6.15: Carbon numbering scheme for DOSN

This sample is again a liquid which freezes at 212 K, therefore the temperature range for studying this compound is very narrow. The ^{13}C CP/MAS NMR spectra (Fig. 6.16) show the expected four resonances which sharpen as the sample is cooled. The molecule, therefore, does not have the plastic phase seen in the BHMCP dioxaspiro derivatives, but there is molecular motion which appears to be causing some maximum dipolar broadening. The temperature range available and the signal strength means that measurement of ^{13}C $T_{1\rho}$ values was not feasible.

Fig. 6.16: ^{13}C CP/MAS NMR spectra of (a) DOSN and (b) BNDD.

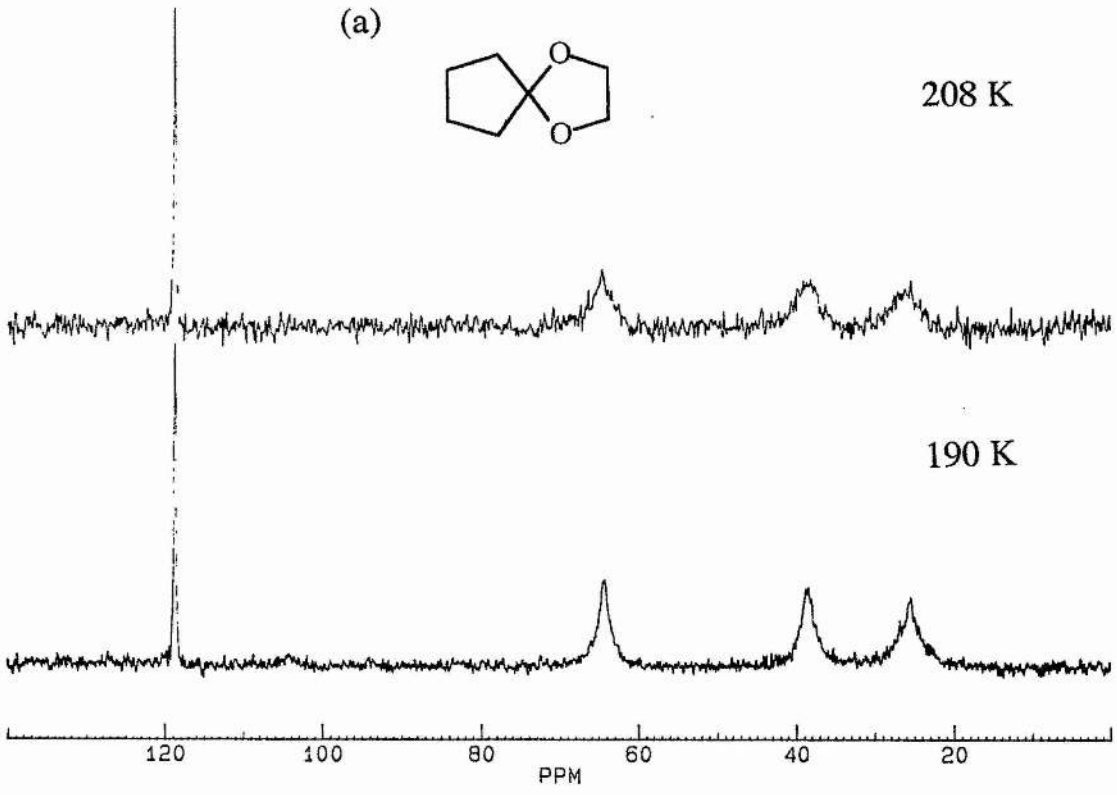

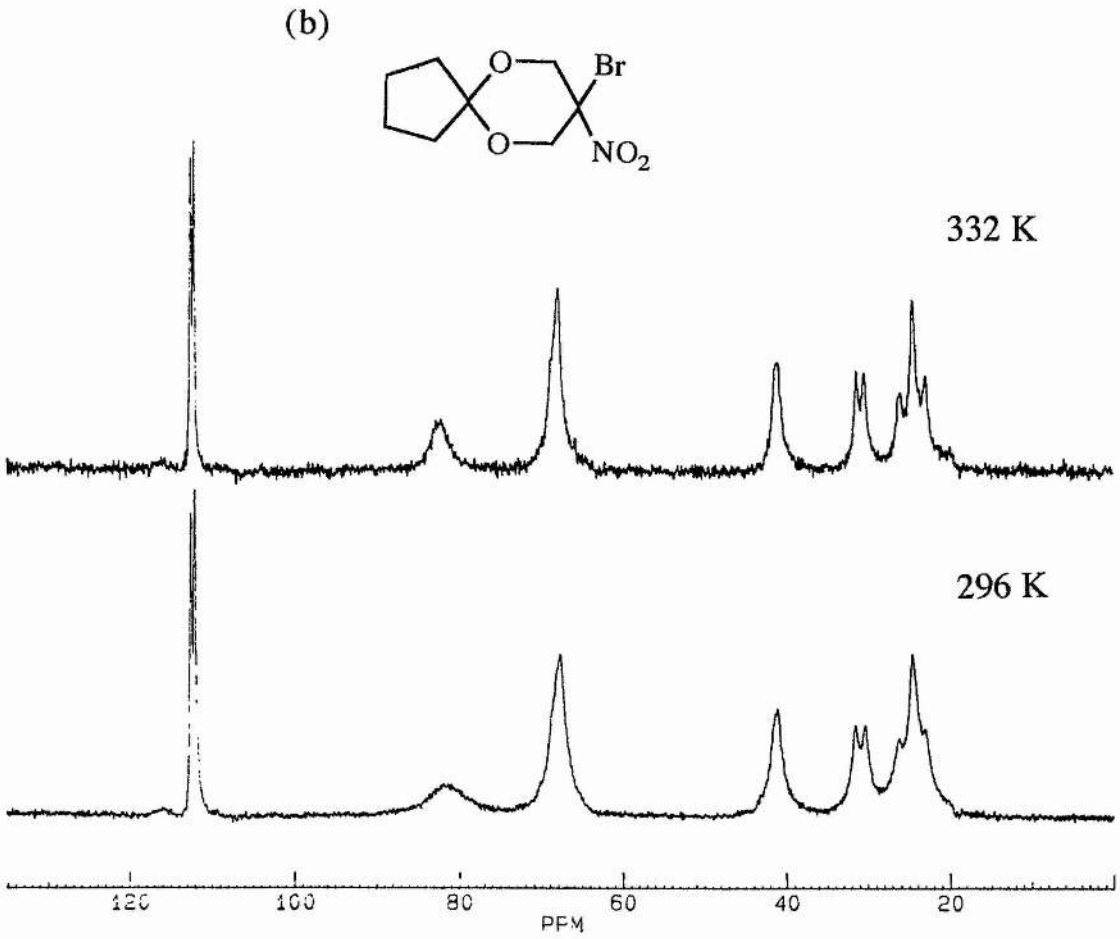

6.2.2 3-Bromo-3-nitro-1,5-dioxaspiro[5.4]decane (BNDD)

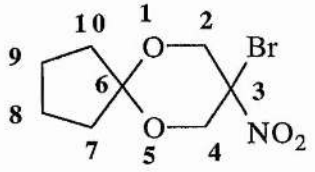

Fig. 6.17: Carbon numbering scheme for BNDD

The sample is a solid with a melting point of 80-82 °C. The ^{13}C CP/MAS NMR spectra of the compound (Fig. 6.16) show more than one resonance for each carbon, with the assignments in Table 6.5.

Carbon	δ_c (ppm)
2,4	67.7
3	82.0
6	112.0 +112.5
7,10	30.3 + 31.5 + 41.1
8,9	23.0 +24.5 +26.1

Table 6.5: ^{13}C chemical shifts (ppm) for BNDD at RT.

The only change on warming of the sample is that the resonances all sharpen which leads to the further splitting of the C(6), C(7,10) and C(8,9) resonances. The presence of two resonances for C(6) indicates that this compound has two molecules in the asymmetric unit. This explains the splitting patterns of C(7,10) and C(8,9) if it is assumed that the resonances at 24.5 and 41.1 are two overlapping resonances. The resonances for C(2,4) and C(3), which are broad, must also contain two resonances. The sharpening of the resonances on warming indicates there is some motion in the molecule, but it is centred on C(3) and so is likely to be motion in the six membered ring. The measurement of $T_{1\rho}$ values was not feasible because the compound had a very long ^1H T_1 relaxation time.

6.2.3 2-Chloromethyl-1,4-dioxaspiro[4.4]nonane (CMDN)

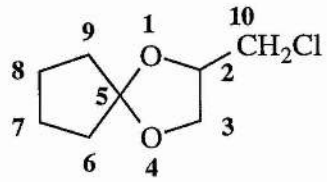

Fig. 6.18: Carbon numbering scheme for CMDN.

This compound freezes at *ca* 236 K, and the ^{13}C HPDEC spectrum (Fig. 6.19) at 234 K shows very sharp resonances for each carbon. The resonances then broaden when the sample is cooled to 230 K and then the signal disappears at 224 K. The ^{13}C CP/MAS NMR spectrum at 223 K (Fig. 6.19), however, reveals very broad resonances for the ring carbons and a change in chemical shift for the resonances, most dramatically in C(7,8) (Table 6.6).

Carbon	phase I	phase II
2	75.3	74.4
3	67.5	67.6
5	119.9	120.8
6,9	36.5 + 36.9	38.1
7,8	23.9 + 24.3	27.30
10	44.9	43.9 + 46.5

Table 6.6: ^{13}C NMR chemical shifts (ppm) for CMDN.

The other interesting difference is that C(10) is now split by residual dipolar coupling to the chlorine of 355 Hz. This suggests that the chloromethyl group is not freely rotating in phase II as it is in phase I and so the dipolar interaction is not averaged out. Dipolar coupling has been measured before in the solid state,[56] to be *ca* 420 Hz and which is of the same order as this example. The sample showed no further changes on cooling to 212 K.

Fig. 6.19: ^{13}C NMR spectra of CMDN.

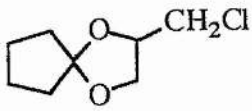

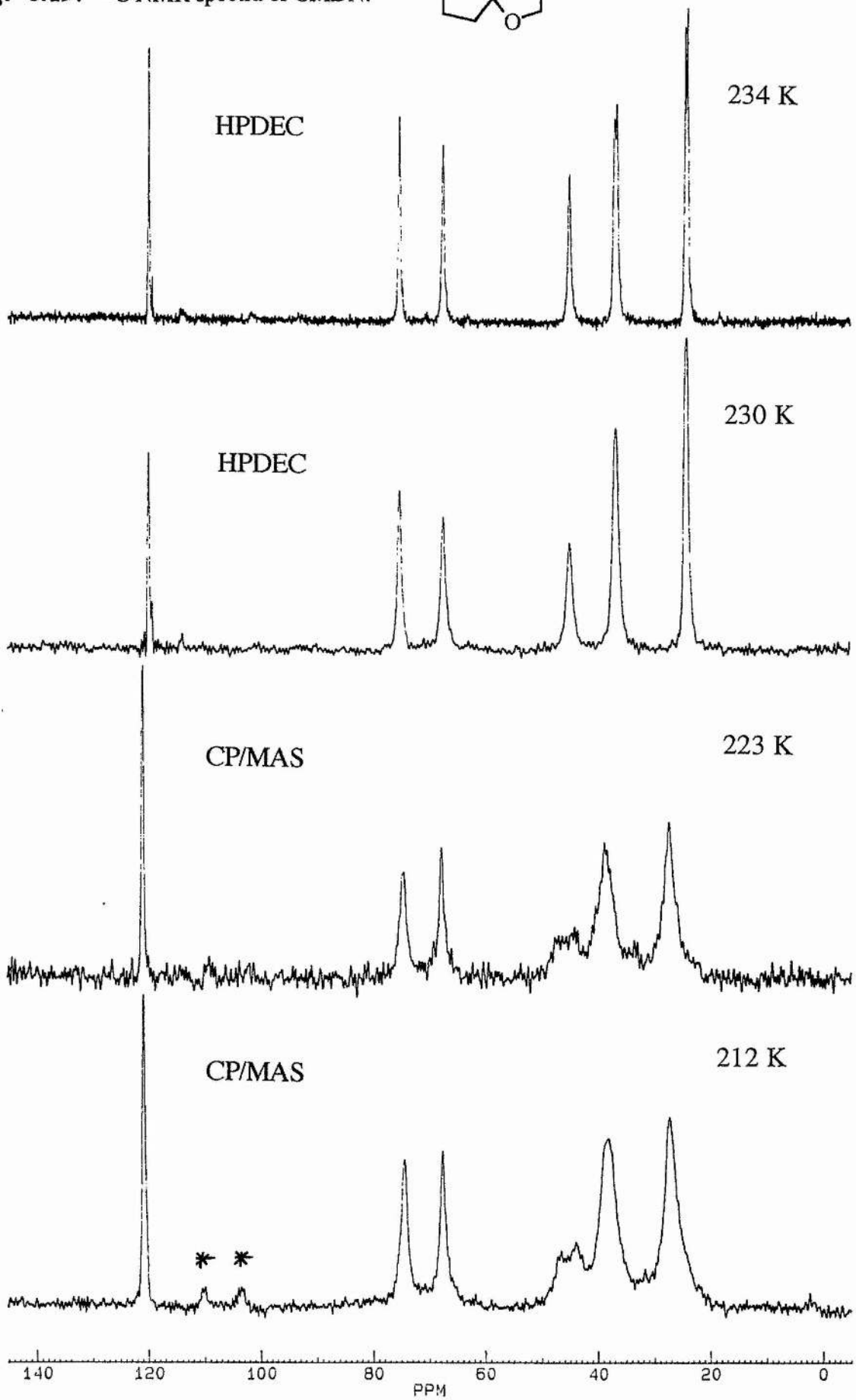

6.3 *trans*-1,2-cyclopentanediol (*t*-CPD)

The ^{13}C CP/MAS NMR spectra reported by Lambert *et al.*[51] show a dramatic broadening and sharpening of all the resonances as the temperature is varied, consistent with maximum dipolar broadening and indicating that it is a good sample for study by ^{13}C $T_{1\rho}$. The ^{13}C CP/MAS NMR spectra (Fig. 6.20) show maximum dipolar broadening at *ca* 240 K which is 30° lower than observed by Lambert *et al.* The temperatures that have been reported by Lambert *et al.* are from an uncalibrated probe and so do not correspond to our calibrated temperatures. The resulting $T_{1\rho}$ plot (Fig. 6.21) shows the expected minimum (*ca* 242 K) for each carbon.

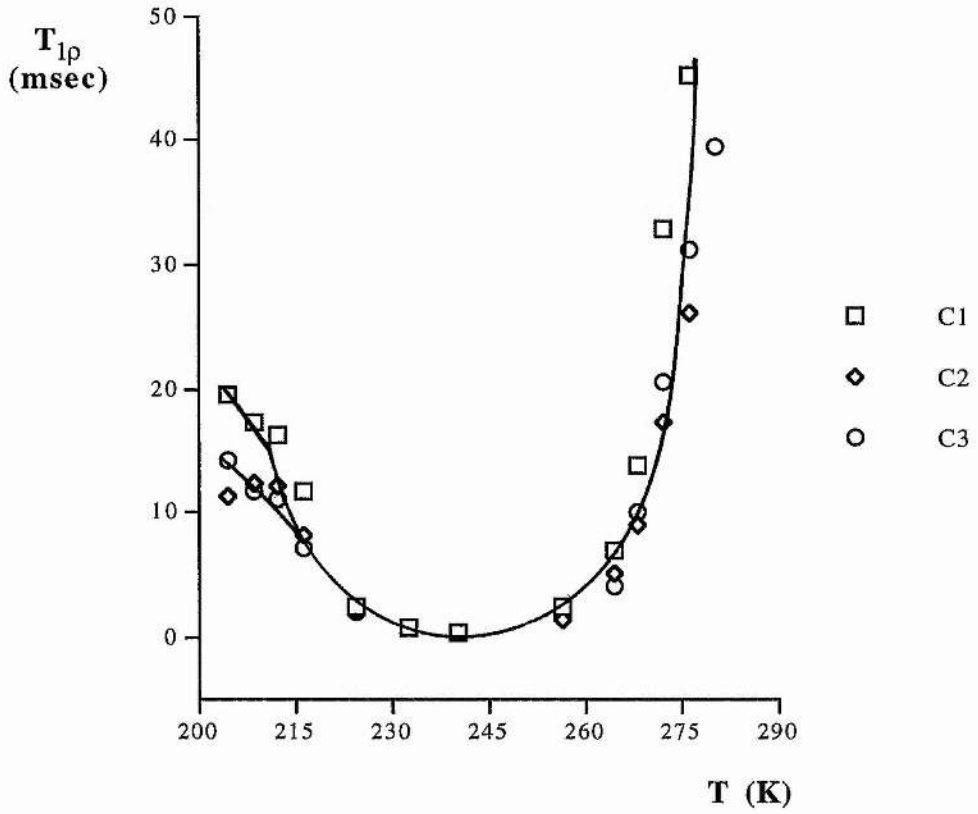

Fig. 6.21: $T_{1\rho}$ plot for C(1), C(2) and C(3) in *t*-CPD [ω_1 = 49.0 kHz]

The ^{13}C CP/MAS NMR spectra of *t*-CPD (-O^{2}H) gives a very similar series of spectra (Fig. 6.22). This indicates that the process is not hydrogen bond exchange.

Fig. 6.20: ^{13}C CP/MAS NMR spectra of *t*-CPD.

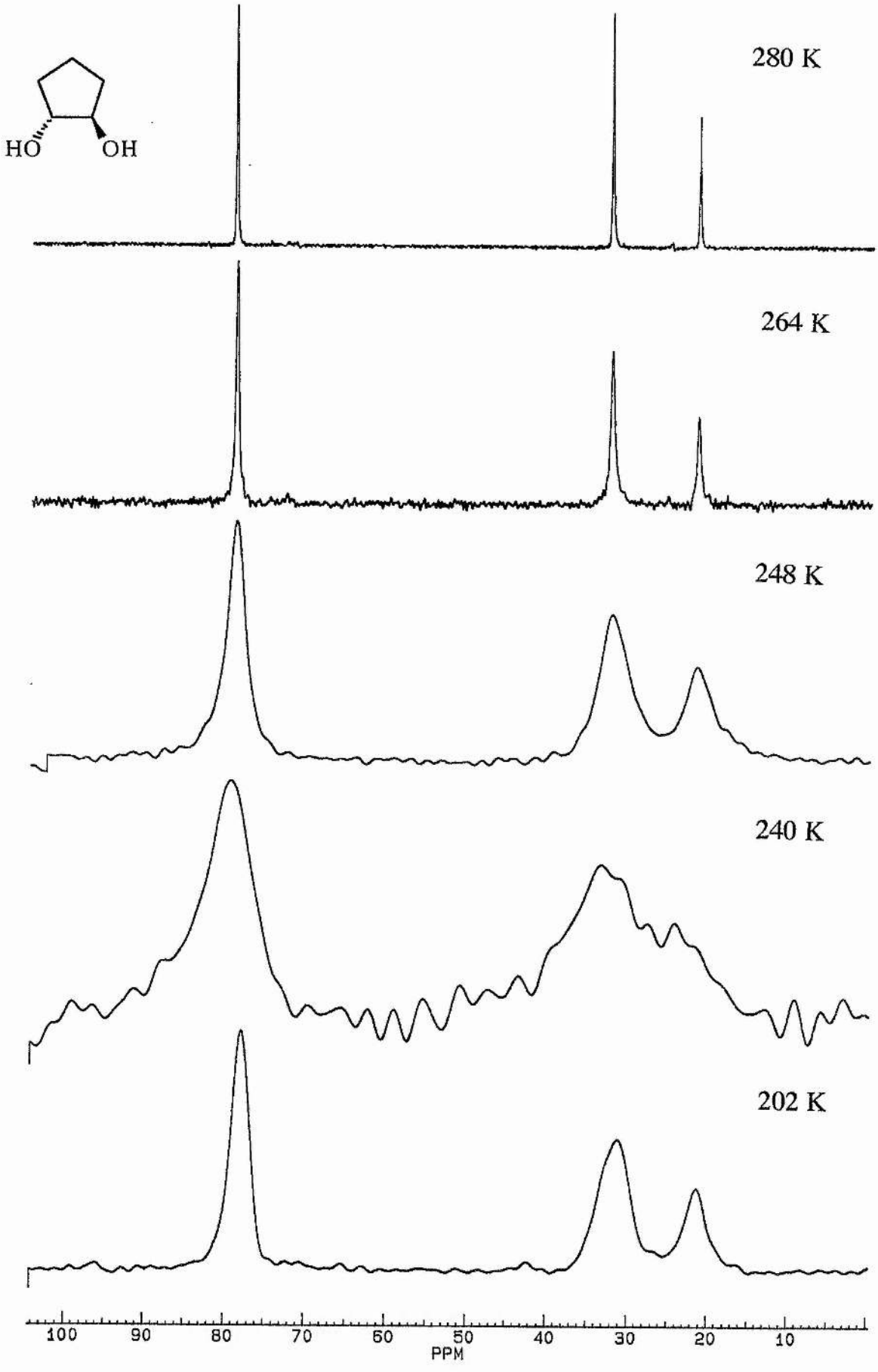

Fig. 6.22: ^{13}C CP/MAS NMR spectra of *t*-CPD (-O^{2}H).

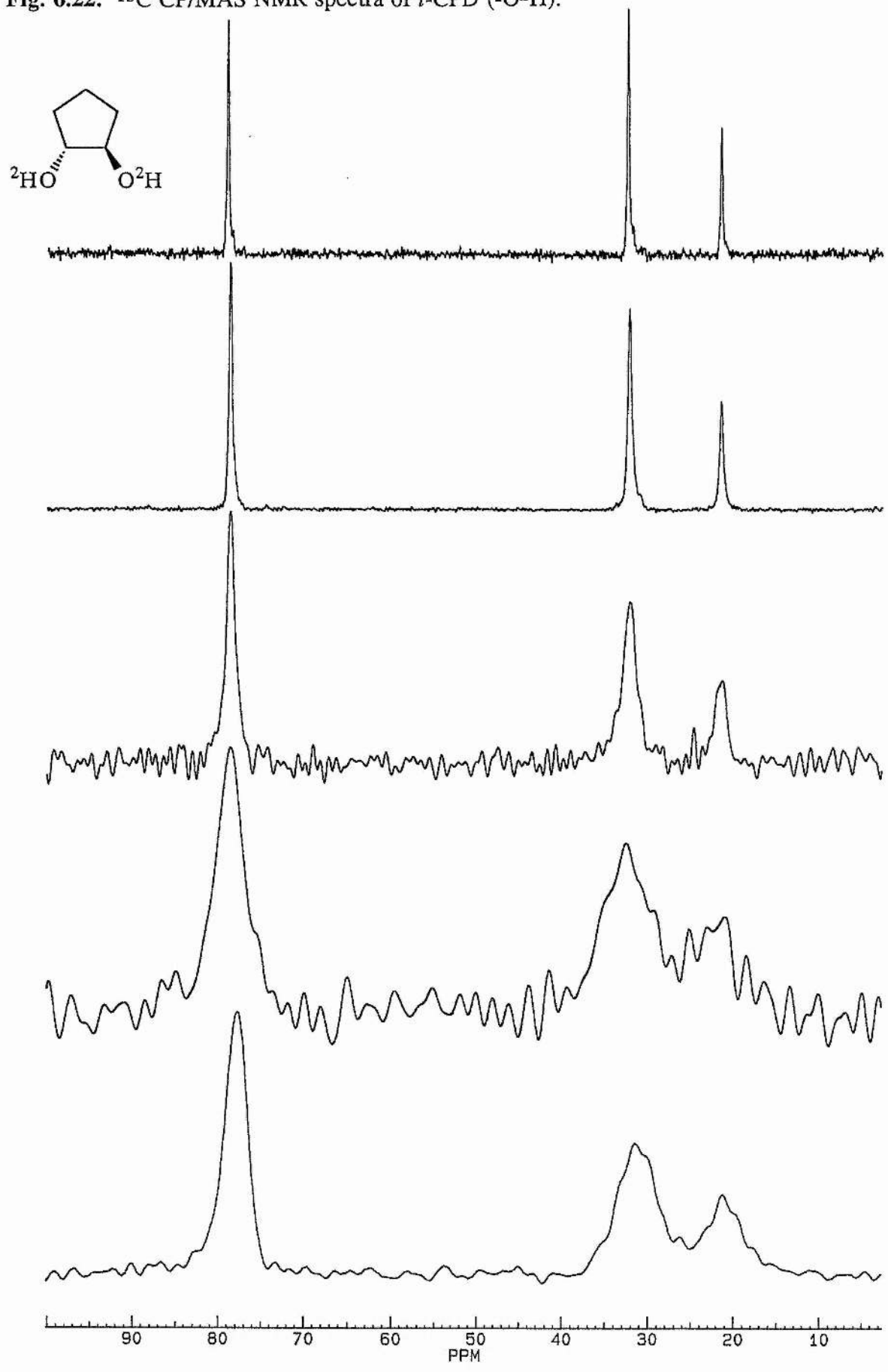

The resulting Eyring plot (Fig. 6.23) uses the average values from the three resonances taken from the $T_{1\rho}$ and rate data (Table 6.7). The data is plotted over the range 212 - 276 K because below this temperature the $T_{1\rho}$ values are not following the expected bell shaped curve. This indicates a change in activation energy of the process or that the $T_{1\rho}$ values are being modulated by another process.

	C(1)		C(2)		C(3)	
Temp (K)	**$T_{1\rho}$ (msec)**	**k x 10^5 (s^{-1})**	**$T_{1\rho}$ (msec)**	**k x 10^5 (s^{-1})**	**$T_{1\rho}$ (msec)**	**k x 10^5 (s^{-1})**
276	45.3	927	26.1	641	31.3	641
272	32.9	676	17.2	424	20.5	420
268	13.8	284	9.02	222	9.93	204
264	6.99	143	5.07	197	4.08	83.3
256	2.33	47.6	1.33	32.5	1.83	37.3
240	0.37	1.57	0.30	1.65	0.35	1.74
232	0.75	0.64	0.78	0.51	0.81	0.59
224	2.48	0.19	2.07	0.19	1.94	0.24
216	11.7	0.040	8.25	0.047	7.07	0.065
212	16.2	0.029	12.1	0.032	11.0	0.042

Table 6.7: $T_{1\rho}$ values and rates for *t*-CPD [ω_1 = 49.0 kHz, B^2 = 2.05 x 10^9 for C(1, 3) and 2.46 x 10^9 for C(2)]

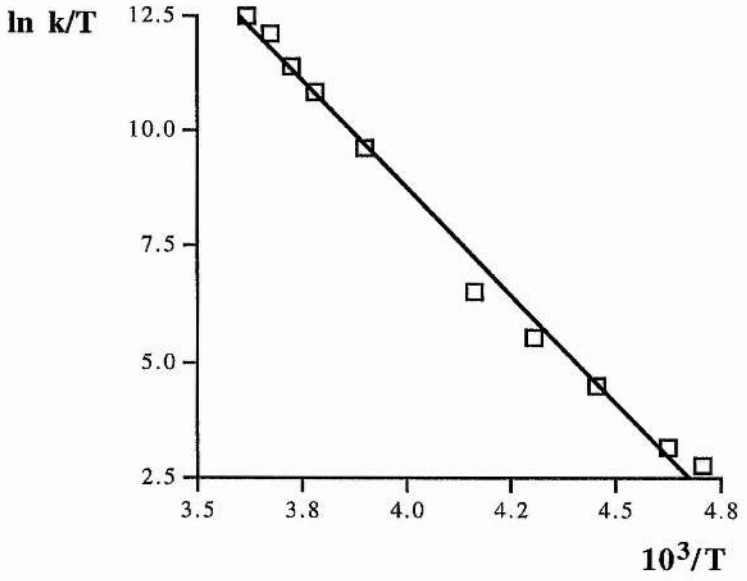

$\Delta H^{\ddagger}$ = +77.0 ± 2.6 kJ mol^{-1}

$\Delta S^{\ddagger}$ = +183.4 ± 10.9 J K^{-1} mol^{-1}

Fig. 6.23: Eyring plot of all three resonances in *t*-CPD

The free energy of activation is slightly larger than values calculated for molecular motion in the tetraalkyl compounds, but the entropy of activation is very much larger. The large positive entropy of activation, +183 J K^{-1} mol^{-1}, found here is surprising but the calculated error of ± 10.9 (95% confidence limits) show that it is significantly larger than zero. The discussion in section 1.4 shows that entropies of activation in solids are properties of the solid and not of the molecule. This results is, however, the most extreme example yet found.

6.3 4,4-Dimethyl-*trans*-1,2-cyclopentanediol (DMCD)

The ^{13}C CP/MAS NMR spectrum of DMCD at 219 K (Fig. 6.24) shows seven resonances for the carbon atoms (Fig. 6.25).

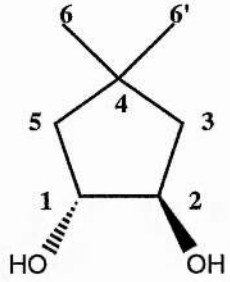

Fig. 6.25: Carbon atom numbering scheme for DMCD

The methylene resonances, C(3,5), (doublet *ca* 45 ppm) and the methyl resonance, C(6,6'), (doublet + broad singlet *ca* 35 ppm) are the resonances that are split. The C(1,2) resonance (76.0 ppm) and the quaternary carbon C(4) (32.0 ppm) are singlets. The identification of the quaternary carbon was achieved with the use of an NQS spectrum. This showed the disappearance of the methylene carbons and a marked reduction in the methyl resonances (32.4 - 35.5 ppm) relative to the quaternary carbon (32.0 ppm). On warming to 284 K (Fig. 6.24) the high field methyl resonance has sharpened. At 294 K two of the methyl resonances have coalesced (Fig. 6.24) with the third low field resonance coalescing at 306 K. The C(3,5) resonances also coalesce and this is complete at 303 K. Therefore, the free energies of activation ($\Delta G_c^{\ddagger}$) were calculated (Table 6.8):

Carbon	T_c (K)	$\Delta\nu$ (Hz)	$\Delta G_c^{\ddagger}$ (kJ mol^{-1})
3,5	303	288	58.3
6,6'	294, 306	172, 356	57.0, 58.4

Table 6.8: Coalescence data for the methylene and methyl carbons.

Fig. 6.24: ^{13}C CP/MAS NMR spectra of DMCD.

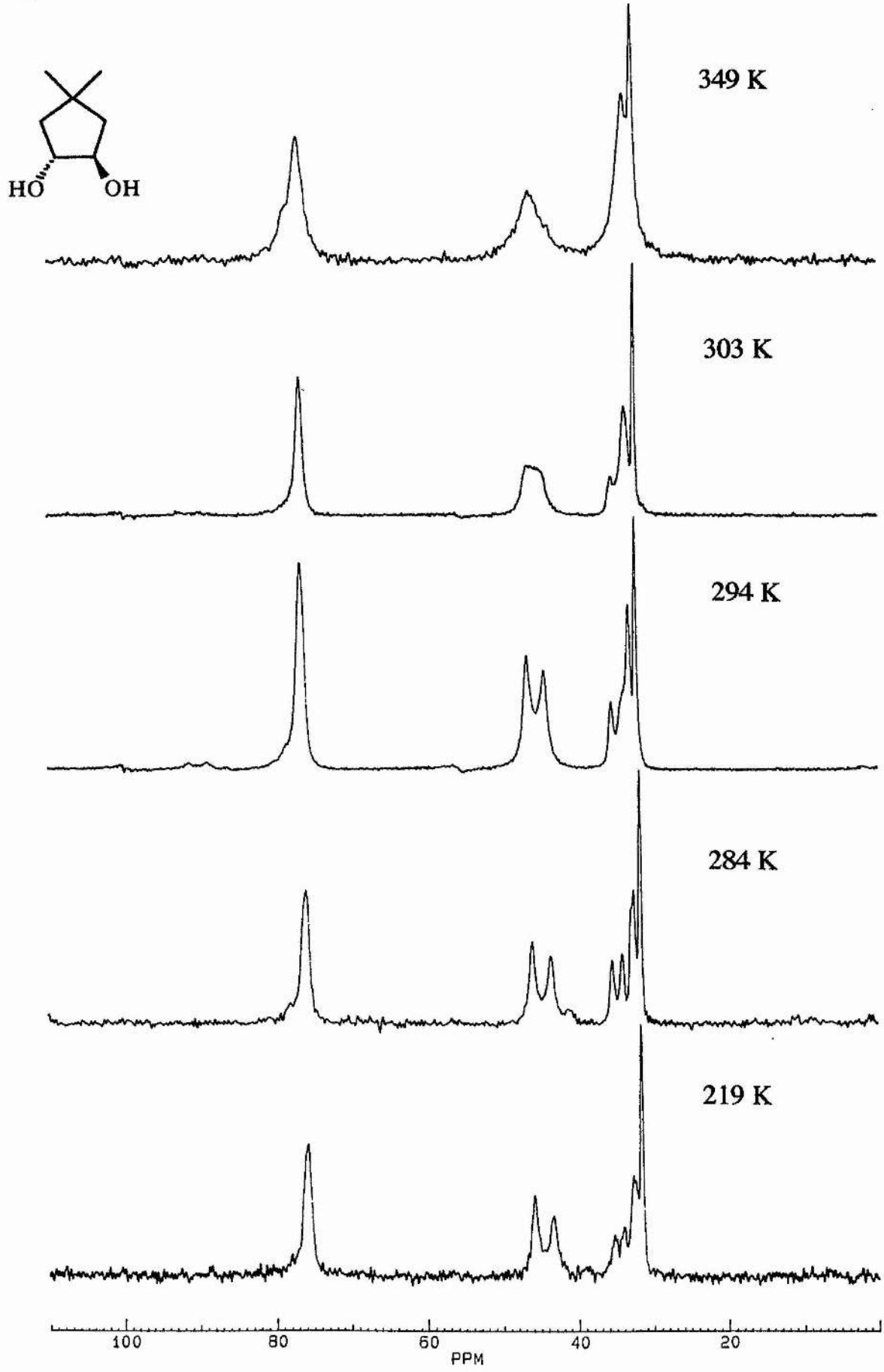

These values of $\Delta G_c^{\ddagger}$ are similar to those found for BHMCP (i.e. 60.8 and 60.2 kJ mol^{-1}). At 349 K (Fig. 6.24) there is a single resonance for each of the four chemical environments. All the resonances are showing signs of maximum dipolar broadening and the C(1,2) resonance has a low field shoulder. The presence of dipolar broadening in the sample led to the measurement of $T_{1\rho}$ values at high temperature. The resulting ^{13}C $T_{1\rho}$ plots (Fig. 6.26) show that C(1,2) and C(3,5) much shorter $T_{1\rho}$ values than C(4) and C(6,6').

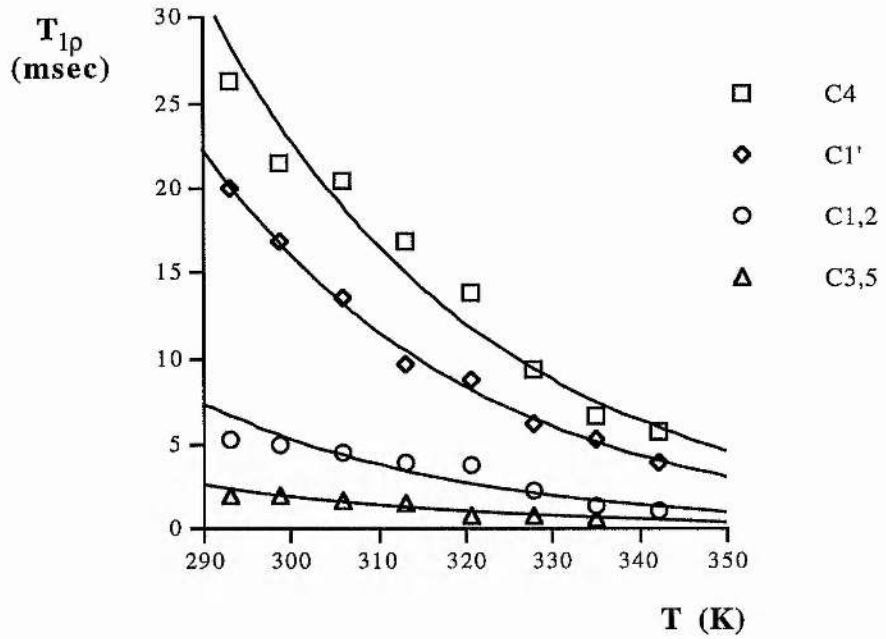

Fig. 6.26: $T_{1\rho}$ plot for the four resonances in DMCD

Therefore, the carbons experiencing the largest motion are C(1,2) and C(3,5). This is completely different to *trans*-1,2-cyclopentanediol (*t*-CPD) where the three resonances have very similar ^{13}C $T_{1\rho}$ values. The motion in DMCD must, therefore, be different to that in *t*-CPD. The possibility of hydrogen bond exchange or flipping, therefore seems likely especially when the $\Delta G_c^{\ddagger}$ values are considered.

The $T_{1\rho}$ values (Table 6.9) allow an Arrhenius plot (Fig. 6.27) which gives activation energies very much lower to those of $\Delta G_c^{\ddagger}$.

Temp (K)	C(1,2)	C(3,5)	C(4)	C(6,6')
342	1.10		5.69	3.94
335	1.43	0.62	6.73	5.28
328	2.24	0.85	9.37	6.25
320	3.82	0.85	13.8	8.82
313	4.00	1.59	16.9	9.71
306	4.54	1.69	20.5	13.5
299	5.04	2.45	21.6	16.9
293	5.36	1.97	26.3	20.0

Table 6.9: Values of $T_{1\rho}$ (msec) for the four resonances in DMCD [ω_1 = 42.2 kHz].

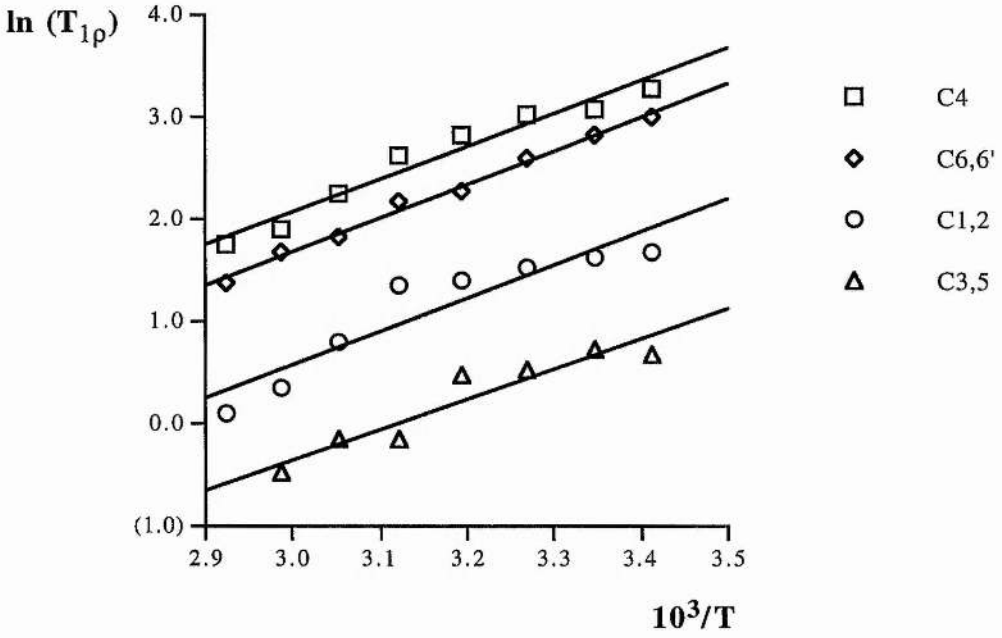

Carbon	E_a (kJ mol^{-1})
1,2	27.0 ± 4.2
3,5	25.8 ± 3.7
4	25.2 ± 2.4
6,6'	27.3 ± 1.0

Fig. 6.27: Arrhenius plot and activation energies for the four resonances in DMCD.

The activation energies are considerably lower than the $\Delta G_c^{\ddagger}$ indicating that it is not the same process that is being measured. To check whether hydrogen bonding is a factor in the coalescence process the hydroxyl groups were deuteriated. The resulting ^{13}C CP/MAS NMR spectra showed that the coalescence temperatures were slightly higher. The resulting $\Delta G_c^{\ddagger}$ values (Table 6.10) are, therefore, slightly higher as well. These results agree with those for 1,1-(bishydroxymethyl)cycloheptane and 2,2-dimethylpropane-1,2-diol.[55] This, therefore, indicates that hydrogen bond exchange is a possible cause of the coalescence and the $T_{1\rho}$ effect.

Carbon	T_c (K)	$\Delta\nu$ (Hz)	$\Delta G_c^{\ddagger}$ (-O^{2}H)	$\Delta G_c^{\ddagger}$ (-O^{1}H)
3,5	308	292	59.1	58.3
6	298	143	58.7	57.0
6'	315	311	60.1	58.4

Table 6.10: Data and $\Delta G_c^{\ddagger}$ values (kJ mol^{-1}) for DMCD (-O^{2}H) and (-O^{1}H)

The four methyl resonances at low temperature says that there must be at least two molecules in the asymmetric unit. The coalescence of the methyls must be by a process that interconverts the environment of these molecules and this must also give a two fold symmetry to the individual molecules because with the same $\Delta G_c^{\ddagger}$ C(3) and C(5) coalesce. Two possible structures (Fig. 6.29) in the solid are dimers (1) or long chains of molecules (2). The two structures could by a process of hydrogen bond flipping and a pseudo rotation of both rings result in the exchange of the carbon resonances.

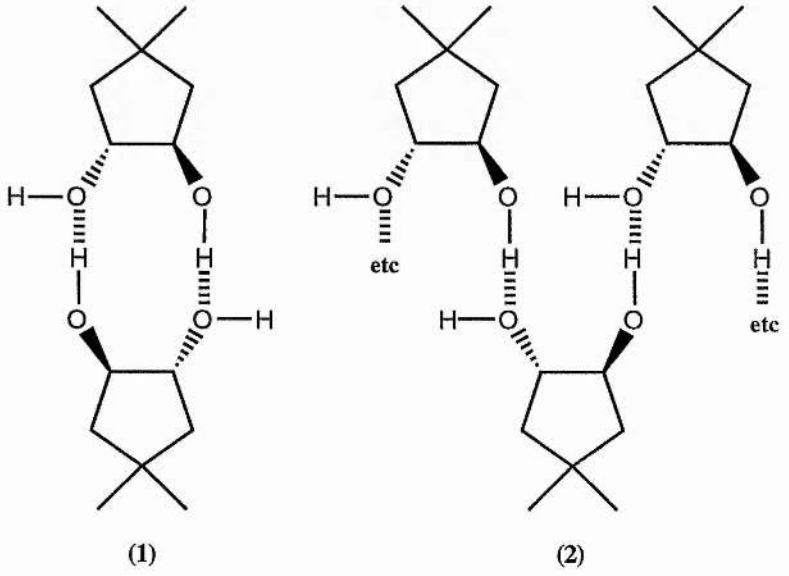

Fig. 6.29: Possible H-bonded structures of DMCD.

The ^{13}C $T_{1\rho}$ values give very much lower activation energies and cannot be due to the same process and so this is process 2. Process 1 might contribute to the $T_{1\rho}$ relaxation but cannot be the only process. Process 1 shows a ^{2}H-bond effect and, therefore, involves H-bond making/breaking. Process 2 is clearly greatest on C(1,2) and more so on C(3,5) (from the $T_{1\rho}$ values) and so is probably a restricted pseudorotation or wobbling of the methine and methylene groups.

The use of a 2D CP/EXSY pulse sequence confirms that the methylene carbons are exchanging [Fig. 6.30 (a)] as well as the methyl resonances at 35.6 and 34.9 ppm [(Fig. 6.30(b)]. The exchange of the central methyl resonance (34.3 ppm) with the high field resonance (34.9 ppm) cannot be seen due to interference from the quaternary resonance. The two low field resonances do not appear to be exchanging. These spectra suggest that in one form the methyl resonances are not equivalent and then after pseudorotation and/or H-bond exchange they convert into an equivalent environment.

6.4 Sulpholane

Another five membered ring compound studied by Lambert *et al.*[51] was sulpholane which showed maximum dipolar broadening and coalescence phenomena. The ^{13}C CP/MAS NMR spectra (Fig. 6.31) that have been recorded in the present study, confirm these findings. The temperatures that Lambert *et al.* quoted are again called into question with the solid state ^{13}C CP/MAS spectrum at +38 °C when sulpholane melts at +27 °C. Lambert *et al.* report only two phases with a phase transition at 288 K. The earlier ^{1}H spin-lattice relaxation study by Kydon *et al.*[57] showed that sulpholane has two plastic phases (T_{tr} = 296 K) and two crystalline phases (T_{tr} = 246 K). The phase above 288 K is confirmed as a likely plastic phase because the signal is much stronger using HPDEC as opposed to CP/MAS. The phase transition at 296 K (phase I - II) did not result in any change of the ^{13}C chemical shifts [Fig. 6.31(a)]. The transition at 288 K (phase II - III), however, did result in a much broader spectrum (Fig. 6.25) and the two resonances are now split. The upfield resonances then decrease in intensity as the sample is further cooled. The reason for the two resonances for each carbon appears to be hysteresis effects because supercooled phase II that has been reported to persist to 267 K.[58] Therefore, the free energy calculations made by Lambert *et al.* are not valid because the two resonances are from different phases and a coalescence temperature of 288 K is given which is the plastic to non-plastic phase transition.

Fig. 6.30 (a): ^{13}C 2D CP/EXSY spectrum of DMCD showing methylene exchange.

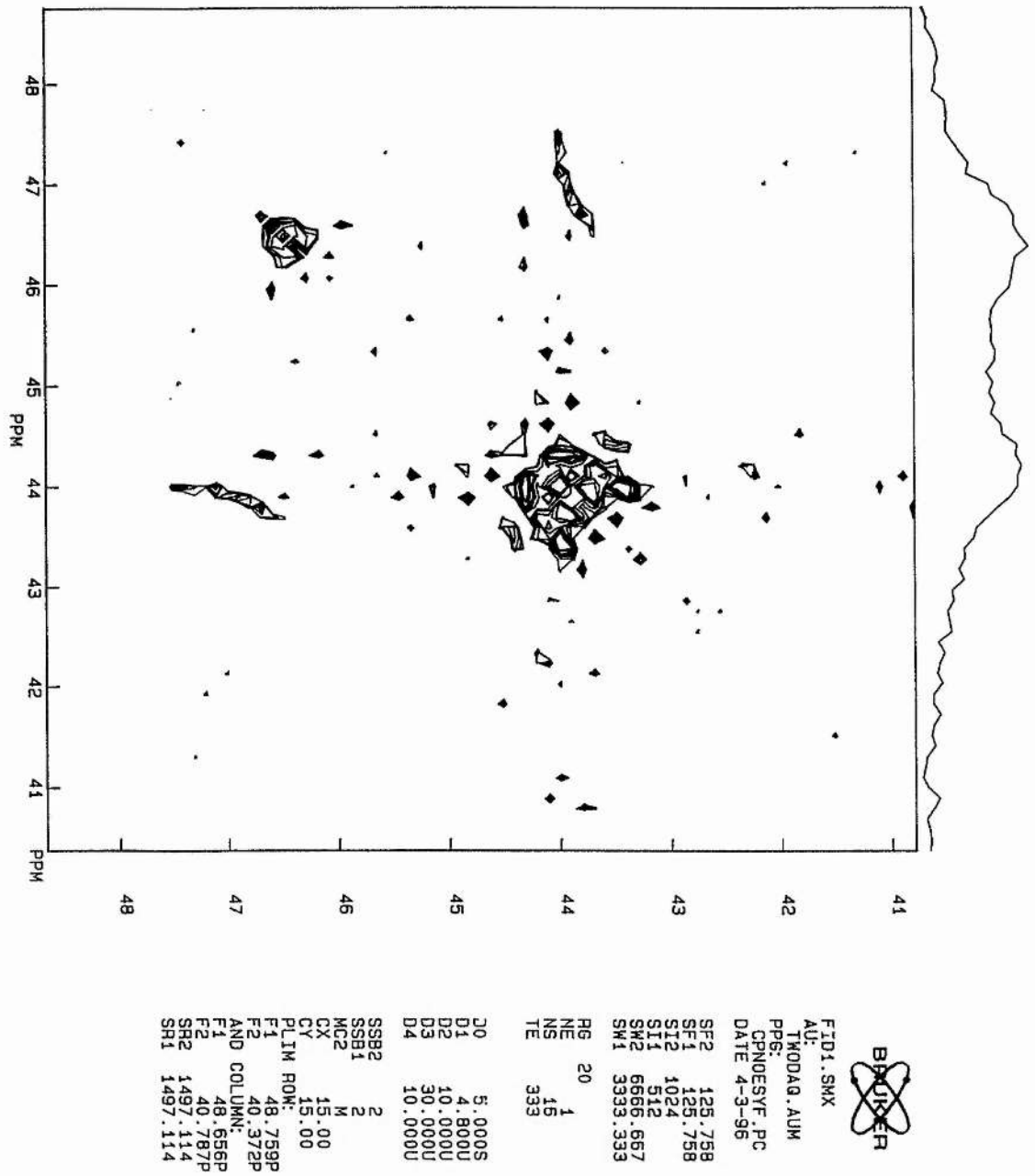

Fig. 6.30 (b): ^{13}C 2D CP/EXSY spectrum of DMCD showing methyl exchange.

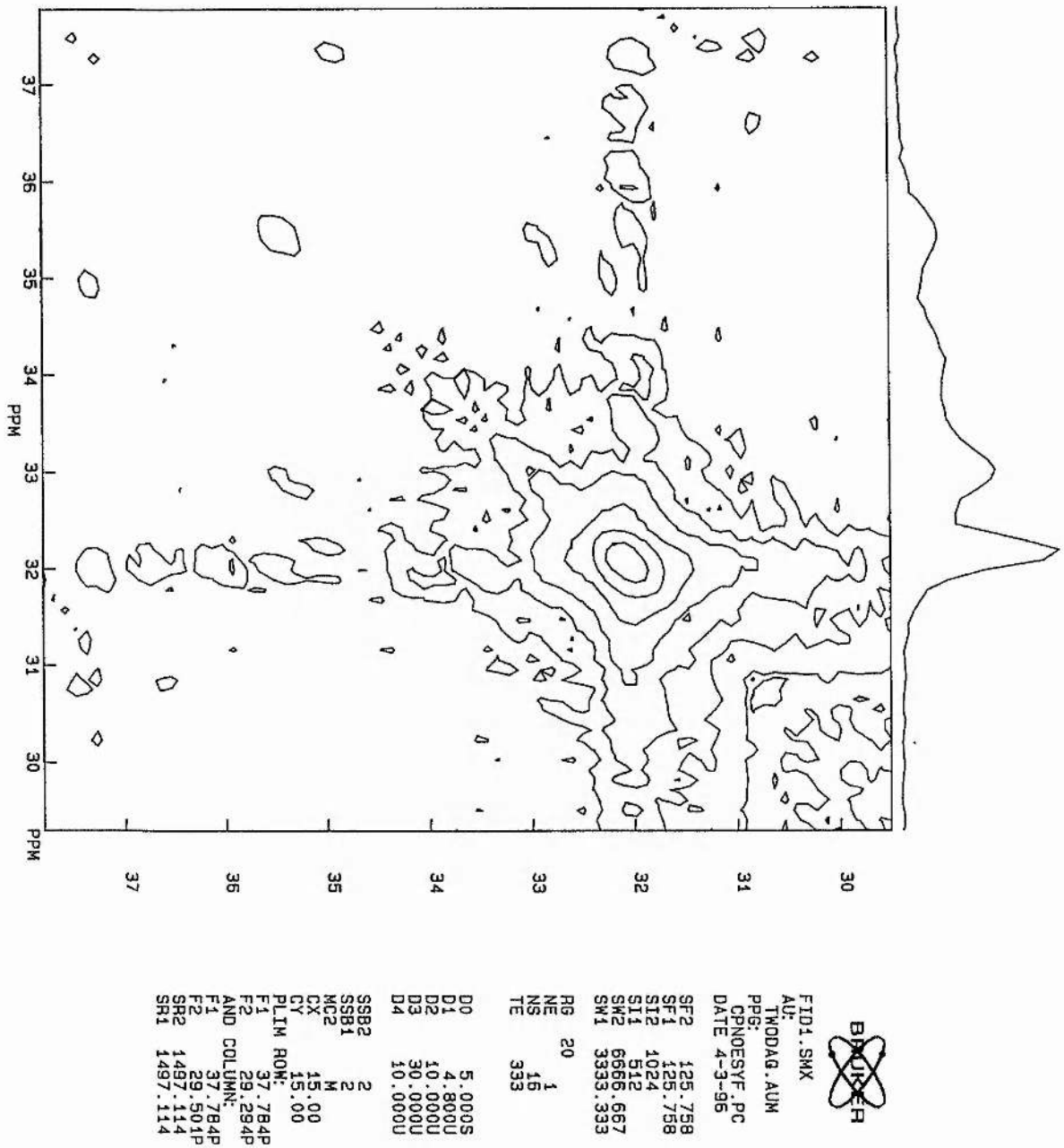

Fig. 6.31(a): ^{13}C CP/MAS NMR spectra of sulpholane.

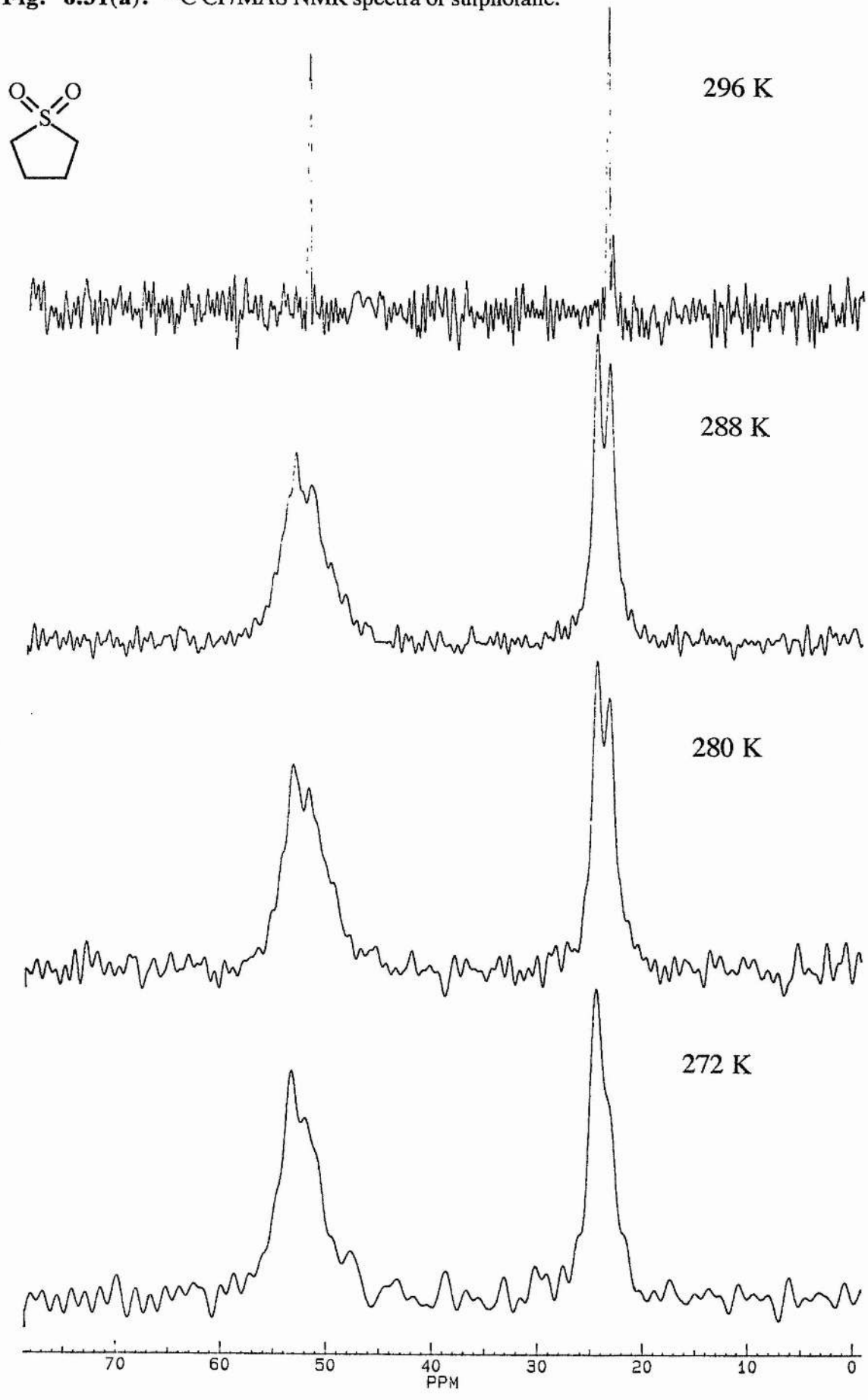

Fig. 6.31(b): ^{13}C CP/MAS NMR spectra of sulpholane.

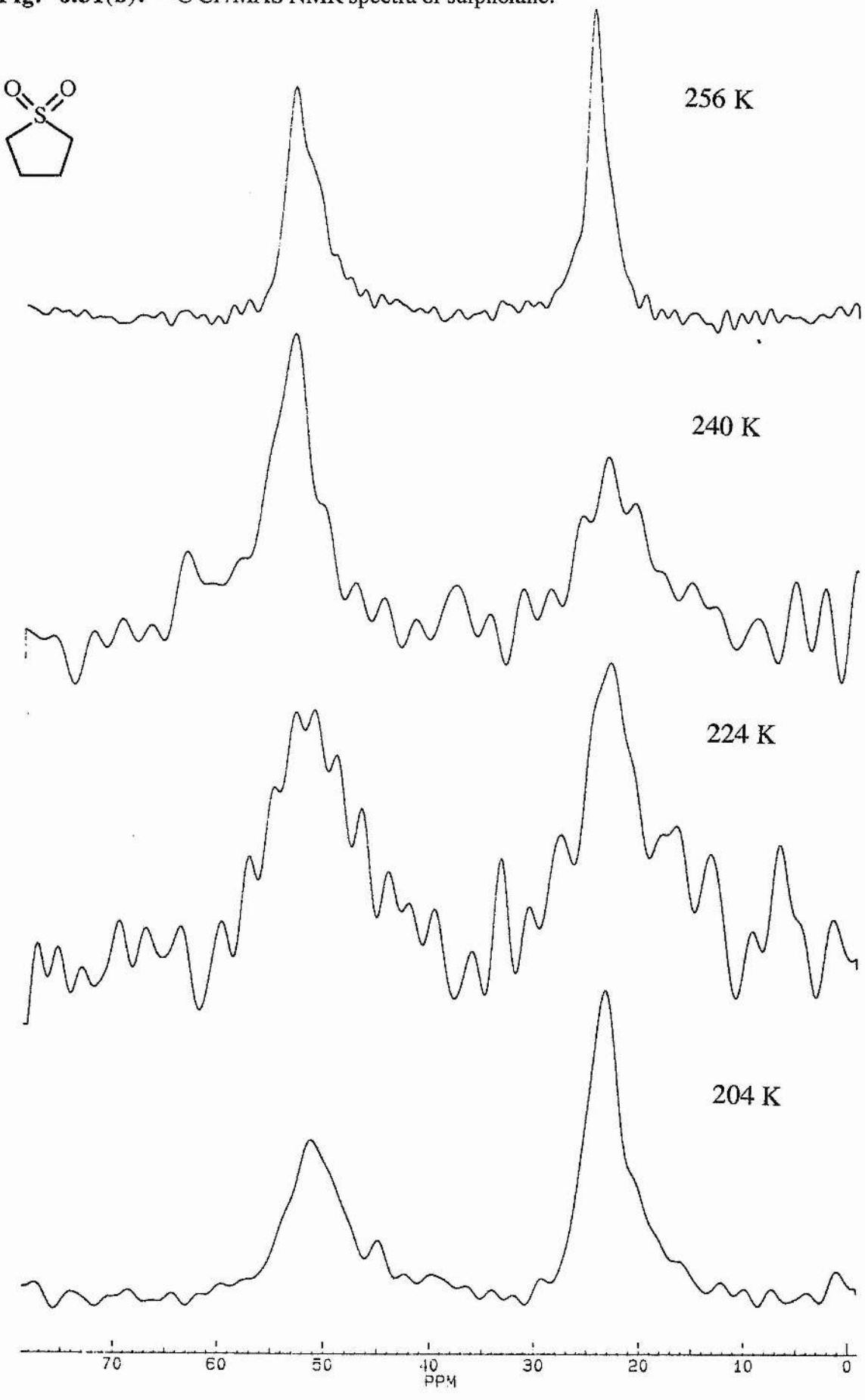

When the sample is cooled further to 240 K [(Fig. 6.31(b)] a deterioration in cross polarisation efficiency becomes evident along with the associated maximum dipolar broadening. The signal at *ca* 235 K is very poor and so the next spectrum given at 224 K is below the minimum for $T_{1\rho}$ [Fig. 6.31(b)]. The ^{13}C $T_{1\rho}$ plot (Fig. 6.32) of sulpholane confirms the minimum at *ca* 230 K. The resonances then sharpen slightly on further cooling to 204 K [(Fig. 6.31(b)]. The decoalescence reported by Lambert *et al.* at low temperature is not seen. The $T_{1\rho}$ plot shows no obvious discontinuity at the supposed phase transition at 246 K reported by Kydon *et al.* The phase change comes very close to the $T_{1\rho}$ minimum (*ca* 235 K) and so any small discontinuity might be difficult to see because the gradient of the curve is changing rapidly. The large jump in $T_{1\rho}$ values seen in 3,3-diethylpentane, however, contradicts this statement. The data reported by Kydon *et al.* shows only a very small jump in ^{1}H $T_{1\rho}$ values which would not be apparent in the ^{13}C $T_{1\rho}$ values because of the larger errors involved.

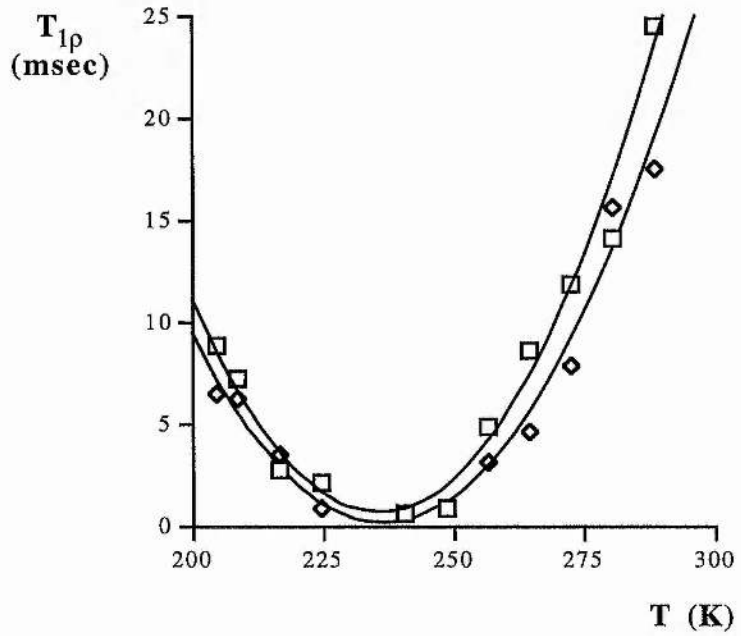

Fig. 6.32: ^{13}C $T_{1\rho}$ plot of C(1) and C(2) in sulpholane [ω_1 =51.4 kHz].

The other problem with the $T_{1\rho}$ plot is that due to the temperature limitations of the probe only four points below the proposed phase transition could be obtained. Therefore, the change in gradient of the $T_{1\rho}$ values reported in the literature,[57] before and after the phase change is not obvious because of the lack of data. The ^{13}C $T_{1\rho}$ data and rates (Table 6.12) show that the values for C(1) and C(2) are very similar. The data is, therefore, combined to reduce errors for the Eyring plot (Fig. 6.33).

	C(1)		C(2)	
Temp. (K)	**$T_{1\rho}$ (msec)**	**k x 10^5 (s^{-1})**	**$T_{1\rho}$ (msec)**	**k x 10^5 (s^{-1})**
288	24.5	330	17.5	305
280	14.2	191	15.6	272
272	11.8	159	7.83	137
264	8.66	89.3	4.55	79.4
256	4.89	65.8	3.17	55.2
248	0.82	10.0	0.80	13.2
240	0.65	7.35		
224	2.12	0.37	0.80	0.79
216	2.72	0.29	3.54	0.17
208	7.19	0.11	6.23	0.096
204	8.81	0.089	6.54	0.092

Table 6.12: $T_{1\rho}$ values and rates for C(1,2) in sulpholane [ω_1 = 51.4 kHz, $B^2 = 1.35 \times 10^9$ and 1.74×10^9 for C(1,2) respectively].

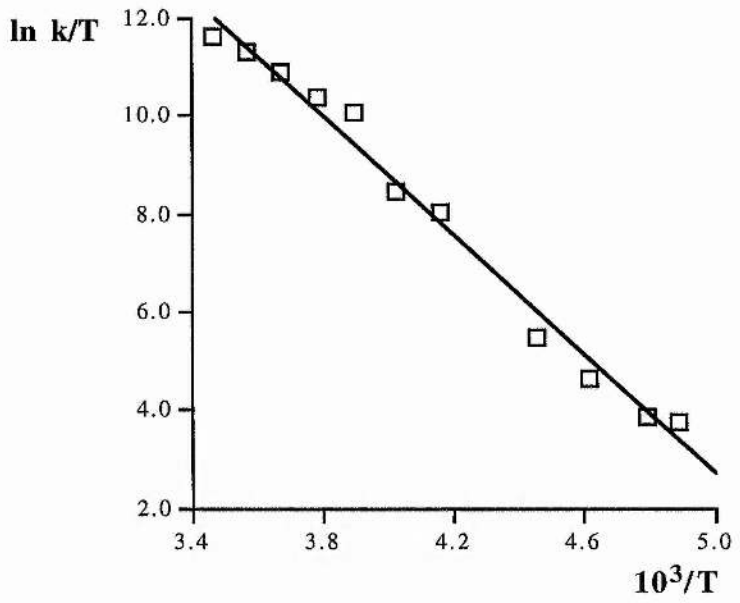

$\Delta H^{\ddagger} = +50.6 \pm 2.1$ kJ mol^{-1}

$\Delta S^{\ddagger} = +77.9 \pm 8.6$ J K^{-1} mol^{-1}

Fig. 6.33: Eyring plot and activation parameters for sulpholane using the combined data of C(1) and C(2).

The activation energy can also be obtained from an Arrhenius plot ($E_a = 52.6 \pm 2.1$ kJ mol^{-1}) and is the same as the value given for phase III (288 - 246 K, $E_a = 52 \pm 2$) in the literature.[57] The activation energy for phase IV is much lower (23 ± 2) and so the four low temperature points would be expected not to tie in with the points from above 246 K. The four low temperature points are too close to the minimum and so an Arrhenius plot of these points is meaningless. The sample is known to show some hysteresis at the phase transitions and so these points may well still belong to phase III.

The entropy of activation is again large and positive as in *t*-CPD. This suggests that the processes in the two compounds could be similar. The two motions possible in sulpholane are rotation about a two fold axis and ring puckering.[57] The latter is reported to be significant in narrowing the absorption line below 77 K.[57] The second moment is then reduced as the amplitude of the ring puckering increases between 77 and 160 K. Two fold rotation then reduces the second moment further on warming to 250 K. Therefore, it is most likely to be the two fold rotation that is modulating the ^{13}C $T_{1\rho}$ values.

CONCLUSION

Conclusion

This study of crystalline organic solids by NMR and in particular using ^{13}C $T_{1\rho}$ measurements has shown that there are many varied conformational processes occurring in the solid state. An advantage of ^{13}C $T_{1\rho}$ as opposed to proton relaxation measurements is that data can be recorded for each carbon resonance resolved. This allows the identification of the parts of the molecule experiencing the largest amplitude of motion and helps elucidate the nature of the dynamic processes.

The tetraalkylmethanes have shown that phase changes can cause large jumps in rates of molecular motion (3,3-diethylpentane) or instigation of a different dynamic process altogether (4,4-dipropylheptane).

The tetraalkyl ammonium and phosphonium salts have shown a variety of molecular motion i.e. cation tumbling, alkyl group rotation and librations. The compounds are shown to be influenced greatly by the structure e.g. compare activation parameters for TMPCl and TMPBr with TMPI. Therefore, a study by X-ray diffraction of these compounds would help to explain the differences seen between and both the enthalpies of activation and entropies of activation calculated for the series of compounds. Although the entropies of activation have large inherent errors they provide information about the solid lattice and so a correlation with X-ray structures should arise. X-ray diffraction studies would also confirm the cause of the different chemical shifts of each of the four chains and the observation of more than one molecule in the asymmetric unit observed for the tetrabutyl ammonium halides and periodate and the tetrabutyl phosphonium halides. This is assumed to be due to the proximity of the anion as observed in TPAI.[43]

The cyclopentane analogues show a variety of molecular motion attributed to H-bond exchange (BHMCP), H-bond exchange with associated large amplitude motions of the ring (*t*-CPD), H-bond exchange at low temperature then large amplitude motions of the ring (DMCD) and rotation about a two fold axis (sulpholane).

The observation of H-bond exchange in BHMCP appears to be confirmed by the deuteriated compound. The different behaviour of the spectrum as the temperature is varied however, indicates a different crystal structure and so analysis by X-ray diffraction would be very informative. The ester and bicyclic derivatives also show no signs of motion of the ring carbons and so lend support to the argument of H-bond exchange in BHMCP. The crystal structures of these compounds are likely to be

somewhat different to that of BHMCP so do not necessarily give information about the parent diol.

The proposed dimers or longer chains of molecules and more than one molecule in the asymmetric in DMCD could also be confirmed by X-ray diffraction. X-ray methods may not however, be able to distinguish between sites due to the rapid interconversion indicated by the NMR results.

The very large positive entropies of activation for *t*-CPD and sulpholane are interesting because generally this is not the case[7,18-20,49] and merit further investigation. Other factors deriving from the structure of the solid must be responsible. In the case of *t*-CPD it is presumably H-bond exchange and for sulpholane it is molecular dipole interactions of the SO_2 group that are important.

The present study has, therefore, shown the variety of molecular motions that can be studied using ^{13}C $T_{1\rho}$ measurements. It has also been shown that information on the solid structure of the compounds can be deduced not just from the chemical shifts, but also from the activation parameters.

Appendix 1

DSC plots

3,3-diethylpentane ($^2H_{20}$)

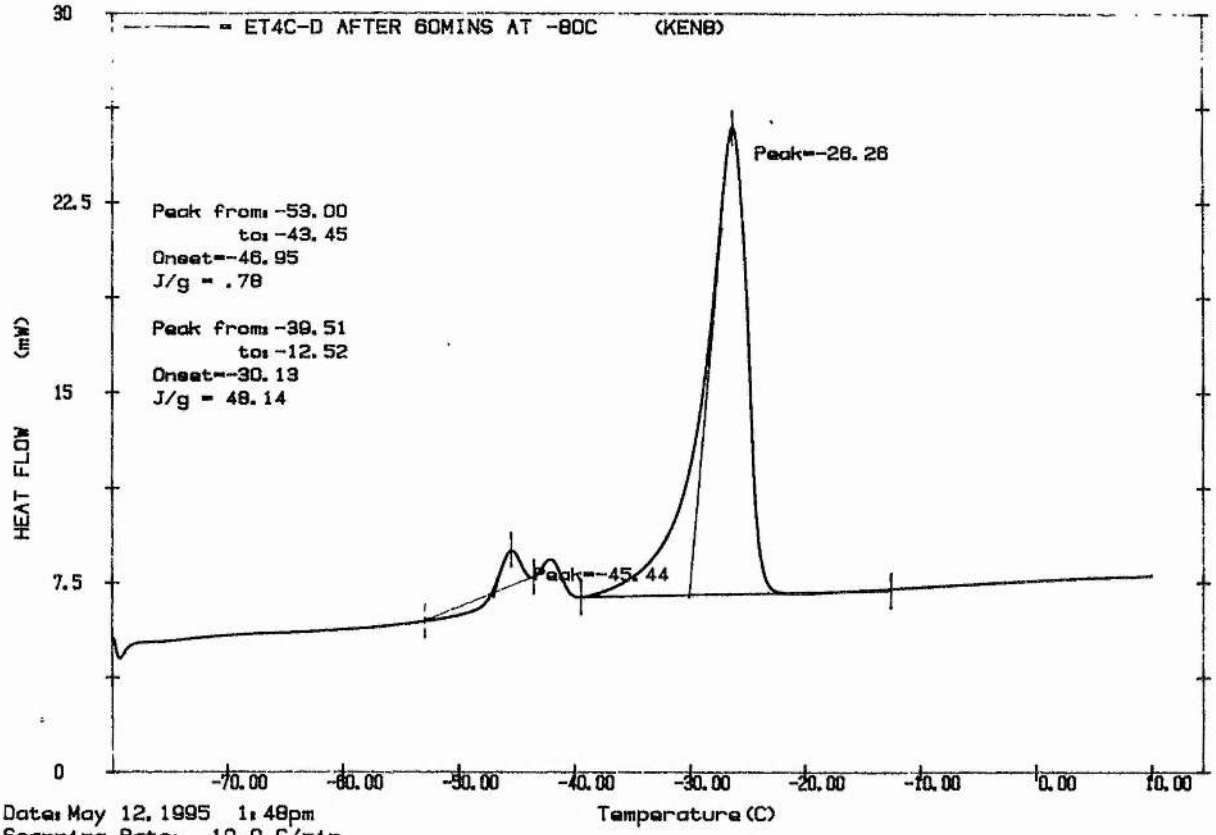

Date: May 12, 1995 1:48pm
Scanning Rate: 10.0 C/min
Sample Wt: 10.000 mg Path: C:\PE\
File 1: KEN8 *J. SMITH*

ST ANDREWS UNIVERSITY

4,4-dipropylheptane

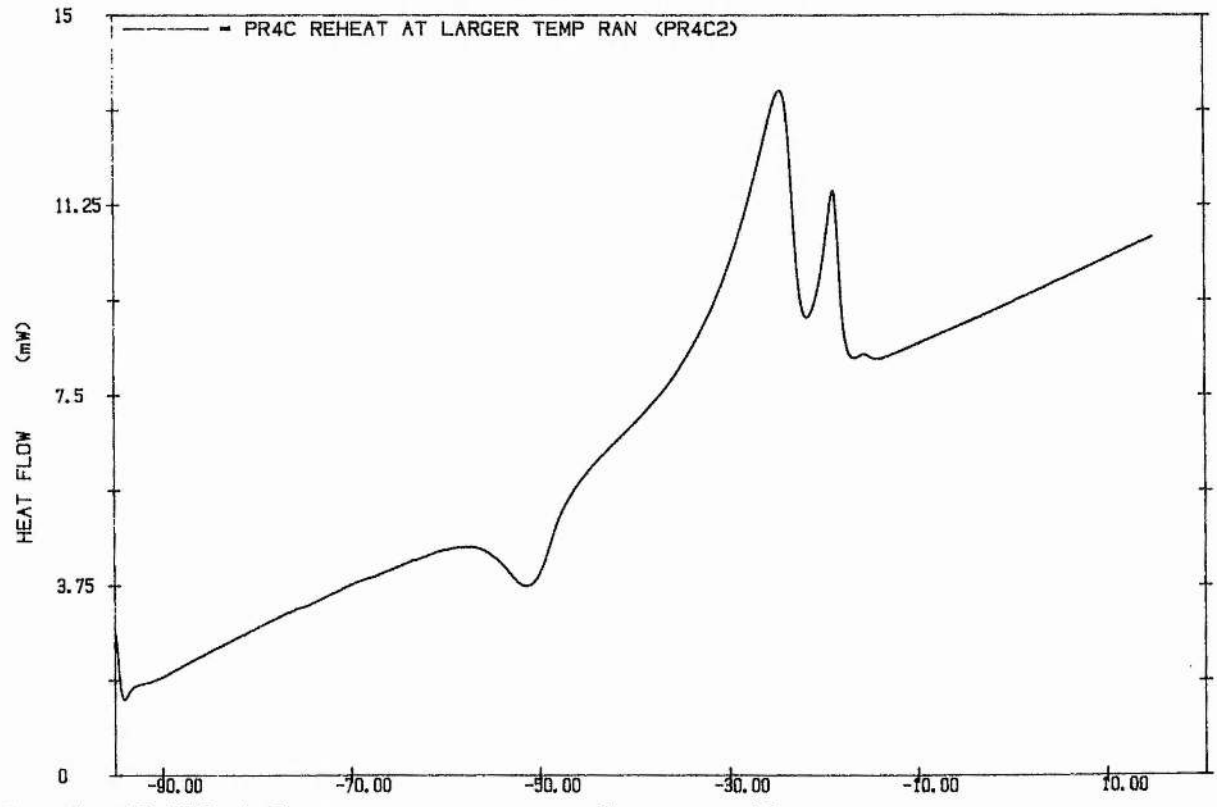

Date: Mar 15, 1996 1:29pm
Scanning Rate: 10.0 C/min

Tetrabutylammonium chloride

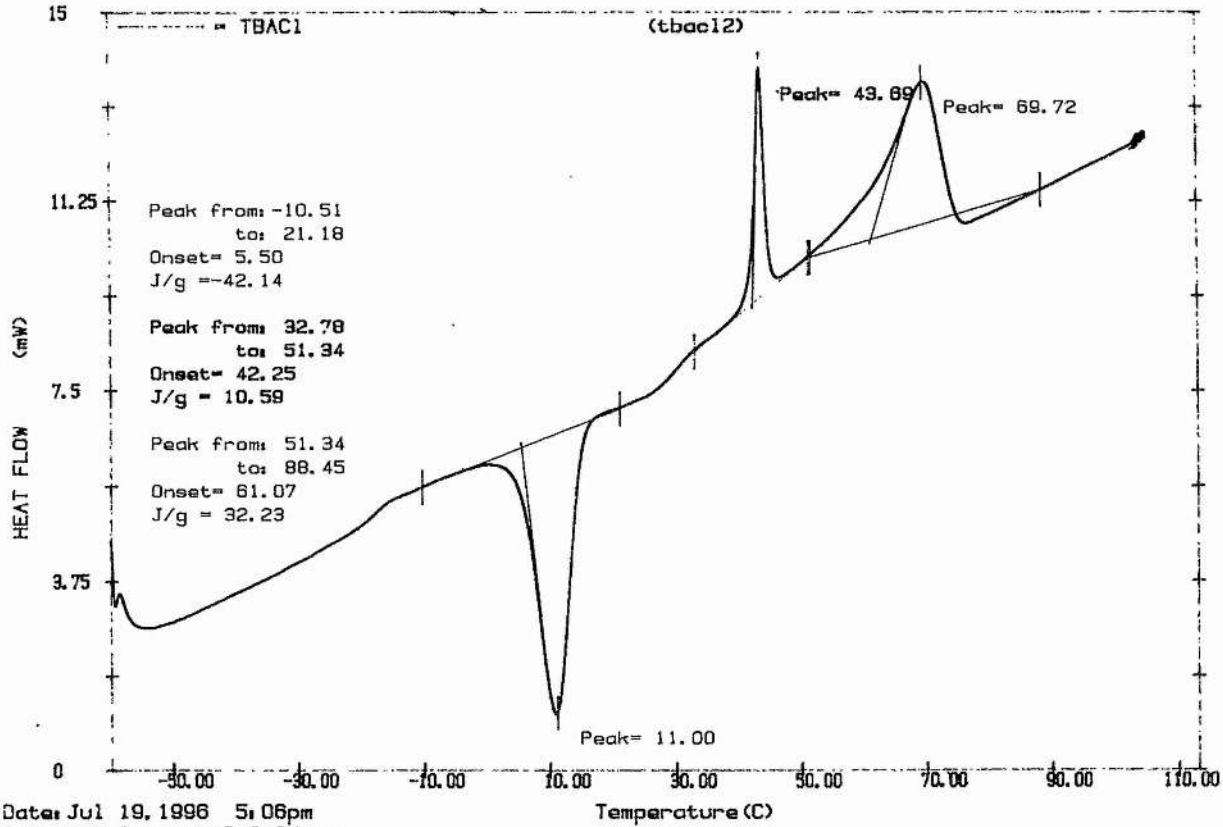

Date: Jul 19, 1996 5:06pm
Scanning Rate: 10.0 C/min
Sample Wt: 4.800 mg Path: C:\PE\
File 1: TBACL2 KEN

ST ANDREWS UNIVERSITY

Tetrabutylammonium iodate

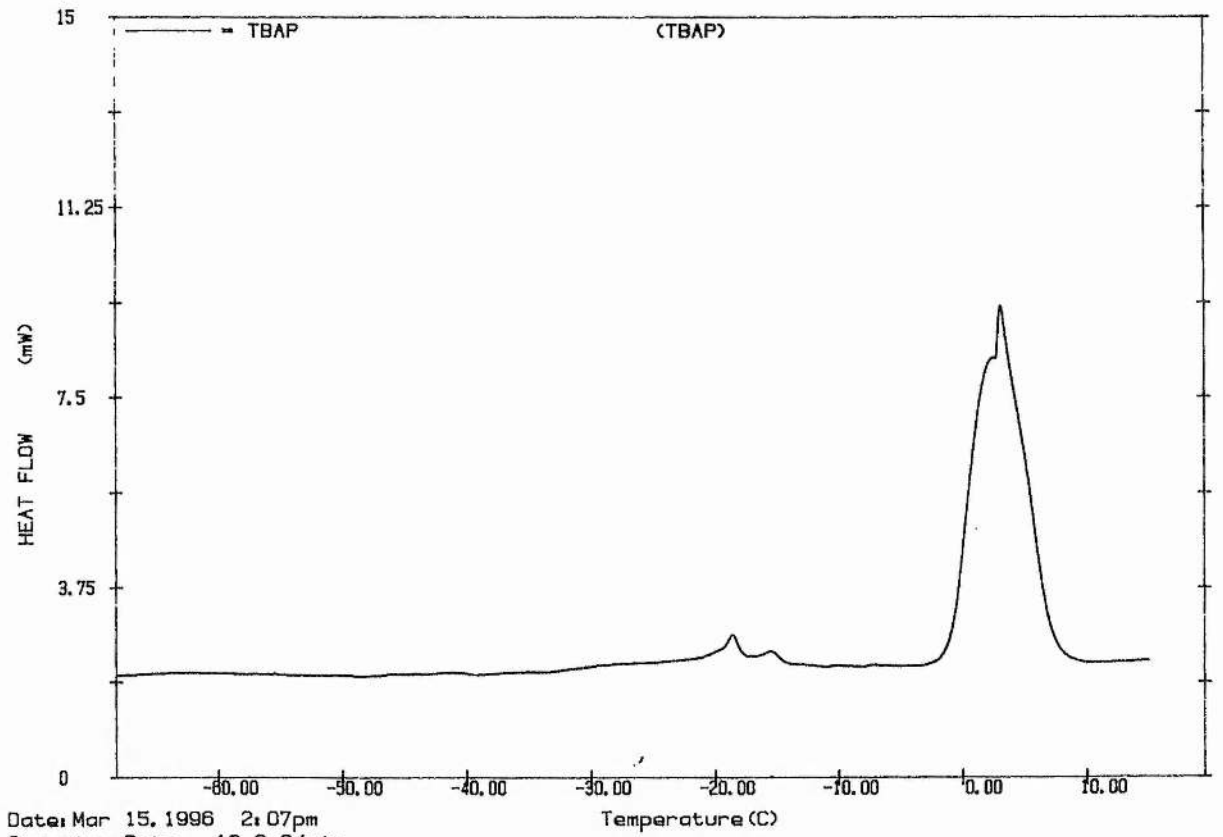

Date: Mar 15, 1996 2:07pm
Scanning Rate: 10.0 C/min
Sample Wt: 5.000 mg Path: C:\PE\

Tetraethylphosponium chloride

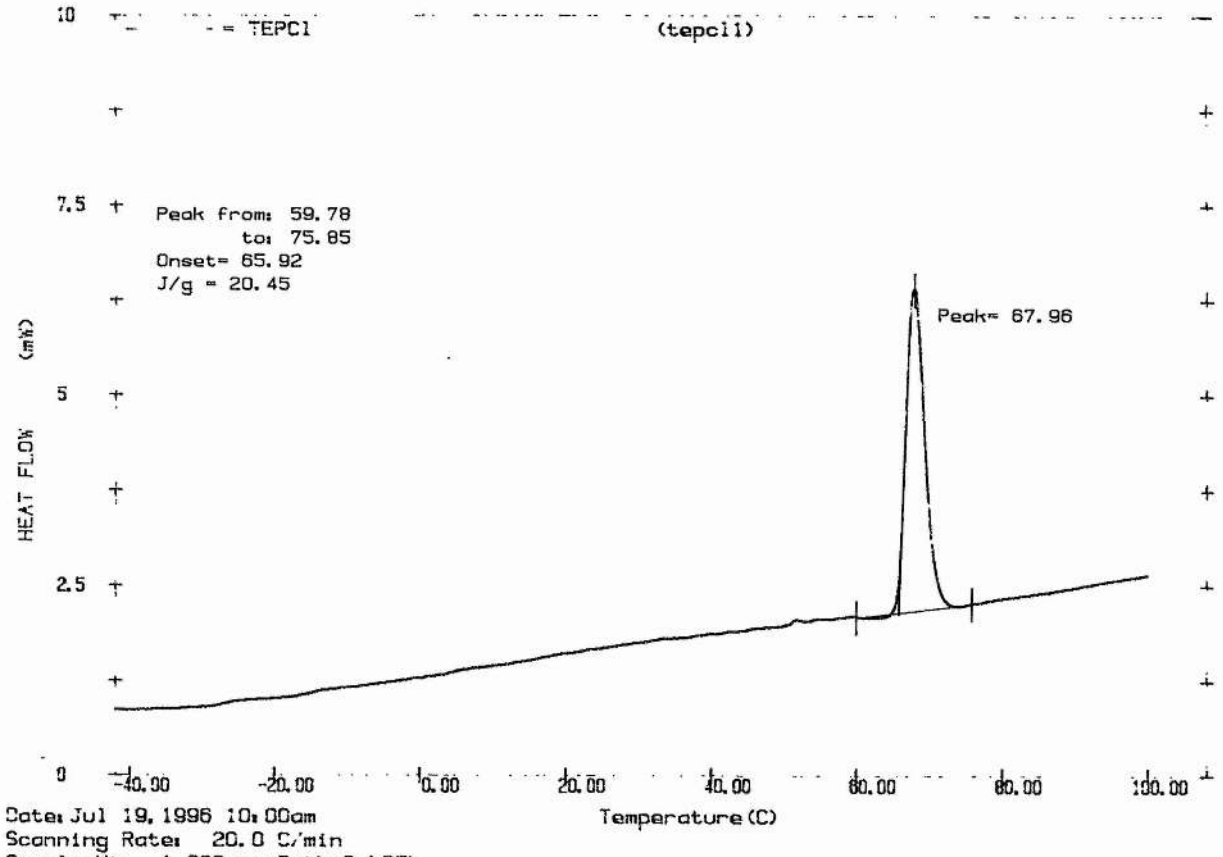

Date: Jul 19, 1996 10:00am
Scanning Rate: 20.0 C/min
Sample Wt: 1.800 mg Path: C:\PE\
File 1: TEPCL1 KEN

ST ANDREWS UNIVERSITY

Tetraethylphosponium bromide

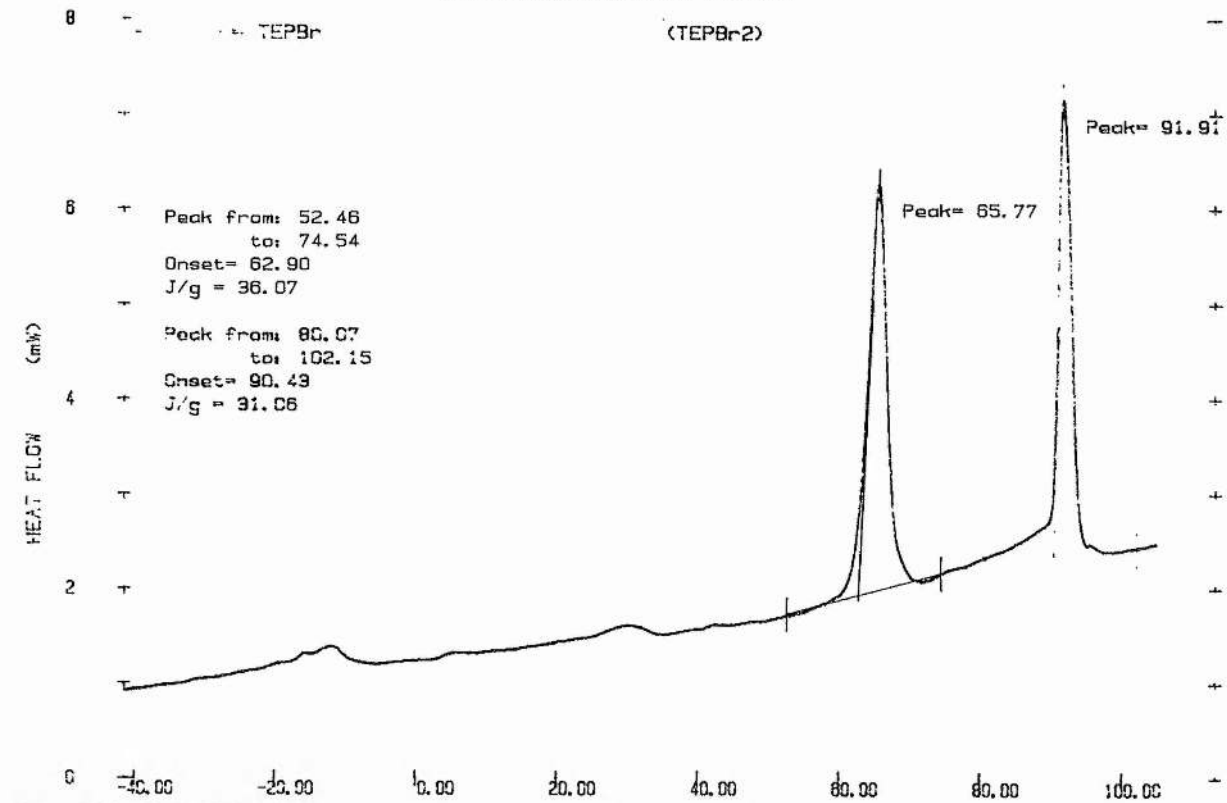

Date: Jul 19, 1996 10:27am
Scanning Rate: 10.0 C/min
Sample Wt: 2.300 mg Path: C:\PE\

ST ANDREWS UNIVERSITY

Tetraethylphosponium iodide

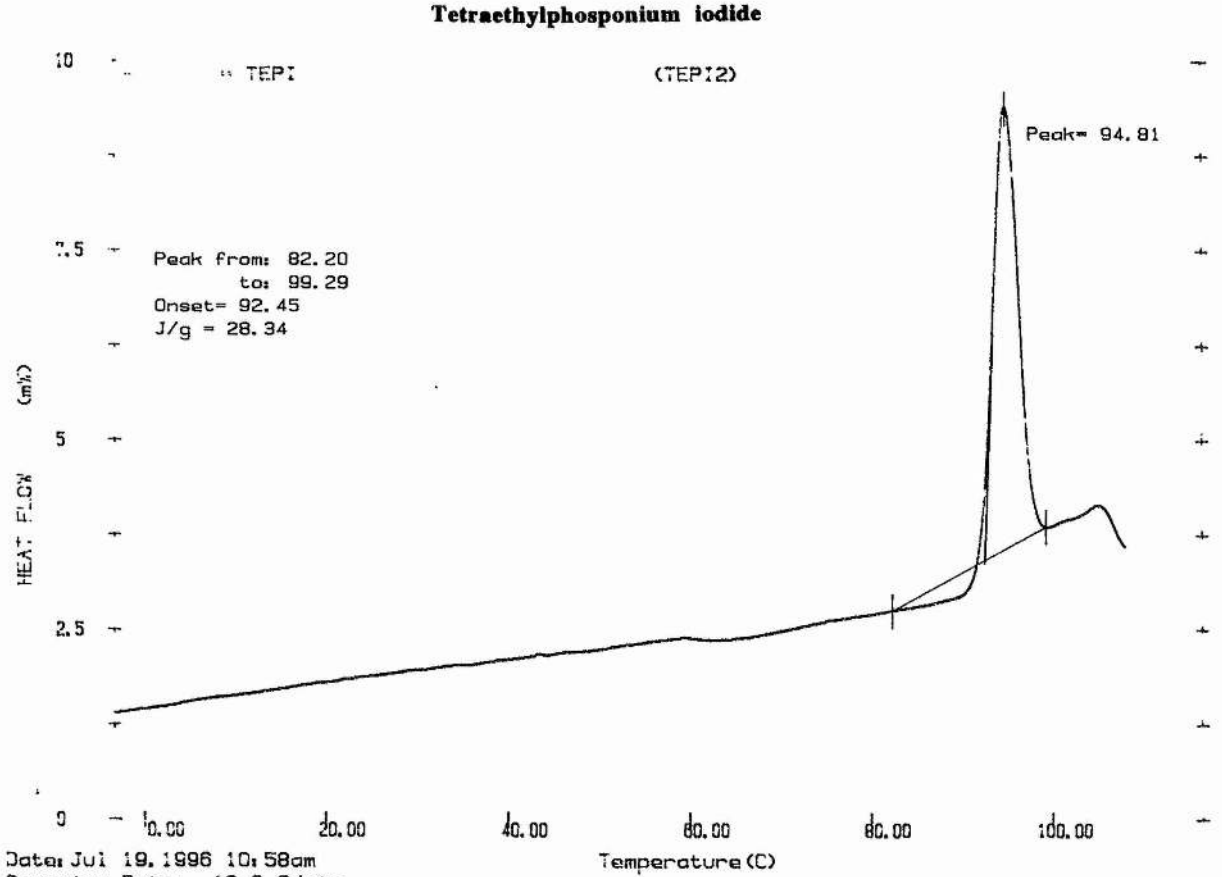

Tetrabutylphosphonium chloride

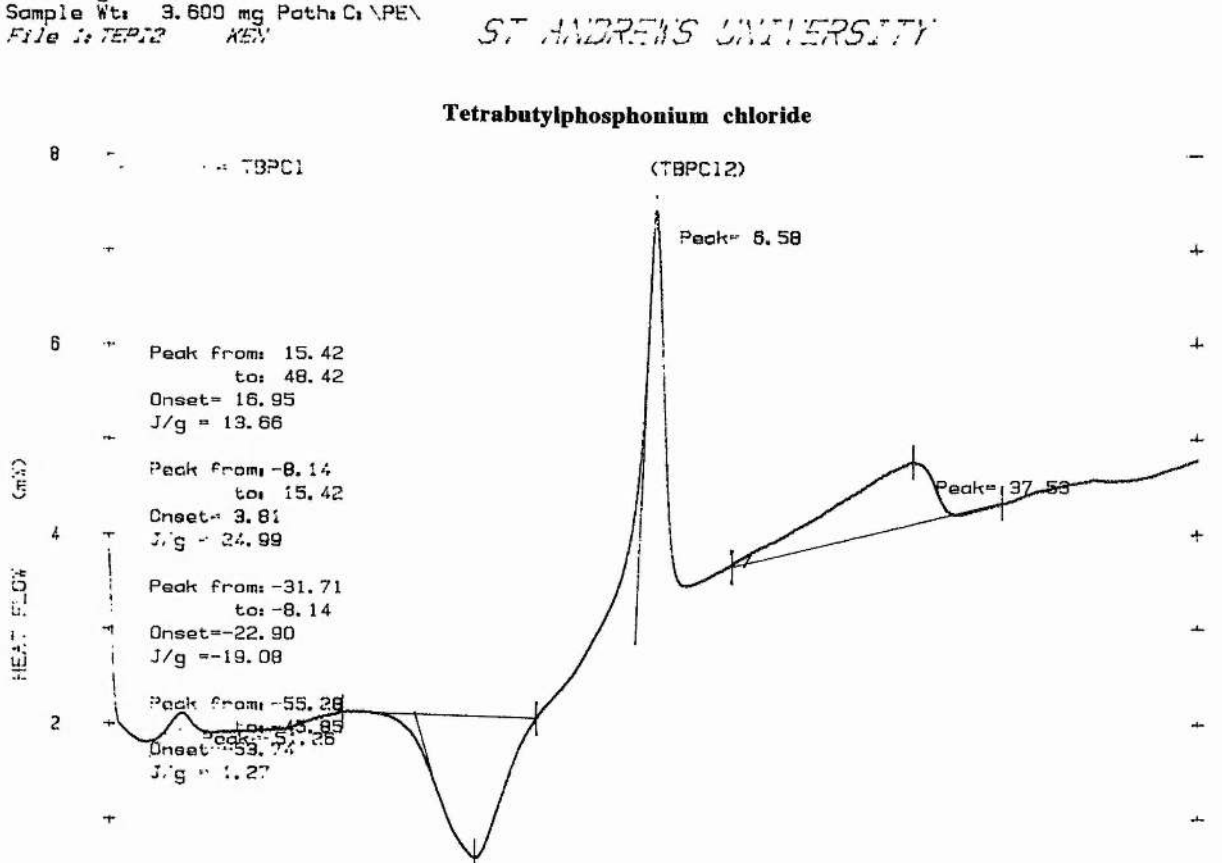

Tetrabutylphosphonium bromide

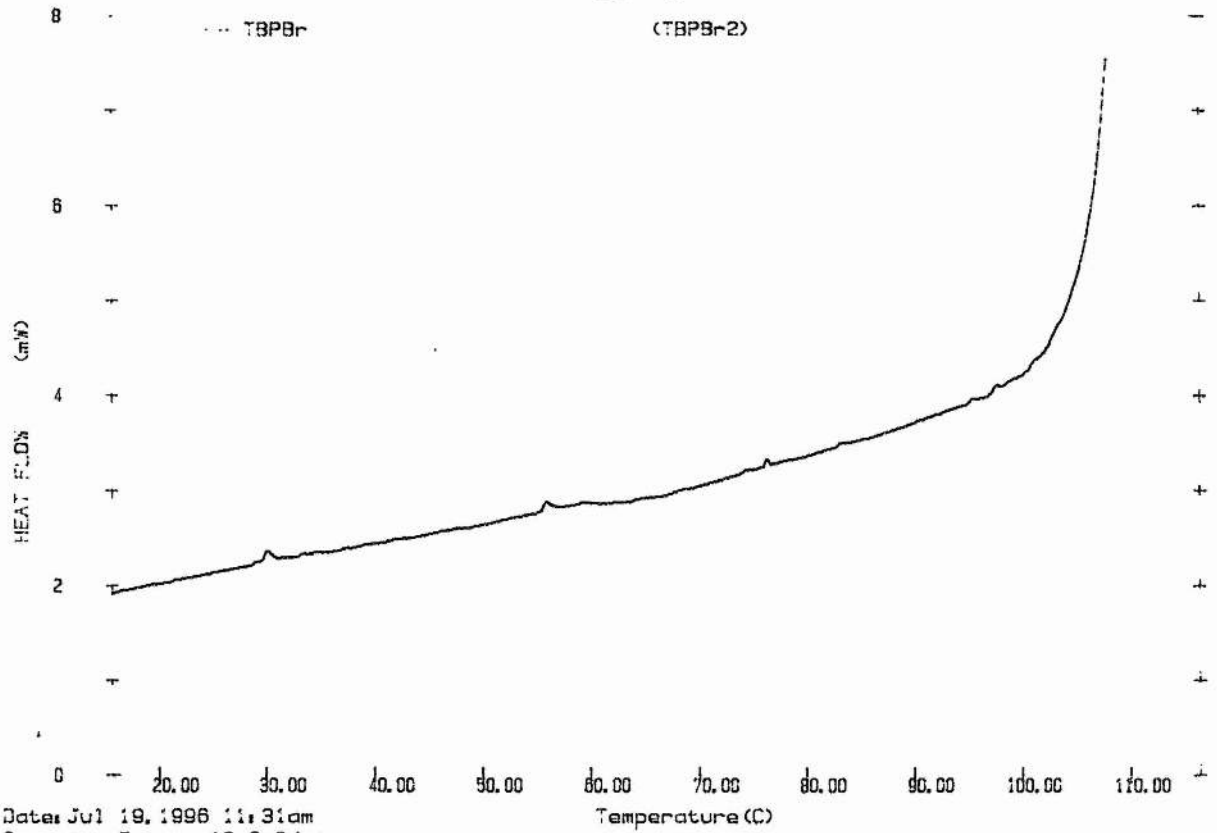

Date: Jul 19, 1996 11:31am
Scanning Rate: 10.0 C/min
Sample Wt: 1.600 mg Path: C:\PE\
File 1: TBPBR2 XEN

Tetrabutylphosphonium iodide

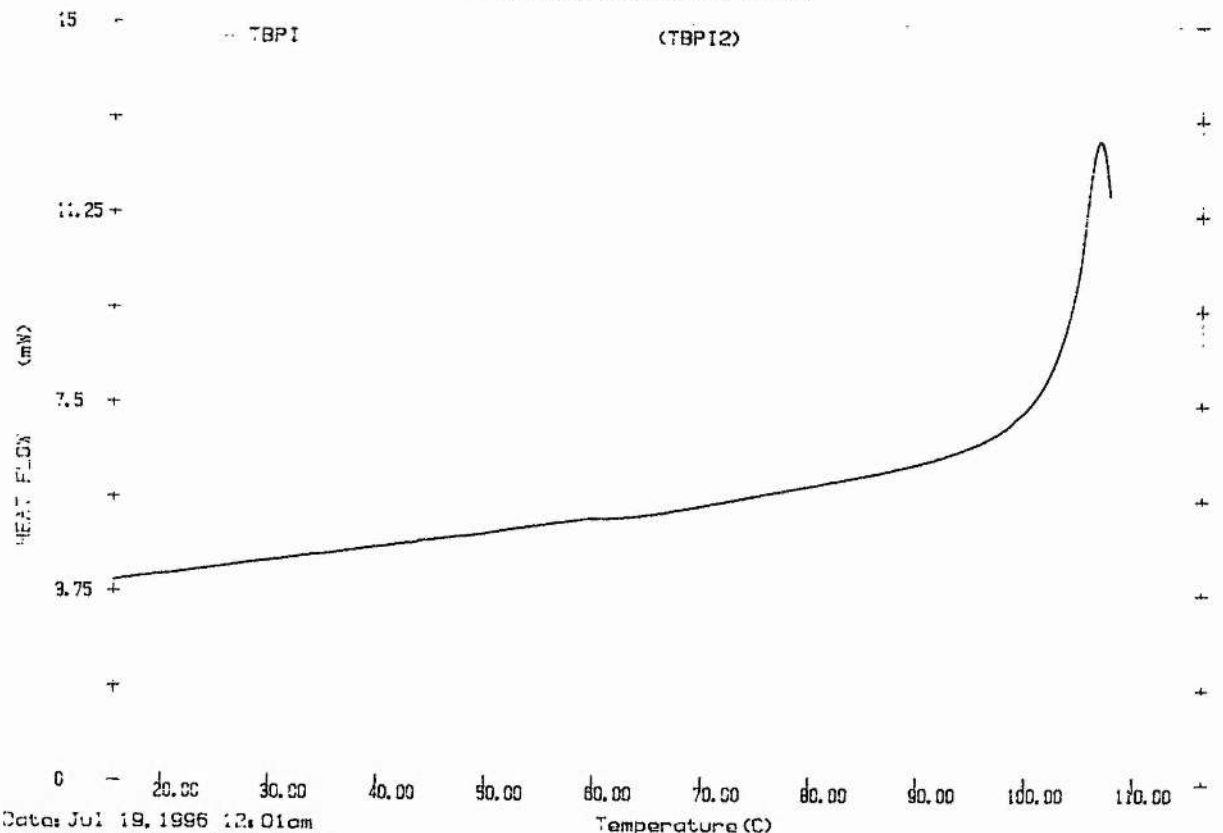

Date: Jul 19, 1996 12:01am
Scanning Rate: 10.0 C/min
Sample Wt: 5.400 mg Path: C:\PE\

References

1 a) L.V. Van Gerven, *Nuclear Magnetic Reasonance in Solids*, Plenum Press, New York, 1977.

b) H. Gunther, *NMR Spectroscopy (second edition)*, John Wiley and Sons Ltd, Chichester, 1992.

c) E. Fukishima and S.B.W.Roeder, *Experimental Pulse NMR*, Addison-Wesley, Massachusetts, 1981.

d) J.K.M. Sanders and B.K. Hunter, *Modern NMR Spectroscopy (second edition)*, Oxford University Press, Oxford, 1993.

e) M. Mehring, *High Resolution NMR Spectroscopy in Solids*, Springer-Verlag, New York, 1976.

f) C.A. Fyfe, *Solid State NMR For Chemists*, C.F.C. Press: Ontario 1984.

2 G.E. Pake, *J. Chem. Phys.*, **16**, 327, 1948.

3 N. Bloembergen, E.M. Purcell and R.V. Pound, *Phys. Rev.*, **73**, 679, 1948.

4 E.R. Andrew and R.G. Eades, *Proc. Roy. Soc. A*, **216**, 398, 1953.

5 G.P. Jones, *Phys. Rev.*, **148**, 332, 1966.

6 G.P. Jones, *Phys. Lett.*, **22**, 390, 1966.

7 F.G. Riddell, S. Arumugam, K.D.M. Harris, M. Rogerson and J.H. Strange, *J. Am. Chem. Soc.*, **115**, 1881, 1993.

8 D.L. Vanderhart and A.N. Garroway, *J. Chem. Phys.*, **74**, 2721, 1981.

9 J. Jeener and P. Broekaert, *Phys. Rev.*, **157**, 232, 1966.

10 R.C. Keller, M.S. Coffey, M.J. Lizak, M.S. Conradi and W Bunnelle, *J. Phys. Chem.*, **93**, 3832, 1989.

11 E.R. Andrew and R.G. Eades, *Proc. Roy. Soc. A*, **216**, 537, 1953.

12 J.S. Waugh and É.I. Fedin, *Sov. Phys.-Solid State*, **4**, 1633, 1963.

13 J. Tsau and D.F.R. Gilson, *Can. J. Chem.*, **48**, 717. 1970.

14 S. Mooibroek and R.E. Wasylishen, *Can. J. Chem.*, **63**, 2926, 1985.

15 (a) J. Jeener, B.H. Meier, P. Bachmann and R.R. Ernst, *J. Chem. Phys.*, 71, 4546, 1979.

(b) C.L. Perrin and T.J. Dwyer, *Chem. Rev.*, **90**, 935, 1990.

16 H.S. Gutowsky and C.H. Holm, *J. Chem. Phys.*, **25**, 1228, 1956.

17 W.P. Rothwell and J.S. Waugh, *J. Chem. Phys.*, **74**, 2721, 1981.

18 F.G. Riddell, G. Bernáth and F. Fülöp, *J. Am. Chem. Soc.*, **117**, 2327, 1994.

19 F.G. Riddell, M. Bremner and J.H. Strange, *Magn. Res. Chem.*, **32**, 118, 1994.

20 F.G. Riddell and M. Rogerson, *J. Chem. Soc., Perkin Trans. 2*, 493, 1996.

21 W.M. Schubert, and S.M. Leahy, *J. Am. Chem. Soc.*, **79**, 381, 1957.

22 M.S. Newman, D.H. Busch, G.E. Cheney and C.R. Gustafson, *Inorg. Chem.*, **11**, 2890, 1972.

23 E. Buchta and K. Giebel, *Chem. Abs.*, **56**, 15381, 1962.

24 V. Petrow, O. Stephenson and A.M. Wild, *Chem. Abs.*, **54**, 16457, 1960.

25 Aldrich Catalogue/Handbook of fine Chemicals, U.K., 427, 1994-1995.

26 F.B. Thole and J.F. Thorpe, *J. Chem. Soc.*, **99**, 420, 1911.

27 G. Kommpa, *Ber.*, **32**, 1421, 1899.

28 H. Kwart and J.A. Ford, Jr., *J. Org. Chem.*, **24**, 2060, 1959.

29 R.Ya. Levina and N.N. Mezentsova, *Chem. Abs.*, 8977g, 1958.

30 A.W. Horton, *J. Am. Chem. Soc.*, **69**, 182, 1947.

31 G.T. Morgan, S.R. Carter and A.E. Duck, *J. Chem. Soc.*, **127**, 1252, 1925.

32 A.D. Petrov and E.A. Chernyshev, *Chem. Abs.*, **48**, 565e, 1952.

33 Organic Syntheses, Coll. Vol. II, John Wiley and Sons Inc., New York, 476, 1943.

34 a) H.S. Gutowsky and G.E. Pake, *J.Chem. Phys.*, **18**, 162, 1950.
b) J.G. Powles and H.S. Gutowsky, *J.Chem. Phys.*, **21**, 1695, 1953.

35 R.W. Alder, C.M. Maunder and A.G. Orpen, *Tet. Lett.*, **31**, 6717, 1990.

36 H.L. Finke, J.F. Messerly and D.R. Douslin, *J. Chem. Thermodynamics*, **8**, 965, 1976.

37 M.S. Greenfield, A.D. Ronemus, R.L. Vold, R.R. Vold, P.D. Ellis and T.E. Raidy, *J. Mag. Res.*, **72**, 89, 1987.

38 (a) E.R. Andrew and P.C. Canepa, *J. Mag. Res.*, **7**, 429, 1972.
(b) D.J. Blears and S.S. Danyluk, *J. Phys. Chem.*, **72**, 2269, 1968.
(c) M. Polak and M. Sheinblatt, *J. Mag. Res.*, **12**, 261, 1973.
(d) S.B.W. Roeder and D.C. Douglass, *J.Chem. Phys.*, **52**, 5525, 1970
(e) J. Dufourcq and B. Lemanceau, *J.Chim. Phys.*, **67**, 9, 1970.
(f) M. Mahajan and B.D. Nageswara Rao, *J. Phys. Chem. Solids.*, **33**, 2191, 1972.

39 S. Albert, H.S.Gutowsky and J.A. Ripmeester, *J. Chem. Phys.*, **56**, 3672, 1972.

40 A.A.V. Gibson and R.E. Raab, *J. Chem. Phys.*, **11**, 4688, 1972.

41 A. Xenopoulos, A.H. Narten, and J. Cheng and B. Wunderlich, *J. Non-Cryst.*

Solids, **131-133**, 113, 1991.

42 A. Xenopoulos, J. Cheng, M. Yasuniwa and B. Wunderlich, *Mol. Cryst. Liq. Cryst.*, **219**, 63, 1992.

43 J. Cheng, A. Xenopoulos, and B. Wunderlich, *Mol. Cryst. Liq. Cryst.*, **220**, 105, 1992.

44 J. Cheng, A. Xenopoulos, and B. Wunderlich, *Mol. Cryst. Liq. Cryst.*, **220**, 127, 1992.

45 P.J. Barrie and J.E. Anderson, *J. Chem. Soc. Perkin. Trans.* 2, 2031, 1992.

46 F.G. Riddell, K.S.Cameron and W.B. Turnbull, *Mag. Res. Chem.*, **33**, 841, 1995.

47 B. Szafranska and Z. Pajak, *J. Mol. Struc.*, **99**, 147, 1983.

48 T.T. Ang and B.A. Dunell, *Can. J. Chem.*, **54**, 1985, 1976.

49 M. Rogerson, University of St. Andrews, Ph.D. Thesis, 1995.

50 J.B. Lambert, L. Xue and S.C. Howard, *J. Am. Chem. Soc.*, **113**, 8958, 1991.

51 J.B. Lambert, S.C. Johnson and L. Xue, *J. Am. Chem. Soc.*, **116**, 6167, 1994.

52 E.L. Eliel and S.H. Wilen, *Stereochemostry of organic compounds*, John Wiley & Sons , Inc., New York, 1994.

53 J.B. Hendrickson, *J. Am. Chem. Soc.*, **89**, 7047, 1967.

54 F.A. Rushworth, *Proc. Roy. Soc. A*, **222**, 526, 1954.

55 F.G.Riddell, V. Weiss, R.A. Spark and L. Lethbridge, unpublished results.

56 R.K. Harris, M.M. Sünnetcioglu, K.S. Cameron and F.G. Riddell, *Mag. Reson. Chem.*, **31**, 963, 1993.

57 D.W. Kydon, A.R Sharp, M.E. Hale and A. Watton, *J.Chem. Phys.*, **72**, 6153, 1980.

58 D.F.R. Gilson and P.P. Saviotti, *J. Chem. Soc. Faraday Trans. II*, 1, 1974.

I'm closin' the book
On the pages and the text
And I don't really care
What happens next
I'm just going
I'm going
I'm gone

Bob Dylan 1973